A STUDY OF CORRECTIONS FOR MATRIX AND PARTICLE SIZE EFFECTS IN THE X-RAY FLUORESCENCE SPECTROCHEMICAL ANALYSIS OF BAUXITE ORE

John H.E. Lawson

A THESIS

in

The Department

of

Chemistry

Presented in Partial Fulfillment of the Requirements for
the Degree of Master of Science at
Sir George Williams University
Montreal, Canada

February, 1974

ABSTRACT

This thesis presents the use of x-ray fluorescence spectrometry for the analysis of bauxite ore in the presence of particle size effects and interelement effects. The investigation basically involves the attempt to analyse coarse bauxite ore, from different geographical regions, without destroying the constitution of the material.

A chapter is devoted to the general description of the method of x-ray fluorescence spectrochemical analysis. The origin and characteristics of x-rays, the instrumentation and the data handling are discussed in some detail for the benefit of those who know little of this analytical technique.

The selection of instrumental parameters is carefully described with reference to the particular analysis of bauxite ore samples keeping the number of variables to a minimum.

Particle size effects are investigated and are shown to be significant in bauxite analysis. The possibility of eliminating or correcting for such effects is considered.

Finally, interelement effects in bauxite analysis are examined. The Lachance and Traill correction procedure is shown to be effective if the determination of interelement effect correction coefficients is carried out with actual bauxite samples.

This thesis is
dedicated to my
devoted parents.

ACKNOWLEDGEMENT

I wish to express my sincere appreciation to Professor J.G. Dick for his effort in initializing the project and for his valuable guidance throughout the investigation.

I gratefully acknowledge the many people at Alcan Research and Development Ltd. who strived to bring industry and academia closer together through the organization of this project. I especially thank Robson Black for his assistance in outlining the problem to be investigated and for his close following of the research.

I wish to thank Alcan Research and Development Ltd. for supplying all the necessary materials, for the use of their x-ray equipment and especially for the support grant.

I am particularly grateful to my close friend Alan Fraser for the many helpful and encouraging discussions which allowed me to overcome some difficult portions of my work. I also thank David Hall and Douglas Bickley for their interest in my project.

My deepest gratitude goes to Diane Lawson for the valuable time and effort which she spent to help type this thesis over the many months of its preparation.

Finally, I wish to thank my dear mother, Ann Lawson, for her continuing patience, understanding and encouragement through the many years of my studies.

TABLE OF CONTENTS

LIST OF TABLES

LIST OF FIGURES

CHAPTER 1

INTRODUCTION

Bauxite is a non-homogeneous clay-like mineral composite containing mostly hydrous oxides of aluminum. It is found in pockets on the surface of Tertiary terrains as a result of intense chemical weathering of basic igneous rock. The aluminum oxide is extracted from the bauxite and is electrolytically reduced to aluminum metal. The bauxites of greatest commercial interest are composed chiefly of the minerals listed in TABLE 1-1 [1] with minor constituents being aluminian goethite (a solid solution of aluminum in $Fe_2O_3 \cdot H_2O$) and oxides of calcium, phosphorous, vanadium, manganese, zinc and gallium. The quantities of the major minerals can vary considerably depending on the region from which the bauxite originates. Rough composition ranges for the major components are as follows: 40 - 60% Al_2O_3; 1 - 10% SiO_2; 1 - 3% TiO_2 and 5 - 30% Fe_2O_3.

The method of extraction of pure alumina from bauxite is known as the Bayer process. Bauxite from different regions is mixed and fed via several hoppers to the digestion tank. The quantity of bauxite is controlled by gates at the base of each hopper. A strong caustic soda solution (~ 45% NaOH) is added and the mixture is digested for several hours at a temperature between 160° and 170° C. and at a pressure of about 100 psi. The alumina goes into solution as the sodium salt ($NaAlO_2$).

TABLE 1-1

PRINCIPAL MINERALS IN BAUXITE

MINERAL	COMPOSITION
Gibbsite	$Al_2O_3 \cdot 3H_2O$
Boehmite	$Al_2O_3 \cdot H_2O$
Kaolinite	$Al_2O_3 \cdot 2SiO_2 \cdot 2H_2O$
Hematite	Fe_2O_3
Goethite	$Fe_2O_3 \cdot H_2O$
Quartz	SiO_2
Anatase	TiO_2

The solution is filtered, diluted with an equal volume of water and allowed to stand for 36 to 48 hours. Some fine seed alumina is added to help in the precipitation of almost pure crystalline aluminum hydroxide. The product is removed by filtration, washed and calcined. The filtrate is reinforced with caustic soda and used again.

The alumina yield is not simply dependent on the amount of alumina in the bauxite but it depends on the amounts of iron oxide and silica. The silica affects the process by using up some of the caustic. The quantity of caustic that is added to the digester feed is critical. If there is too much caustic it will come out of the supersaturated solution and clog the pipes. If there is too little caustic the process efficiency decreases because some of the alumina is not dissolved. The iron content influences the filtering process of the Bayer liquors [2,3]. If there is not much iron in the bauxite, some laterite(bauxite with a high iron content) is added to the digester feed to facilitate transformation of iron minerals to forms which settle more rapidly.

The concentrations of the major components of the bauxite must be known with reasonable accuracy in order that adjustments can be made to the Bayer process to give maximum production of alumina. Ideally, if the digester feed is controlled to maintain a constant amount of each of the major components, the parameters for the extraction process can remain fixed.

The evaluation of a new bauxite deposit involves the examination of thousands of drill hole samples. To analyze them chemically involves extensive and costly procedures especially for the determination of alumina content. Usually the amounts of the other major components are secured by wet chemical methods and a by-difference value for alumina is calculated. In most cases this method is generally satisfactory but it can be subject to large errors, especially where exploration samples are concerned when very little is known about the mineralogical make up of the bauxite.

As instrumental methods of chemical analysis became more prominent and reliable, the problem of bauxite analysis was viewed under a different light. The principal requirement was that the method must involve a minimum of sample preparation. This eliminated methods where the sample must be in solution as is the case for spectrophotometry and atomic absorption spectrometry. X-ray methods of analysis seemed to offer an excellent means of solving the problem. A fair amount of work has been done on the use of x-ray methods for chemical analysis, but there is very little literature on the quantitative x-ray analysis of multicomponent mixtures on a mass production basis.

X-ray diffraction was first used because it gives information on the compounds present, rather than on the elements or chemical groups. This method is reasonably accurate if all major constituents are determined and adjusted to 100 percent, but it requires considerable time to set up calibrations. The standards used must be very similar

to the unknown materials to be analysed. Bauxite deposits from two regions may not be, and usually are not, compatible because their mineralogical compositions are not similar. Thus separate calibrations are required for different types of bauxite. The x-ray diffraction method has become more useful qualitatively rather than quantitatively. It is now mostly used as a sorting method and as a means to obtain useful mineral ratios.

The method which seems to be more applicable to production scale bauxite analysis is x-ray secondary-emission or x-ray fluorescence (XRF) spectroscopy. There are four main advantages. Firstly, materials can be analysed as liquids, solids or powders and in most cases the sample need not be destroyed. For bauxite, a soft granular substance, the preparation can be restricted to simple grinding of the sample to a suitable particle size. This could be done in a matter of minutes. Secondly, instrument calibration is considerably simplified. The analysis involves the determination of elemental percentages. For this reason it is not necessary to give any consideration to the mineralogical form of the sample and synthetic standards might be used. Thirdly, the determination of a number of elements can be done at the same time, usually with just simple revision of instrumental parameters. The time for analysis of one element is usually less than one minute. Finally, the method possibly lends itself to automation with computer data acquisition and process control.

As in all analytical methods, x-ray fluorescence analysis

presents certain problems which must be overcome. The difficulty is basically due to the sample itself. The validity of the analytical determination depends on the physical structure and chemical composition of the sample.

The problem of physical structure could be solved if the sample was completely homogeneous with a particle size somewhat less than the depth of penetration of the x-rays under consideration. This would be the case if a solution was made of the sample. However, keeping powder analysis with minimum sample preparation in mind, all mineral powders act heterogeneously in the presence of x-rays and for production analysis the required particle size is highly impractical.

The problem of chemical composition is generally referred to as the matrix effect. The observed intensity of a characteristic radiation of one element is directly affected by the presence of all other elements (the matrix) in the sample. Depending on the atomic number of the elements involved and the energy of the characteristic incident radiation, one element may absorb or enhance (either true or pseudo-enhancement) the secondary radiation being generated by another element. These effects cannot be eliminated but a considerable amount of work has been done to either correct for the effects mathematically or make the effects negligible by changing the basic composition of the sample.

Present bauxite analysis by XRF spectrometry does not eliminate the particle size effects and matrix effects. However, these effects have been reduced significantly by using standards which are

essentially the same physically and chemically as the unknown samples. This is a limited solution to the problem of bauxite analysis in that it cannot be applied to different bauxite types. The ideal analytical set up would be obtained if corrections could be devised to eliminate the problems of matrix effects and particle size effects when applied to any type of bauxite regardless of origin. Under such conditions an automated process control situation could be developed. Different bauxite types would be loaded into separate hoppers with the feed from these hoppers being continually sampled and analytically investigated by XRF spectrometric analysis. A computer would acquire the x-ray data, calculate the elemental percentages of the bauxite and adjust the feed gates on the hoppers. The digester feed would be controlled to give a constant composition that would allow the variables of the Bayer extraction process to be fixed for maximum efficiency in alumina production.

The program projected for this study of the XRF spectrometric analysis of bauxite was two-fold and involved:

1) The investigation of whether or not particle size effects could be observed in the x-ray spectrochemical analysis of bauxite ores and, if such effects were observed, to investigate the possibility of deriving particle size effect correction factors or coefficients capable of eliminating or minimizing these effects.
2) The investigation of the matrix absorption and enhancement effects in the x-ray spectrochemical analysis of bauxite ores and to derive, if possible, matrix effect correction factors

or coefficients capable of eliminating or minimizing these effects.

CHAPTER 2

X-RAY FLUORESCENCE SPECTROMETRY

The aim of this chapter is by no means to present a thorough description of the technique of x-ray fluorescence spectrometry. Detailed information concerning the basics, the general applications of conventional equipment and the sophisticated theory and components required for special applications can be found in numerous texts, reviews and papers. Particular reference is made to the book by E. P. Bertin [4] which seems to thoroughly cover the principles and practice of x-ray techniques from preliminary experiments to modern techniques. The 619 pages of text are referenced with an extensive bibliography.

The primary intention here is to present some of the basic principles behind this analytical technique in terms of the origin and properties of x-rays and to describe the essential details of the instrumentation involved. A cursory discussion of some of the inherent problems and attempts to eliminate them is developed with respect to the effects of sample preparation, homogeneity and particle size as well as interelement interactions.

2-1 ORIGIN OF X-RAY SPECTRA

The x-ray region of the electromagnetic spectrum is generally considered to lie in the wavelength range of 0.1 to 50 angstroms (Å). Shorter wavelengths belong to the gamma ray region while longer wavelengths are considered part of the soft x-ray and vacuum ultraviolet region. X-rays are emitted from an element as a result of bombardment by high energy electrons. The resultant x-ray spectrum is complex and involves a characteristic line spectrum of discrete wavelengths that is superimposed on top of a broad band spectrum of continuous radiation.

The continuum is characterized by a short wavelength limit corresponding to the maximum energy of the impinging electrons, a peak maximum which occurs at about double the short wavelength limit and a trailing-off in intensity at long wavelengths. This radiation is a result of the deceleration of the exciting electrons upon impact with the target material. As a consequence, the intensity of the continuum varies directly with the applied voltage and current for the electron beam, as well as with the atomic number of the target element.

The characteristic line spectrum is adequately explained in terms of the Bohr atom concept. If the electron beam should cause ejection of one or more electrons from an inner electron shell a "positive hole" is created. This atomic instability is relieved by single or multiple electron transitions from the outer orbitals. With this electron transfer, characteristic radiation is emitted at a

wavelength equivalent to the change of energy state of the electron. If an electron is removed from the K-shell (innermost) and replaced by an electron from the L-shell (next innermost) radiation known as K_α radiation may be generated. The emission of an L line could follow with an electron from the M-shell filling the hole in the L-shell. Subsequent transitions and emissions may continue until the energy transfer is equivalent to that associated with the outer orbital electron vibration.

The true x-ray line spectrum is considerably more complicated. The Pauli exclusion principle states that no two electrons can have the same quantum numbers (n, l, m, s) which define the electron energy state. The principal quantum number (n) can have integral values of 1, 2, 3, etc. corresponding to the K, L, M, etc. electron shells. The angular quantum number (l) defines the orbital shape and can take on values from $(n-1)$ to 0. The magnetic quantum number (m), defined by the projection of the angular momentum (l) upon the direction of the magnetic field, can have values of $+l$, $-l$, or 0. Finally, the spin quantum number (s) has a value of either $+ {}^1/_2$ or $- {}^1/_2$. The selection rules, for the determination of allowable transitions, state that $\Delta l = \pm 1$ and $\Delta J = 0$ or ± 1 where J is the vector sum of l and s. The x-ray spectrum is thus comprised of a number of groups (one K group, three L groups, five M groups, etc.) each containing several characteristic lines. Naturally, the number of spectral lines increase as the atomic number increases. A light element may only have a few lines

in its x-ray spectrum but for a very heavy element more than 50 different electron transitions and hence x-ray lines are possible. This would give rise to an extremely complicated spectrum if all lines were observed. Fortunately, only a fraction of these lines may be detected due to the very low line intensity of x-rays originating from the outer electron interactions.

The intensity of each spectral line depends on the transition probability which is a function of the different electron energy states in the orbitals. Thus for a given atom the intensity ratios of the various lines would always be the same. However, for different atoms, and hence different orbital and electron energy states, the intensity ratios within a given series would change in favour of low energy transitions for the low atomic number elements. For example, the ratio of $K\alpha$ to $K\beta$ intensity is much larger for the light elements. For aluminum this ratio is 25:1 while it is only 3:1 for tin. In general, only the K series or L series lines are of sufficient intensity to be useful for spectrochemical analysis.

The expression relating the wavelength of x-rays to their energy in volts is known as the Duane-Hunt law and is developed [4] as indicated below.

The energy of electromagnetic radiation is given by the expression

$$E = h\nu = hc/\lambda \qquad 2\text{-}1$$

where E is the photon energy in ergs, h is Planck's constant

(6.624×10^{-27} erg sec), C is the velocity of light (2.998×10^{10} cm/sec), ν is the frequency (Hz) and λ is the wavelength (cm) of the radiation.

For x-ray generation the exciting electron has an energy of

$$E_e = eV \qquad 2\text{-}2$$

where e is the electronic charge in electrostatic units (4.8×10^{-10} esu) and V is the applied potential in volts. In the ideal case, all of the energy of the electron would be transferred to the x-ray photon hence

$$E_e = eV = hc/\lambda \qquad 2\text{-}3$$

and

$$\lambda = hc/eV \qquad 2\text{-}4$$

Substituting in the values of h, c and e and converting centimeters to angstroms (10^8 Å/cm) and electrostatic units to volts (300 V/esu), EQUATION 2-4 becomes the Duane-Hunt law

$$\lambda = 12{,}400/V \qquad 2\text{-}5$$

where λ is in angstroms and V is in volts.

This expression is used extensively in XRF spectrometry and is especially useful for the determination of selective excitation conditions.

The preceding discussion describes the result of primary excitation of x-ray spectra by high energy electrons. When x-rays are used for excitation, the resultant secondary-emission is characterized by only a line spectrum. As mentioned previously, a continuum is caused by an incremental energy loss process by impinging electrons. For primary x-ray photons this stepwise reduction of energy is impossible and thus a continuum cannot exist in a secondary-emission spectrum.

2-2 PROPERTIES OF X-RAYS

In x-ray fluorescence spectrometry the excitation of the x-ray secondary-emission spectrum is achieved by irradiation of the sample with x-rays of selected wavelength as determined by the target material of an x-ray tube. The propagation of x-rays, both primary and secondary, is determined first by their energy and second by the type of medium through which they travel. Basically, x-rays may be transmitted, absorbed, scattered or diffracted. The properties of absorption and incoherent scatter show the particle nature of x-rays while coherent scatter and diffraction display their wave character.

It is reasonable to assume that radiation absorption is

inversely proportional to the radiation energy. The greater the energy the greater the penetration power. Since the electrons of atoms occur in discrete energy levels, it is expected that the absorption of primary radiation would not be a continuous function of the energy of that radiation. Abrupt discontinuities occur and are known as absorption edges. An electron will only be expelled from any given level if enough energy is applied. Below this energy the incident radiation would not be absorbed while above the minimum required energy for electron expulsion (absorption edge energy) the radiation is absorbed and an electron is removed. For each electron energy level there is an absorption edge. It is this principle that is applied for selective elemental line excitation.

Whenever x-rays pass through a material there is always some loss of intensity by absorption. The degree of absorption of radiation of any wavelength by any element is expressed in terms of absorption coefficients. These coefficients are determined from the Lambert law,

$$I = I_o \exp(-\mu t) \qquad 2\text{-}6$$

which relates the incident radiation intensity (I_o) to the emergent radiation intensity (I) after passing through an absorber of thickness t centimeters. The linear absorption coefficient (μ) represents absorption per unit thickness and has units of reciprocal centimeters. Three other absorption coefficients are derived from the Lambert equation. The most important is the mass-absorption coefficient (μm)

which gives absorption per unit mass in units of square centimeters per gram,

$$\mu m = \mu/\rho \qquad 2\cdot7$$

where ρ is the density of the absorber in grams per cubic centimeter. This absorption coefficient is a function of only the wavelength of the radiation and the atomic number of the absorbing element. The other two coefficients, which are rarely used, are the atomic absorption coefficient (absorption per gram)

$$\mu a = \mu/N \qquad 2\cdot8$$

where N is the number of atoms per cubic centimeter and the molar absorption coefficient (absorption per mole)

$$\mu mol = \mu m \cdot A \qquad 2\cdot9$$

where A is the atomic weight in grams per mole.

The absorption coefficients show the loss of intensity when x-rays traverse a material. They are composite in nature representing the true photoelectric absorption, where the photon energy is transferred to an orbital electron, and a scattering process where the photons are dispersed from their path. The photoelectron absorption and x-ray

generation have been discussed (SECTION 2·1). The process of x-ray scattering can be coherent (Rayleigh scatter) where the x-ray photon collides with an electron and is deflected without loss of energy, or incoherent (Compton scatter) where the scattered photon has lost some of its energy to the electron.

Extensive treatment of the calculation of the x-ray mass-absorption coefficients has been carried out by Victoreen [5]. Very briefly, an equation was developed in a simplified format relating the mass-absorption coefficient (μ/ρ) to atomic parameters and the wavelength (λ) of the incident radfation.

$$\mu/\rho = C\lambda^3 - D\lambda^4 + \sigma_e N_o \frac{Z}{A} \qquad 2\cdot10$$

where Z is the atomic number, A is the atomic weight, N_o is Avagadro's number and σ_e is the electron scattering coefficient. The coefficients C and D are complex wavelength factors. The terms σ_e, C and D all represent very elaborate expressions of atomic energy states. The reader is referred to the original publication for any further details concerning the calculation of mass-absorption coefficients.

For complex materials (more than one element) a mass-absorption coefficient can be calculated for the compound. This is done by consideration of the individual element mass-absorption coefficients and their appropriate weighting factors.

$$\mu m \text{ (compound)} = \sum_i (\mu m_i \cdot X_i) \qquad 2.11$$

where μm (compound) is the mass-absorption coefficient of the compound which is the sum of the products of the individual mass-absorption coefficient (μm_i) and the weight fraction (X_i) of each element in the compound.

Recalling the discussion on the x-ray continuum, it was mentioned that a secondary-emission continuum could not occur. However, some continuous radiation is in fact observed in the secondary spectrum. This is attributed to the Compton (incoherent) scattering of the primary continuum.

The principle of Rayleigh (coherent) scattering is the basis of crystal dispersion, the backbone of x-ray spectrometric analysis. In XRF spectrometry all wavelengths of the secondary radiation are emitted simultaneously. The analyser crystal of the spectrometer disperses these x-rays in order, so that each wavelength may be examined separately.

A crystal is regarded as a number of planes of atoms. Incident radiation is scattered in all directions by each atom in the crystal lattice. Nevertheless, only in certain directions do these scattered x-rays undergo reinforcement to produce a diffracted beam. There are three conditions for diffraction to occur:

1) With reference to the plane of diffraction in the crystal, the angles of the incident and diffracted beams are equal;

2) the directions of the incident and diffracted beams, and the normal to the diffracting planes are coplanar;

3) radiation reinforcement occurs when the difference in path length is an integral number of wavelengths.

These conditions are summarized in the Bragg equation

$$n\lambda = 2d \sin\theta \qquad 2\text{-}12$$

where:

λ = the wavelength of the incident radiation

θ = the angle of incidence

d = the interplanar spacing of the crystal

n = the order of diffraction

2-3 INSTRUMENTATION

The chemical analysis by x-ray fluorescence spectrometry involves five basic processes. The first is the excitation of the characteristic x-ray spectrum of the sample. The second is the dispersion of the radiated sample beam which is determined by the arrangement of the goniometer. This includes the sample position, collimation, crystal(s) and goniometer geometry. The third process is the detection of the dispersed spectral radiation. Fourthly, the detected radiation is subjected to pulse height (energy) selection and

line intensities are recorded. The above four stages represent that portion of x-ray analysis that is directly related to the x-ray spectrometer. The fifth and final process involves data reduction and conversion from x-ray line intensities to analytical concentrations.

2.3.1 X-RAY EXCITATION

The first stage of the x-ray spectrometer involves the source of primary excitation. Originally, x-rays were generated by direct electron excitation. This method of excitation imposes many restrictions on the type of sample that may be examined. Since high vacuum conditions are required it is necessary for the sample to be solid and non-volatile. With the sample acting as an anode there exists a problem of poor conductivity and local heating. In general, present spectrometers utilize an x-ray tube as the sourse of primary excitation.

The x-ray tube, for conventional applications, is constructed of a filament (cathode) and a target (anode) inside a sealed evacuated tube. A tungsten filament is heated by a current to produce a high electron density and electron emission. The intensity of emission being directly proportional to the applied current. These electrons are accelerated by a large potential difference between the filament and the anode. The target for the high energy electron beam is constructed of a layer of pure element against a copper background. When the high energy electrons strike the anode, a large amount of heat is given off.

Only about one percent of the applied power is transferred to useful characteristic x-ray radiation. For this reason the target material is mounted on or incorporated in a copper base that is water cooled to dissipate the heat being evolved. Without this, the target would have a very short life. For practical purposes, common x-ray tubes for x-ray fluorescence spectrometry are made with refractory target materials such as chromium, molybdenum or tungsten. Platinum may also be used in some circumstances. For x-ray diffraction spectrometry it is not necessary to have as much power. Hence the selection of diffraction tubes include target materials of iron, cobalt, nickel, copper and silver. The generated x-rays pass through a window, usually beryllium, that is situated in the side of the tube head. For some spectrometers an end window x-ray tube is required.

For special applications there are other types of x-ray tubes. The dual target x-ray tube is constructed similarly as the standard tube with the exception that the target surface is composed of two separate target elements. Focusing of the electron beam by an external control selects which target is used. With the appropriate choice of target materials there would be no need to change tubes. Usually the two elements used are chromium and tungsten.

In cases where very special excitation conditions are required, such as examination of ultra-soft radiation, a demountable x-ray tube may be selected. With this type of tube (easy target replacement) there is no restriction as to the type of target material. Also, higher power

may be used since target life is not important. Continuous evacuation of the tube permits removal of the window material. With this, the sample may be placed close to the target giving much better excitation. The sample may even be used as the target. Finally, there is the Henke tube [6] which is specially designed for wavelengths greater than 15 angstroms.

2-3-2 SPECTROGONIOMETER

Most spectrometers are designed with the sample positioned such that it is irradiated by the primary x-ray beam either from below (inverted optics) or from above (normal optics). A spectrometer with inverted optics requires, for analysis of loose powders or liquids, that the sample holder have a Mylar (polyethylene terephthalate) window. This is highly undesirable, due to radiation absorption, if long wavelengths are to be examined. For such analyses the use of a normal optics spectrometer is advantageous.

The angle of incidence of the primary radiation may be either 60 degrees or 45 degrees for standard spectrometers. There is, of course, no restriction that only these angles may be used. For the special simultaneous spectrometers the incident angle is 90 degrees. With this arrangement the complete sample is evenly irradiated. However, in most other spectrometers the sample holder is designed to rotate

allowing uniform sample irradiation. The 45 degree arrangement has the advantage of simplifying the post-data collection calculations. As an example, consideration of the depth of penetration requires inclusion of a spectrometer geometry factor which is the ratio of the sine of the incident angle to the sine of the take-off angle. For a 45 degree geometry this factor is 1, while for a 60 degree geometry this factor is the square root of three.

The goniometer is basically a system of slits or collimators and a monochromator or analyser crystal. The most common spectrometer arrangement invokes the principle of reflection from a single flat crystal. Other modifications include reflection from a single curved crystal, transmission through a curved crystal and double flat-crystal reflection.

In x-ray analysis it is desirable to have a colinear radiation beam. However, sample excitation causes x-rays to be radiated in all directions. Slits or multiple slit (Soller) collimators are normally used to restrict the divergence of the x-rays. In general, these devices do not restrict radiation that is parallel to the crystal axis. To achieve this a multiple tube collimator is required.

The analyser crystal is the basis of x-ray analysis, serving the purpose of separating the sample radiation beam into its individual wavelength components. This process (diffraction) has been described in Section 2.2. There is a wide selection of materials for analyser

crystals [4] some of which are shown in TABLE 2·1.

Four main geometric arrangements of the spectrometer are described [7] as shown in FIGURES 2·1 - 2·4 representing the four main methods of analysis. The most popular of these, because of its simplicity is the single flat-crystal reflection method (FIGURE 2·1). This arrangement involves a source collimator, the analyser crystal and a detector collimator. As the crystal rotates through an angle "theta" (θ) the detector moves through an angle 2 "theta" (2θ) intercepting the diffracted radiation. The wavelength of the radiation is determined by the Bragg equation (EQUATION 2·12). The intensity and resolution are dependent on the degree of collimation and the type of analyser crystal.

The second method (FIGURE 2·2) involves reflection from a curved crystal. As in the previous method the crystal and detector are rotated through angles of θ and 2θ respectively. A slit is used in place of the source collimator which must lie on a focusing circle governed by the equation

$$\ell = \frac{n\lambda}{d} \cdot \frac{R}{2} = R \sin\theta \qquad 2\cdot13$$

where ℓ is the distance between the slit and the crystal axis and R is the diameter of the focal circle which is the radius of curvature of the crystal. The advantage of this method is that exceptionally high intensities are obtainable. Unfortunately, to cover a large wavelength range, several crystals of different curvature are required.

TABLE 2-1

COMMON ANALYSER CRYSTALS

CRYSTAL NAME	CHEMICAL FORMULA OR SYMBOL	CRYSTAL SPACING 2d (A)	USEFUL WAVELENGTH REGION (A)
QUARTZ	SiO_2	1.624	0.142 - 1.55 (hard)
LITHIUM FLUORIDE	LiF(200)	4.028	0.351 - 3.84 (medium)
PENTAERYTHRITOL	PET	8.742	0.762 - 8.34 (soft)
POTASSIUM HYDROGEN PHTHALATE	KHP	26.63	2.32 - 25.40 (very soft)
LEAD STEARATE	PbSt	100.4	8.75 - 95.75 (ultra soft)

FIGURE 2-1

XRF spectrometer geometric arrangement for analysis by the single flat-crystal reflection method.

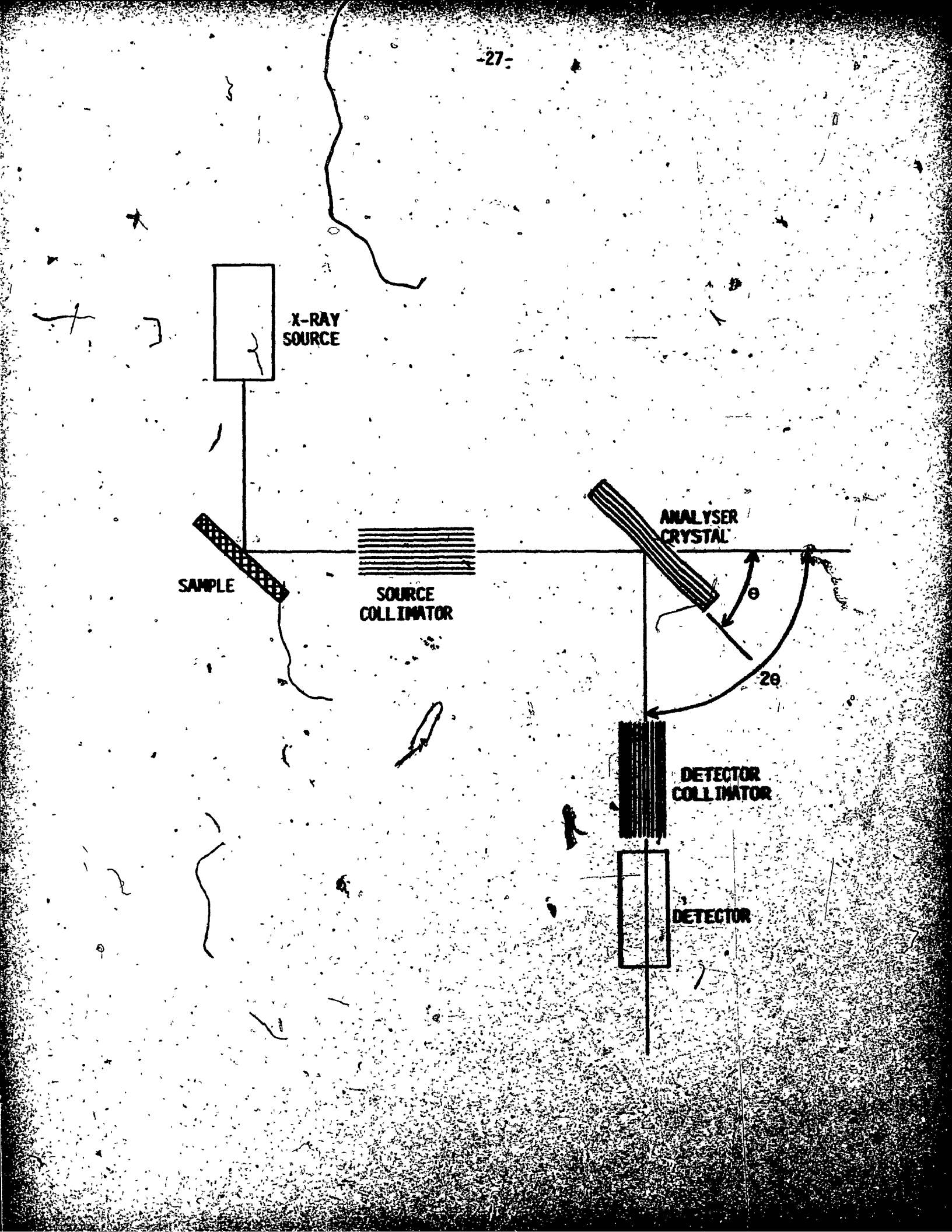
X-RAY
SOURCE
SAMPLE
SOURCE
COLLIMATOR
ANALYSER
CRYSTAL
θ
2θ
DETECTOR
COLLIMATOR
DETECTOR

FIGURE 2·2

XRF spectrometer geometric arrangement for analysis by the curved crystal reflection method.

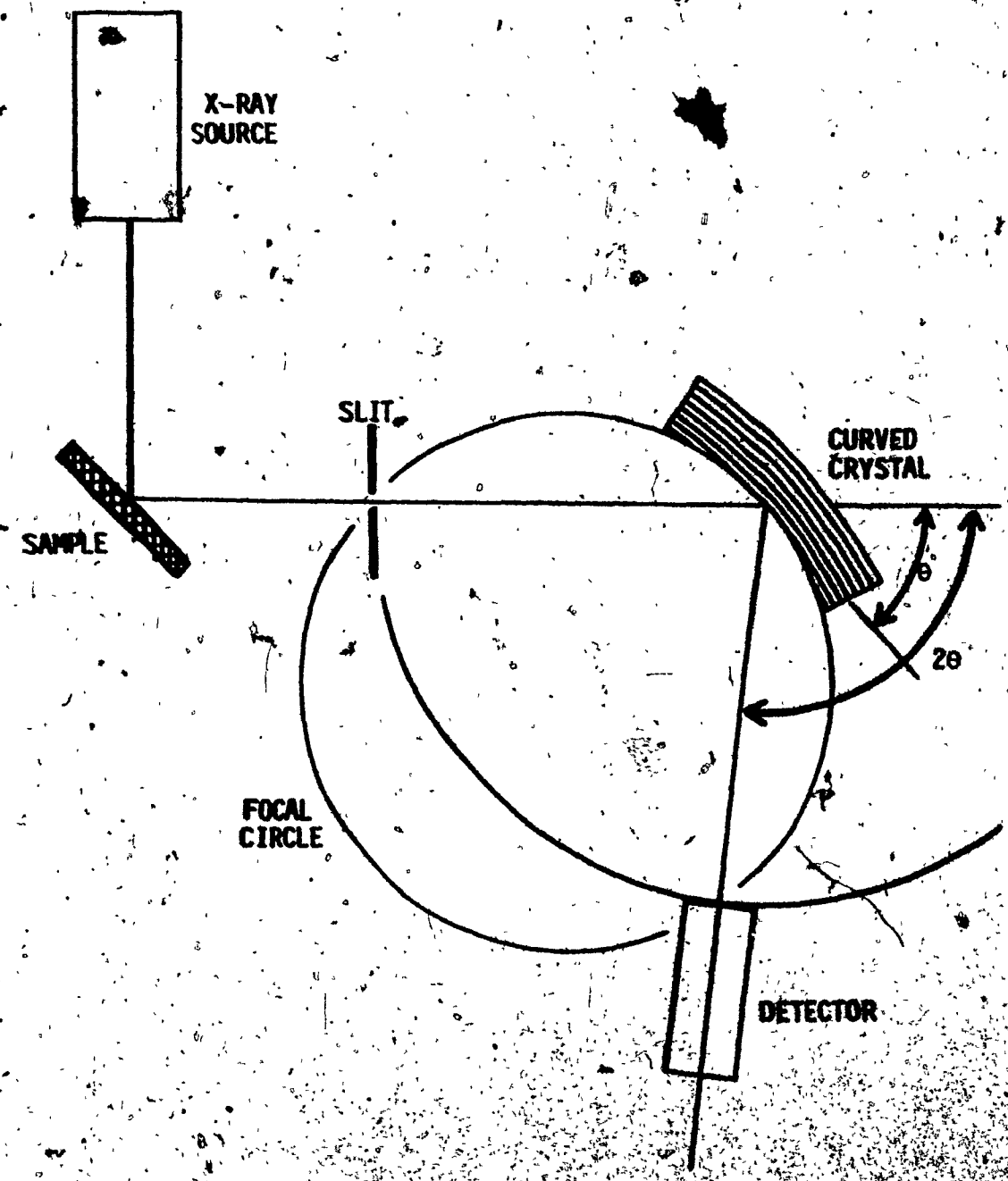
X-RAY
SOURCE
SLIT
CURVED
CRYSTAL
SAMPLE
θ
2θ
FOCAL
CIRCLE
DETECTOR

In the third method (FIGURE 2·3) the sample beam is transmitted through a curved crystal made of a thin slab of mica. There is no source slit or collimator. The radiation is diffracted by crystal planes which are normal to the crystal surface. The crystal is bent to a radius equal to the diameter of the focal circle. Wavelengths which satisfy the Bragg equation are focused at the detector slit. Although the intensity of the transmitted radiation is rather low, only the one crystal is required for the analysis of the complete spectral range.

The method of double crystal reflection (FIGURE 2·4) requires no slits or collimators. Sample radiation is diffracted from the first crystal onto the second crystal where only those wavelengths satisfying the Bragg equation are diffracted to the detector. Only a fraction of the sample wavelengths are allowed to fall on the second crystal for any particular setting of the first crystal. It is necessary to rotate and translate the first crystal to cover the complete wavelength range. This method gives good resolution but a substantial loss of intensity as compared to single crystal reflection with collimation.

The effective range of the spectrometer (single flat-crystal reflection) is determined by the type and size of the analyser crystal and the width of the source collimator. The maximum wavelength limit, ideally, is equal to the 2d spacing of the crystal. This is equivalent to a 2θ angle of 180 degrees which is physically impossible since the detector would have to be in the same axis as the radiation source. The maximum limit is thus determined by the construction of the goniometer

FIGURE 2-3

XRF spectrometer geometric arrangement for analysis by the curved crystal transmission method.

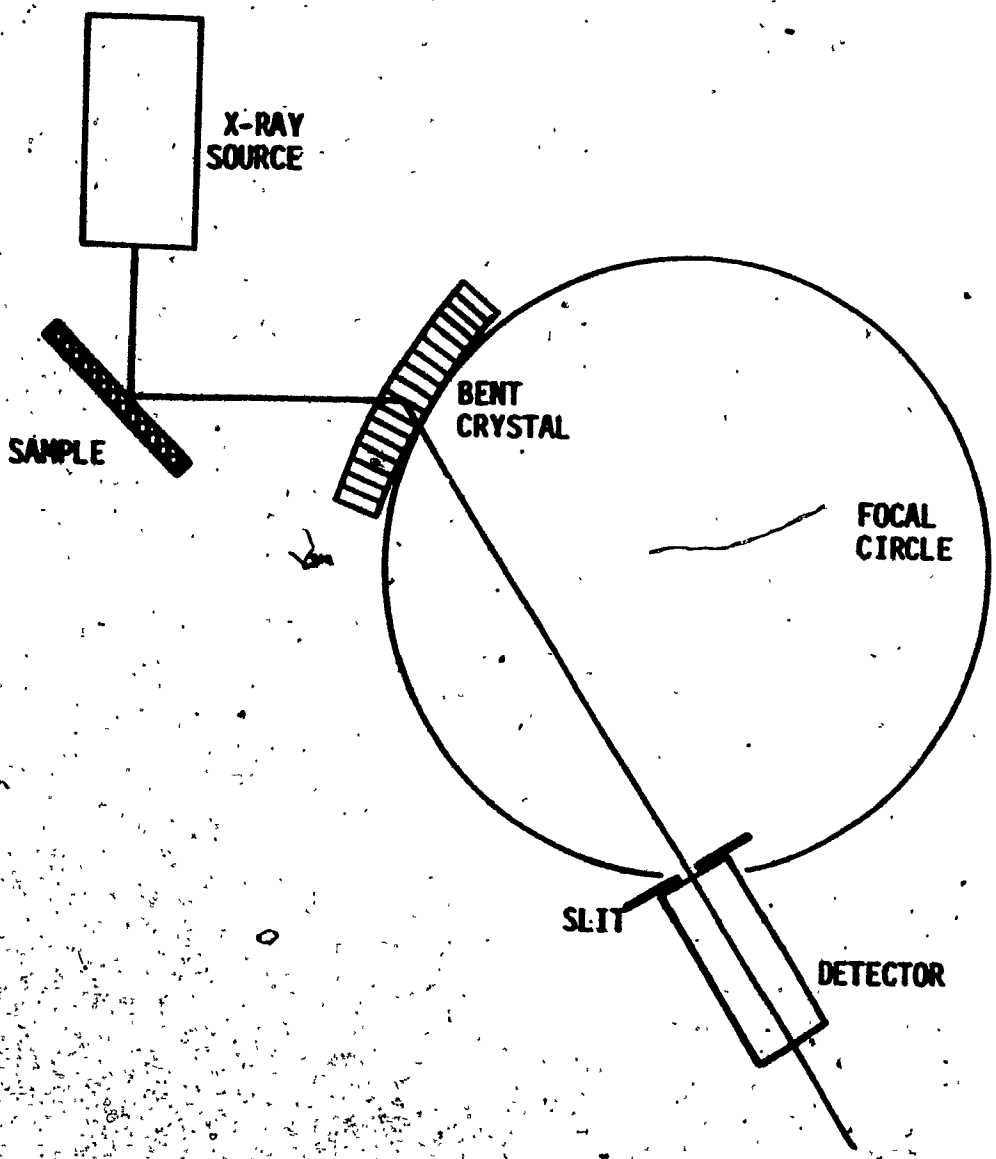
X-RAY
SOURCE
SAMPLE
BENT
CRYSTAL
FOCAL
CIRCLE
SLIT
DETECTOR

FIGURE 2-4

XRF spectrometer geometric arrangement for analysis by the double flat-crystal reflection method.

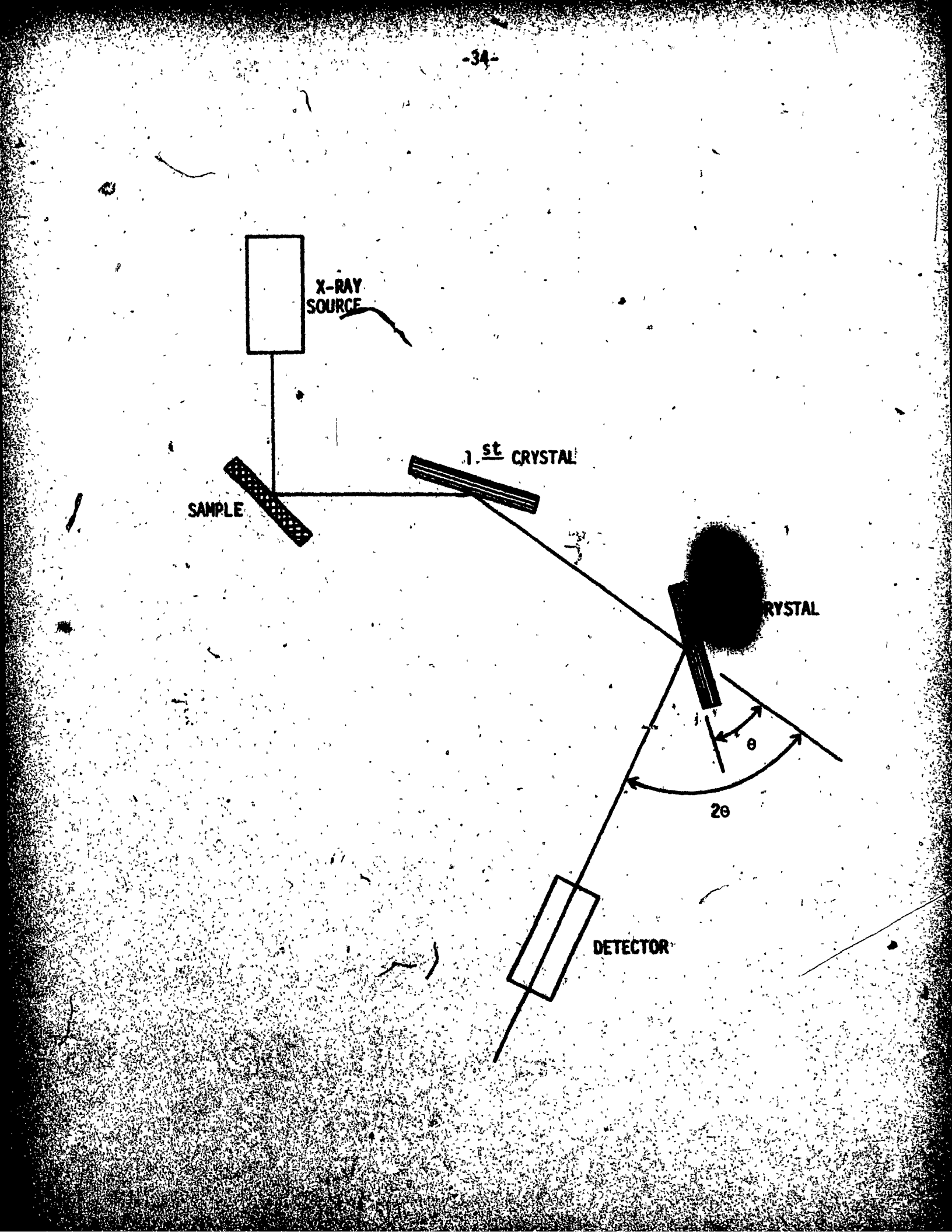
X-RAY
SOURCE
1. st CRYSTAL
SAMPLE
RYSTAL
θ
2θ
DETECTOR

where the detector arm comes in contact with the sample chamber or the x-ray tube. For most spectrometers this means a 2θ angle of about 145 degrees. The minimum effective wavelength limit is determined by the minimum angle at which the complete collimated sample beam falls on the analyser crystal. The average crystal of about 3 inches long, with a collimator 0.5 inches wide, would result in a minimum 2θ angle of about 20 degrees. For smaller angles some of the sample beam passes the crystal and hence is not diffracted to the detector. Radiation is still detected but with a decreased intensity. At very small angles some of the primary radiation enters the detector. The practical minimum 2θ angle is determined to be about 10 degrees.

2-3-3 DETECTION

Essentially there are three types of x-ray detectors. For qualitative work the photographic plate is quite adequate but this technique is not well suited to quantitative determinations. Electronic devices such as scintillation detectors and gas-filled detectors are normally used in XRF spectrometry. The basic principle behind x-ray detection is the conversion of the high energy radiation to a form of lower energy that may be detected by conventional equipment.

The scintillator crystal or phosphor of a scintillation detector converts x-rays to light photons. The x-rays promote valence

electrons to higher energy states and light, visible and ultraviolet, is emitted when the electrons return to the normal state. The crystal is fixed to a standard photomultiplier tube which converts the light photons to electrical pulses.

The scintillator material must have a high enough absorption coefficient to absorb most or all of the incident x-rays. It must have a high light photon output relative to the x-ray photon energy. The emitted light photons must be transmitted through the material without absorption and their energy must match the spectral sensitivity of the photocathode in the photomultiplier tube. Also, the response time of the electron transition must be small enough to allow sufficiently high counting rates. For x-ray spectrometry the scintillator material is thallium-activated sodium iodide which adequately displays the above requirements.

In the photomultiplier tube the light photons strike a photocathode which generates photoelectrons. These photoelectrons are attracted to the first of a series of dynodes causing emission of two to four electrons. Each of these electrons are attracted to the second dynode, which is at a slightly higher potential, causing emission of an additional two to four electrons. The tube contains many of these dynodes (9 - 14) resulting in a large electronic gain of each light photon incident on the tube.

There is a proportional relationship between incident x-ray

energy and the output electrical pulse of the scintillation detector. An assumption is made that the light photons being generated in the scintillator crystal are all of equivalent energy. If all the x-ray energy is converted into light photons it is expected that the number of light photons produced is equal to the energy of the x-rays divided by the energy of the light photons. Thus the higher the x-ray energy the more light photons will be produced and the larger the voltage pulse being generated by the photomultiplier tube.

The gas-filled detector is constructed of a cylindrical cathode, an axial thin-wire anode, a gas filling and has either an end or side window. There are several types of gas-filled detectors which are distinguished from each other by the applied voltage, the window material, the type of gas filling and whether the gas chamber is sealed or permits gas flow.

In x-ray spectrometry a detector is only useful if the output signal is directly proportional to the energy of the incident radiation. At low and high applied potential the gas-filled detectors do not operate proportionately and for simplicity these detectors will not be discussed. The sealed proportional counter has limited use since its detectable wavelength range is about the same as the scintillation counter. Also, the gas filling must be replaced periodically. The most widely used gas-filled detector is the gas-flow proportional counter.

The operation of these detectors is basically the same. The

gas filling provides the energy conversion from x-ray photons to electrical charge through the process of ionization. The gas is usually a noble gas (He, Ne, Ar, Kr, Xe) which is mixed with a low percentage of some organic vapour (CO_2, CH_4, C_2H_6, etc.) acting as a quench gas to terminate the ionization. The most common gas filling is "P10" which is 90% argon and 10% methane. For ultra-soft radiation, mixtures of neon or helium with a quench gas may be used.

The process of gas ionization by high energy electrons or x-ray photons is a common phenomenon. However, under normal circumstances, the ion pair will quickly recombine. The measurement of the degree of ionization requires that the two separate ions be separated and kept apart. This is performed by applying a large potential difference across the ionization chamber. The electron moves to the anode and the positive ion moves to the cathode. At low potentials there is one electron collected at the anode for each electron formed by the ionization. This means the gas amplification factor is one. If the applied potential is high enough the electrons will accelerate and upon collision with other gas molecules will cause further ionization. The electrons so produced will similarly cause further ionization. This process of one electron initiating the formation of thousands of other electrons is called Townsend avalanching. Depending on the detector voltage, the gas amplification factor in the proportional region can vary from 10^2 to 10^5. At very high potentials (Geiger-counter region) avalanching is so extensive that one x-ray photon causes complete ionization within the gas

volume and all proportionality disappears.

For the detector to generate an output pulse that is proportional to the incident x-ray energy, all the electrons formed by the ionization and avalanching must reach the anode wire before the positive ions are neutralized at the cathode. The purpose of the quench gas is to terminate the ionization by undergoing permanent decomposition by supplying electrons to the positive ions. By this process the relatively immobile positive gas ions are replaced by even more immobile positive molecules. A positively charged envelope is formed around the anode. This shielding effectively reduces the potential between the anode and cathode thus preventing generalized avalanching and complete discharge of the counter.

As with the scintillation counter, the gas proportional flow counter produces output pulses in direct proportion to the energy of the x-ray photon. The number of ion pairs produced is directly related to the photon energy and is equal to the energy of the x-ray divided by the effective ionization potential of the detector gas. For a particular applied potential the number of electrons reaching the anode is proportional to the number of ion pairs. Thus pulse height voltage is representative of the incident x-ray energy.

Under normal operating conditions the number of voltage pulses produced by the detector varies as the intensity of the incident x-rays. However, at high count rates the linear relationship does not hold. The recovery time of a detector is the time required, after an initial pulse,

to produce a second pulse of similar pulse height. If the period between incident photons is smaller than the recovery time, the detector may generate an output pulse but it will be shifted to a lower pulse height energy. Considering more intense radiation, a point is reached when the photon frequency causes too small a pulse height to be counted. This time is known as the resolving time and is sometimes referred to as the detector dead time. The true dead time is the period after an initial photon, in which the detector has no response to a second photon. The small (uncounted) output pulses, in effect, extend the resolving time of the detector. As the incident x-ray intensity is increased there occurs a greater number of these small (uncounted) output pulses. This results in a choking effect where the measured intensity decreases with increasing incident intensity.

Compensation may be made for the effect of intensity loss with high count rate. First the detector resolving time is empirically determined using the following relationship

$$I_t = \frac{I_m}{1 - I_m T} \qquad 2\text{-}14$$

where I_t is the true intensity, I_m is the measured intensity and T is the resolving time of the detector. Using this same expression the true intensity may be calculated for the high count rates. Another approach to the problem is to determine at what count rate the detector begins to deviate from linearity. If all count rates are kept below this value

then there would be no significant loss in the observed intensities.

For the scintillation counter (SC), which has a dead time of about 0.1 μsec, a one percent intensity deviation occurs at about 100,000 counts per second. The proportional flow counter (PFC) has a dead time about twice that of the SC thus giving the same intensity deviation at one half the counting rate.

The resolution of a detector is determined by the width of its pulse height distribution at half of the peak maximum relative to the average pulse height. Normally this property of a detector is determined experimentally and it may be energy dependent. In general, the resolution of the PFC is about 15 percent while that of the SC is about three to four times larger.

All detectors do not have the same efficiency for all wavelengths of incident x-ray photons. The SC is useful for the hard radiation (wavelength range 0.1 - 4 Å) while the PFC can be used for soft radiation (wavelength range 1 - 10 Å). A combination of these two detectors, the double window PFC fixed in front of the SC, provides good efficiency for most normal applications of XRF spectrometry. As in the case of x-ray tubes, special detectors must be used for ultra-soft radiation.

2-3-4 PULSE HEIGHT SELECTION

The pulse height produced by the detector relates to the energy of the x-rays. However, there may be x-rays of several different wavelengths incident on the detector at any one time. For example, a second order diffraction line of wavelength 2Å will appear at the same 2θ angle as a first order diffraction line of wavelength 4Å. Other wavelengths may arise from secondary x-ray emission of the radiation path atmosphere, the analyser crystal, the detector gas (for the PFC) or the scintillator crystal (for the SC). This multiple line overlap cannot be allowed to exist if quantitative results are to be obtained. Isolation of the detector pulses of similar amplitude may be achieved by pulse height selection. This involves the imposition of upper and lower pulse height or energy limits (pulse height window) such that x-ray wavelengths incident on the detector that fall above or below these limits would not be counted.

The main components of a pulse height analyser include a gain selector, a mode selector, a lower level helipot and an upper level helipot. Some spectrometers have the option of an automatic lower level scan selector which is used to display the pulse height distribution.

The function of the gain control is to attenuate the electronic pulses coming from the detector before they enter the linear amplifier. Attenuation of the detector output signal essentially allows higher energy x-rays to be counted. If the pulse height window were set to

accept all pulses equivalent to an x-ray energy between 2 and 4 keV at a gain setting of 10; then for the same helipot settings at gain 2 the energy accepted would be between 10 and 20 keV. The actual helipot scale is floating and must be calibrated to any energy scale. The procedure of calibration involves the use of a monochromatic radiation source such as Fe55 placed in front of the detector. The pulse height window is set about the energy of this radiation with a width of 0.2 keV. For Fe55 (5.9 keV) the lower level helipot is set at 5.8 and the upper level helipot is set at 6.0. The detector high voltage is then adjusted to give a maximum count rate. The analyser helipot readings should now read directly in keV values. The upper and lower energy discrimination levels for pulse height analysis of any line may be set according to the energy of the x-rays.

There are three modes of the pulse height analyser which determine the relationship between the upper and lower level helipot settings. Data collection by the integral mode allows counting of all pulses having a height greater than the lower level. This mode is only used when there seems to be no need for a particular pulse height selection. The lower level is simply set to exclude any background noise pulses. For the 100 percent mode both the upper and lower levels are set to specific values and all energies between these levels are counted. This is the normal mode for pulse height selection. The window mode relates the upper level directly to the lower level. Setting of the upper level helipot determines the width (ΔE) of the pulse height selection which may be above the lower level (E_L) [i.e. $E_L + \Delta E$] or

centralize about the lower level [i.e. $E_L \pm {}^1/_2\Delta E$]. The window mode is used mainly to determine pulse height distributions but it is also useful if a standard pulse height width is desired for the examination of a number of different spectral lines.

Many x-ray spectrometer models only have a single channel pulse height analyser. The discriminator settings must be reset for each analytical line under investigation. The simultaneous spectrometers require many separate pulse height analyser channels, one for each wavelength being detected. The automatic spectrometer [8] employs automatic pulse height selection. This is achieved by causing all pulses, through selective amplification, to fall within a preset fixed upper and lower level pulse height setting. The degree of pulse amplification is electronically controlled according to the spectrometer diffraction angle. Alternatively, the pulse height window may be shifted in proportion to the spectrometer diffraction angle. The analyser is operated in the window mode and the lower level is automatically controlled to correspond to the detected radiation energy.

2.4 SELECTION OF OPERATING CONDITIONS

The first step in chemical analysis by XRF spectrometry is the determination of the numerous instrumental parameters. Appropriate conditions are selected, given the various elements that are to be investigated together with any restrictions that are to be imposed for

a particular analytical problem. The following gives just a brief outline of the steps and considerations that must be performed in order to set up the spectrometer to collect spectral line intensity data. Each of the points mentioned are discussed in detail in SECTION 3·4 as they apply to the particular problem of the analysis of bauxite ore.

The primary consideration involves the various spectral line energies of absorption and emission and the efficiency of excitation through the choice of x-ray tube and generator (kV, mA) settings. Next the propagation and dispersion of the secondary-emission x-ray spectrum must be evaluated. The necessity of a special atmosphere throughout the radiation path is dependent on the energy and absorption characteristics of the wavelength being determined. Selection of the analyser crystal and the degree of collimation depends on the spectral line energy and intensity as well as any restriction on the resolution required. For each element the goniometer settings must be selected according to the choice of analyser crystal and radiation energy. The detection method and pulse height selection are chosen for each x-ray wavelength. This is simply done by determining the pulse height distribution using the appropriate detector and selecting the desired pulse height discrimination limits. Finally, there is a choice of collecting the data with reference to a fixed count or a fixed time. For minimum counting error and better precision where data acquisition time is not too important, the fixed count method may be selected. If analysis time is critical and some precision may be sacrificed, the fixed time method is usually preferred.

2-5 EFFECTS OF THE SAMPLE ON XRF SPECTRAL INTENSITIES

The accuracy of XRF spectrochemical analysis is dependent on the physical and compositional make-up of the sample under investigation. Intensity variations caused by the sample must first be identified as to their origin. Subsequently, steps must be taken to either eliminate or make negligible such effects. Through special sample preparation methods and empirically or theoretically derived correction procedures, attempts may be made toward this end.

Of primary consideration are the physical effects of surface roughness and particle size. Directly connected with these is the effect of a heterogeneous sample. Naturally, these three problems are only significant when powder analysis is concerned. Solids (alloys) or solid solutions (fused samples) are homogenous and non-particulate. Only the surface finish need be considered in the preparation of the sample.

The compositional effects are two fold in nature. Of minor importance is the shift of the characteristic spectral line energy with variation of the chemical state of the atoms being examined. Finally, and most significantly, are the effects of radiation absorption or enhancement by elemental interaction (matrix effects) that are prevalent in all specimens.

2-5-1 SURFACE ROUGHNESS, PARTICLE SIZE AND HETEROGENEITY EFFECTS

The excitation and emission of secondary x-ray spectra is a surface phenomenon. The depth being dependent on the energy of the excitation source and the absorption properties of the sample. Under normal analysis conditions, the average depth of penetration of the primary and secondary x-rays is less than 100 microns. However, for long wavelength radiation (e.g. Al Kα) the penetration depth is reduced to less than 20 microns. Obviously, any surface irregularities may cause significant interference with the spectral line intensities.

A considerable amount of work has been done by other authors with respect to the identification and characterization of surface roughness and particle size effects with and without a homogeneous sample. Most notably are the papers by F. Claisse[9-12], F. Claisse and C. Samson[13], E.L. Gunn[14] and K.W. Madlem[15]. It has been established that at a very small grain size (<1μ) or at a large grain size (>1000μ) there is no dependence of x-ray intensity on grain size. There is, however, a significant decrease in the total x-ray intensity for the large particles. Between the two limits, the normal region of particle size, there is severe x-ray intensity variation with grain size. The subsequent discussion is an attempt to explain the existence of the physical effects within a sample.

Consider first the pure particle size effect which is not to be confused with the particle size effect associated with a heterogeneous sample. In this case, all particles are of the same uniform composition. If there is a variation in particle size throughout the sample, the particle size effect is effectively reduced or eliminated. The smaller particles will fill in the spaces between the larger particles forming, essentially, a solid sample with a flat surface. As shown in FIGURE 2-5 (A), the detected x-rays will originate from the complete sample surface.

As the diameter of the particles becomes larger than the penetration depth there is a loss of x-ray intensity. Only part of the surface area produces x-rays that actually reach the detector. FIGURE 2-5 (B) represents a sample surface where the x-ray penetration depth is approximately one quarter of the particle size. It may be seen that the area irradiated by the primary x-rays is not the same area from which x-rays may be detected. As a result, by comparison to a flat sample (FIGURE 2-5 (A)), the area from which x-rays actually are detected is considerably smaller when the sample is comprised of large particles.

Samples that are mixtures of elements or compounds require a slightly more sophisticated treatment when considering particle size effects. Heterogeneity effects come into play when all the particles do not have the same composition. For this situation, absorption properties must be considered. Basically, the effects of

FIGURE 2·5

Area of effective x-ray excitation for :-

(A) a homogeneous sample in which the particle size is much less than the penetration depth of the primary x-ray beam;

(B) a homogeneous sample in which the particle size is about four times the penetration depth of the primary x-ray beam.

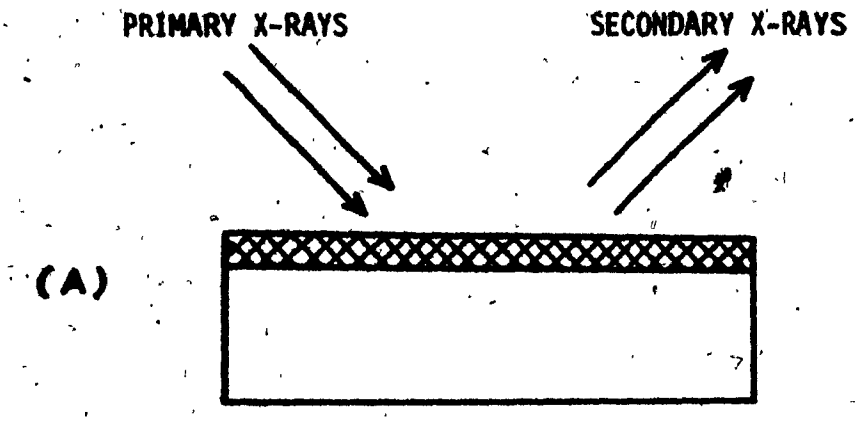
PRIMARY X-RAYS
SECONDARY X-RAYS
(A)

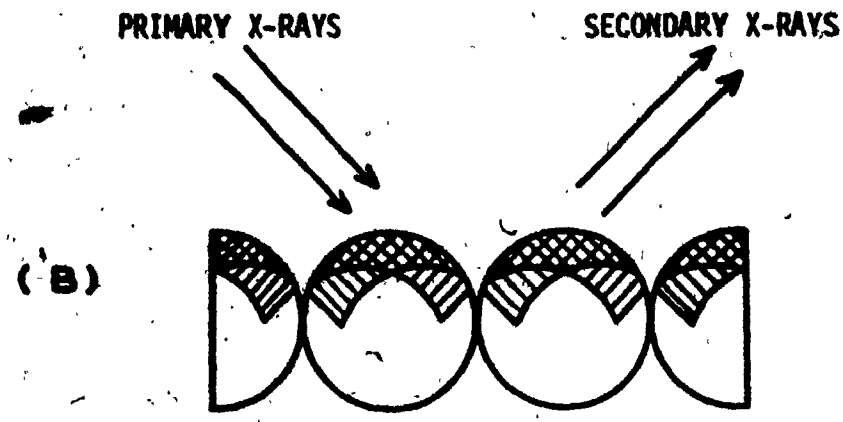
PRIMARY X-RAYS
SECONDARY X-RAYS
(B)

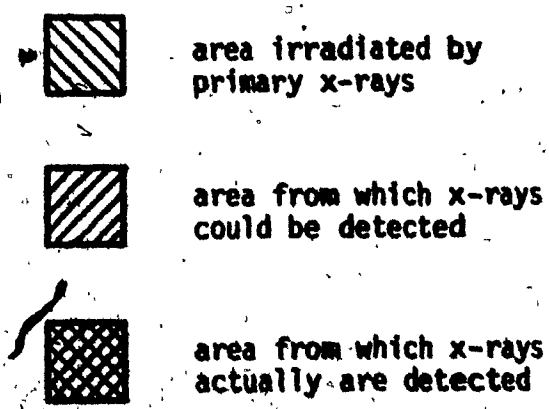
area irradiated by primary x-rays
area from which x-rays could be detected
area from which x-rays actually are detected

heterogeneity are simply a combination of matrix (interelement) effects and particle size effects.

A diagramatic representation is shown in FIGURE 2·6 of a sample containing two compounds of equal proportion. For this illustration, the x-ray intensities for elements X and Y are being examined. The element X occurs only in the cross-hatched particles (X-particles) while the element Y occurs only in the other particles (Y-particles). The compounds are (A) in the form of fine (uniform size) powders, homogeneously dispersed; (B) in the form of coarse (uniform size) powders, homogeneously dispersed; (C) in the form where one compound has a larger grain size than the other compound. For all three cases the relative x-ray intensities and the nature of the sample effect depends on the difference in the absorption properties of the two kinds of particles.

Firstly, consider that the X-particle absorbs radiation similarly as the Y-particle. Assume that each small particle is equivalent to 2 "absorption units" and the effective penetration depth is equal to 4 "absorption units". Therefore, the top two rows of small particles are involved in x-ray production. For FIGURES 2·6 (A) and 2·6 (B) where the grains (groups of small particles) are of uniform size, an equivalent number of small particles (8) for both X and Y contribute to the total x-ray intensity. When the respective sizes of the grains are different (FIGURE 2·6 (C)) there is a larger proportion of the smaller particles (6 X-particles compared to 10 Y-particles) that contribute to the total x-ray intensity.

FIGURE 2·6

Representation of the surface of a sample containing a mixture of two components in equal proportion where :-

(A) both components are fine grains that are dispersed homogeneously;

(B) both components are coarse grains that are dispersed homogeneously;

(C) the two components are of different grain size.

(A) HOMOGENEOUS SAMPLE — 1 particle per grain (X & Y)

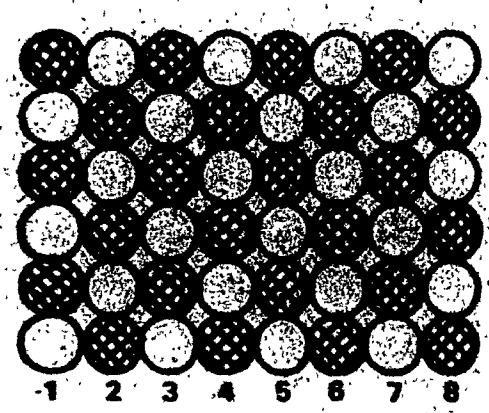

(B) HOMOGENEOUS SAMPLE — 4 particles per grain (X & Y)

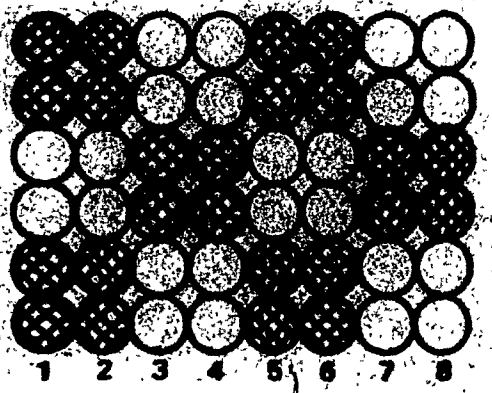

(C) HETEROGENEOUS SAMPLE — 24 X-particles per grain (X)
1 Y-particle per grain (Y)

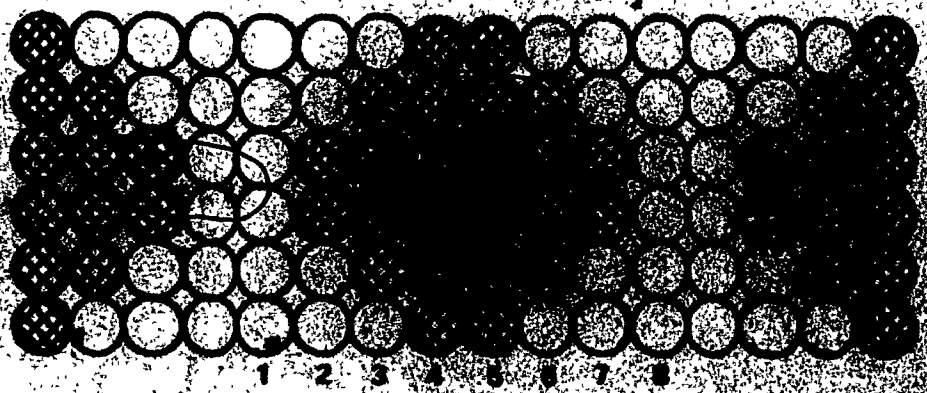

Now consider the more practical situation where the two particles have different absorption properties. While keeping the effective penetration depth equal to 4 "absorption units" assume that the radiation penetrates through twice as many Y-particles as X-particles. That is, the X-particle is equivalent to the 2 "absorption units" as before but the Y-particle is now equivalent to just 1 "absorption unit". The three situations (A),(B) and (C), described by FIGURE 2.6, are represented in TABLE 2.2 showing the different proportions of the X-particles and Y-particles that contribute to the total x-ray intensity.

As the grains become larger, there is less shielding of the heavy absorber X-particles deeper within the sample but more shielding of the light absorber Y-particles. Hence, there appears to be more X-particles than Y-particles. With a difference in grain size between the two absorbing substances the resultant x-ray intensity ratio will change in favour of the smaller particles. What must also be kept in mind, due to the shielding effect, is that the heterogeneous particle size effect is variable depending on whether the larger particle is the heavy or the light absorber. The intensity loss is much greater for the large particle if it is the light absorber.

It is easily seen from the above argument that homogeneity, both compositional and particle size, is a necessity for accurate XRF spectrochemical analysis. Attempts to correct for or eliminate these sample effects have, so far, required an alteration of the sample. Most desirable, since it retains the sample composition,

TABLE 2-2

PARTICLE EXCITATION SHOWING HETEROGENEITY EFFECTS

SAMPLE	A		B		C	
TYPE OF PARTICLE	X	Y	X	Y	X	Y
NUMBER OF EXCITED PARTICLES						
column 1	1.5	1	2	0	0	4
column 2	1	2	2	0	1	2
column 3	1.5	1	1	2	1.5	1
column 4	1	2	1	2	2	0
column 5	1.5	1	2	0	2	0
column 6	1	2	2	0	1.5	1
column 7	1.5	1	1	2	1	2
column 8	1	2	1	2	0	4
TOTAL EXCITED PARTICLES	10	12	12	8	9	14

is the reduction of the particle size by excessive grinding toward the ideal <5μ size. In the past this was not practical and workers resorted to other methods. Such procedures include adding an internal standard to the sample[16], dilution of the sample by a heavy or a light matrix[12] and forming a solid solution by fusion[9,11,15]. Little or no work was attempted in the analysis of coarse (50-100μ) particulate material. Now suitable rapid grinding techniques and equipment are available which facilitate accurate XRF analysis without particle size effects.

2-5-2 EFFECT OF CHEMICAL STATE

The energy and intensity of secondary-emission radiation that is produced by an element is, in general, dependent on the atomic number and concentration of that element. This statement, although quite valid, is only applicable to cursory investigations of x-ray spectra. As discussed in the previous section, the detected x-ray intensity is affected considerably by particle size, grain size and heterogeneity. For detailed spectral analysis a less significant but very important factor comes into play. The different chemical states of the elements cause variations in the energy and intensity of the x-ray spectral lines.

The effect of chemical state is two fold in nature. The properties of atomic oxidation state and chemical combination state

both influence the x-ray absorption and emission of the elements. As mentioned previously, the phenomena of x-ray absorption and emission involve the transference of energy and electrons within the atomic electron shells. Consequently, any alteration of electron configuration is expected to cause variations in the x-ray spectra.

Now, a change of oxidation state rearranges the electron shells in different energy states. Also, changes in the state of chemical combination is associated with the degree of atomic crowding.

The following two points may be noted. Firstly, the characteristics of x-ray lines resulting from outer electron transitions would be affected most prominently by chemical state variations. Secondly, the effects of chemical state would be more pronounced for low atomic number elements where there are fewer electron shells and consequently the valence (outer) electrons are nearer to the atomic nucleus.

Early workers, Siegbahn and Magnusson[17] examined the series spectra of aluminum. Aluminum metal displayed a single broad band with a sharp limit on the short wavelength side. This shape, characteristic of metals, was attributed to transitions from the levels of the conduction electrons. For aluminum oxide (Al_2O_3) two separate peaks were observed at 184.0 Å and 198.6 Å. Examination of the K spectra of Al and Al_2O_3, Siegbahn and Karlsson[18], produced similar results.

Later, Siegbahn and Magnusson[19] showed that the silicon L spectrum contained two peaks for both Si and SiO_2. However, the wavelengths were 134.3 Å and 138.2 Å for Si as opposed to 130.7 Å and 139.5 Å respectively for SiO_2. Complementing this work, Koffman and Moll[20] showed that there was a significant wavelength shift of the Si Kα lines in the x-ray spectra of various silicates as compared to the x-ray spectrum of silicon metal.

Zemany[21] went on step further and specifically examined the x-ray spectra of different valence states of sulphur and manganese. It was pointed out that the wavelength shifts due to chemical oxidation state are relatively small but significant intensity errors may be introduced. For example, consider that the goniometer setting for the S Kα peak maximum had been determined using sodium sulphide ($Na_2S \cdot 9H_2O$)(-2 oxidation state). This same angle if used to examine sodium sulphate (Na_2SO_4)(+6 oxidation state) introduces a 15% intensity loss as a result of the S Kα line being measured away from the peak maximum.

In an attempt to calculate x-ray spectral intensities, Claisse and Samson[13] showed that the fluorescent yield of an element was dependent on the chemical composition of the compound containing that element. They determined a direct relationship between interatomic distance and the fluorescent yield.

Along similar lines, Fisher and Baun[22] established that the

effects of electronic structure and interatomic bonding can be correlated according to the groups of the periodic table.

2·5·3 EFFECTS OF ELEMENTAL INTERACTION (MATRIX EFFECTS)

Quantitative chemical analysis by x-ray fluorescence would be a simple matter if there were no interelement effects. The characteristic line intensities of the x-ray spectra corresponding to the particular elements in the sample would thus be directly proportional to the respective atomic densities. A simple intensity ratio between the samples and the pure-element standards would suffice to determine elemental concentrations. This is of coarse neglecting any kind of particle size or heterogeneity effects.

Unfortunately, this ideal relationship would only apply if the incident x-rays caused excitation of just the single layer of atoms that make up the surface of the sample. Since different atoms require different excitation conditions in order to produce a secondary x-ray spectrum, it immediately follows that all atoms will exhibit different absorption properties. Hence, the degree of primary x-ray absorption and secondary x-ray emission of atoms below the sample surface is directly dependent on the nature of the atoms which occur closer to the surface.

The interelement effects arise in three ways. Firstly, the incident x-rays penetrate a significant distance below the surface of the sample. In doing so, the elemental absorption properties determine the degree of penetration and hence the number of atoms being excited.

Secondly, the characteristic secondary-emission radiation must pass through and escape from the sample in order for it to be detected. Now, each element will emit secondary radiation of different energy. The matrix (all other elements within the sample) will correspondingly exhibit different absorption characteristics toward each energy. The result is that x-ray line intensities become attenuated to various degrees depending on the line energy and the composition of the matrix.

Thirdly, if an element absorbs secondary radiation being emitted by other elements in the matrix, it may subsequently produce secondary radiation. This would add to the secondary radiation already being generated through absorption of the primary excitation energy. The spectral line intensity is thus increased by this process, commonly referred to as the matrix enhancement effect. The effects of matrix absorption and enhancement may be described with the aid of FIGURE 2-5 which shows the radiated x-ray intensity of an element as a function of its concentration in a simple binary system. Curve A shows the general appearance of the intensity function under conditions of either matrix enhancement or negative absorption. In this case the second

FIGURE 2-7

Relationship of x-ray line intensity as a function of concentration for one element of a binary system when :-

(A) that element is the heavy absorber;

(B) both elements possess similar absorption properties;

(C) that element is the light absorber.

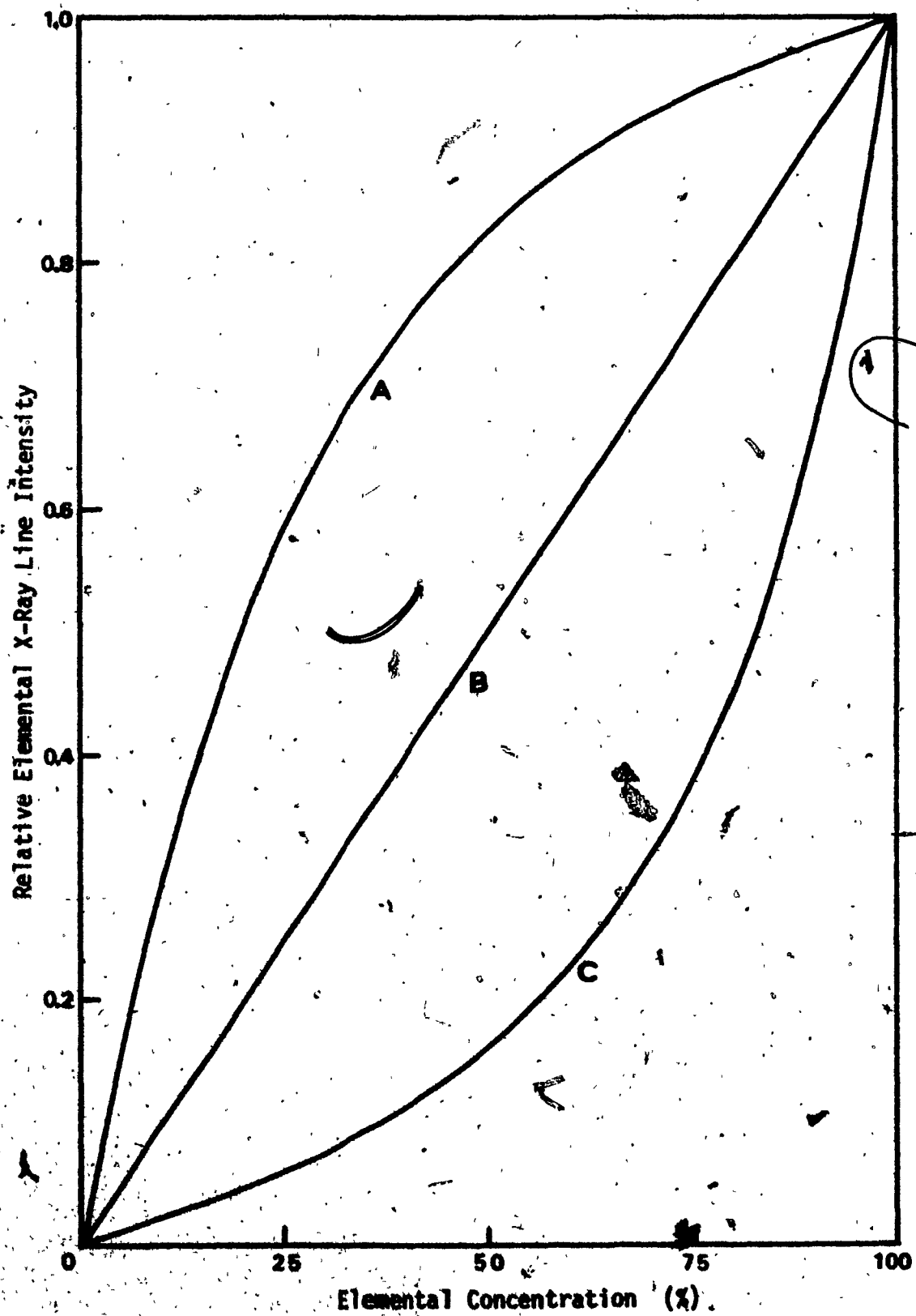
1.0
0.8
0.6
0.4
0.2
0
25
50
75
100
A
B
C
Relative Elemental X-Ray Line Intensity
Elemental Concentration (%)

element produces x-rays of higher energy than the absorption edge energy of the first element. The measured radiation is artificially enhanced at low concentrations of the analysed element. This enhancement effect falls off as the second element becomes the minor constituent. If the two elements have very different mass absorption coefficients, a similarly shaped curve occurs when the second element is the light absorber. Curve B displays the linear relationship of the intensity function that might be observed if the two elements had very similar x-ray absorption properties. Curve C represents the intensity function that might result if the absorption edge energy of the second element is below the energy of the radiation being emitted by the first element. For this situation the radiation for the analysed element is highly absorbed at low concentrations. Again, the effect of absorption disappears as the heavy absorber becomes the minor constituent.

In short, the effect of the matrix is simply described as follows. The intensity - concentration relationship for each element is primarily a function of the elemental concentration, the absorption properties and the emission properties of that element. In addition to this the relationship is proportional to the absorption properties and concentrations of all other elements in the sample matrix.

This most serious problem of the interelement effect exists for all multicomponent materials. The effects may be quite small and simple or very large and complex depending on the substances

present. In order to achieve accurate quantitative analysis by XRF spectrometry, many workers have attempted to eliminate or correct for these effects.

The methods of approach may be generalized into three types :

(1) The spectrometer is calibrated over small concentration ranges using standards that closely resemble the unknown samples. Concentrations are determined from the ratios of net x-ray intensities for the unknowns and standards. In this method the matrix is regarded as being constant and accurate analysis is possible. The advantage here is the speed of analysis. Unfortunately, many standards are required and significant errors are introduced when dealing with samples of varied origins.

(2) The sample is diluted with a suitable material in order to reduce the matrix effects to a negligible level. As in the first case, intensity ratios (unknown / standard) are used to determine elemental concentrations. This method has the drawback that the sample must be destroyed and sample preparation time may be lengthened considerably. Also, the x-ray intensities are deminished, due to the dilution factor, resulting in a loss of sensitivity.

(3) Mathematical correction procedures are applied to compensate for the interelement effects.

First, theoretical correction factors may be determined from the characteristic x-ray properties of the elements.

Application of these factors to the measured x-ray intensities produces a direct quantitative determination. However, the x-ray absorption and emission within a complex matrix is not completely understood, especially in the light element region. Large errors may exist in the analysis of non-ideal sample materials.

Second, correction factors may be determined empirically and applied to the measured intensities to give the desired analytical results. Again, this method requires a certain number of well-analysed standards. For this method there is not such a strict dependence on compositional compatibility between the standards and the unknowns.

The direct calibration and comparison method has been and still is extensively used for quantitative XRF spectrometry. Although considerable care and time is required to set up the calibrations, the subsequent routine chemical analysis is very simple and rapid.

Except in the case of alloy materials, the trend in a large number of laboratories is to employ the sample dilution method to assist in the elimination of the sample effects which interfere with the intensity - concentration relationships. The remainder of this section is intended to shed some light on the various attempts by certain workers to evaluate matrix effects, devise correction factors, and develop accurate x-ray spectrochemical analysis procedures in the presence of these effects.

Ambrose et al[23] showed the effectiveness of borate fusions in destroying effects due to grain size, heterogeneity and mineralogical variations, as well as to reduce the interelement effects. The addition of a heavy absorber, as described by Claisse[9] and modified by Rose et al[24] (use of lanthanum oxide), was proven to reduce matrix effects to a very low level.

With the increased availability of small low-cost computers, many workers have been encouraged to include some form of mathematical correction procedure in the conversion of measured x-ray intensities to elemental concentrations.

Gunn[25] believed in the use of working calibration curves. However, instead of adding a heavy absorber to produce a constant matrix absorption, he included a computer-determined mass absorption correction factor. Unfortunately, an error of 15% to 20% was inherent in the working curves that were developed for some volcanic rock analysis. The mass absorption correction factors, being determined for pure samples, were obviously not suitable for this type of practical analysis.

Sherman[26] preferred the pure theoretical approach and came up with a rigorous mathematical model to represent a mixture of elements being irradiated by high intensity x-rays. Under the assumption of monochromatic incident radiation, the emitted x-ray intensity of an element was correlated to the concentration,

absorption coefficient and emission coefficient. Enhancement effects were also considered. The results were extremely complex and did not seem to have practical significance.

Lucas-Tooth, in a preliminary investigation with Price[27] and a detailed investigation with Pyne[28], developed a much more simple empirical method of matrix effect correction. The elemental concentrations were related to the measured x-ray intensities of all elements in the sample and the respective, empirically determined, interelement effect constants. The method was subjected to a severe test in the analysis of multicomponent alloy steels. The results displayed a high degree of analytical accuracy and precision. Other workers, Sanderson and Yeck[29], applied the Lucas-Tooth method with similar success for light elements in iron and titanium ores.

About the same time that Sherman was developing the mathematical model, Beattie and Brissey[30] developed a simple empirical first-order linear correction procedure to overcome the matrix effects. Matrix effect constants were deduced from binary sample concentrations and x-ray intensities. The computation was carried out by solving a set of simultaneous equations. The method required that one element (the most abundant) be distinguished from the other elements in order to arrive at the best solution. This was considered a disadvantage by some other workers.

The best-known and most extensively practiced approach to the correction of interelement effects is the Lachance and

Traill method[31-37]. The method is based on the relationship that " the relative intensity of a constituent is directly proportional to its weight fraction and inversely proportional to 1 plus the sum of the products of the weight fractions of the remaining constituents times their respective alpha constants "; the alpha constants representing the empirically determined quantitative measures of the interelement effects. The relationship is simply shown in the following equation.

$$R_A = \frac{W_A}{1 + \sum_j \alpha_{Aj} W_j} \qquad 2\text{-}15$$

where:

R_A = the relative intensity for element A as compared to the intensity for pure element A

W_A = the weight fraction of element A

W_j = the weight fraction of element j

α_{Aj} = the alpha constant representing the interelement effect of the matrix element j on the intensity for element A

The method, developed for binary alloy systems, was extended to include the solution of multicomponent systems in x-ray diffraction, x-ray fluorescence and electron probe analysis. The alpha constants, once determined, were postulated to be applicable

to any spectrometer system having the same geometry and using similar analysis conditions. The matrix effect problem was thus solved and the quantitative determination was reduced to the measurement of characteristic x-ray intensity followed by a simple solution of linear equations.

The computer applications to XRF spectrometry have been excellently described by Mitchell[38] showing the advantages and the disadvantages of various statistical techniques. The Lachance and Traill method, where the concentration is the dependent variable and the intensity is the independent variable, was shown to be more useful than the Lucas-Tooth method where the intensity is the dependent variable and the concentration is the independent variable. A comparison between a least-squares solution and a multiple regression solution indicates a preference for the regression method where the dependent variable is related to several independent variables.

Other workers, Jenkins and Whitelaw[40], have attempted both the methods of Lachance and Traill and Lucas-Tooth. A preference was shown for the use of a slightly modified Lachance and Traill expression which included dead-time and background corrections.

Criss and Birks[41] developed a method that was very similar to that of Lachance and Traill. The difference appeared in the determination of the alpha coefficients. Criss and Birks preferred to determine them from fundamental absorption parameters rather than

from empirical solutions through regression analysis or the solving of simultaneous equations. Stephenson[42] investigated various methods and elected to use the Criss and Birks method because of the fundamental parameter approach.

The list of interelement effect correction methods does not stop here by any means. Authors such as Poole and Holloway[43] and McKinney and Rosenberg[44] have developed their own particular method to suit their own desires and needs.

Matrix effect correction procedures are not always necessary. However, if experimental results indicate that they are required, several methods may be attempted. The final selection may be made on the basis of the degree of complexity or, more importantly, on the effectiveness with which the method eliminates the particular elemental interferences.

CHAPTER 3

EXPERIMENTAL

3-1 SAMPLE DESCRIPTION

3-1-1 BAUXITE SAMPLES

The Aluminum Company of Canada (Alcan), Arvida, Que., supplied all of the bauxite samples used in this investigation. These samples originated from five different geographical regions. From the large number of samples available, a selection of ten to fifteen samples from each region was made. This was done to ensure that the total sample lot would represent the complete range of compositions, including the minimum and maximum values, of all the regions.

The sixty-three bauxites selected include 12 samples from Jamaica, 13 samples from Guyana (Demerara), 14 samples from Brazil, 9 samples from West Africa (Boke) and 15 samples from Australia. Also included in the sample lot are 3 samples from the Alcan "Accuracy Program" and 4 samples from the National Bureau of Standards. The "Accuracy Program" samples represent large quantities of bauxites that are periodically analysed by Alcan as a means of checking the accuracy of their analytical methods.

The identification and chemical composition of the bauxite samples are shown in TABLES 3·1 to 3·6. Except for the NBS samples, which are supplied with analytical data, the chemical composition was determined by Alcan. The values for the alumina (AT_2O_3) content are by-difference values except where direct analysis is indicated. The bauxites have been assigned sample numbers from 1 to 70 for simplicity in future reference.

In addition, Alcan supplied large quantities (300 - 400 grams) of coarse bauxite ore from the above mentioned five regions. These samples were provided for that part of this project dealing with particle size effects. The chemical compositions of these bauxites (supplied by Alcan) are shown in TABLE 3·7. Due to the very coarse nature of this material and its heterogeneity, the percentage composition values shown may not be truly representative of the bauxite ore received. However, an accurate analysis of these coarse bauxites was not pertinent to the proposed investigation.

The bauxites varied considerably in physical state and colour. Although most of the samples were received as fine powders, several were of a particle size much larger than 10 mesh (2 mm.). Attempts to crush the coarse materials revealed that some bauxite types were significantly harder than others. It was also noted that there are significant hardness differences within some bauxite types. While one type would crush uniformly another type would contain pieces of material much harder than the remainder of the sample. The colours of the bauxite ores were

TABLE 3-1

CHEMICAL COMPOSITION OF JAMAICA BAUXITE SAMPLES

SAMPLE	IDENTIFICATION	% Fe_2O_3	% TiO_2	% SiO_2	% Al_2O_3
# 1	JM 453	20.0	2.80	0.33	48.6
# 2	JM 454	18.1	2.70	1.44	47.2
# 3	JM 634	17.9	2.48	5.72	44.2
# 4	JM 635	18.4	2.41	3.57	46.9
# 5	JM 661	18.1	2.43	5.67	46.5
# 6	JM 662	18.8	2.25	0.64	45.8
# 7	JM 917	19.7	3.31	0.34	47.2
# 8	JM 918	17.9	2.68	0.64	49.5
# 9	JM 919	19.6	2.23	6.65	43.9
#10	JM 920	18.1	2.57	8.94	45.4
#11	JM 921	18.8	2.71	3.13	47.1
#12	JM 922	20.2	2.80	2.84	45.8

RANGES	% Fe_2O_3	17.9 - 20.2
	% TiO_2	2.2 - 3.3
	% SiO_2	0.3 - 8.9
	% Al_2O_3	43.9 - 49.5

TABLE 3·2

CHEMICAL COMPOSITION OF GUYANA (DEMERARA) BAUXITE SAMPLES

SAMPLE	IDENTIFICATION	% Fe_2O_3	% TiO_2	% SiO_2	% Al_2O_3
#17	DM CAA	2.1	2.6	2.1	60.3
#18	DM CAE	1.4	1.7	19.8	52.1
#19	DM CAF	2.0	2.4	25.8	47.7
#20	DM CAG	4.3	3.8	28.8	44.4
#21	DM CAH	2.3	1.9	35.5	42.7
#22	DM CAI	0.2	1.3	40.2	41.8
#23	DM CAJ	14.5	0.8	60.5	3.3*
#24	DM CAK	0.7	2.1	6.8	60.0
#25	DM CAM	25.4	1.1	35.7	25.9
#26	DM CAN	28.6	1.0	6.7	36.4
#27	DM CAO	38.0	1.4	24.7	23.7
#28	DM CAQ	48.4	0.9	6.6	18.3
#29	DM CAR	53.7	1.7	8.8	8.9

* by direct chemical analysis

RANGES		
	% Fe_2O_3	0.2 - 53.7
	% TiO_2	0.8 - 3.8
	% SiO_2	2.1 - 60.5
	% Al_2O_3	3.3 - 60.3

TABLE 3-3

CHEMICAL COMPOSITION OF BRAZIL (AMAZON) BAUXITE SAMPLES

SAMPLE	IDENTIFICATION	% Fe_2O_3	% TiO_2	% SiO_2	% Al_2O_3
#30	BZ 30A S/L	18.1	2.7	1.1	50.4
#31	BZ 30B S/L	9.0	2.5	1.1	56.8
#32	BZ 61A S/L	27.4	2.3	6.9	41.3
#33	BZ 62A S/L	25.4	1.6	10.7	40.4
#34	BZ 67A S/L	22.8	1.9	8.2	43.7
#35	BZ 128A S/L	36.8	2.0	1.7	38.0
#36	BZ 140A S/L	18.5	2.4	2.3	50.0
#37	BZ 19A +20M	31.9	2.0	0.9	41.8
#38	BZ 30B +20M	7.0	2.3	0.9	59.0
#39	BZ 61A +20M	23.7	1.9	4.5	45.7
#40	BZ 74A +20M	20.3	1.3	6.5	46.5
#41	BZ 93B +20M	22.7	2.2	0.7	47.2
#42	BZ 121A +20M	21.7	1.5	2.9	48.0
#43	BZ 138A +20M	15.3	1.7	2.5	52.5

RANGES		
	% Fe_2O_3	7.0 - 36.8
	% TiO_2	1.3 - 2.7
	% SiO_2	0.7 - 10.7
	% Al_2O_3	38.0 - 59.0

TABLE 3-4

CHEMICAL COMPOSITION OF WEST AFRICA (BOKE) BAUXITE SAMPLES

SAMPLE	IDENTIFICATION	% Fe_2O_3	% TiO_2	% SiO_2	% Al_2O_3*
#44	BK 14134	14.05	2.67	1.20	52.01
#45	BK 14135	12.08	2.46	0.81	53.18
#46	BK 16726	7.48	4.81	0.80	56.24
#47	BK 19356	3.61	4.87	0.40	61.23
#48	BK 19987	6.40	3.54	1.12	57.54
#49	BK 20497	4.59	5.61	0.53	57.8
#50	BK 38741	1.48	3.38	0.45	63.7
#51	BK 38742	3.99	3.74	0.53	59.5
#52	BK 38743	3.19	3.72	0.57	60.0

* by direct chemical analysis

RANGES		
	% Fe_2O_3	1.48 - 14.05
	% TiO_2	2.46 - 5.61
	% SiO_2	0.40 - 1.20
	% Al_2O_3	52.01 - 63.7

TABLE 3·5

CHEMICAL COMPOSITION OF AUSTRALIA BAUXITE SAMPLES

SAMPLE	IDENTIFICATION	% Fe_2O_3	% TiO_2	% SiO_2	% Al_2O_3
#56	AU TH1A	5.3	2.54	22.2	39.8
#57	AU TH1E	9.8	2.16	32.4	34.9
#58	AU TH3B	12.1	2.00	22.8	40.4
#59	AU TH3C	17.2	1.76	25.5	36.3
#60	AU TH5B	9.1	2.41	17.5	46.1
#61	AU TH5E	14.9	1.76	35.7	31.6
#62	AU TH5G	2.8	1.80	53.3	27.4
#63	AU TH5H	3.8	1.87	48.0	30.6
#64	AU TH6G	6.0	1.22	53.6	26.0
#65	AU TH6H	4.5	1.17	58.1	23.6
#66	AU TH7A	8.0	2.21	24.6	41.6
#67	AU TH7C	8.7	2.32	9.0	51.9
#68	AU TH7E	14.4	1.96	16.9	43.5
#69	AU TH7F	11.6	2.10	21.6	42.5
#70	AU TH7G	15.6	1.69	33.7	32.4

RANGES	% Fe_2O_3	2.8 - 17.2
	% TiO_2	1.17 - 2.54
	% SiO_2	9.0 - 58.1
	% Al_2O_3	23.6 - 51.9

TABLE 3·6

CHEMICAL COMPOSITION OF NATIONAL BUREAU OF STANDARDS AND ALCAN "ACCURACY PROGRAM" BAUXITE SAMPLES

SAMPLE	IDENTIFICATION	% Fe_2O_3	% TiO_2	% SiO_2	% Al_2O_3*
#13	NBS 69A	5.82	2.78	6.01	55.0
#14	AP CAA	1.84	2.56	5.25	59.7
#15	AP CAB	1.84	2.54	4.99	59.3
#16	AP CAC	7.20	1.22	8.87	56.2
#53	NBS 78	0.79	3.37	20.69	69.97
#54	NBS 97	0.98	2.38	42.87	38.77
#55	NBS 98	2.05	1.43	59.11	25.54

* by direct chemical analysis

TABLE 3·7

CHEMICAL COMPOSITION OF COARSE BAUXITE SAMPLES

REGION	% Fe_2O_3	% TiO_2	% SiO_2	% Al_2O_3*
BOKE	5.20	3.05	0.86	58.67
AUSTRALIA**	17.10	2.96	4.88	54.83
DEMERARA	4.3	2.48	3.8	59.0
JAMAICA	17.9	2.48	5.72	44.2
AMAZON	11.2	1.15	3.45	55.1

* by direct chemical analysis
** pre-ground to -10 mesh powder

diverse from a deep red brown, characteristic of materials containing hematite, through orange to yellow, characteristic of materials containing aluminian goethite[2] and finally to almost white or grey where the material contained very little hematite.

3·1·2 SYNTHETIC SAMPLES

Throughout the investigation a large number of synthetic mixtures were prepared in order to examine the problem of matrix effects and matric effect corrections. The materials used in the preparation of these mixtures consisted of anhydrous ferric oxide (Fe_2O_3), anhydrous titanic oxide (TiO_2), silicon carbide (SiC), quartz (SiO_2), aluminum oxide (Al_2O_3), lithium carbonate (Li_2CO_3) and lithium hydroxide ($LiOH \cdot H_2O$). The quartz (Ottawa sand, 99.9% SiO_2 minimum) was supplied by Dr. Guy Perrault, Ecole Polytechnique, Montreal. It had been prepared by grinding the sand (using a Shatterbox with a tungsten carbide grinding vial) to a fine powder where about 80 percent of the material had a particle size less than 200 mesh (74 microns). The material was said to contain 150 ppm cobalt and 200 ppm tungsten carbide. These small impurities were not expected to cause any significant error, and their presence was in general ignored. The aluminum oxide was supplied by Alcan and was a sample of alumina fine seed that is used to facilitate precipitation in the Bayer extraction process. This material was accompanied by a particle size distribution chart showing that about 94 percent of the particles were of a size less than 200 mesh (74 microns).

FIGURE 3-1 is a bar graph representation of this chart.

The synthetic samples were prepared by mixing together carefully weighed amounts of either one, two or all of the elements (Al, Si, Ti or Fe in their respective compounds) using either lithium carbonate or lithium hydroxide as a base matrix. It was noted that most of the pure materials were hygroscopic, particularly the ferric oxide and the lithium hydroxide. A study was made of the rate of absorption of water by dried (12 hours in vacuo) lithium hydroxide. This compound was the most hygroscopic of those handled, gaining in the long term over one-third of its original dried weight. After 8 hours of exposure to the atmosphere, the dried lithium hydroxide had attained 98 percent of the final projected weight gain. FIGURE 3-2 shows the increase of weight with respect to time of exposure for lithium hydroxide.

In view of the above results, and the need to know accurate concentration values for the synthetic samples, it was deemed necessary to make initial sample weighings in a dry environment. Subsequently the samples were exposed to the moisture in the atmosphere prior to the determination of a final sample weight. The individual pure materials were first vacuum dried for twelve hours. The mixtures were then prepared, under dry nitrogen, by weighing out the appropriate quantities of the desired pure components. The final sample weight was procured following a period of 24 to 36 hours in which the material was exposed to air. The synthetic samples were finally mixed for 15 minutes using a rotating ball mill.

FIGURE 3-1

Particle size distribution of alumina fine seed.

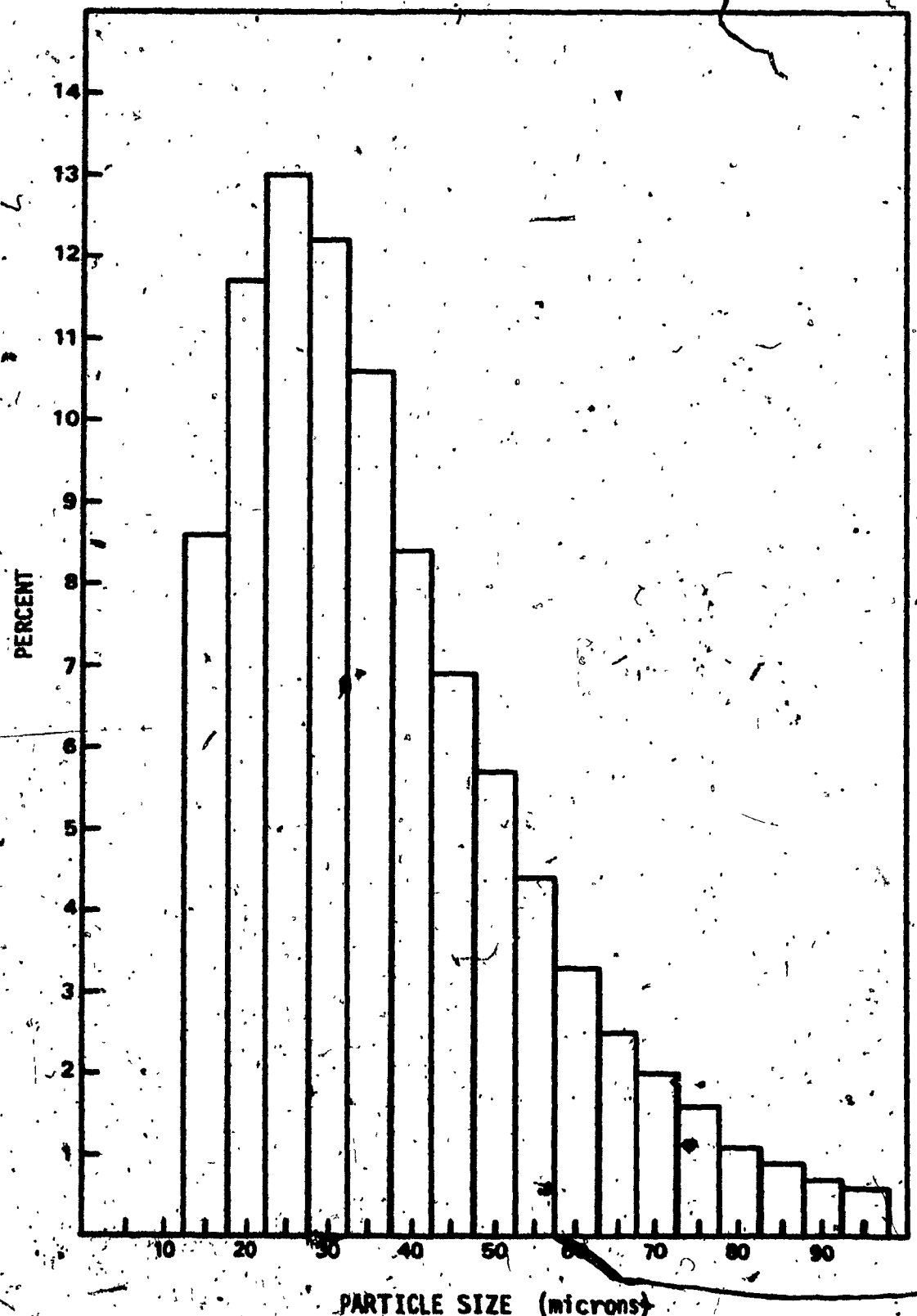
PERCENT
14
13
12
11
10
9
8
7
6
5
4
3
2
1
10
20
30
40
50
70
80
90
PARTICLE SIZE (microns)

FIGURE 3-2

Weight increase of lithium hydroxide as a function of the period of exposure to air.

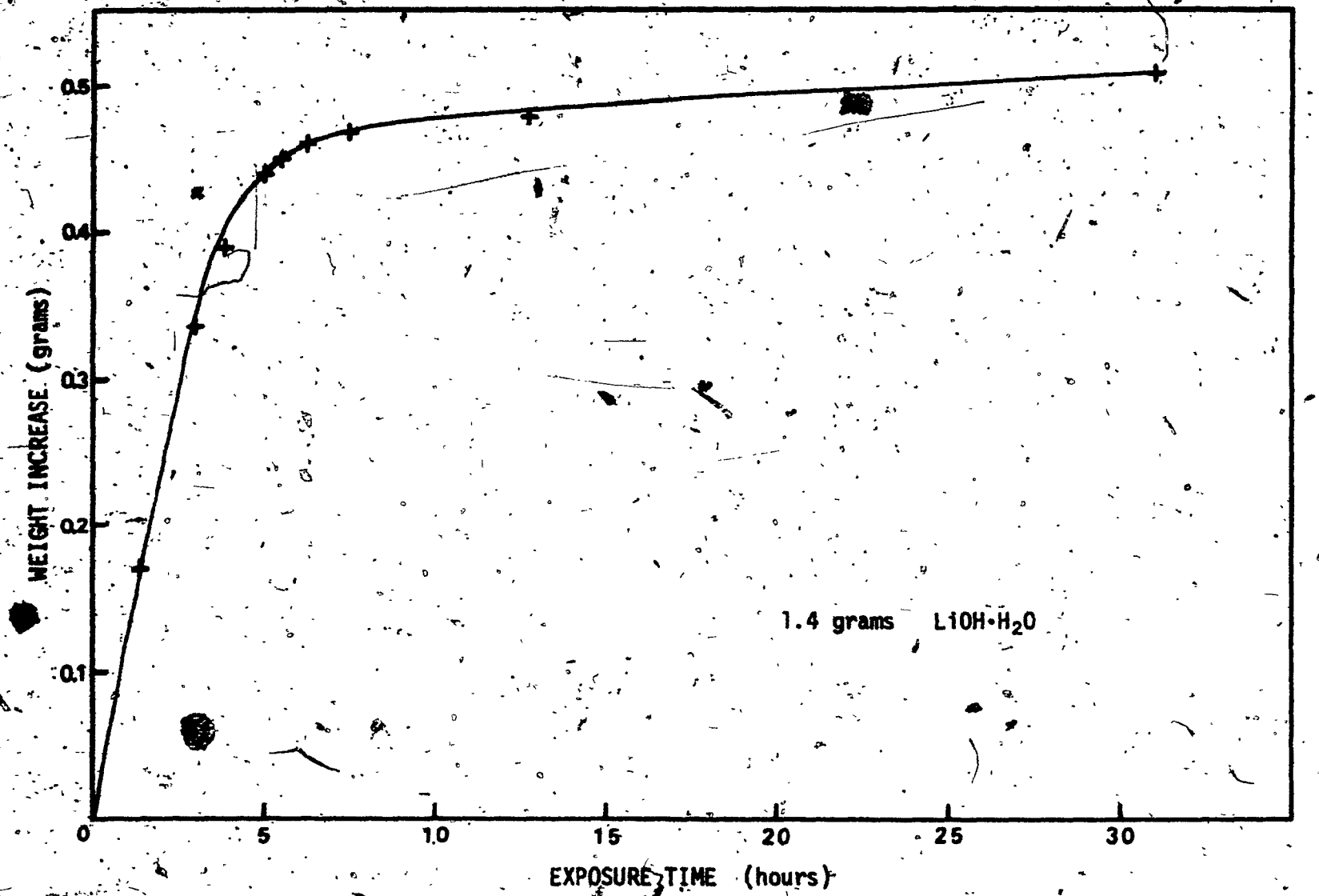
WEIGHT INCREASE (grams)
0.5
0.4
0.3
0.2
0.1
0
5
10
15
20
25
30
EXPOSURE TIME (hours)
1.4 grams LiOH·H2O

3-2 SAMPLE PREPARATION (BRIQUETTING TECHNIQUE)

Powdered bauxite ore analysis by x-ray fluorescence spectroscopy can be performed with the sample as a loose powder or by the preparation of self-supporting sample pellets or briquettes. The sample chamber configuration of the x-ray goniometer usually requires a thin Mylar film specimen retainer covering the irradiated surface for loose powder analysis. This is extremely unfavourable in the investigation of a light element, due to significant absorption of the long wavelength radiation. In addition, a critical volume of a loose power is comprised of air holes between the particles, again resulting in an adverse situation relative to low-energy radiation absorption. For these reasons, and to obtain the advantage of reducing the particle size effects, all of the powdered bauxite ore samples and the synthetic samples to be used for XRF spectrochemical analysis were prepared by the briquetting technique.

Briquette formation involves placing the powder material in a cylindrical die in a hydraulic press, sufficient pressure (20,000 to 50,000 psi) being applied to form a compact disc which can be handled almost as a solid specimen. In the case of bauxite ore samples, the powder is not very cohesive resulting in somewhat fragile briquettes. To fortify the specimen disc, fibrous cellulose is added prior to compacting to form a strong backing material.

The die assembly (Spex # 3622 Evacuable X-Ray Die) or

briquetting mold consists of a heavy cylindrical chamber ($1\frac{1}{4}$ inch diameter) with a removable base, two polished metal inserts to secure a smooth surface finish on the briquette and a piston to apply the required pressure. The die is assembled with the base and one metal insert placed in the bottom of the cylinder with the polished face uppermost. About 5 grams of cellulose powder is loaded in the die and is tamped lightly with the piston. The piston is withdrawn and about 0.5 to 1 gram of the bauxite ore (sufficient material to produce a briquette sample depth in excess of the penetration depth of the x-rays) is placed in the cylinder and carefully spread evenly over the packed cellulose surface. The second metal insert is placed in the cylinder with the polished face downwards and pressed down with the piston. The die assembly is placed in the hydraulic press and a load of 40,000 psi is applied, retained for several seconds and then released. The base is removed from the briquetting mold. Pressure is then reapplied to the piston to force the completed briquette out of the mold. The cellulose backing now provides an excellent surface for marking the sample identification.

3.3 EQUIPMENT

The x-ray fluorescence spectrographic data was acquired using a Picker Nuclear Spectro-Diffractometer System. This instrument is a single-channel manual spectrometer consisting of an ultrastable high voltage generator (model 6238H), various interchangeable x-ray tubes

(type OEG 60), goniometer (model 6239B) (method of analysis by reflection from a single flat crystal) and a radiation analyser (model 6245).

The solid state DC generator has a maximum voltage setting of 60 kilovolts (kV) with a stability of 0.1 percent and a maximum current setting of 50 milliamperes(mA) with a stability of 0.02 percent. The generator has the capability for simultaneous operation of two x-ray tubes, one in the fluorescence mode and the other in the diffraction mode.

The primary x-ray radiation is generated by using a chromium target or a tungsten target, end window, x-ray tube having a maximum power rating of 1800 watts. The sample is irradiated from above with the incident angle of the primary x-ray beam being equal to 45 degrees, this being of course the same as the take-off angle for the secondary radiation. Provision is made for sample rotation.

The goniometer is adapted for helium gas flow through the specimen chamber and the optical path. The analyser crystals available are lithium fluoride (LiF, (200) reflection plane, $2d = 4.03$ Å), penta erythritol (PET, (002) reflection plane, $2d = 8.74$ Å) or ammonium dihydrogen phosphate (ADP, (110) reflection plane, $2d = 10.64$ Å).

Collimation of the secondary radiation being emitted by the sample is achieved with a Soller collimator, positioned between the sample chamber and the crystal chamber, which limits the beam divergence to two degrees. For the dispersed beam a coarse or fine Soller collimator

is used between the crystal chamber and the detector. The secondary beam divergence is limited to 0.39 degrees for coarse collimation or 0.175 degrees for fine collimation. A gas proportional flow counter or a scintillation counter is used for radiation detection. The flow gas for the proportional counter is 10 percent methane in argon ("P10").

The transistorized radiation analyser consists of a dual range power supply, a low range of 400 - 1600 V for the scintillation counter and a high range of 800 - 3200 V for the proportional flow counter, a pulse height selector, and scalar and ratemeter displays. Data acquisition is achieved through a fixed time or fixed count mode. Data recording is attained via a strip chart recorder for analog output or a data printer for digital output.

A portion of the work concerning particle size effects was performed at Alcan, Arvida, where a Philips Automatic X-Ray Spectrometer Type PW 1210 was used. The two spectrometers are basically similar as far as the x-ray generation and detection components are concerned. However, advantageous features of the Philips spectrometer are as follows:

1) The sample chamber and optical path can be evacuated;
2) four specimens can be accommodated within the sample chamber;
3) the unit can be programmed to automatically perform consecutive analytical determinations of up to 15 different elements.

All computations were carried out using a Hewlett-Packard (HP) model 2114A mini computer having a 8K - 16 bit word memory package. Peripheral units include a HP2737A High Speed Punched Tape Reader

(HP-modified Remex model RT0302RA/S44 Tape Transport) (Reading speed: 300 characters per second) for program and data input, a HP2020A Digital Tape Unit for data storage on magnetic tape, a Houston Instrument COMPLOT model DP-1-5 Digital Incremental Plotter (plot increment: 0.005 inches) and a HP2752A teleprinter (HP-modified Teletype model ASR33-TC) for data output.

3·4 INSTRUMENTAL PARAMETERS

The initial objective for the XRF spectrochemical analysis of bauxite ore samples was to establish a single set of instrumental parameters that would be suitable for the determination of all the elements concerned. Consideration was given to the energy and intensity of the excitation radiation, the efficiency and resolution of the analysing crystal, the detector characteristics, the pulse height selector settings and some sources of error. Due to the inherent nature of the elements under investigation and the principles of XRF spectrochemical analysis, it was not possible to devise a consistent set of parameters that would favour the best analytical conditions for every element.

This investigation was primarily concerned only with the analysis of the four major components of bauxite ore. The analytes in question were aluminum, silicon, titanium and iron having atomic numbers 13, 14, 22 and 26 respectively. TABLE 3·8 shows some data from the

TABLE 3-8

X-RAY DATA FOR K SERIES SPECTRA OF Al, Si, Ti, Fe

ELEMENT	Al	Si	Ti	Fe
K excitation potential (keV)	1.559	1.838	4.965	7.112
K absorption edge (Å)	7.951	6.745	2.497	1.743
Kα analyte line (Å)	8.339	7.126	2.750	1.937
$K\alpha_1$ analyte line (Å)	8.338	7.125	2.749	1.936
$K\alpha_2$ analyte line (Å)	8.341	7.127	2.753	1.940
$K\beta_1$ analyte line (Å)	7.981	6.769	2.514	1.757

X-Ray Periodic Table[45] indicating the K excitation potential, the wavelength of the K absorption edge, and the wavelengths of the secondary emission spectral lines for these four elements.

3.4.1 SELECTION OF X-RAY TUBE

For maximum efficiency of x-ray spectral line excitation the primary radiation should have a wavelength near the short wavelength side of the absorption edge. If there is an intense line, characteristic of the x-ray tube target, near this wavelength it would contribute the most to the excitation of the secondary-emission x-ray spectrum. Otherwise, the continuum from the x-ray tube target would present the primary source of excitation.

The most intense line (Kα) produced from the chromium target x-ray tube has a wavelength of 2.291 angstroms (useful for excitation of characteristic x-ray radiation of elements lighter than vanadium). This line represents almost 65 percent of the total spectrum of chromium. Considering the tungsten target x-ray tube, the most intense lines (useful for excitation of the secondary-emission x-ray spectra of elements of atomic number 28 or less) are those of the L series. The radiated intensity of the tungsten Lα line (about 1.5 Å) together with the tungsten Lβ line (about 1.3 Å) only represents roughly 18 percent of the total spectrum of tungsten. While the characteristic lines of tungsten will cause excitation of the spectral lines of aluminum, silicon, titanium and iron, the characteristic lines of chromium will only excite the

spectra of aluminum, silicon and titanium. It is necessary to rely on the chromium continuum to induce excitation of the characteristic spectrum of iron. However, the iron K absorption edge (1.743 Å) is not far above the energy of the chromium Kα line (2.291 Å) and consequently the chromium continuum, just above the iron K absorption edge, would be quite intense. There is apparently a large difference between the relative quantities of primary excitation radiation being generated by the chromium target and tungsten target x-ray tubes. This would seem to indicate a three to four fold intensity advantage in favour of the use of the chromium target tube. The actual intensity advantage is considerably smaller than this because the overall tungsten spectrum intensity is about three times the intensity of the chromium spectrum.

The efficiency of x-ray production must also be considered. The intensity of the analyte line that can be detected is dependent on the depth of penetration or the amount of absorption of the primary radiation. It is also dependent on the degree of absorption of the secondary radiation between the point of origin within the sample and the sample surface. For the detection of a particular analyte line the mass absorption coefficients for all elements in the specimen must be considered for all primary excitation wavelengths.

It has been shown[4] that for a pure element an efficiency factor may be defined by the following equation:

$$T_{\lambda_P,\lambda_L} = \frac{\mu_{A,\lambda_P}}{\mu_{A,\lambda_P} + A\,\mu_{A,\lambda_L}} \qquad 3.1$$

where:

T_{λ_P, λ_L} represents the efficiency factor for the primary wavelength λ_P in exciting the analyte - line of wavelength λ_L.

μ_{A,λ_P} is the mass absorption coefficient of pure element A for λ_P.

μ_{A,λ_L} is the mass absorption coefficient of pure element A for λ_L.

A is the spectrometer geometry factor which is equal to $\sin\phi_1 / \sin\phi_2$ where ϕ_1 is the angle of incidence of the primary x-ray beam and ϕ_2 is the take-off angle of the secondary-emission x-ray beam.

The particular arrangement of the Picker spectro-diffractometer (incident angle equals take-off angle equals 45 degrees) defines the spectrometer geometry factor (A) to be equal to unity. TABLE 3-9 shows the mass absorption coefficients[46] of the analytes aluminum, silicon, titanium and iron for the approximate wavelength of chromium $K\alpha$ and $K\beta$ radiation, tungsten $L\alpha_1$ and $L\beta_1$ radiation and the analyte characteristic $K\alpha$ radiation. These values were applied to EQUATION 3-1 and the calculated efficiency factors are shown in TABLE 3-10 for the chromium and tungsten lines indicated. There are no entries for the excitation of iron radiation by the chromium $K\alpha$ or $K\beta$ lines since this process does not exist.

TABLE 3-9

MASS ABSORPTION COEFFICIENTS

λ (Å)	line	Al	Si	Ti	Fe
2.28	CrKα	153	193	565	115
2.1	CrKβ	117	146	475	91
1.5	$WL\alpha_1$	45	57	190	284
1.3	$WL\beta_1$	30	37.5	127	201
8.34	AlKα	330	480	2000	2910
7.08	Si[illegible]	3170	315	1300	2040
2.76	Ti[illegible]	263	328	114	193
1.93	FeKα	94	116	377	71

TABLE 3-10

EFFICIENCY FACTORS

λ (Å)	line	Al	Si	Ti	Fe
2.28	CrKα	.317	.380	.832	-
2.1	CrKβ	.262	.317	.806	-
1.5	$WL\alpha_1$	.120	.153	.625	.800
1.3	$WL\beta_1$	.083	.106	.527	.739

A comparison of the actual spectral intensities obtainable with the tungsten or chromium target x-ray tubes was desired. Keeping all instrumental parameters constant, except the primary excitation source, a portion of the bauxite spectrum (covering the wavelengths between 1.592 Å and 2.846 Å) was examined. The fixed parameters that were selected are indicated in TABLE 3·11 and the sample used was the National Bureau of Standards Bauxite sample NBS 69A (#13 in TABLE 3·6). FIGURE 3·3 shows the spectrum using the tungsten target x-ray tube. The iron Kα line maximum intensity is about 150 kcps. (no dead time correction) while the titanium Kα line maximum intensity is about 30 kcps. The small peak observed for chromium Kα line is due to the presence of 0.05 percent chromate (Cr_2O_3) in the sample. FIGURE 3·4 shows the corresponding spectrum using the chromium target x-ray tube. It was noted that the iron Kα intensity had decreased to about 30 kcps. (the same as the TiKα intensity when excited by tungsten radiation). However, the titanium Kα intensity had increased to about 88 kcps. (no dead time correction). The intensity of the characteristic radiation of silicon and aluminum was expected to increase similarly.

The chromium target x-ray tube introduces the chromium lines into the spectrum. It appeared that there is no significant spectral line overlap in this region. Apart from causing an increase in background intensity for the iron and titanium lines it was expected that the chromium lines would not appreciably affect the accuracy in the analysis of bauxite ore.

TABLE 3·11

INSTRUMENT PARAMETERS

HIGH VOLTAGE GENERATOR	50 kV	36 mA
HELIUM GAS FLOW	5 cfh	
DISPERSION CRYSTAL	PET	2d = 8.74 Å
COLLIMATION	COARSE	
DETECTOR	PROPORTIONAL FLOW	
HIGH VOLTAGE	3.20 HELIPOT (1.06 kV)	
P10 GAS FLOW	0.25 cfh	
PULSE HEIGHT ANALYSER		
MODE -	LOWER LEVEL 0.50	
GAIN 10		
SPECTROMETER ANGLES		
OMEGA (ω)	0.0 degrees	
2 THETA (2θ)	SCAN 21° to 38°	
	SCAN SPEED 1° /min.	

FIGURE 3-3

X-ray spectral scan (1.592 Å to 2.846 Å) for bauxite sample NBS 69A. Excitation by a tungsten target x-ray tube.

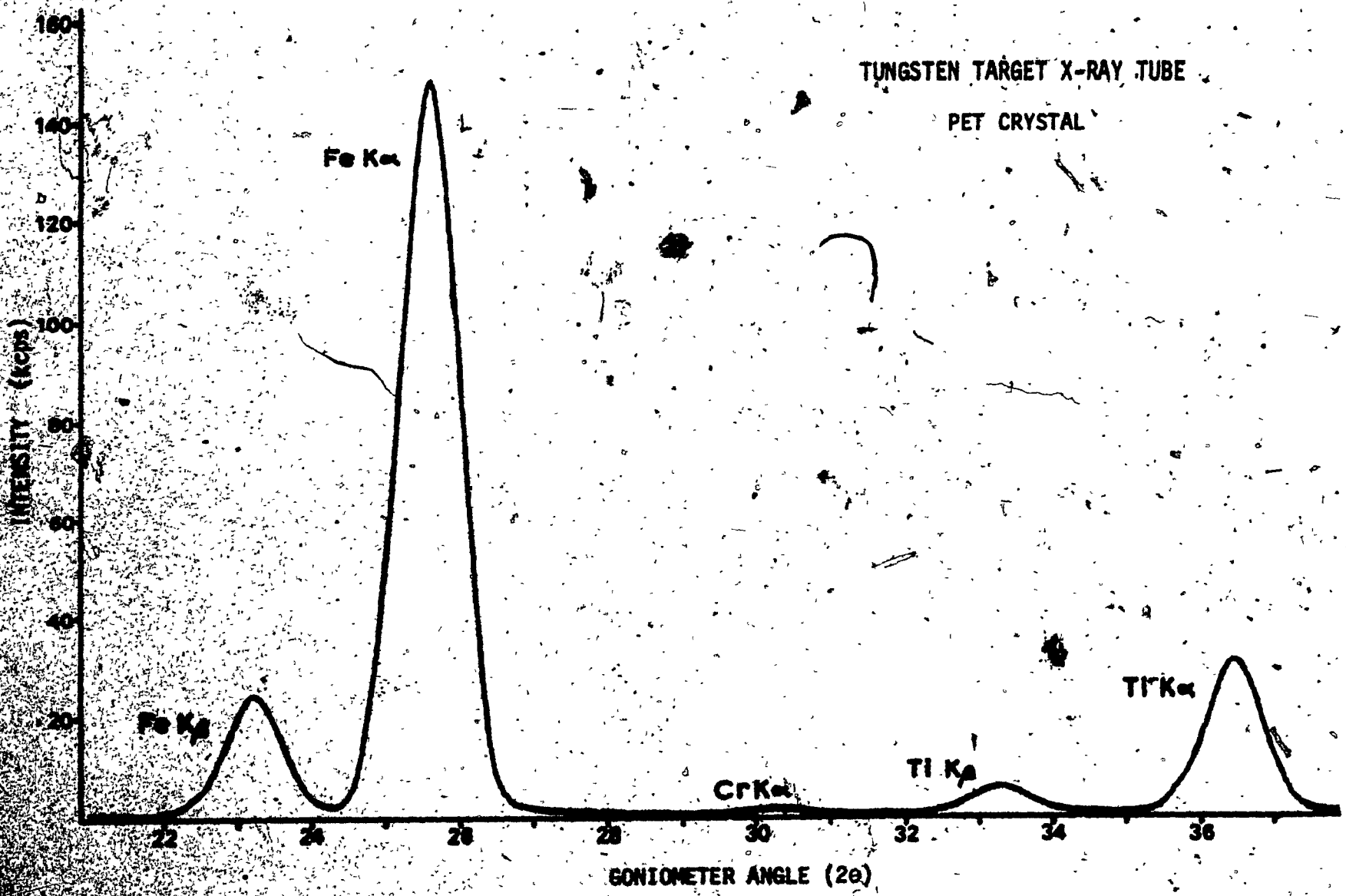
TUNGSTEN TARGET X-RAY TUBE
PET CRYSTAL
Fe Kα
Fe Kβ
Cr Kα
Ti Kβ
Ti Kα
INTENSITY (kcps)
160
140
120
100
80
60
40
20
22
24
26
28
30
32
34
36
GONIOMETER ANGLE (2θ)

FIGURE 3-4

X-ray spectral scan (1.592 Å to 2.846 Å) for bauxite sample NBS 69A. Excitation by a chromium target x-ray tube.

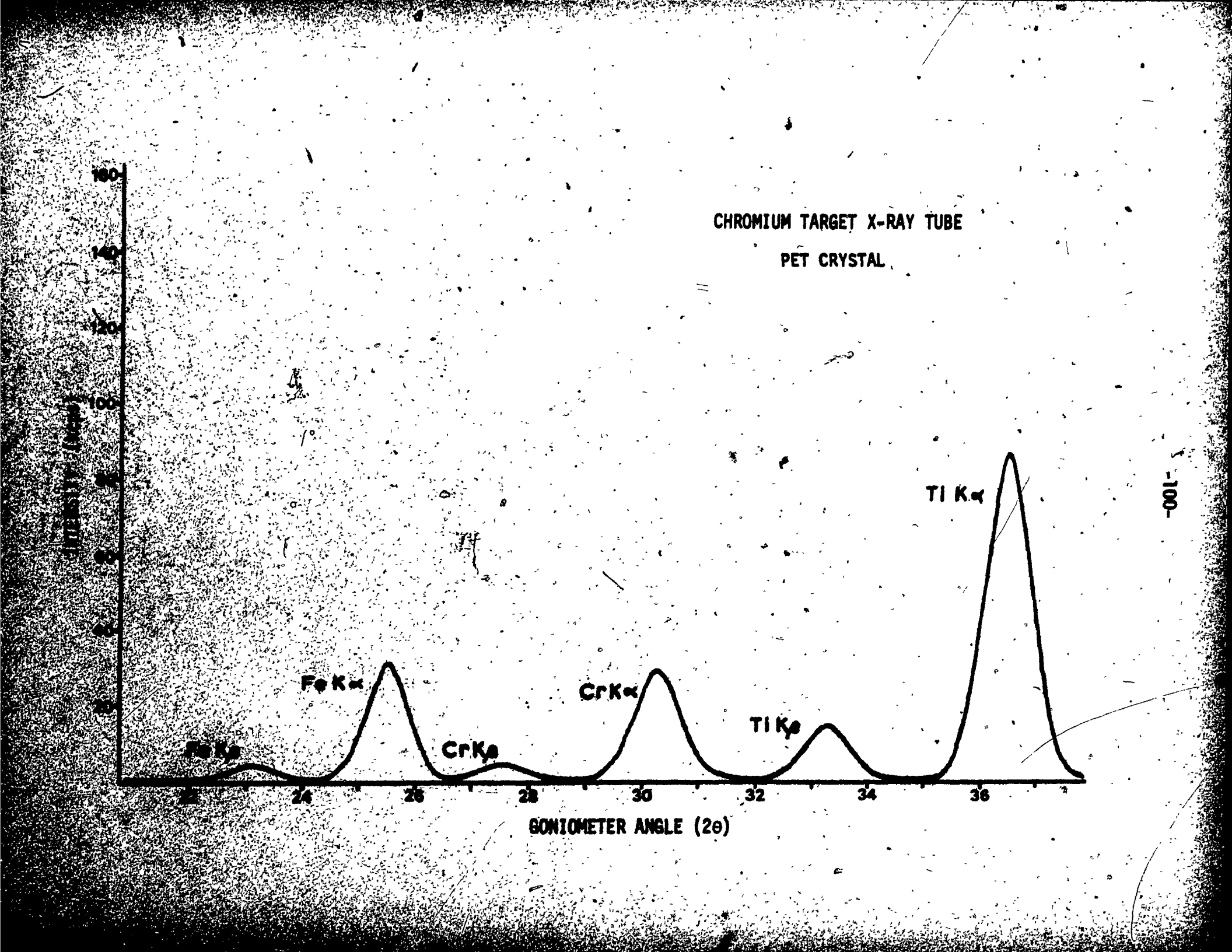
CHROMIUM TARGET X-RAY TUBE
PET CRYSTAL
160
140
120
100
80
60
40
20
Fe Kβ
Fe Kα
Cr Kβ
Cr Kα
Ti Kβ
Ti Kα
22
24
26
28
30
32
34
36
GONIOMETER ANGLE (2θ)
-100-

It was apparent from the calculated efficiency factors and the observed spectral scans that the tungsten target x-ray tube would only be required for efficient excitation of the iron spectrum. The chromium target x-ray tube has a considerable advantage with respect to the efficiency of excitation of aluminum, silicon and titanium x-ray spectra. As outlined previously, it was desired to have a minimum number of varying instrumental parameters. To this end, a sacrifice of intensity of iron radiation was made in favour of the attainment of maximum efficiency of excitation and intensity of the long wavelength radiation. The chromium target x-ray tube was selected for the analysis of all elements (Al, Si, Ti and Fe) in bauxite ore.

3-4-2 SELECTION OF ATMOSPHERE

The atmosphere within the radiation path of the goniometer was chosen to be air for the analysis of iron while for the analysis of titanium, silicon and aluminum the crystal chamber and specimen chamber were purged with helium. The rate of flow of helium was adjusted to 5 cubic feet per hour (cfh) in order to allow the intensity of aluminum $K\alpha$ radiation to return to a plateau value within ten seconds following a sample change.

Atmospheric absorption is not significant for radiation having a wavelength of about 2.5 angstroms or smaller. It was observed that the transmission of titanium $K\alpha$ radiation (2.75 Å) was considerably diminished by an air atmosphere (a ratio of intensity in helium to

intensity in air of abgut 5 to 1) while the radiation of silicon and aluminum were almost completely absorbed. A helium path was required for silicon and aluminum analysis. The analysis of titanium could have been done with an air atmosphere but due to the low amount of titanium in bauxite a helium atmosphere was used.

3·4·3 SELECTION OF ANALYSER CRYSTAL

The LiF(200) crystal has excellent properties as far as reflectivity, resolution, thermal expansion coefficient and the number of elements for which it can be used. Unfortunately, the practical useful range of this crystal (0.351 Å to 3.84 Å), while being very suitable for the analysis of iron and titanium lines, does not include the long wavelength lines of silicon and aluminum.

The ADP crystal is adaptable for the analysis of the low energy lines. However, it has poor properties of low reflectivity and low resolution especially for the higher energy lines. Added to this is the high background introduced by the phosphorous Kα lines. For these reasons this crystal was expected to be impractical for the analysis in question.

The PET crystal has high reflectivity, moderate resolution and does not emit any secondary radiation. This crystal will diffract radiation having a wavelength as long as 8.40 angstroms which just includes the aluminum Kα line. The iron Kα line is diffracted at a

2 "theta" angle of about 26 degrees which is just about the minimum of the effective range of the spectrometer. Below this angle the intensities fall off because the crystal does not intersect the complete incident radiation beam. The unfavourable qualities of the PET crystal are that it has a large coefficient of thermal expansion, it deteriorates with age and it is quite fragile.

The PET crystal appears to have adequate resolution of the higher energy lines as shown by FIGURE 3·4. The only significant inter-element line interference might be the overlap of the CrKβ line with the FeKα line. However, the chromium line intensity, from the x-ray tube target, does not depend on the sample and would not affect the analysis of iron. Another factor in favour of using the PET crystal, in preference to the LiF crystal for the analysis of iron and titanium, is that the crystal reflectivity is greater. An intensity comparison is shown in FIGURE 3·5 for the FeKα line and in FIGURE 3·6 for the TiKα line. The instrumental parameters, with respect to generator setting, collimation, detection and pulse height analysis, used to obtain these spectral scans were the same as those indicated in TABLE 3·11. A helium atmosphere was not used. Tungsten radiation was used for the excitation of the FeKα line while chromium radiation was used for the excitation of the TiKα line. The intensities diffracted by the LiF crystal with reference to the intensities diffracted by the PET crystal are about 80 percent for the FeKα line and 50 percent for the TiKα line. It was concluded that the PET crystal was the best all around crystal for use in the analysis of bauxite.

FIGURE 3·5

Spectral scans of the iron Kα line (excited by tungsten Kα radiation) using the analyser crystals penta erythritol (PET) and lithium fluoride (LiF).

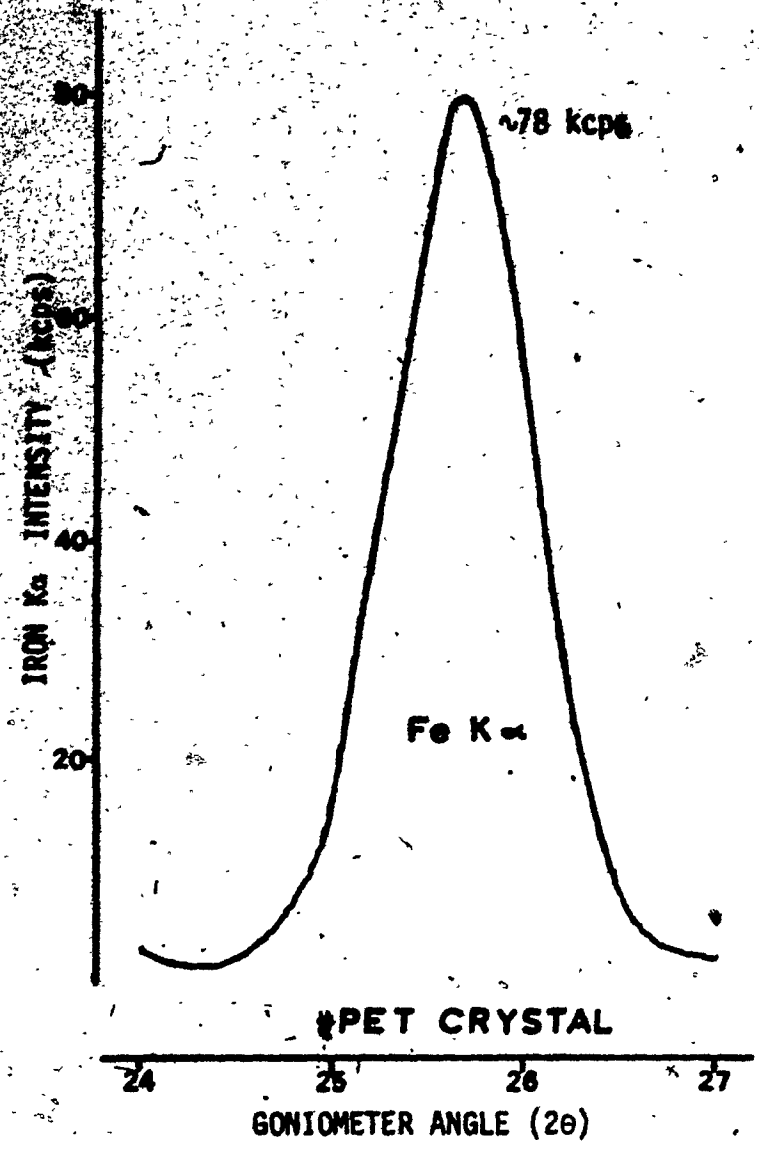
IRON Kα INTENSITY (kcps)
80
60
40
20
~78 kcps
Fe Kα
PET CRYSTAL
24
25
26
27
GONIOMETER ANGLE (2θ)

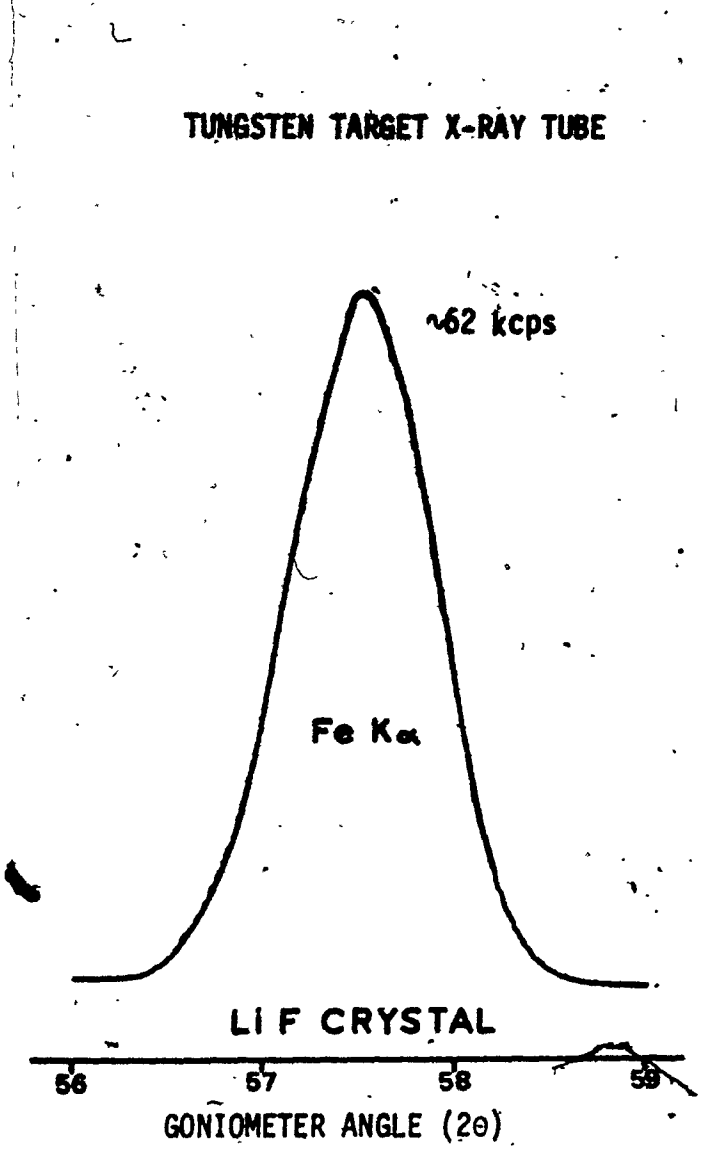
TUNGSTEN TARGET X-RAY TUBE
~62 kcps
Fe Kα
LiF CRYSTAL
56
57
58
59
GONIOMETER ANGLE (2θ)

FIGURE 3-6

Spectral scans of the titanium Kα line (excited by chromium Kα radiation) using the analyser crystals penta erythritol (PET) and lithium fluoride (LiF).

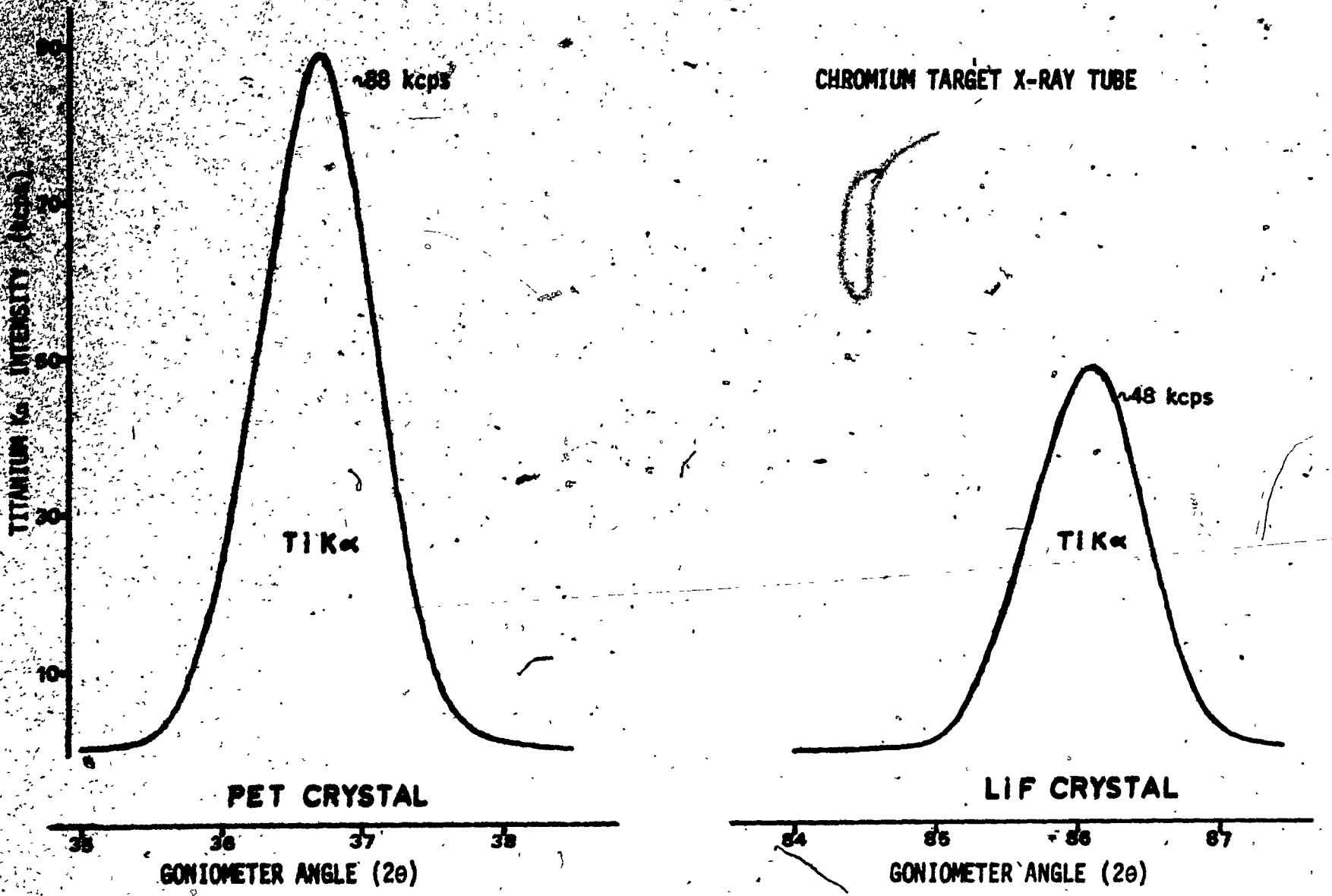
CHROMIUM TARGET X-RAY TUBE
~88 kcps
TiKα
PET CRYSTAL
TITANIUM Kα INTENSITY (kcps)
90
70
50
30
10
35
36
37
38
GONIOMETER ANGLE (2θ)
~48 kcps
TiKα
LIF CRYSTAL
84
85
86
87
GONIOMETER ANGLE (2θ)

3·4·4 SELECTION OF COLLIMATION

The collimation was selected to be coarse due to the premium on intensity for the long wavelength radiation of silicon and aluminum. FIGURE 3·7 shows the difference between coarse and fine collimation on the spectral scan of the FeKα and Kβ lines. Parameters with respect to generator setting, analyser crystal, detection and pulse height analysis were the same as those indicated in TABLE 3·11. It is clear that any resolution problem is eliminated by the fine collimator. Unfortunately, the intensity of the lines is diminished by about 50 percent. It would have been better to use the fine collimator for the analysis of iron and titanium to eliminate any spectral line overlap but for simplicity only one collimator was used for all elements.

3·4·5 SELECTION OF DETECTOR

The gas proportional flow counter (PFC) was chosen in preference to the scintillation counter (SC) for the radiation detection of Al, Si, Ti and Fe. The PFC has the advantage over the SC in that the background noise level is much lower (approximately 0.2 cps for the PFC as opposed to 10 cps for the SC). The detector energy resolution was determined to be about 20 percent for the PFC and about 60 percent for the SC using Fe55 as the radiation source.

The dead time for the PFC is about twice that of the SC. As a result, the PFC linearity is only good up to an intensity of about

FIGURE 3-7

Spectral scans showing the effect of coarse and fine collimation on the intensity and resolution of the iron Kα and Kβ lines using the PET analyser crystal.

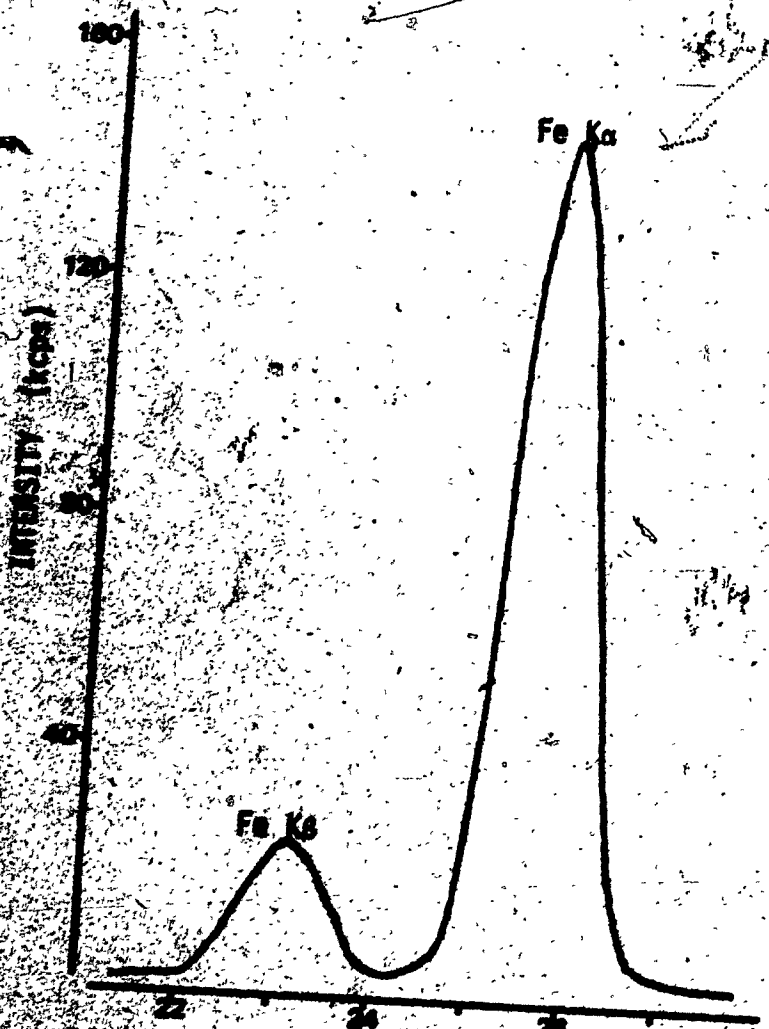

COARSE COLLIMATION

(TUNGSTEN TARGET X-RAY TUBE)

(PET CRYSTAL)

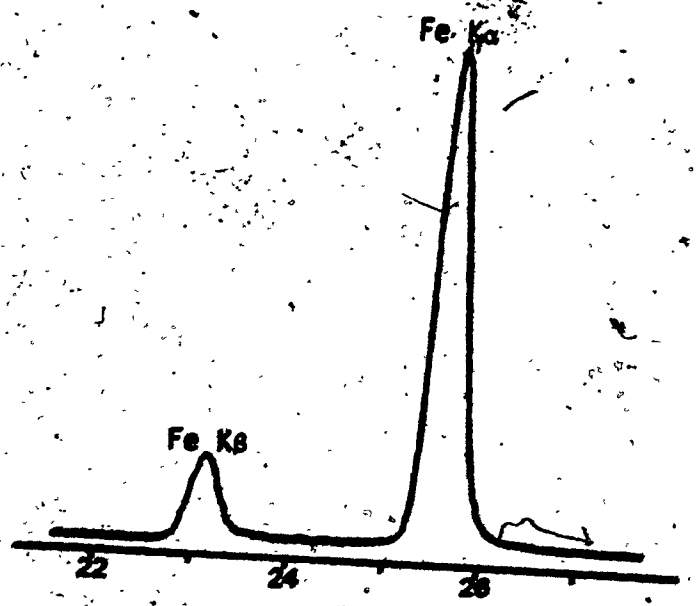

FINE COLLIMATION

50,000 cps while the SC maintains its linearity up to about 100,000 cps. FIGURE 3-8 shows the observed relationship of AlKα intensity as a function of x-ray tube current (high voltage set at 50 kV) for the proportional flow counter.

Finally, and most important, the useful wavelength range of the PFC is 0.7 to 10 angstroms while that of the SC is only 0.1 to 3 angstroms. The SC could not detect the long wavelength radiation of silicon and aluminum. To add to this, the efficiency of the SC is less than the PFC for the detection of iron and titanium radiation[46].

With the selection of the proportional counter, the gas flow rate had to be established. It was noted that with no pulse height selection, variation of the rate of flow of the "P10" gas made little effect on the counting intensity. However, the PFC is well known to display a shift of pulse height distribution towards smaller pulse sizes with increasing counting rate. This presents severe problems when the analysis scheme depends heavily on well defined limits of pulse height distribution. It has been shown[47] that this shift can be reduced by decreasing the rate of flow of the counter gas. Of course there is a minimum gas flow below which the counter does not operate properly.

The warm up time must also be considered. The lower the flow rate the longer the period required to completely flush out the gas chamber. In the case of bauxite analysis it was found unnecessary to apply stringent limits on the pulse height selection due to the lack of interfering lines. A short warm up period was desired in preference to

FIGURE 3-8

Observed intensity of the aluminum Kα line as a function of the intensity of the primary excitation source (chromium Kα) using the gas proportional flow counter.

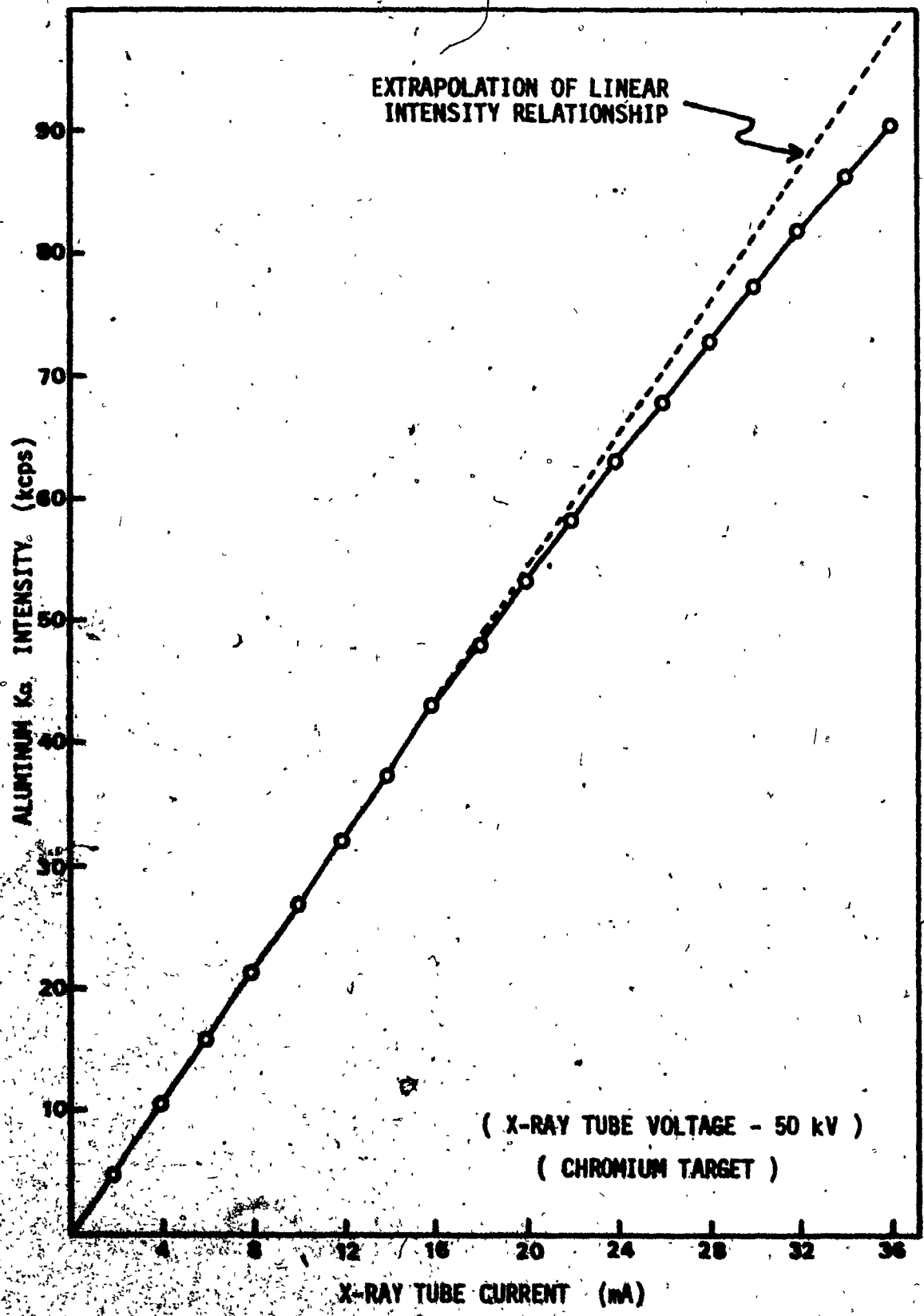
EXTRAPOLATION OF LINEAR
INTENSITY RELATIONSHIP
ALUMINUM Kα INTENSITY (kcps)
90
80
70
60
50
40
30
20
10
(X-RAY TUBE VOLTAGE - 50 kV)
(CHROMIUM TARGET)
4
8
12
16
20
24
28
32
36
X-RAY TUBE CURRENT (mA)

a small pulse height window. The usual range of gas flow rate varies from 0.05 to 0.5 cfh and for this investigation the flow of the "P10" gas was set at 0.25 cfh.

3-4-6 SELECTION OF POWER SETTINGS FOR THE X-RAY TUBE

Once the x-ray tube and detector had been selected it was necessary to determine the power settings (kV and mA) of the high voltage supply to the x-ray tube. Establishment of these parameters first involves the consideration of the absorption edge energies of the elements being investigated and second involves the dead time of the detection system.

As mentioned previously, the x-ray spectral lines for any element can be excited when the potential of the x-ray tube exceeds the excitation potential or absorption edge potential of that element. Below this potential there is no excitation of secondary spectra. However, unless the applied potential is considerably larger than the absorption edge energy, the excitation process is inefficient. Above this potential (3 to 4 times the absorption edge energy) the excitation is much more effective resulting in more intense spectra. The K absorption edge energies for aluminum, silicon, titanium and iron have been shown in TABLE 3-8. Choosing a factor of four, the minimum applied high voltage settings for effective spectral excitation of these elements were determined to be 6.236 kV for Al, 7.362 kV for Si, 19.860 kV for Ti and 28.448 kV for Fe. As the analysis of bauxite ore samples was

restricted to the determination of just these four elements it was obvious that there would be no problem with insufficient excitation of secondary x-ray spectra; the minimum kV requirements being easily obtainable with the equipment at hand.

For the analysis of aluminum, due to poor efficiency of excitation by the primary x-ray beam (see TABLE 3-10) and atmospheric absorption of low energy radiation, it was deemed necessary to operate the x-ray generator at maximum allowable power (50kV and 36mA) even though the average bauxite sample contains about 25 percent aluminum. A similar generator setting when applied to the determination of titanium would result in exceptionally high counts even for the low percentages of this element (less than 3 percent) that occur in bauxite ores.

It was desired to select generator operating conditions such that the intensity of any analyte line being examined would not be so great as to cause a loss of linearity and choking effect of the detector. The need to apply dead time correction methods is thus eliminated. This presents the second consideration. As described before (see FIGURE 3-8) the proportional flow counter begins to deviate from linearity for counting rates above 50,000 cps. The generator settings were selected accordingly.

Adjustments of the generator settings were carried out while examining samples containing high concentrations of the elements. From the seventy bauxite samples, four were selected to represent the maximum concentration for each of the four elements. These samples were

DM CAA (#17) for aluminum containing 60.3 percent Al_2O_3, DM CAJ (#23) for silicon containing 60.5 percent SiO_2, BK 20497 (#49) for titanium containing 5.61 percent TiO_2 and DM CAR (#29) for iron containing 53.7 percent Fe_2O_3. It was decided to use a high voltage setting not lower than 40 kV to ensure efficient x-ray excitation. The maximum allowable counting rate was selected to be 40,000 cps to ensure detector linearity. TABLE 3·12 shows the final generator settings determined for the four elements along with the corresponding Kα radiation intensities.

3·4·7 SELECTION OF GONIOMETER ANGLES

To this point there was no optimization of the goniometer settings. With the establishment of the parameters of x-ray generation, radiation path atmosphere, dispersion, collimation and detection it was now necessary to accurately determine the angles of the goniometer at which the intensity of the characteristic radiation would be measured.

First a choice had to be made as to which spectral line would be used for the analysis of the elements. A spectral scan covering the complete range of the spectrometer was procured for the NBS 69A bauxite sample. With the PET analyser crystal and a 2 "theta" range of 20 degrees to 147.7 degrees this spectrum included the wavelengths of 1.52 Å to 8.40 Å for first order lines and proportionate wavelengths of second, third and fourth order lines.

The higher energy region of the spectrum (FIGURE 3·4) appears

TABLE 3-12

X-RAY GENERATOR SETTINGS

Element	Al	Si	Ti	Fe
Sample	DM CAA	CM CAJ	DK 20497	DM CAR
% Element	31.91	28.28	3.36	37.56
kV	50	50	40	40
mA	36	36	10	20
K_α count rate cps	15K	16K	34K	37K

somewhat congested with a fairly high background intensity (about 500 cps). For this reason the possibility of using higher order lines was examined for the determination of intensities for iron and titanium. The background intensity for the second order lines of iron and titanium was considerably lower than the first order lines by a factor of 10 to 20. However, the peak intensities were similarly diminished resulting in approximately the same peak to background ratios. For the second order lines the spectra are spread out more; but, as mentioned before, there seemed to be no significant spectral line overlap of the first order lines. The conclusion was made that there was no advantage to use the second order lines in preference to the first order lines. Similarly there was no advantage to use any Kβ lines instead of the Kα lines. Thus the first order Kα lines were selected for the analysis of all the elements.

For each spectral line there were four angles that had to be determined. First the "omega" and 2 "theta" angles were adjusted in succession to give a maximum radiation intensity at the peak position. Then a 2 "theta" scan about the central peak position was obtained in order to select the 2 "theta" angles, on each side of the peak, at which background intensity counts would be measured. The resultant angles are shown in TABLE 3-13. Where possible, the background counts were taken about 3 degrees on either side of the central peak maximum. With the exception of both sides of the silicon Kα line and the lower energy side of the titanium Kα line it was necessary to take background readings nearer to the peak angle due to the close proximity of other

TABLE 3-13

GONIOMETER ANGLES (PET CRYSTAL)

Element	Al	Si	Ti	Fe
ω	+0.05°	+0.05°	+0.05°	+0.05°
Peak 2θ	145.42°	109.42°	36.87°	25.80°
$Bg_1 2\theta$	143.70°	106.42°	35.10°	24.36°
$Bg_2 2\theta$	147.50°	112.42°	39.50°	26.96°

spectral lines. In these cases each background angle was selected at the point of minimum intensity between the spectral lines.

3·4·8 SELECTION OF PULSE HEIGHT ANALYSER SETTINGS

The next step was the selection of the low and high energy limits for the pulse height analysis. For bauxite ore it was considered that the use of pulse height selection was not required. Since the concentrations of any element other than Al, Si, Ti or Fe were of little significance, it was expected that the intensity of any resultant spectral line would be negligible. For each element (Kα line) an energy scan using a 0.2 keV energy window was determined. It was noted for all four elements that there were no interfering spectral lines near the characteristic wavelengths of the elements. Nevertheless, pulse height selection was employed with a very wide energy window to reduce the background noise level.

Keeping in mind the shift of the pulse height distribution with count rate, the pulse height analysis energy limits were selected accordingly. From the complete group of bauxite samples for each element three samples, representing the minimum, average and maximum concentrations for that element, were used to evaluate the actual variation of the pulse height. The samples of maximum concentration had been previously selected for the determination of the high voltage generator settings. Eight additional selections were required. The four samples representing the average concentrations were DM CAI (#22) for Al containing 41.8% Al_2O_3,

DH CAA (#17) for Si containing 2.1% SiO_2, NBS 69A (#13) for Ti containing 2.78% TiO_2 and JM 922 (#12) for Fe containing 20.2% Fe_2O_3. The four samples representing the minimum concentrations were Dm CAJ (#23) for Al containing 3.3% Al_2O_3, JM 453 (#1) for Si containing 0.33% SiO_2, DH CAJ (#23) for Ti containing 0.8% TiO_2 and CH CAI (#22) for Fe containing 0.2% Fe_2O_3.

The gain selector was set at 5 for all elements. Calibration of the pulse height analyser was performed by adjusting the detector high voltage to give maximum intensity with the PHA (0.2 keV window) set at the energy of the spectral line. The sample used for the calibration procedure was the average concentration sample. The pulse height distributions were obtained by scanning the energy from 10 keV to zero with the 0.2 keV window. TABLE 3-14 shows fifteen pulse height distributions that were obtained for the $K\alpha$ radiations. In addition to the twelve selected samples, the distribution of another sample of intermediate concentration for each of Si, Ti and Fe was included. The five values that are shown for the distribution represent the energy (1) where the peak reaches the baseline (low energy side), (2) at the peak half-height (low energy side), (3) at the peak maximum, (4) at the peak half-height (high energy side) and (5) where the peak reaches the baseline (high energy side). From this data the upper and lower energy levels of the pulse height selector were determined as indicated as follows:

TABLE 3-14

PULSE HEIGHT DISTRIBUTIONS

SAMPLE	ELEMENT	% ELEMENT	PULSE HEIGHT DISTRIBUTION* (1)	(2)	(3)	(4)	(5)
DM CAA (#17)	Al	31.91	0.8	1.1	1.4	1.7	2.7
DM CAI (#22)	Al	22.12	0.8	1.2	1.5	1.8	2.8
DM CAJ (#23)	Al	1.75	0.8	1.4	1.7	2.1	3.0
DM CAJ (#23)	Si	28.28	0.7	1.2	1.4	1.8	2.8
DM CAG (#20)	Si	13.46	1.0	1.4	1.7	2.0	3.0
DM CAA (#17)	Si	0.98	1.2	1.6	1.9	2.3	3.0
JM 453 (#1)	Si	0.15	1.4	1.7	2.0	2.3	2.6
BK 20497 (#49)	Ti	3.36	2.2	3.7	4.2	4.8	5.8
DM CAG (#20)	Ti	2.28	2.4	3.9	4.4	4.9	6.0
NBS 69A (#13)	Ti	1.67	2.6	4.0	4.5	5.0	6.2
DM CAJ (#23)	Ti	0.48	3.6	4.4	5.0	5.5	6.4
DM CAR (#29)	Fe	37.56	1.0	4.3	5.1	6.1	7.8
JM 922 (#12)	Fe	14.13	4.6	5.6	6.3	7.2	8.6
NBS 69A (#13)	Fe	4.07	5.4	6.6	7.3	8.2	9.4
DM CAI (#22)	Fe	0.14	6.0	7.3	8.0	8.7	9.6

*pulse height in units of keV

	Lower Level (keV)	Upper Level (keV)
Al	0.5	3.0
Si	0.5	3.0
Ti	0.7	8.5
Fe	1.0	9.5

3.4.9 SELECTION OF COUNTING STANDARDS

Finally a set of four counting standards, one for each element, were selected. These samples were used throughout the investigation to correct for any intensity error caused by instrumental drift. This error may be due to a fluctuation of the power, temperature, humidity or any other such factor. The intensity of the counting standard was measured after every three other samples being examined. If the counting standard intensity either increased or decreased then the corresponding intensities of the other samples were mathematically corrected down or up by the same relative amount. Correction was made for both peak and background counts. For the examination of background count drift, the limitation on the frequency of measurement of the standard was relaxed in some cases.

Originally one sample (NBS 69A) was chosen for the counting standard of all elements. However, it was realized that the counting standard should have a high secondary radiation intensity in order to lessen the relative counting error. For silicon, titanium and iron the samples containing the maximum amounts of the respective elements

(DM CAJ, BK 20497, DM CAR) were selected for standards. The NBS 69A sample was retained as the counting standard for the aluminum radiation.

3.4.10 SELECTION OF THE MODE OF DATA COLLECTION

The fixed time mode of data collection was employed in preference to fixed count mode for simplicity and convenience due to the direct relationship between the actual data values and the concentrations of the elements in the samples. With the exception of silicon analysis, all counting times were 10 seconds. The low percentages of silicon required longer periods in order to acquire sufficient counts to reduce the counting error. A 10 second count was retained for samples containing more than 30 percent SiO_2. For samples containing between 10 and 30 percent SiO_2 a 20 second counting time was selected while for samples with less than 10 percent SiO_2 a 50 second count was employed. It was not practical to take counts for periods longer than 50 seconds.

3.4.11 FINAL INSTRUMENT PARAMETERS (SUMMARY)

The final set of instrumental parameters for the XRF spectrochemical analysis of Al, Si, Ti and Fe in bauxite ore is shown in TABLE 3.15. The value shown for the detector high voltage is only an approximate value since the pulse height analyser was recalibrated, by slight variation of this voltage (maximum ± 10 Volts), each time data was collected for any particular element.

TABLE 3-15

INSTRUMENT PARAMETERS (FINAL)

ELEMENT		Al	Si	Ti	Fe
TUBE TARGET		Cr	Cr	Cr	Cr
	kV	50	50	40	40
	mA	36	36	10	20
SAMPLE ROTATION		ON	ON	ON	ON
HELIUM FLOW		5 cfh	5 cfh	5 cfh	OFF
CRYSTAL		PET	PET	PET	PET
COLLIMATOR		COARSE	COARSE	COARSE	COARSE
DETECTOR		PFC	PFC	PFC	PFC
P10 FLOW		0.25 cfh	0.25 cfh	0.25 cfh	0.25 cfh
HIGH VOLTAGE DETECTOR	~ 3.72 HELIPOT	1.690 kV	1.690 kV	1.690 kV	1.690 kV
PHA	GAIN	5	5	5	5
	MODE	100%	100%	100%	100%
	UPPER LEVEL	3.00	3.00	8.50	9.50
	LOWER LEVEL	0.50	0.50	0.70	1.00
ANGLES (degrees)					
	ω	+0.05	+0.05	+0.05	+0.05
	2θ Peak	145.42	109.42	36.87	28.50
	2θ Background 1	143.70	106.42	35.10	24.36
	2θ Background 2	147.50	112.42	39.50	26.96
COUNTING STANDARD		NBS 69A	DM CAJ	BK 20497	DM CAR
	PEAK COUNTS/sec.	14,000	16,000	34,000	37,000
	Bg1 COUNTS/sec.	860	77	245	440
	Bg2 COUNTS/sec.	250	50	63	550
COUNTING TIME		10 sec.	10 sec. > 30% 20 sec. 10-30% 50 sec. < 10%	10 sec.	10 sec.

3·4·12 DATA COLLECTION PROCEDURE

The general procedure of data acquisition and handling, after sample preparation, involved the set up of the appropriate parameters suitable for the determination of the element in question. Subsequently, for any one lot of samples, the radiation measurements were obtained for all samples at each goniometer angle. That is, for each element in turn all samples were analysed first at the peak angle then at the two background angles. This was done to eliminate any error that may be caused by the adjustment of the goniometer angle. All counts were repeated five times for each specimen. The reported intensities represent the average count of these readings. After collection of the raw data the peak intensities were corrected for instrumental drift, background intensity and different counting times to give net corrected intensities in counts per second. The instrumental drift correction was carried out by the application of EQUATION 3·2.

$$I' = I \times \frac{Is}{1/2\,(Is_1 + Is_2)} \qquad 3\cdot2$$

where:

- I' is the intensity corrected for instrumental drift;
- I is the actual measured intensity;
- Is is the established constant intensity of the counting standard;

Is_1 is the measured intensity of the counting standard taken before the measurement of the sample;

Is_2 is the measured intensity of the counting standard after the measurement of the sample.

The correction for background intensity involved the use of EQUATION 3-3.

$$I_{MEAS} = IPk - \left[IBg_1 + \frac{2\theta Bg_1 - 2\theta Pk}{2\theta Bg_1 - 2\theta Bg_2} (IBg_2 - IBg_1)\right] \qquad 3\text{-}3$$

where:

I_{MEAS} is the net corrected intensity;

IPk is the intensity measured at the peak position;

IBg_1 is the intensity measured at the first background position;

IBg_2 is the intensity measured at the second background position;

2θPk is the 2θ angle of the peak position;

2θBg is the 2θ angle of the first background position;

2θBg is the 2θ angle of the second background position.

The x-ray spectral results are tabulated in APPENDIX A for all the bauxite samples. Included in these tables are the errors inherent in the concentrations of the elements. These errors were determined from the Alcan tolerance limits at the 85 percent confidence level. The net XRF intensities represent the average intensity that has been corrected for instrument drift and background intensities. The relative

counting error represents the error in the average intensity at the 99.7 percent confidence level (3σ). For direct comparison with the relative concentration error it is necessary to multiply the relative counting error by a factor of 0.48 since the 85 percent confidence level is only 1.44σ. Only nine of the 280 net average intensities acquired show a relative counting error greater than 5 percent (3σ).

The intensity vs concentration plots of the x-ray data are shown in FIGURES 3-9 to 3-12. An obvious trend is observed in the analysis for silicon and iron. The SiKα intensity plot deviates toward a higher intensity at higher concentrations. The FeKα intensity plot deviates toward a lower intensity at higher concentrations. The plot for TiKα intensity appears to be similar to the FeKα intensity plot. However, the titanium concentration does not exceed 6% and no definite conclusions may be made. It is noted that the data for AlKα is very scattered which eliminates any conclusion concerning the matrix effect on aluminum. The large scattering is postulated to be partially due to the errors inherent in the by-difference concentration values for the alumina content.

The sampling error was determined for the Jamaica series of bauxite samples. Three briquettes had been prepared for each of the twelve samples. TABLE 3-16 shows for each element the standard deviation (σ) and the relative standard deviation (ϵ) for the average count of each briquette. For each sample the standard deviations are shown in TABLE 3-17. It can be seen by comparison of TABLE 3-16 and TABLE 3-17

FIGURES 3-9 to 3-12

Relationship of x-ray intensity (measured) and the known concentrations for the determination of the principal elements in bauxite (Al, Si, Ti and Fe).

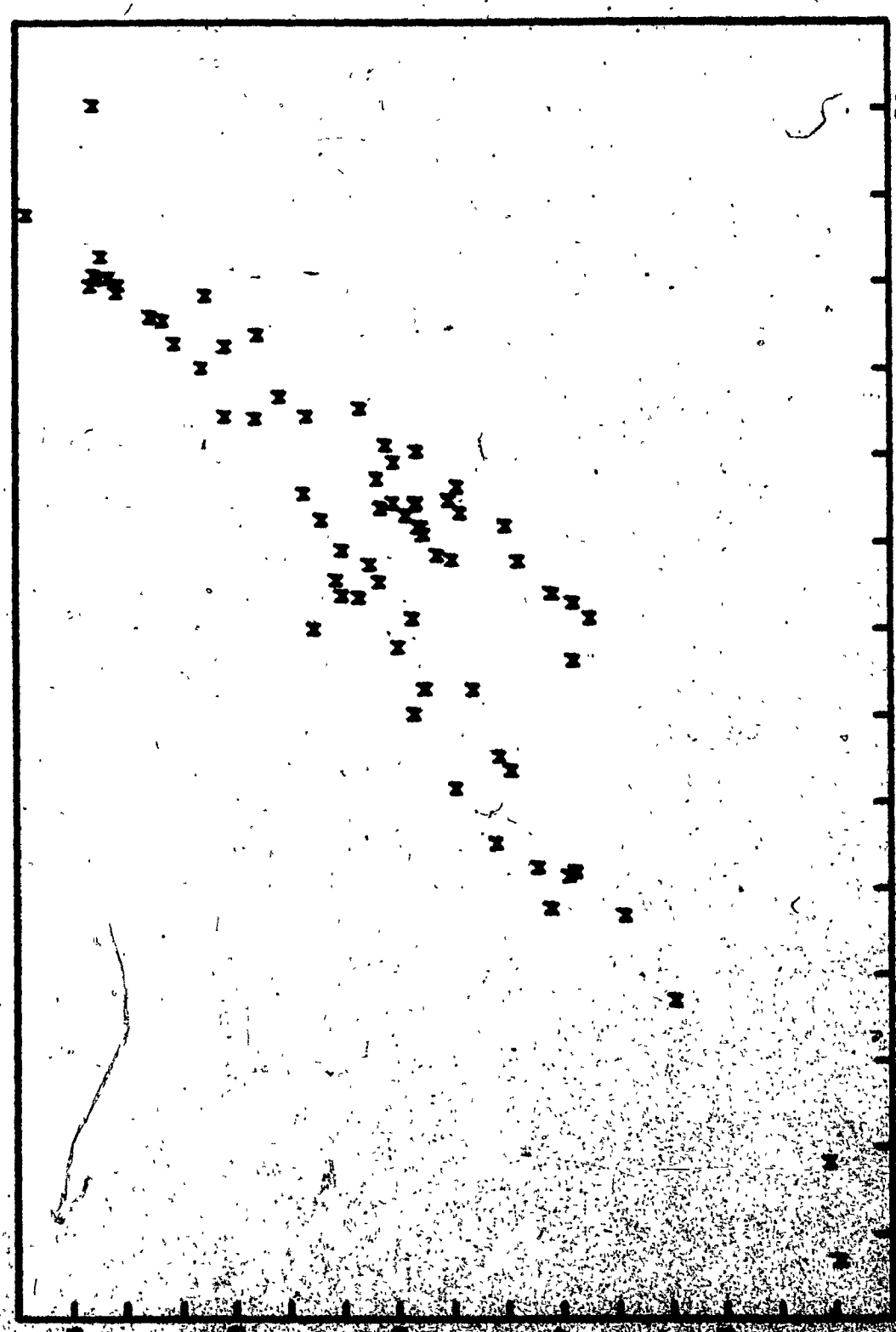
MEASURED AT Kα INTENSITY (kcps)
KNOWN CONCENTRATION OF Al_2O_3 (%)

FIGURE 3-9

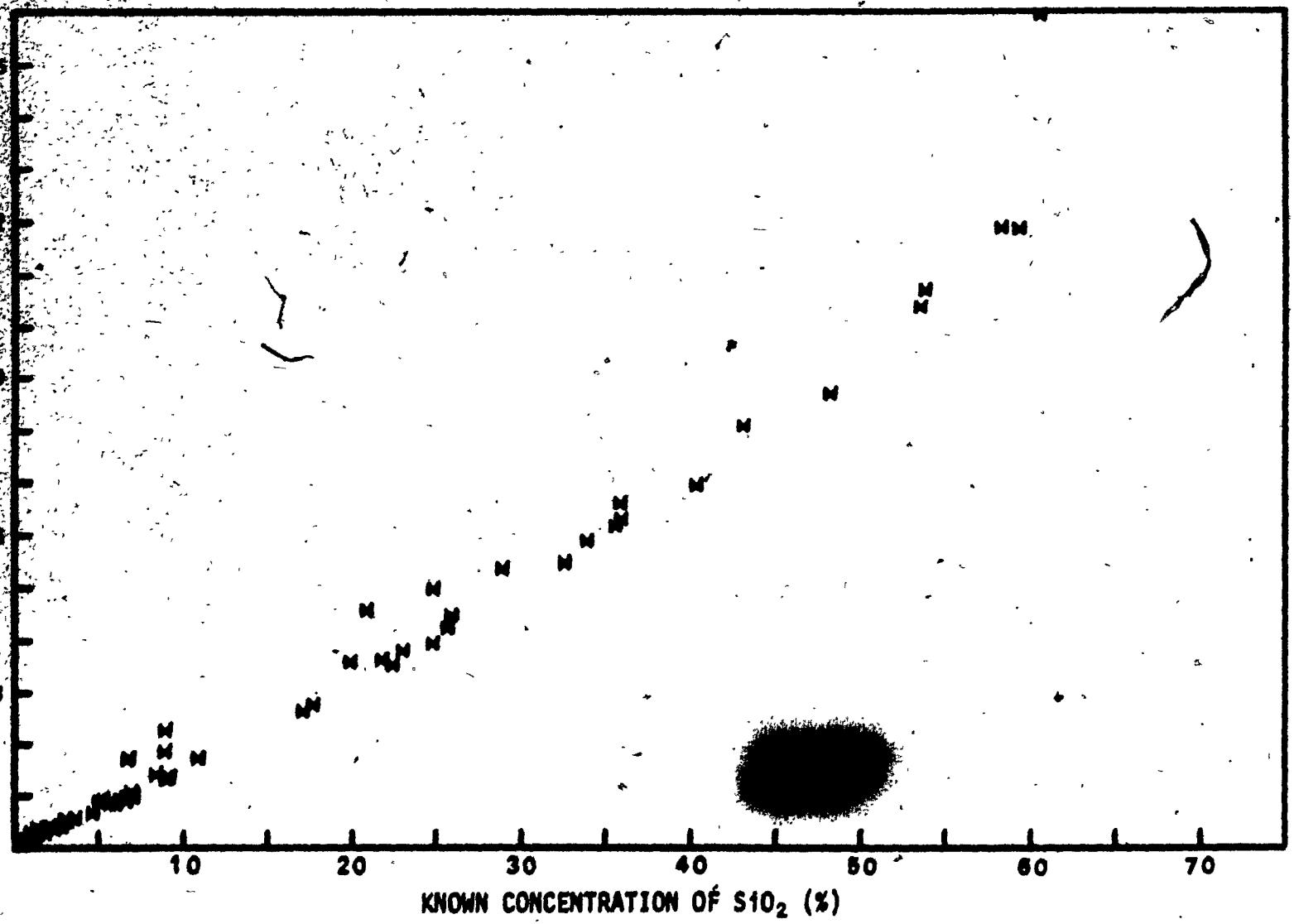
MEASURED Si Kα INTENSITY (kcps)
15
12
9
6
3
10
20
30
40
50
60
70
KNOWN CONCENTRATION OF SiO_2 (%)

FIGURE 3-10

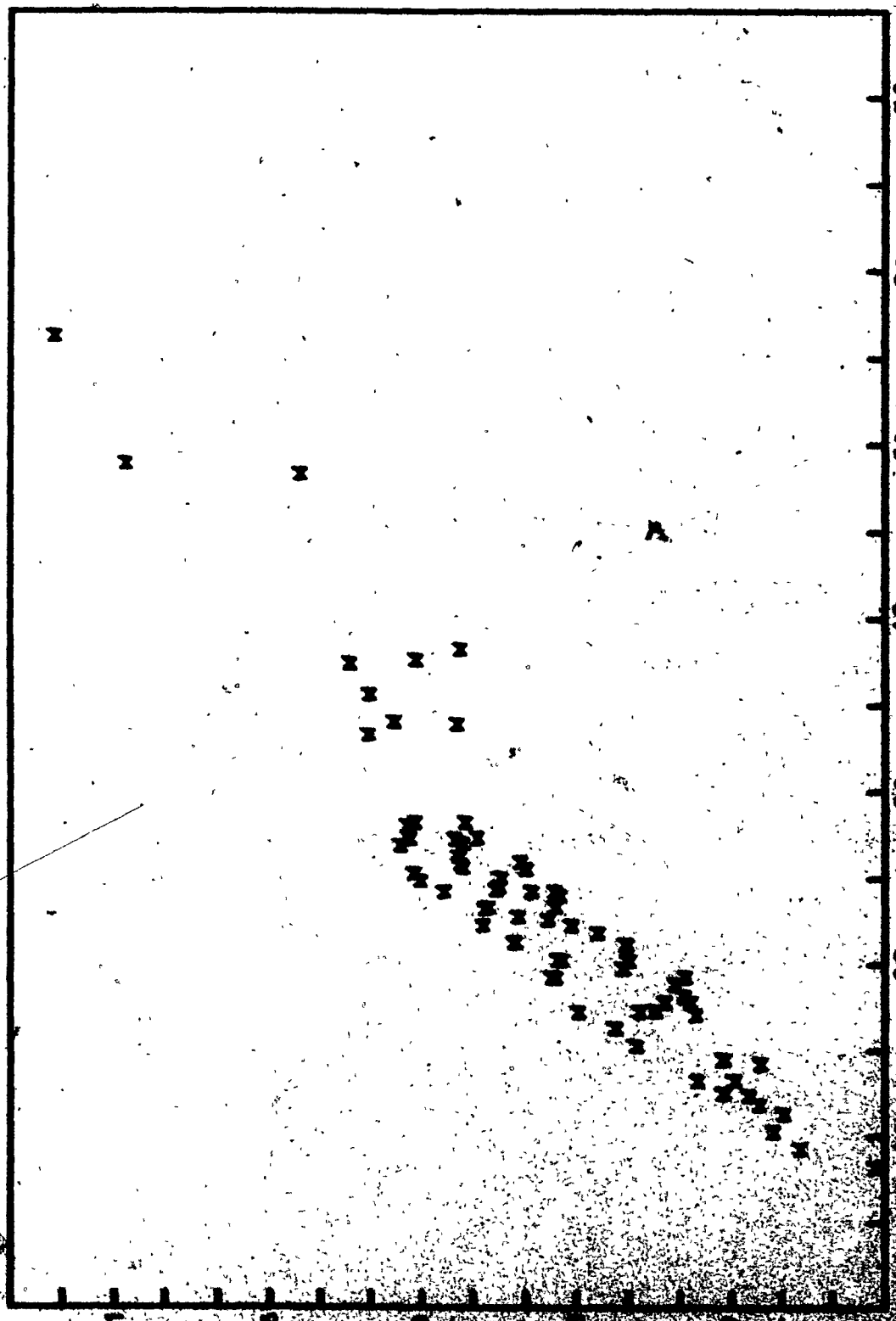

FIGURE 3.11

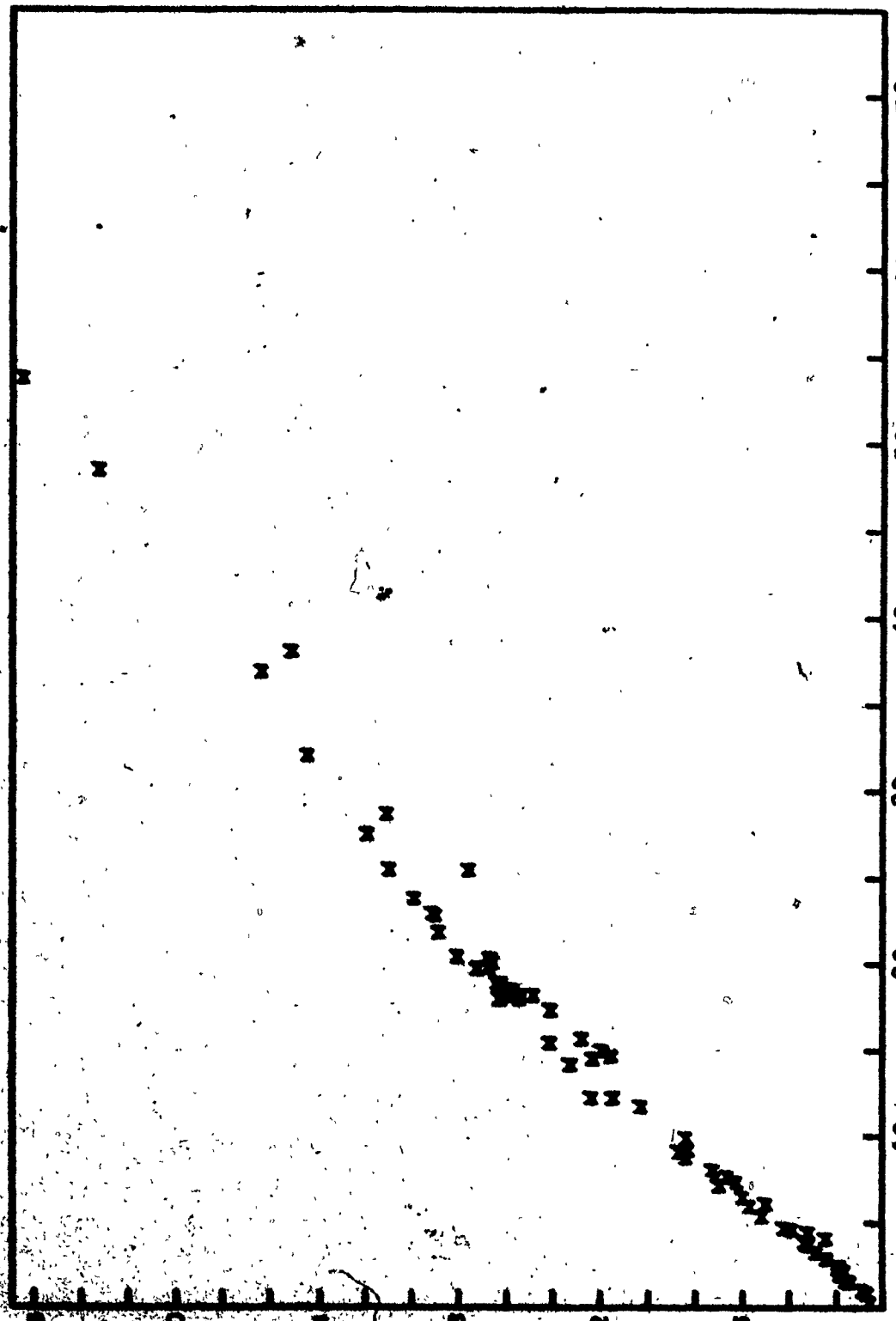
MEASURED Fe Kα INTENSITY (kcps)
0
6
12
18
24
30
36
KNOWN CONCENTRATION OF Fe_2O_3 (%)
10
20
30
40
50
60
70

FIGURE 3-12

TABLE 3-16

EMPIRICAL COUNTING ERRORS - JAMAICA SAMPLES

	Al		Si		Ti		Fe	
Sample	σ cps	3ε	σ cps	3ε	σ cps	3ε	σ cps	3ε
1 A	53	1.61	7	7.43	34	.32	44	.83
B	14	.40	4	4.23	62	.60	59	1.12
C	23	.68	4	4.83	33	.31	50	.97
2 A	55	1.69	10	2.78	54	.56	31	.67
B	14	.43	11	3.21	43	.44	18	.39
C	48	1.48	13	3.46	73	.75	67	1.44
3 A	29	.98	22	1.68	68	.77	58	1.20
B	33	1.10	19	1.43	34	.39	54	1.11
C	49	1.65	17	1.32	58	.66	35	.71
4 A	49	1.48	20	2.63	58	.65	27	.55
B	28	.83	19	2.51	23	.26	20	.39
C	47	1.41	11	1.40	35	.39	27	.54
5 A	56	1.76	17	1.36	74	.83	18	.37
B	57	1.82	8	.65	36	.40	46	.94
C	30	.95	22	1.79	58	.65	48	.97
6 A	17	.54	6	3.88	34	.40	46	.90
B	22	.71	4	2.55	55	.65	38	.74
C	25	.82	5	3.02	46	.55	36	.70
7 A	20	.63	4	5.61	57	.50	37	.70
B	39	1.26	5	5.94	26	.23	45	.87
C	26	.83	4	5.48	57	.50	30	.58
8 A	32	1.00	4	9.83	47	.49	37	.73
B	40	1.24	4	9.56	17	.18	22	.44
C	10	.30	3	7.97	31	.32	28	.55
9 A	30	1.03	22	1.54	18	.22	43	.81
B	24	.82	18	1.26	46	.58	36	.67
C	40	1.38	11	.78	29	.37	74	1.37
10 A	41	1.34	28	1.44	73	.85	62	1.28
B	44	1.43	19	.97	18	.22	52	1.07
C	30	.99	24	1.22	54	.63	17	.35
11 A	30	.97	16	2.30	53	.57	46	.90
B	10	.33	15	2.20	24	.26	36	.71
C	19	.61	12	1.78	77	.83	76	1.50
12 A	47	1.51	7	1.22	47	.49	20	.38
B	42	1.35	6	1.18	40	.42	58	1.02
C	32	1.03	10	1.93	37	.39	41	.79
AVERAGE	33	1.07	12	3.12	45	.49	41	.81

TABLE 3-17

SAMPLING ERROR - JAMAICA SAMPLES

SAMPLE	Al		Si		Ti		Fe	
	σ	3ε	σ	3ε	σ	3ε	σ	3ε
1	127	3.80	9	9.68	55	.52	74	1.42
2	17	.53	23	6.49	78	.80	32	.69
3	14	.45	28	2.11	71	.80	95	1.96
4	27	.80	5	.60	46	.51	74	1.50
5	32	1.02	14	1.16	74	.83	39	0.79
6	7	.21	4	2.44	22	.25	9	.38
7	21	.66	4	4.70	69	.60	20	.39
8	38	1.18	4	9.47	29	.30	20	.39
9	13	.45	2	.11	15	.19	29	.53
10	15	.47	5	.23	17	.20	10	.21
11	14	.43	3	.44	18	.20	49	.96
12	8	.27	3	.60	29	.31	46	.89
AVERAGE	28	.86	9	3.17	44	.46	41	.82

σ in cps

that on the average the sampling error is about the same as the counting error for all four elements. In both cases the same trend is observed with the error decreasing in the series Si >> Al > Fe > Ti.

The detection limits were considered for each of the components in bauxite. These were determined from four selected samples covering the range of concentration for each element. The detection limit was considered as the concentration equivalent of the 3σ counting error for the background intensity. The method of calculation[48] is indicated in TABLE 3·18.

The complete set of detection limits can be found in TABLE 3·19. It was noted, with the exception of the smallest concentration of titanium, that the detection limit became smaller as the concentration decreased. This variation was attributed to a sample matrix effect. The average detection limits for bauxite were determined to be 0.017% Fe_2O_3, 0.002% TiO_2, 0.012% SiO_2 and 0.087% Al_2O_3.

TABLE 3-18

DETECTION LIMIT DETERMINATION

SAMPLE	NBS 69A	
CONCENTRATION	5.82% Fe_2O_3	
peak intensity	51460	counts
background intensity	1380	counts
net intensity	50080	counts
counts per percent Fe_2O_3	8607	
background (3σ) error	111	counts

DETECTION LIMIT = 111 / 8607 = 0.013% Fe_2O_3

TABLE 3-19

DETECTION LIMITS

	SAMPLE	%	PEAK COUNTS	BACKGROUND COUNTS	BACKGROUND 3σ	DETECTION LIMIT(%)
Fe_2O_3	DM CAR	53.7	386290	5370	220	0.031
	JM 454	18.1	137870	2240	142	0.019
	NBS 69A	5.82	51460	1380	111	0.013
	DM CAI	0.20	4030	1010	95	0.005
TiO_2	DM CAG	3.80	174300	970	93	0.002
	NBS 69A	2.78	129880	1260	106	0.002
	JM 454	2.70	170840	1190	103	0.002
	DM CAJ	0.80	13430	340	55	0.003
SiO_2	DM CAJ	60.5	160050	660	77	0.029
	NBS 69A	6.01	39530	280	50	0.008
	JM 454	1.44	11100	230	45	0.006
	JM 453	0.33	2900	170	39	0.004
Al_2O_3	NBS 78	70.0	159780	6820	248	0.109
	NBS 69A	55.0	125960	5710	227	0.099
	JM 454	47.2	93090	4290	196	0.099
	DM CAR	8.9	20620	930	91	0.039

CHAPTER 4

PARTICLE SIZE EFFECTS

4-1 INTRODUCTION

The investigation of matrix effects and matrix effect corrections would only be feasible if the particle size level of the sample was such that the particle size effect would be a minimum. For this reason the first phase of the program involved the investigation of particle size effects.

The preliminary evaluation of the effect of particle size involved a review of the types of sample materials and their absorption properties as they relate to x-ray penetration depths. Experimentally, the initial step was an attempt to determine a particle size effect by the examination of sieved fractions of a pure homogeneous material. In this manner there would be no interference due to compositional variation. The second step was the investigation of sieved fractions of bauxite material. The third and final step involved grinding a coarse sample of bauxite for successive periods of time until a very small particle size (hence minimum particle size effect) was obtained.

4·2 EXPERIMENTAL RESULTS AND DISCUSSION

4·2·1 DEPTH OF PENETRATION

The importance of the x-ray penetration depth with respect to particle size effects (see SECTION 2·5·1) required an initial theoretical examination of the absorption properties of the sample materials. Consideration was given to the penetrating power of the primary chromium Kα radiation and of the characteristic secondary-emission Kα radiations of aluminum, silicon, titanium and iron. The penetration depth calculations were carried out using the Lambert equation (EQUATION 2·6). The selection of sample materials includes the oxides (Al_2O_3, SiO_2, TiO_2, Fe_2O_3) of the four elements and a hypothetical bauxite sample having a composition as follows :-

25% Al	(47.2% Al_2O_3)
3% Si	(6.4% SiO_2)
2% Ti	(3.3% TiO_2)
10% Fe	(14.3% Fe_2O_3)
55% O	
5% H and trace elements	

The relationships of x-ray intensities as a function of sample depth is shown in FIGURES 4·1 to 4·5. The depth at which the x-ray intensity diminished to 0.1% of the incident intensity was assumed to be the penetration depth. TABLE 4·1 gives the calculated penetration depths

FIGURES 4·1 to 4·5

Relationship of x-ray intensity as a function of the depth of material (bauxite, Al_2O_3, SiO_2, TiO_2, Fe_2O_3) for :-

4·1 chromium Kα radiation,

4·2 aluminum Kα radiation,

4·3 silicon Kα radiation,

4·4 titanium Kα radiation,

4·5 iron Kα radiation.

FIGURE 4-1

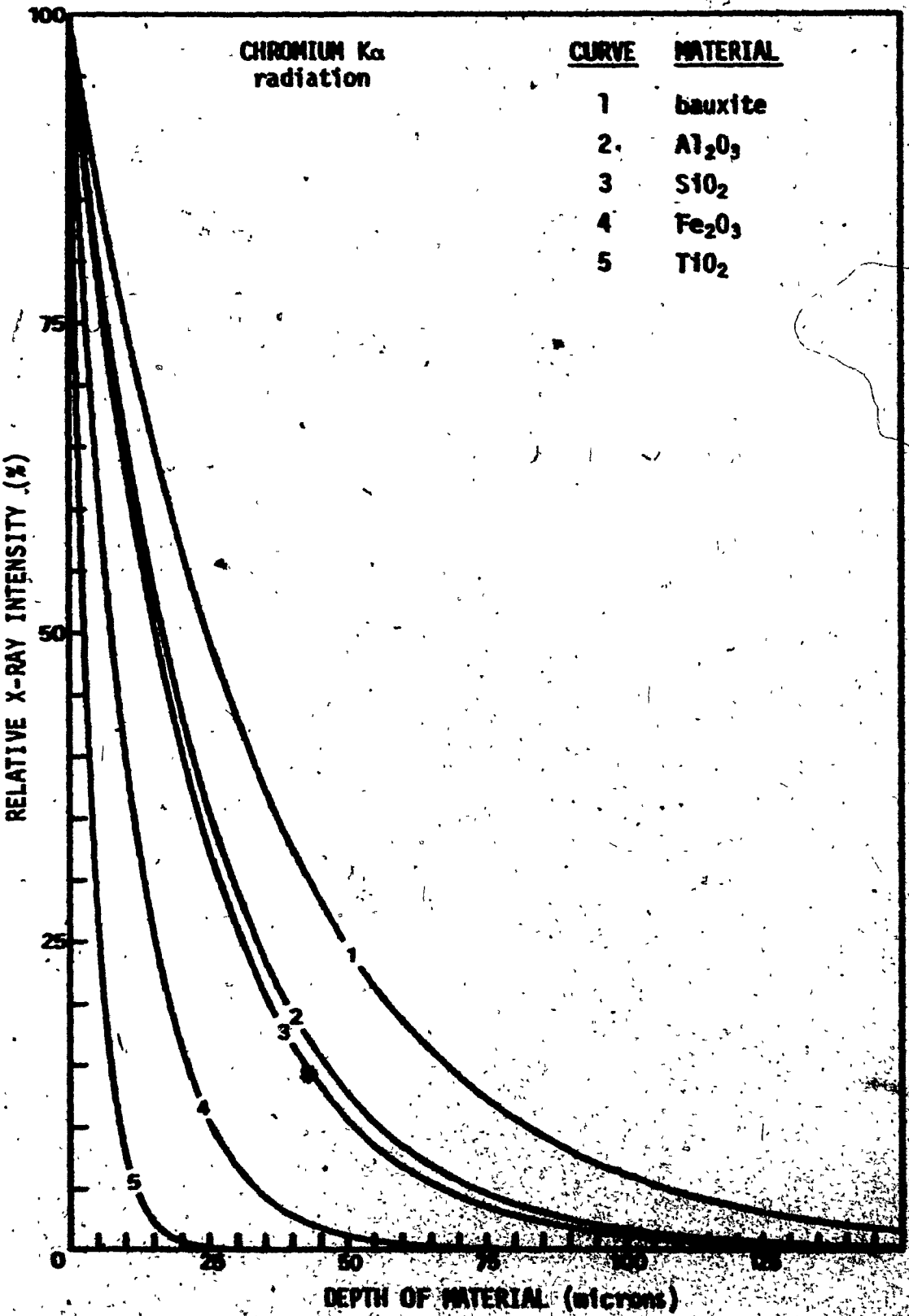
CHROMIUM Kα radiation
CURVE MATERIAL
1 bauxite
2 Al_2O_3
3 SiO_2
4 Fe_2O_3
5 TiO_2
RELATIVE X-RAY INTENSITY (%)
100
75
50
25
0
25
50
75
DEPTH OF MATERIAL (microns)

FIGURE 4-2

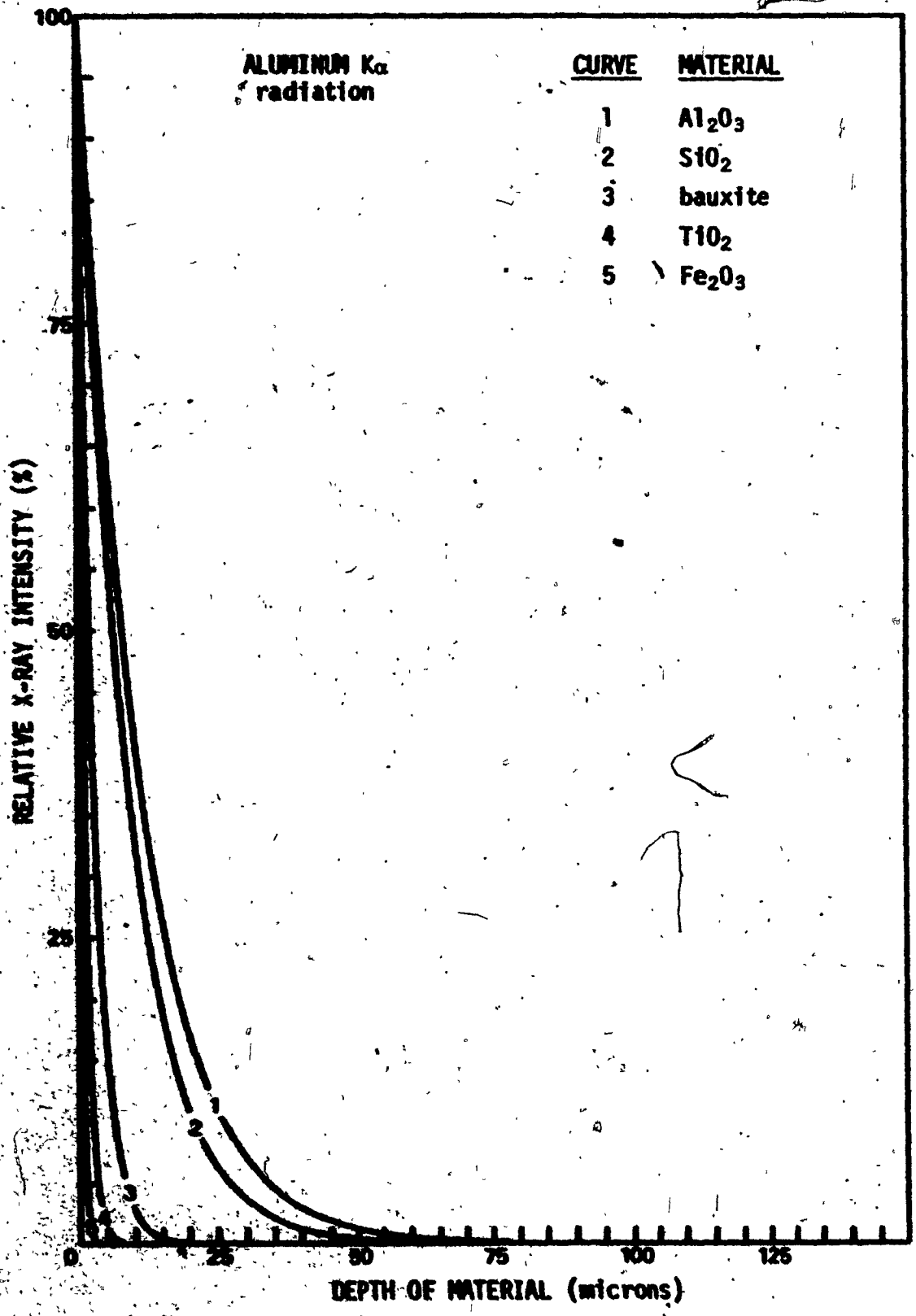
ALUMINUM Kα radiation
CURVE MATERIAL
1 Al_2O_3
2 SiO_2
3 bauxite
4 TiO_2
5 Fe_2O_3
100
75
50
25
0
RELATIVE X-RAY INTENSITY (%)
25
50
75
100
125
DEPTH OF MATERIAL (microns)

FIGURE 4-3

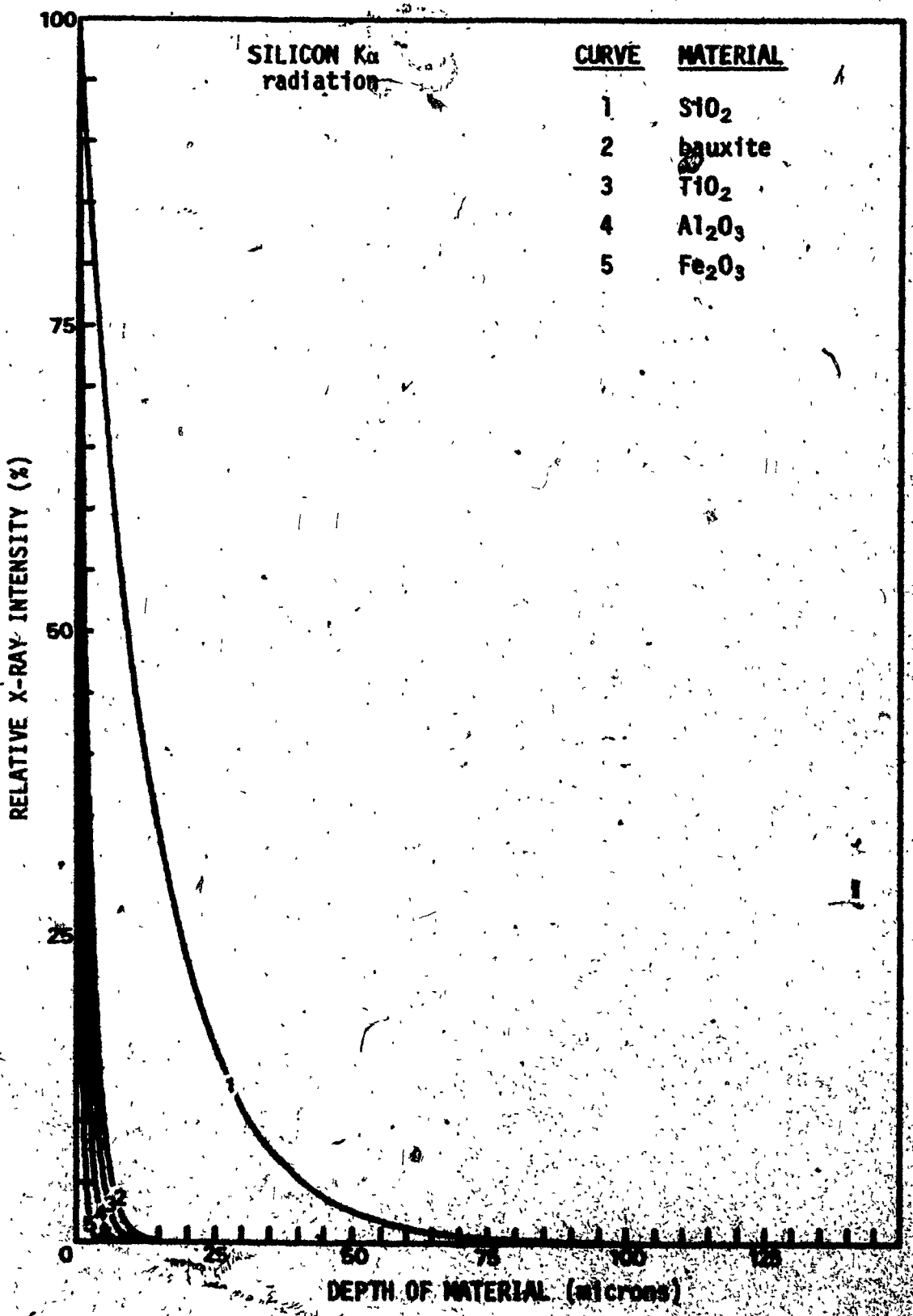
SILICON Kα radiation
CURVE MATERIAL
1 SiO2
2 bauxite
3 TiO2
4 Al2O3
5 Fe2O3
RELATIVE X-RAY INTENSITY (%)
100
75
50
25
0
25
50
75
100
125
DEPTH OF MATERIAL (microns)

FIGURE 4-4

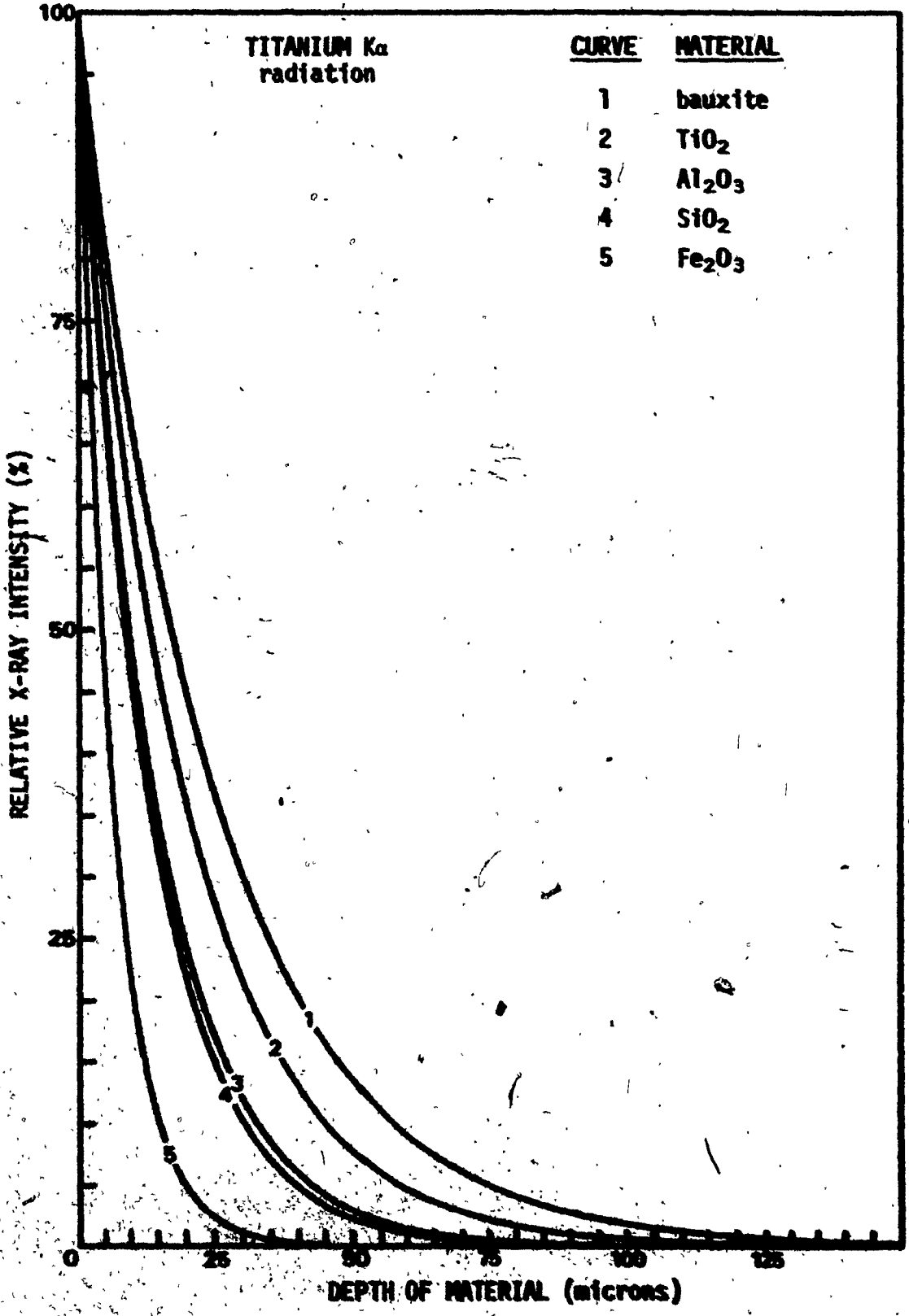
TITANIUM Kα radiation
CURVE MATERIAL
1 bauxite
2 TiO2
3 Al2O3
4 SiO2
5 Fe2O3
RELATIVE X-RAY INTENSITY (%)
100
75
50
25
0
25
50
75
100
125
DEPTH OF MATERIAL (microns)

FIGURE 4-5

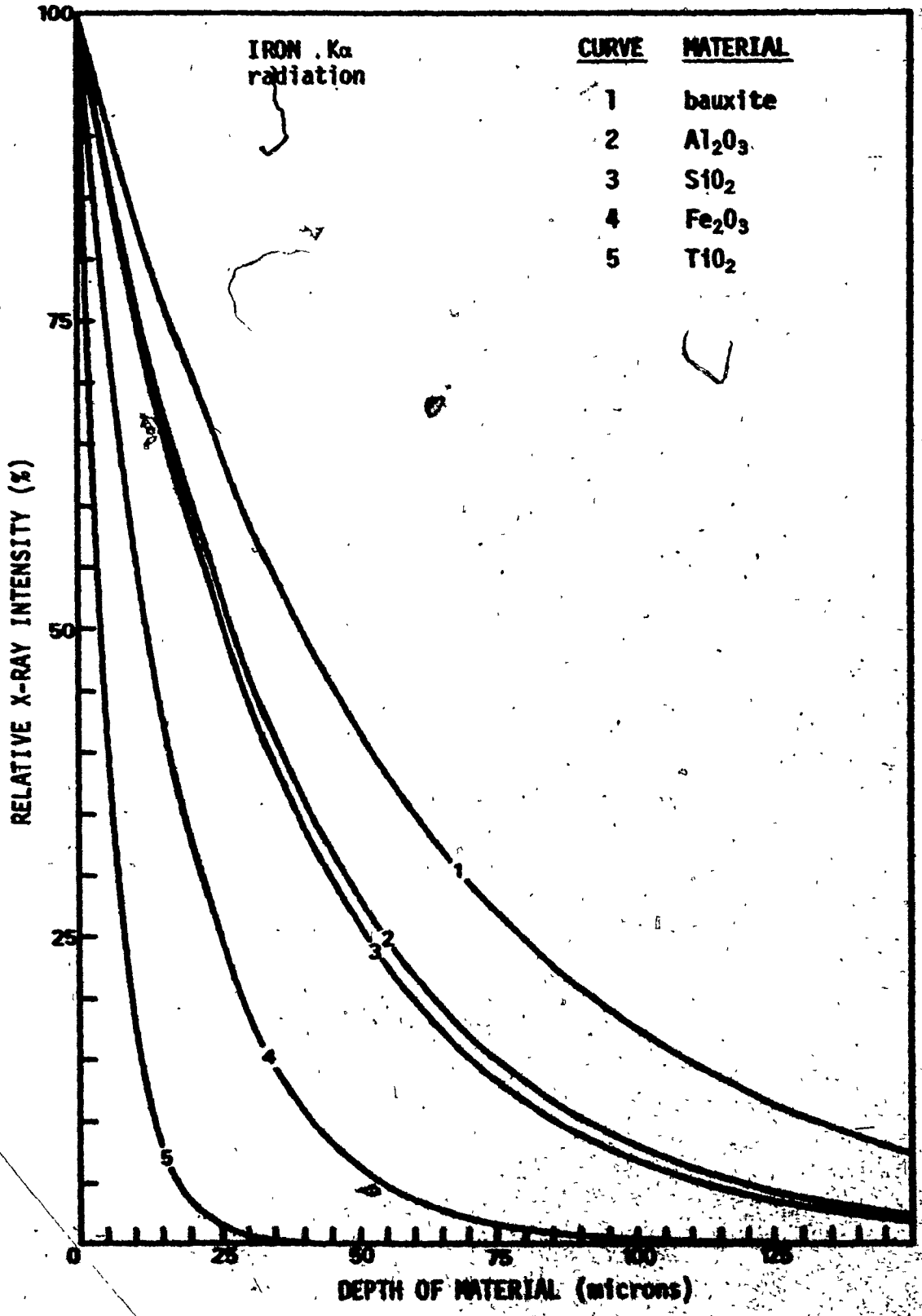
IRON . Kα radiation
CURVE MATERIAL
1 bauxite
2 Al_2O_3
3 SiO_2
4 Fe_2O_3
5 TiO_2
RELATIVE X-RAY INTENSITY (%)
100
75
50
25
0
25
50
75
100
125
DEPTH OF MATERIAL (microns)

TABLE 4-1

X-RAY PENETRATION DEPTHS*

RADIATION	Cr Kα	Al Kα	Si Kα	Ti Kα	Fe Kα
λ	2.28Å	8.34Å	7.08Å	2.76Å	1.93Å
MATERIAL					
Al_2O_3	290	53.7	43.7	169	474
SiO_2	298	47.8	74.4	175	496
TiO_2	44.7	11.3	17.5	205	67.1
Fe_2O_3	107	4.2	6.0	63.8	174
BAUXITE	246	18.8	15.4	172	395

* depth in microns

for the pertinent x-ray wavelengths in the selected materials. It was noted that the primary CrKα radiation will penetrate through bauxite to a depth of about 246 microns (μ). The secondary radiation that may be detected will come from a maximum depth of

18.8 μ for AlKα radiation
15.4 μ for SiKα radiation
172 μ for TiKα radiation
246 μ (CrKα penetration depth) for FeKα radiation.

In these calculations the bauxite sample was assumed to be homogeneous with respect to composition and particle size. These results showed that the particles must be smaller than 15 μ to eliminate a particle size effect in bauxite. However, if there is a compositional variation with particle size, i.e. large particles of one material and small particles of another, it appears that the x-ray penetration depths may vary significantly. For example, consider a large particle of alumina coated with fine particles of iron oxide. In this case a 4.2 μ layer of Fe_2O_3 will completely absorb any AlKα radiation.

4-2-2 INVESTIGATION OF PURE ALUMINA SEED OF KNOWN PARTICLE SIZE DISTRIBUTION

In order to attempt a determination of the approximate critical particle size, below which a particle size effect would not be observed, a bulk sample of pure alumina fine seed was sieved and several fractions, as indicated in TABLE 4-2, were accumulated. It was expected that, since

TABLE 4-2

PARTICLE SIZE ASSOCIATED WITH SIEVED FRACTIONS OF PURE ALUMINA FINE SEED

SAMPLE	SIEVE SIZE (mesh)	PARTICLE SIZE (microns)
A	+150	+100
B	-150 to +180	-100 to +85
C	-180 to +200	-85 to +75
D	-200 to +325	-75 to +44
E	-325 to +400	-44 to +37
F	-400	-37

TABLE 4-3

X-RAY INTENSITY DATA FOR SIEVED ALUMINA FINE SEED

SAMPLE	INTENSITY (cps)	COUNTING ERROR (3σ)
A	11140	100
B	11100	100
C	11150	100
D	11160	100
E	11190	100
F	11180	100

this material was presumably homogeneous, no difficulties with respect to a variation of composition with particle size would be introduced.

Three discs of each size grouping were briquetted at 20 tons and were subjected to x-ray fluorescence (XRF) spectrometric analysis at parameters suitable to aluminum determination. TABLE 4·3 shows the average aluminum counting intensity values that were secured. It will be noted from this data that all sized samples showed the same counting intensity within the 3σ counting error. It was apparent that any significant particle size effect should involve particle sizes more coarse than 100 microns, at least relative to the effect on aluminum counting intensity.

4·2·3 INVESTIGATION OF THE COUNTING INTENSITY FOR VARIOUS ELEMENTS IN SIZED BAUXITE ORE SAMPLES

It was decided, in view of the results obtained in 4·2·2 of the foregoing, to secure several samples of very coarse bauxite ore materials. These samples would be manually ground and size fractioned by sieving. The several size fractions would be examined by XRF to determine the counting intensity for each of the various elements present in significant quantities. Accordingly, Alcan was asked to provide the coarse bauxite samples required. Five of these were submitted, the sources of origin being Amazon (Brazil), Australia, Boke (West Africa), Demerara (Guyana) and Jamaica. Of these samples, only the Australian

material had been pre-ground to less than 10 mesh. The four remaining samples were considerably coarser, varying in main particle size from $^1/_4$" to $^1/_2$", with some accumulation of finer material.

All samples were ground manually with a mortar and pestle until the original bulk sample taken in each case passed through a 10 mesh sieve. The total material was then sieved on a 200 mesh sieve, and the -200 mesh portion set aside. The +200 mesh sample was then carefully sieved so that, finally, a size distribution as shown in TABLE 4-4 was obtained. Because of the length of time involved in the separation process, only three of the bauxite samples were completely separated in this way, these being the Amazon, Boke and Australian materials.

Material from the various size categories was briquetted. The discs were subjected to XRF examination using parameters suitable for the determination of the counting intensities of aluminum, iron, silicon and titanium. TABLES 4-5 to 4-7 show the counting intensities and the percent intensities relative to the highest counting value in each case. The straight line point connecting plots are shown in FIGURES 4-6 to 4-9. The following points may be noted:

IRON

The Amazon and Boke samples show a trend to increased counting intensity with decreasing particle size. The Australian sample showed an initial increase in counting intensity, followed by a decrease and finally by an increase.

TABLE 4-4

PARTICLE SIZE FOR SIEVED FRACTIONS OF BULK BAUXITE

SIEVE SIZE (mesh)	PARTICLE SIZE (microns)
-10 to +20	-2000 to +840
-20 to +40	-840 to +420
-40 to +60	-420 to +250
-60 to +80	-250 to +180
-80 to +100	-180 to +150
-100 to +120	-150 to +125
-120 to +140	-125 to +105
-140 to +160	-105 to +95
-160 to +180	-95 to +85
-180 to +200	-85 to +75
-200	-75

TABLE 4.5

XRF ANALYSIS* AMAZON BULK BAUXITE (sieved)

GRAIN SIZE (mesh)	Fe		Si		Ti		Al	
	Int.	Rel.%	Int.	Rel.%	Int.	Rel.%	Int.	Rel.%
-10 +20	4.75	49.90	0.482	50.31	3.23	57.61	7.27	80.55
-20 +40	5.88	61.76	0.541	56.47	3.54	63.12	6.56	72.65
-40 +60	6.86	72.06	0.664	69.31	4.13	73.66	7.42	82.25
-60 +80	7.34	77.10	0.632	65.97	4.39	78.38	8.28	91.75
-80 +100	7.31	76.79	0.620	64.72	4.32	77.19	8.92	98.80
-100 +120	7.91	83.09	0.704	73.49	4.40	78.46	8.85	98.06
-120 +140	9.52	100.0	0.958	100.0	5.60	100.0	8.54	94.57
-140 +160	9.29	97.58	0.887	92.59	5.36	95.72	8.69	96.27
-180 +200	9.07	95.27	0.793	82.78	5.10	90.96	9.03	100.0

* Intensity in kilo counts per second (kcps)

TABLE 4.6

XRF ANALYSIS* BOKE BULK BAUXITE (sieved)

GRAIN SIZE (mesh)	Fe		Si		Ti		Al	
	Int.	Rel.%	Int.	Rel.%	Int.	Rel.%	Int.	Rel.%
-10 +20	3.66	66.30	0.148	53.24	7.45	66.59	9.60	79.85
-20 +40	3.56	64.49	0.153	54.68	7.11	63.57	9.42	78.32
-40 +60	4.14	75.00	0.164	58.99	8.40	75.10	10.62	88.30
-60 +80	4.56	82.61	0.168	60.43	9.49	84.83	11.02	91.60
-80 +100	4.56	82.61	0.171	61.51	9.98	89.15	11.26	93.62
-100 +120	4.82	87.32	0.175	62.96	10.57	94.47	11.31	94.06
-120 +140	4.96	89.86	0.178	64.03	11.18	99.87	11.10	92.29
-140 +160	5.21	94.38	0.175	62.95	10.85	96.94	11.34	94.30
-160 +180	4.84	87.68	0.178	64.03	10.59	94.65	11.34	94.32
-180 +200	5.41	98.01	0.178	64.03	11.19	100.0	11.41	94.87
-200	5.52	100.0	0.278	100.0	10.86	97.03	12.03	100.0

* Intensity in kilo counts per second (kcps)

TABLE 4-7

XRF ANALYSIS* AUSTRALIA BULK BAUXITE (sieved)

GRAIN SIZE (mesh)	Fe		Si		Ti		Al	
	Int.	Rel.%	Int.	Rel.%	Int.	Rel.%	Int.	Rel.%
-10 +20	8.32	87.21	0.311	36.37	5.76	51.31	7.21	62.97
-20 +40	9.18	96.23	0.354	41.40	7.47	66.59	8.34	72.82
-40 +60	9.54	100.0	0.448	52.40	9.19	81.85	10.25	89.53
-60 +80	9.17	96.12	0.570	66.67	10.02	89.26	10.84	94.62
-80 +100	8.76	91.82	0.690	80.70	10.80	96.23	11.21	97.90
-100 +120	8.52	89.31	0.704	82.34	10.94	97.49	11.43	99.81
-120 +140	8.43	88.36	0.748	87.49	11.17	99.57	11.45	100.0
-140 +160	8.49	88.99	0.782	91.46	11.09	98.84	11.38	99.39
-160 +180	8.50	89.10	0.813	95.09	10.90	97.14	11.44	99.87
-180 +200	8.36	87.63	0.855	100.0	10.98	97.86	11.33	98.95
-200	9.42	98.74	0.742	86.78	11.22	100.0	11.39	99.43

* Intensity in kilo counts per second (kcps)

FIGURES 4·6 to 4·9

Variation of x-ray intensity for size fractioned bauxite materials.

FIGURE 4-6

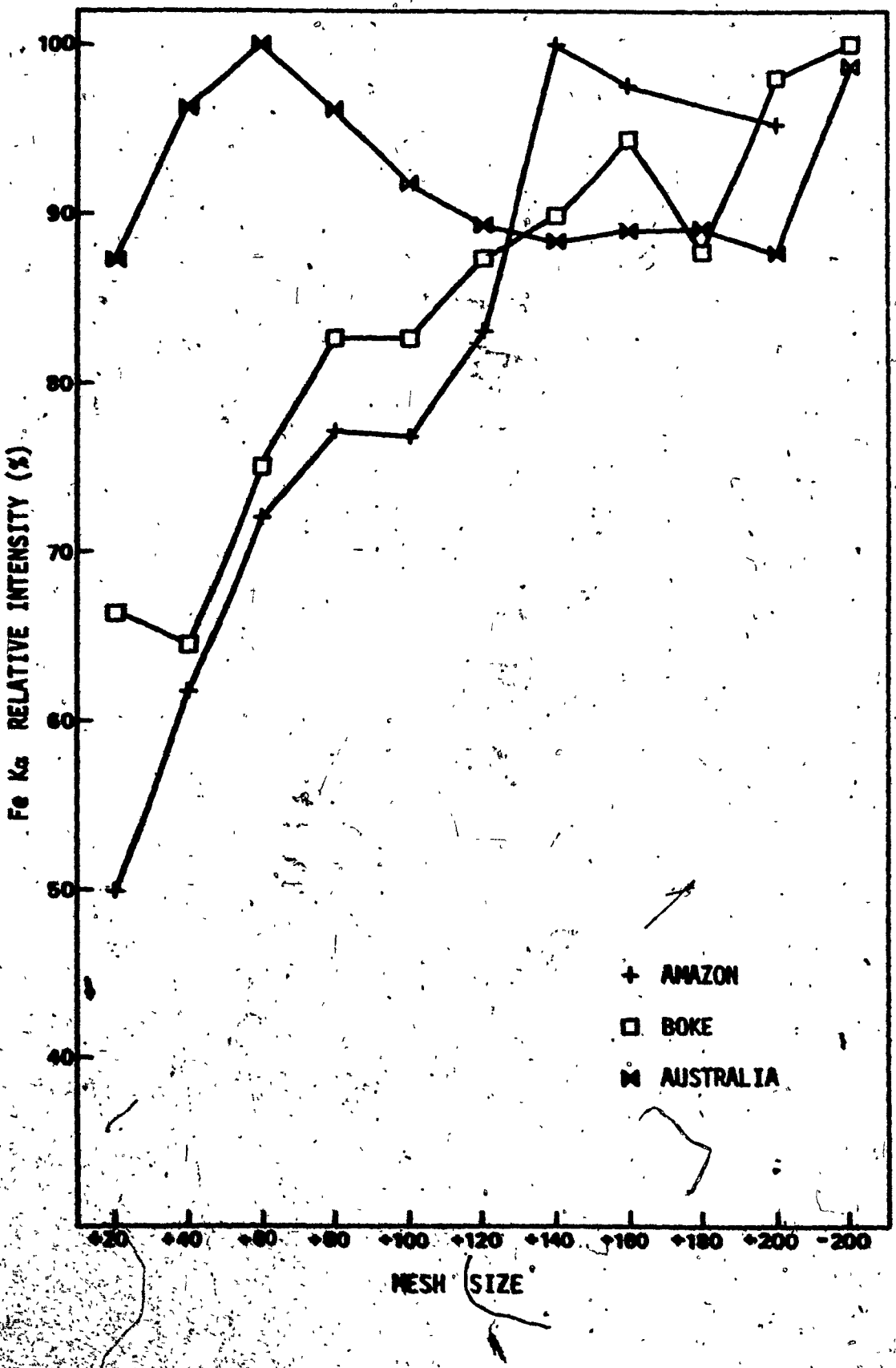
100
90
80
70
60
50
40
Fe Ka RELATIVE INTENSITY (%)
+ AMAZON
□ BOKE
⋈ AUSTRALIA
+20
+40
+60
+80
+100
+120
+140
+160
+180
+200
-200
MESH SIZE

FIGURE 4.7

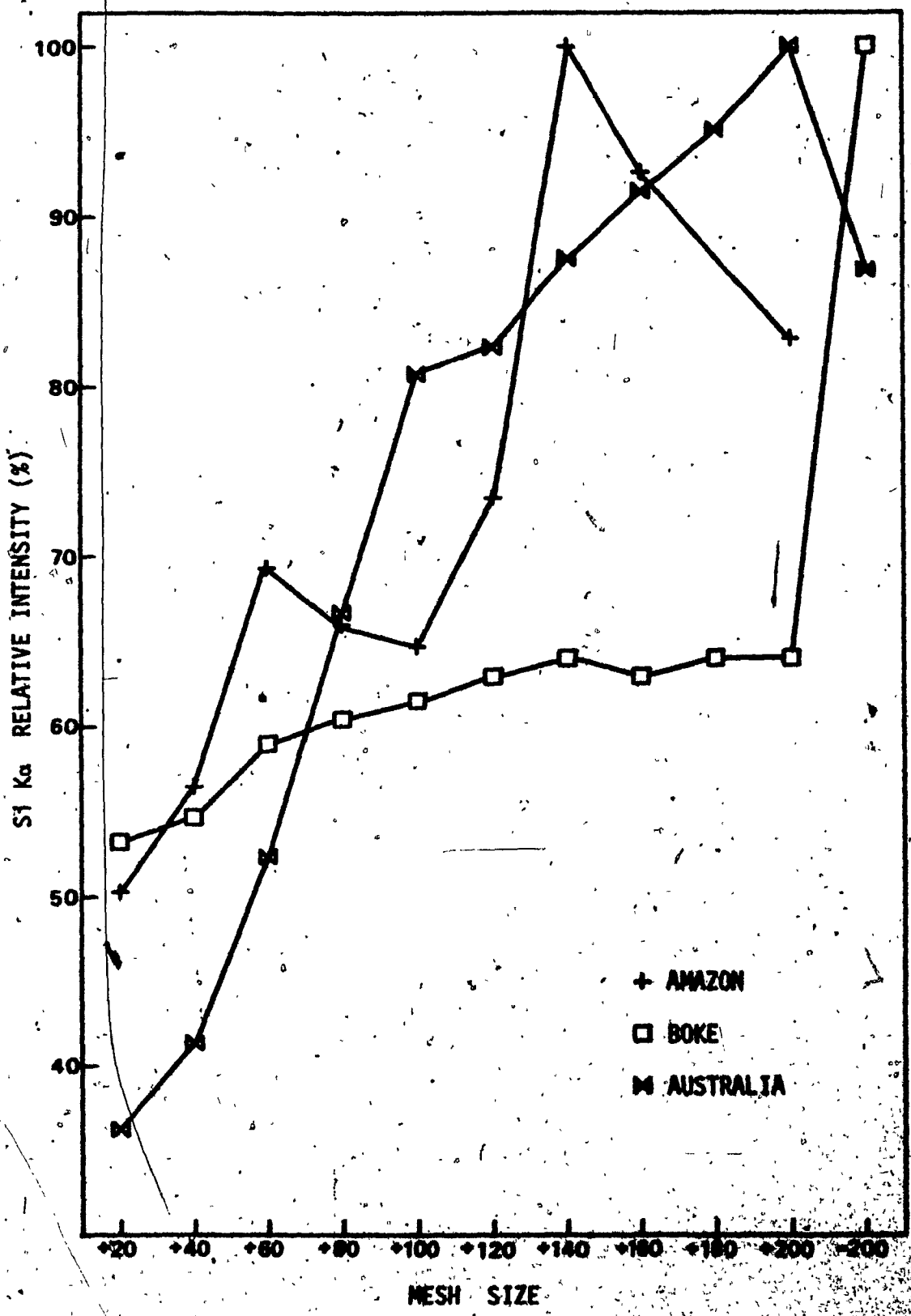
100
90
80
70
60
50
40
Si Kα RELATIVE INTENSITY (%)
+20
+40
+60
+80
+100
+120
+140
+160
+180
+200
-200
MESH SIZE
AMAZON
BOKE
AUSTRALIA

FIGURE 4-8

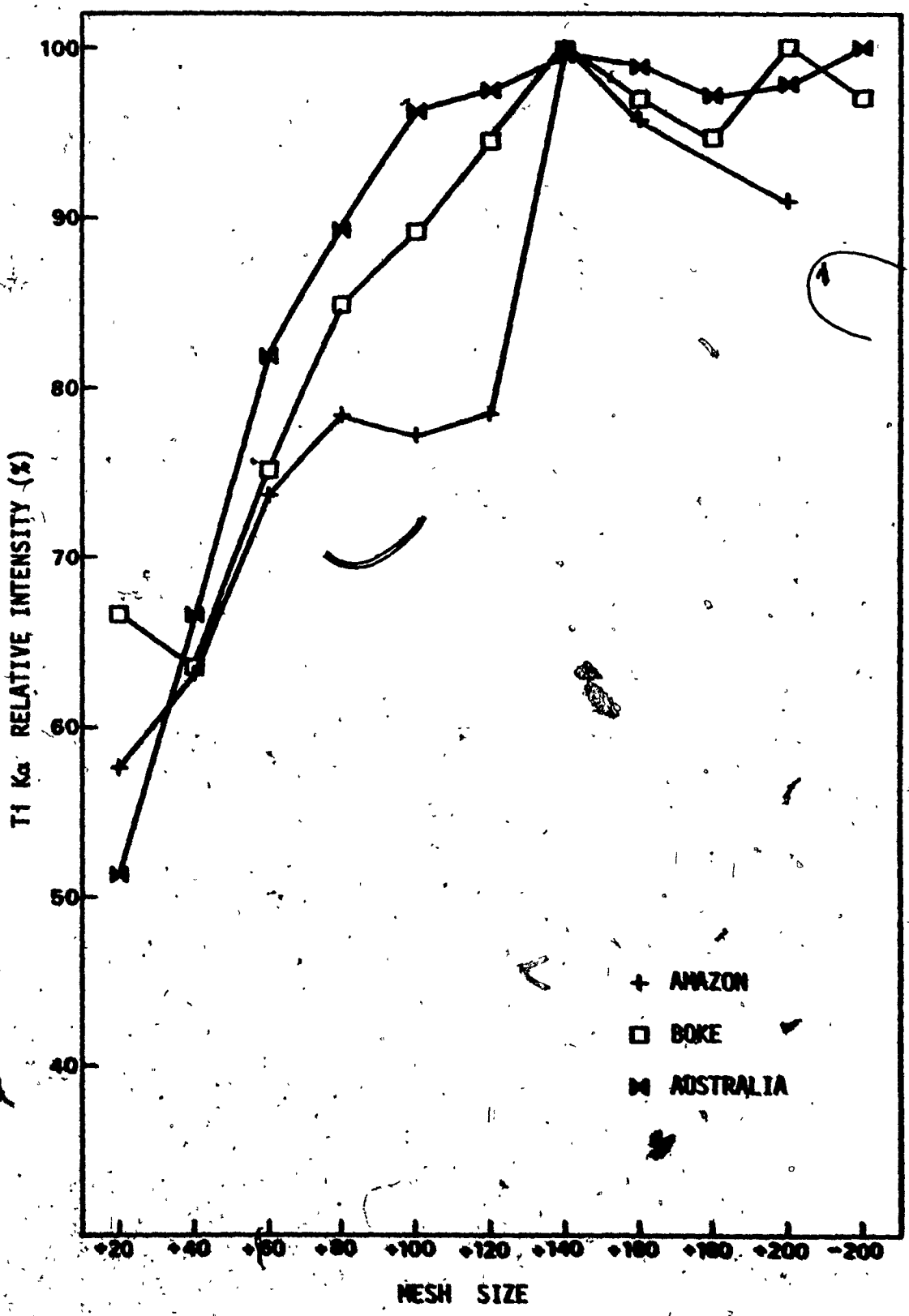
100
90
80
70
60
50
40
Ti Kα RELATIVE INTENSITY (%)
+20
+40
+60
+80
+100
+120
+140
+160
+180
+200
-200
MESH SIZE
AMAZON
BOKE
AUSTRALIA

FIGURE 4-9

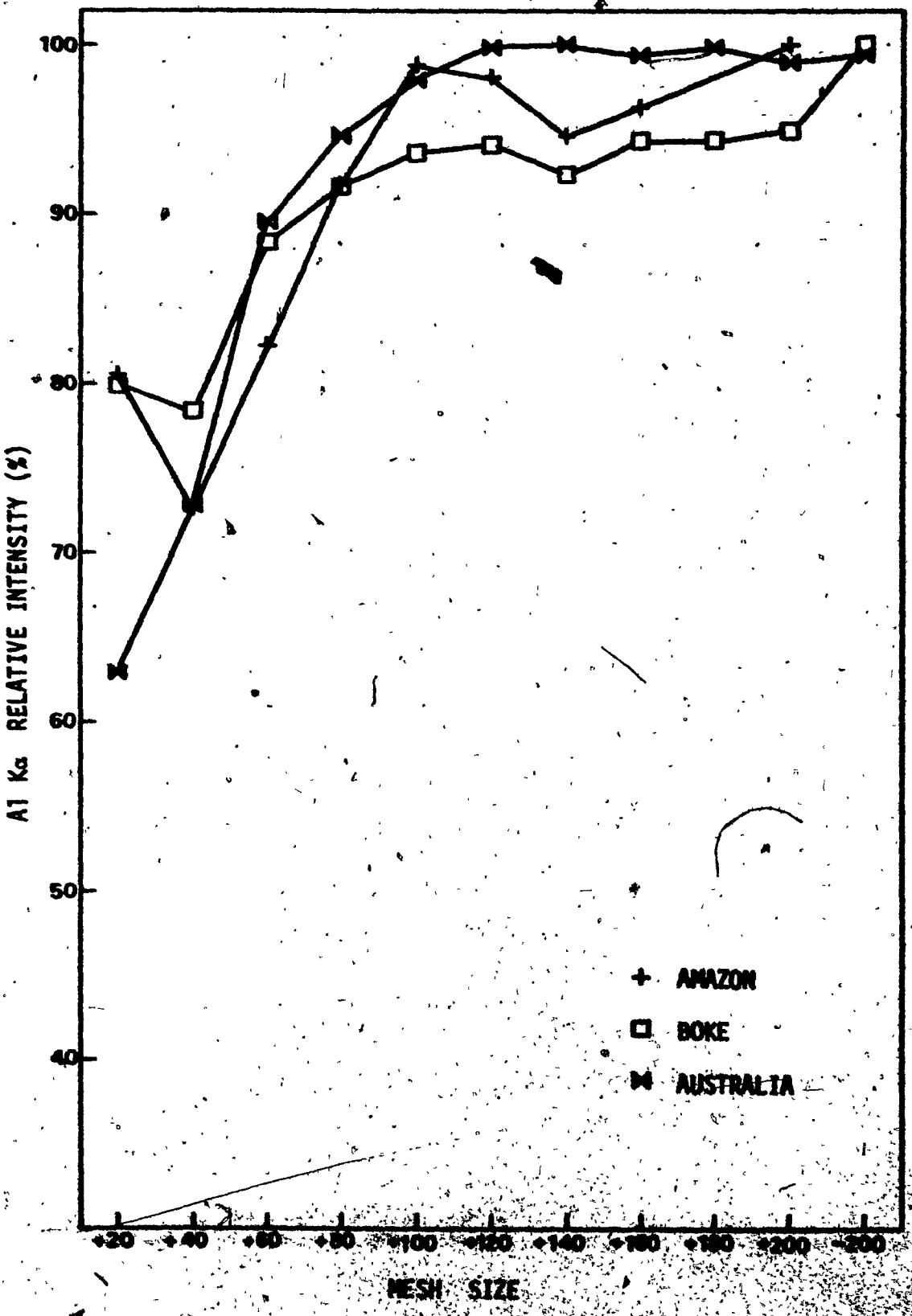
100
90
80
70
60
50
40
Al Kα RELATIVE INTENSITY (%)
AMAZON
BOKE
AUSTRALIA
+20
+40
+60
+80
+100
+120
+140
+160
+180
+200
-200
MESH SIZE

TITANIUM

All of the sample materials, regardless of source, show an increase in counting intensity with decreasing particle size.

SILICON

The Amazon and Australian materials shown counting intensity increasing with decreasing particle size. The Boke material shows the same trend, but with a slow rate of increase initially, followed by a rapid rate of increase.

ALUMINUM

All materials showed, generally, an increase in the counting intensity with decreasing particle size.

The only significant departure from the average behaviour was noted in the case of the iron counting intensity for the Australian material. The departure of the silicon counting intensity from the general trend, noted in the case of the Boke material, may possibly be ascribed to the low silicon content involved, the correspondingly low counting intensity and the associated high relative counting error.

On the basis of the foregoing results, it appeared that a definite particle size effect had been observed, and that the counting intensity increased as the masking effect of the large particles is reduced with decreasing particle size. The departure observed for the

iron counting rate on Australian material may possibly be associated with the fact that this was the only pre-ground material; the larger particles may have been coated with a softer, higher-iron content component in the pre-grinding process.

Despite this apparent evidence of a particle size effect, the possibility that the results observed might have been due to some variations in composition with particle size could not be overlooked. The erratic nature of most of the graphs suggests that there is some other effect superimposed on the particle size effect. It was decided to investigate this point by performing direct wet analysis of several of the size fractions for the Amazon, Boke and Australian materials which had been completely size-fractioned. TABLES 4-8 and 4-9 show the wet analysis results for iron and silicon by size fraction. The methods of analysis used were Alcan Standard Method 194-54 for silicon and Alcan Standard Method 195-54 for iron. These results, on the basis of percent values relative to the highest value for each element in each material, are shown plotted along with the appropriate XRF relative intensities in FIGURES 4-10 to 4-15.

It will be noted that the general trend of counting intensity in each case matches the trend of compositional variation. From this it can be assumed that the particle size effect is very soundly masked by the effect of compositional variation with particle size.

In order to visually record the variation in particle size within a size fraction, even at the fraction level of -200 mesh, the

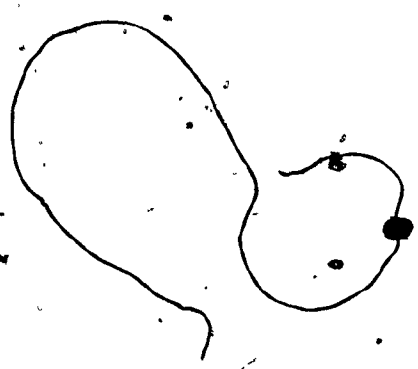

TABLE 4-8

DIRECT (WET) ANALYSIS OF Fe_2O_3 FOR BULK BAUXITE (sieved)

	AMAZON		BOKE		AUSTRALIA	
GRAIN SIZE (mesh)	%	Rel.%	%	Rel.%	%	Rel.%
-10 +20	9.01	66.08	4.50	53.67	21.23	119.3*
-20 +40	9.79	71.78	5.48	70.35	17.75	99.69
-40 +60	11.58	84.96			17.80	100.0
-60 +80	11.66	85.51	7.71	92.00		
-80 +100	11.98	87.85			13.95	78.36
-100 +120	11.65	85.48				
-120 +140	13.63	100.0			13.12	73.67
-140 +160	13.43	98.52	8.38	100.0		
-160 +180			7.52	89.78	13.18	74.01
-180 +200	13.11	96.16				
-200			7.50	89.58	13.55	76.13

* data not included for graph

TABLE 4-9

DIRECT (WET) ANALYSIS OF SiO_2 FOR BULK BAUXITE (sieved)

	AMAZON		BOKE		AUSTRALIA	
GRAIN SIZE (mesh)	%	Rel.%	%	Rel.%	%	Rel.%
-10 +20	3.12	76.65	0.693	38.61	2.31	33.16
-20 +40	3.31	81.50	0.759	42.28	2.43	34.83
-40 +60	3.58	87.99			2.86	41.00
-60 +80	3.82	94.09	0.791	44.07		
-80 +100	3.66	89.96			5.62	80.57
-100 +120	3.28	80.78				
-120 +140	4.06	100.0			6.71	96.23
-140 +160	3.82	94.02	0.924	51.48		
-160 +180			0.964	53.70	6.97	100.0
-180 +200	3.26	80.14				
-200			1.795	100.0	5.67	81.42

FIGURES 4-10 to 4-15

Variation of chemical composition of Fe_2O_3 and SiO_2 for size fractioned bauxite materials compared to the corresponding variation of x-ray intensity.

FIGURE 4-10

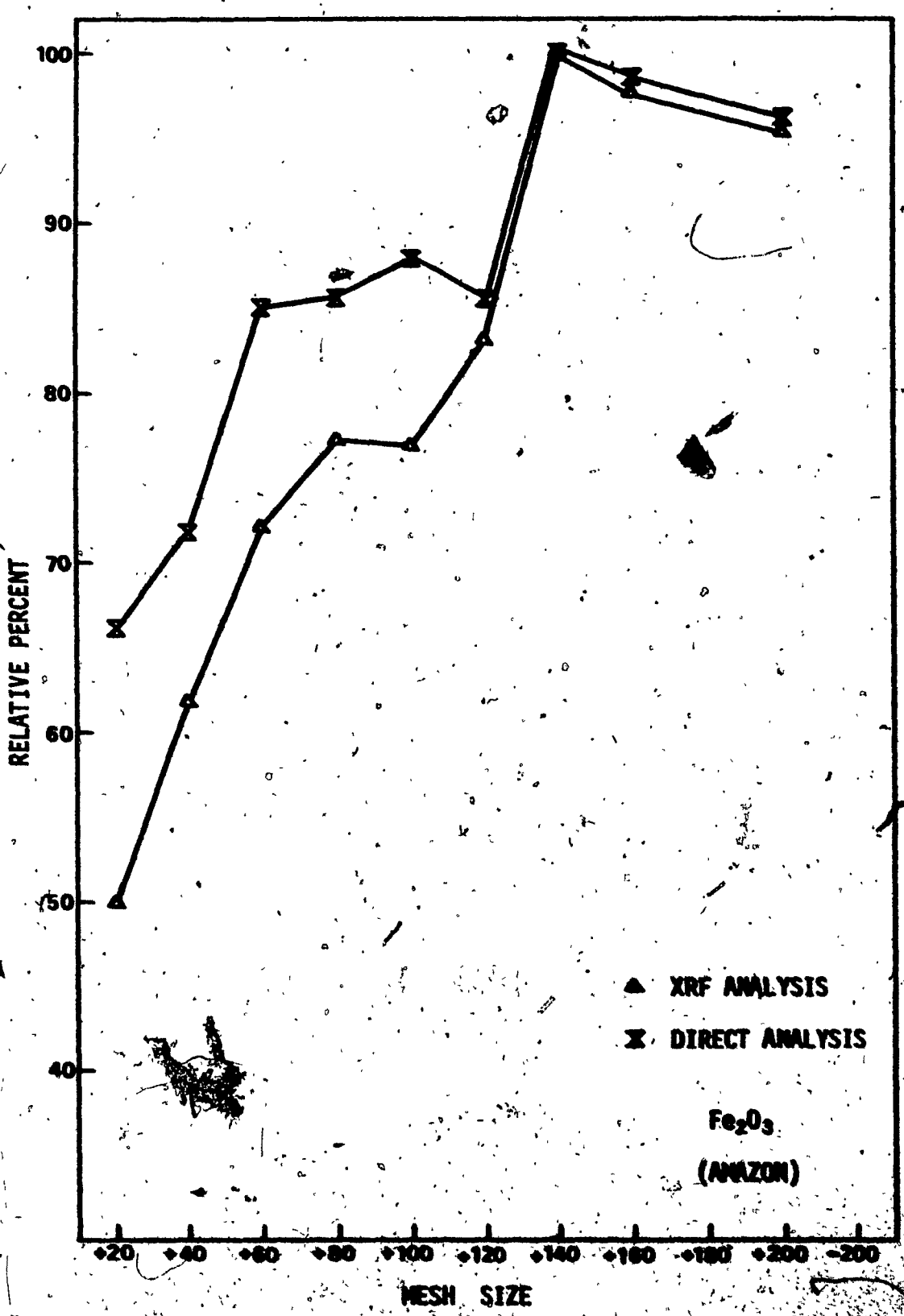
100
90
80
70
60
50
40
RELATIVE PERCENT
XRF ANALYSIS
DIRECT ANALYSIS
Fe_2O_3
(AMAZON)
+20
+40
+60
+80
+100
+120
+140
+160
+180
+200
-200
MESH SIZE

FIGURE 4-11

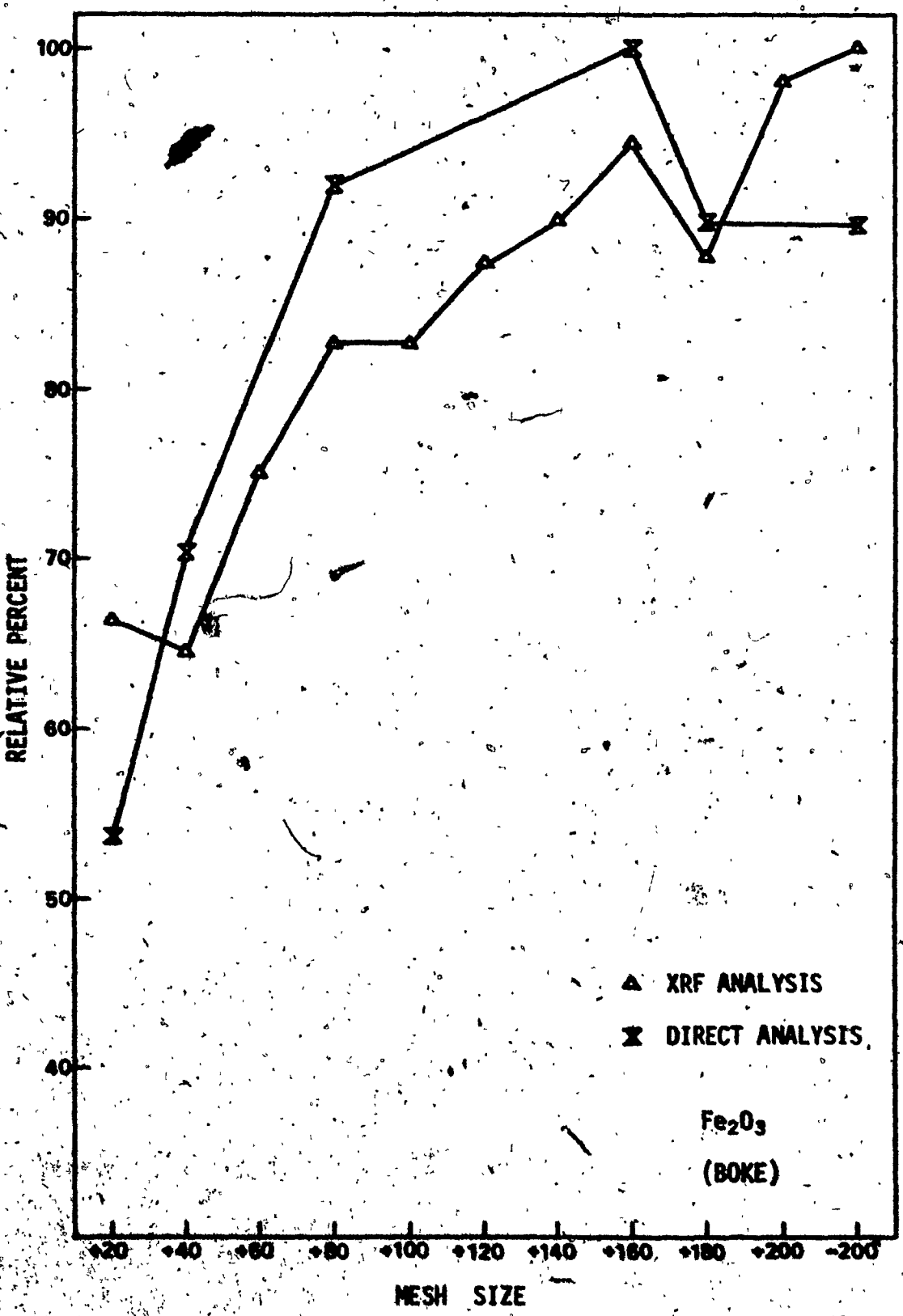
100
90
80
70
60
50
40
RELATIVE PERCENT
XRF ANALYSIS
DIRECT ANALYSIS
Fe_2O_3
(BOKE)
+20
+40
+60
+80
+100
+120
+140
+160
+180
+200
-200
MESH SIZE

FIGURE 4-12

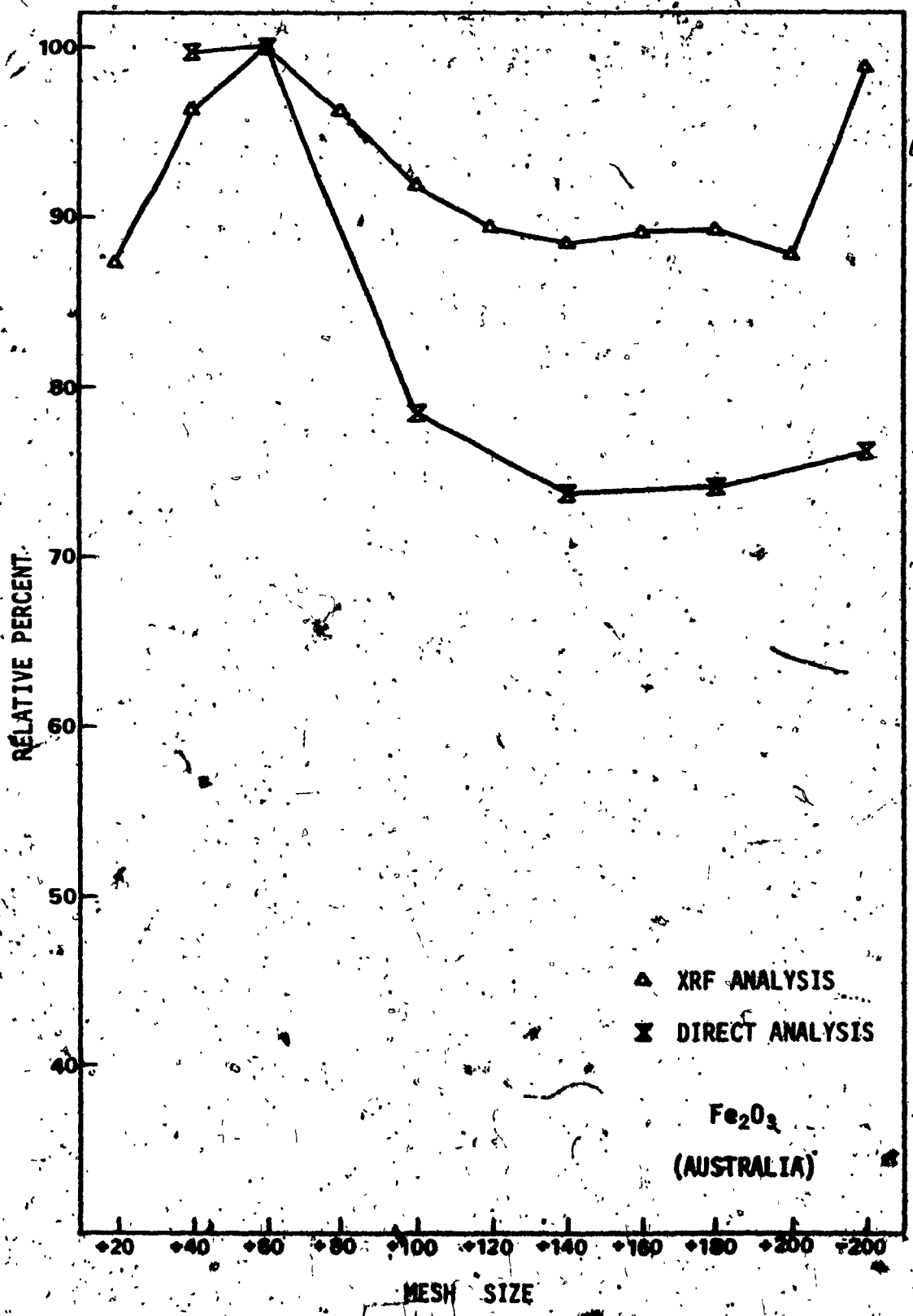
100
90
80
70
60
50
40
RELATIVE PERCENT
△ XRF ANALYSIS
⧗ DIRECT ANALYSIS
Fe_2O_3
(AUSTRALIA)
+20
+40
+60
+80
+100
+120
+140
+160
+180
+200
+200
MESH SIZE

FIGURE 4-13

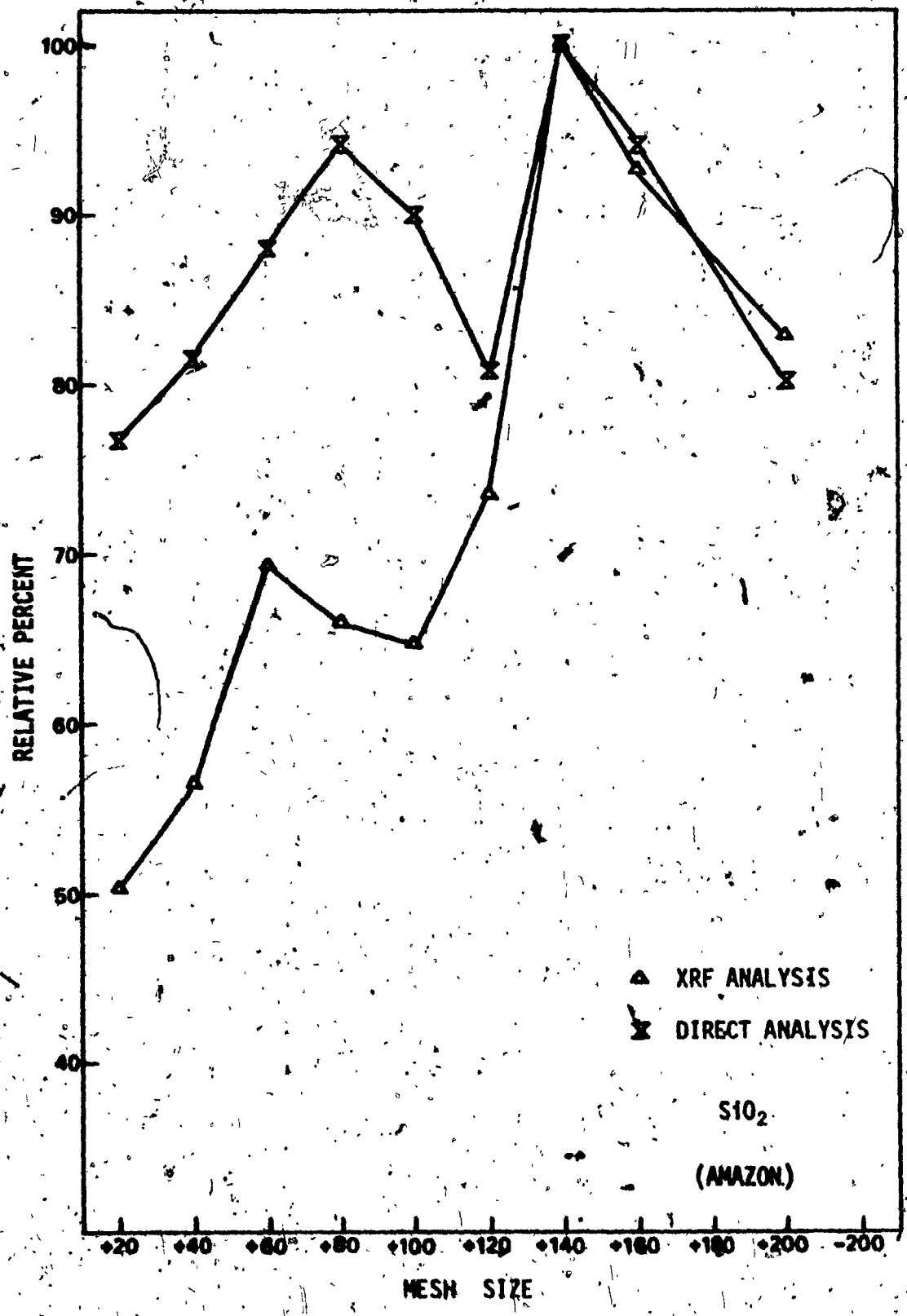
100
90
80
70
60
50
40
RELATIVE PERCENT
XRF ANALYSIS
DIRECT ANALYSIS
SiO_2
(AMAZON)
+20
+40
+60
+80
+100
+120
+140
+160
+180
+200
-200
MESH SIZE

FIGURE 4-14

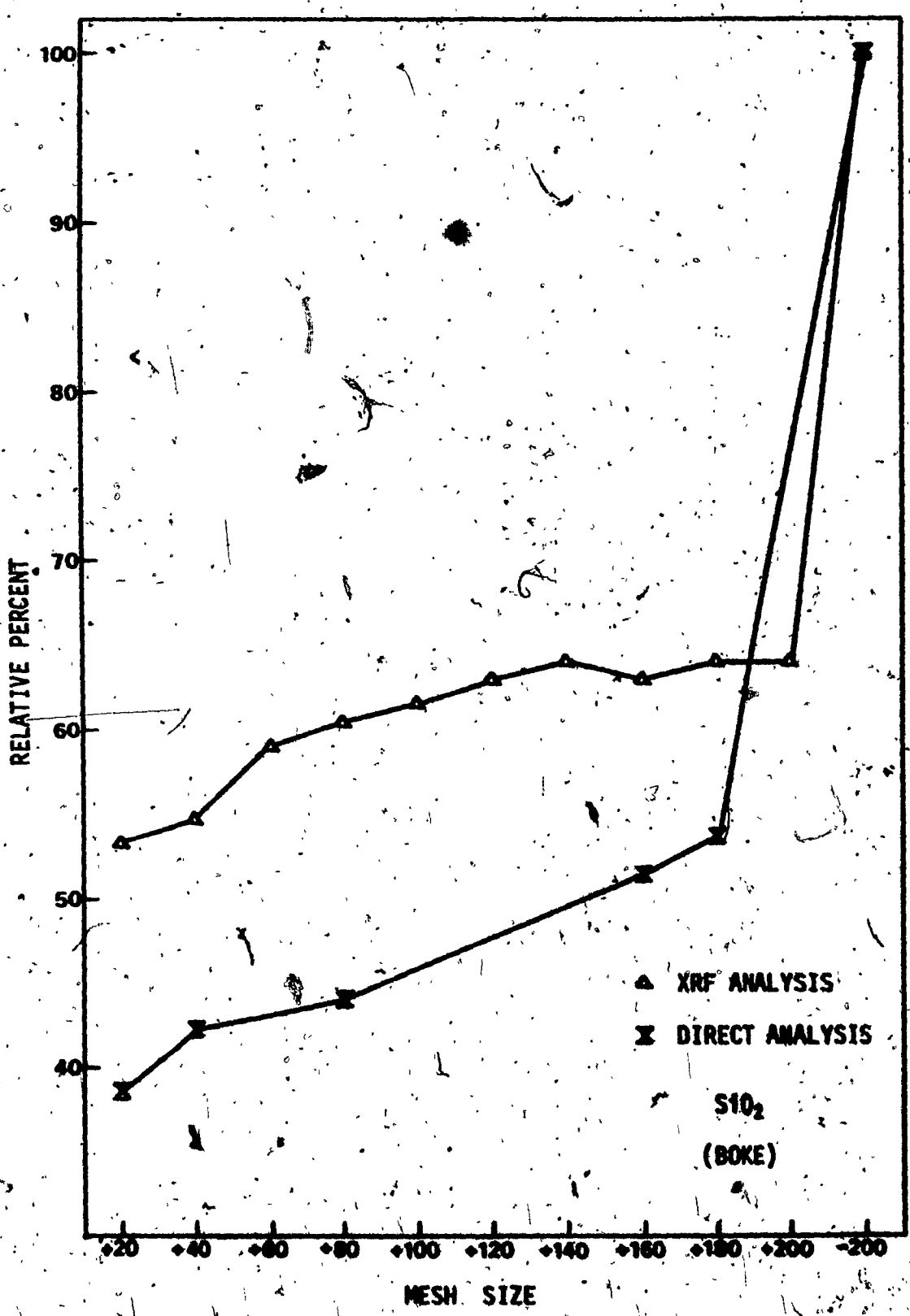
100
90
80
70
60
50
40
RELATIVE PERCENT
XRF ANALYSIS
DIRECT ANALYSIS
SiO_2
(BOKE)
+20
+40
+60
+80
+100
+120
+140
+160
+180
+200
-200
MESH SIZE

FIGURE 4-15

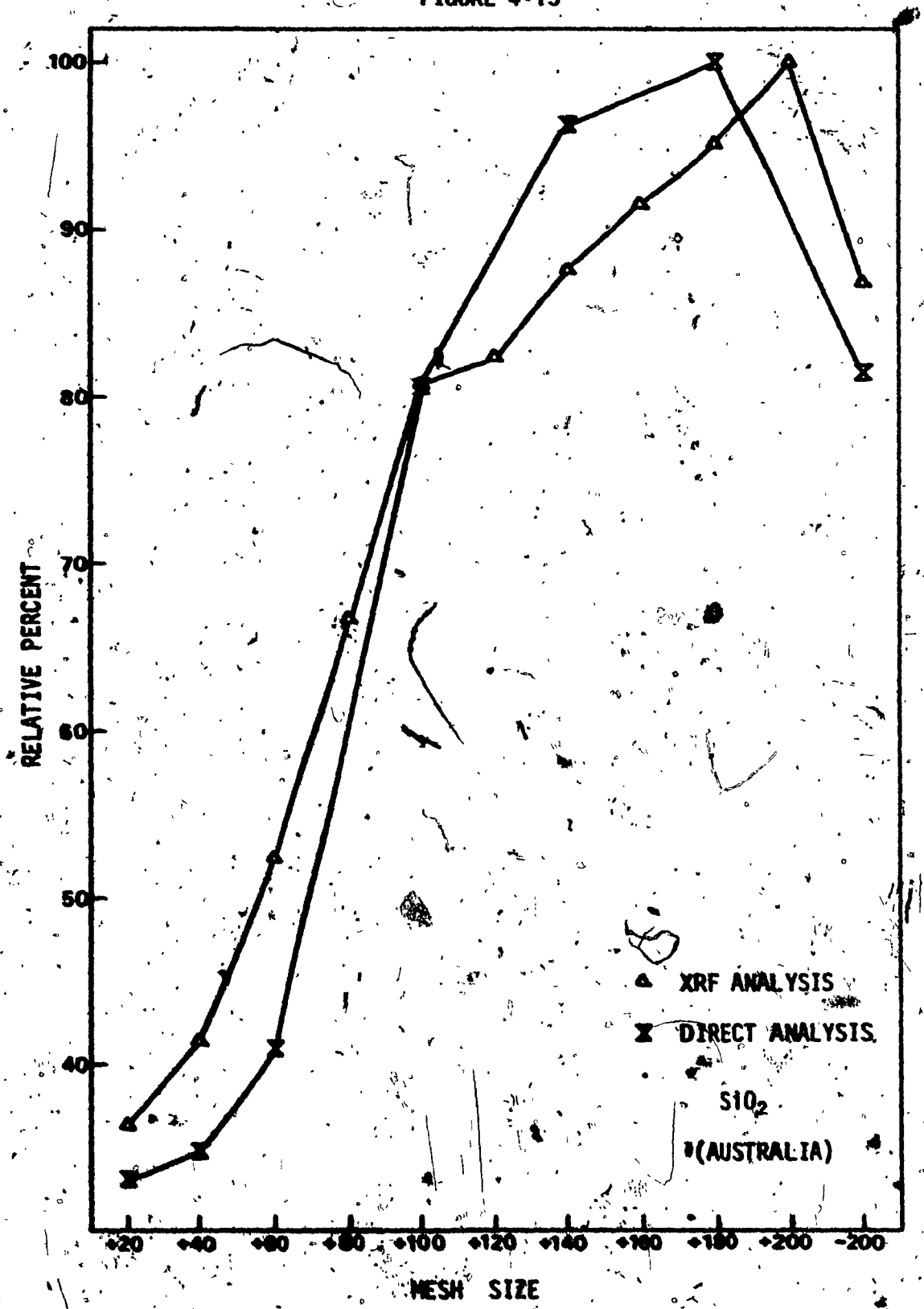
100
90
80
70
60
50
40
RELATIVE PERCENT
+20
+40
+60
+80
+100
+120
+140
+160
+180
+200
-200
MESH SIZE
XRF ANALYSIS
DIRECT ANALYSIS
SiO2
(AUSTRALIA)

Boke sample was dispersed and microphotographed (by Miss S. Wamboldt through Dr. R. A. Westbury, Sir George Williams University) at about 400X magnification. It will be observed from FIGURES 4·16 and 4·17 that the particles vary from a few at 30-65 microns to many at less than 10 microns. In the preparation of a sample disc for XRF analysis, it is possible that a large portion of the surface material of the disc may be made up of the smaller particles. The resultant XRF data might not be subject to any particle size effects. However, unless the sample is homogeneous, the XRF data would not be representative of the total sample.

4·2·4 INVESTIGATION OF THE EFFECT OF GRINDING ON THE COUNTING INTENSITY FOR VARIOUS ELEMENTS IN BAUXITE ORES

It was decided to further investigate the question of particle size effect and particle size compositional variation from a somewhat different approach. To this end, a coarsely sized fraction from each of the five bauxite source materials, procured for the investigation in 4·2·3, was taken and subjected to gradually increased grinding times in a Shatterbox, this phase of the work being performed at Arvida. The fraction taken was the -10 to +20 mesh material. The powder samples were ground for approximately two seconds and the loose powder, in a holder, was examined by XRF relative to aluminum, iron, silicon and titanium counting intensities. The powder was then returned and ground for a similar period of time and re-examined by XRF. This process was

FIGURES 4-16 and 4-17

Microphotographs of sieved (-200 mesh) Boke bulk bauxite.

FIGURE 4-16

MAGNIFICATION 400X (Scale 4mm = 10 microns)

SAMPLE A

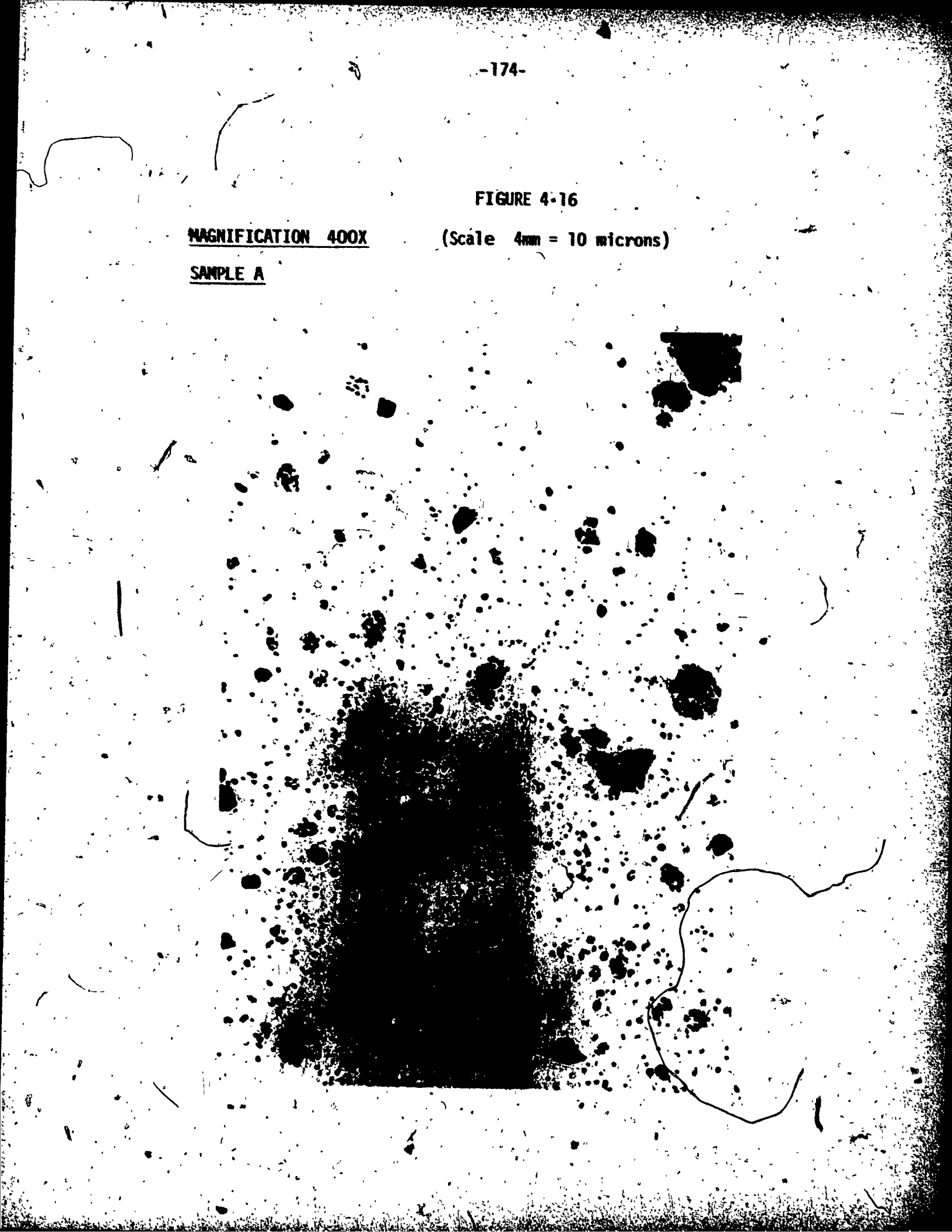

FIGURE 4-17

MAGNIFICATION 400X (Scale, 4mm = 10 microns)

SAMPLE B

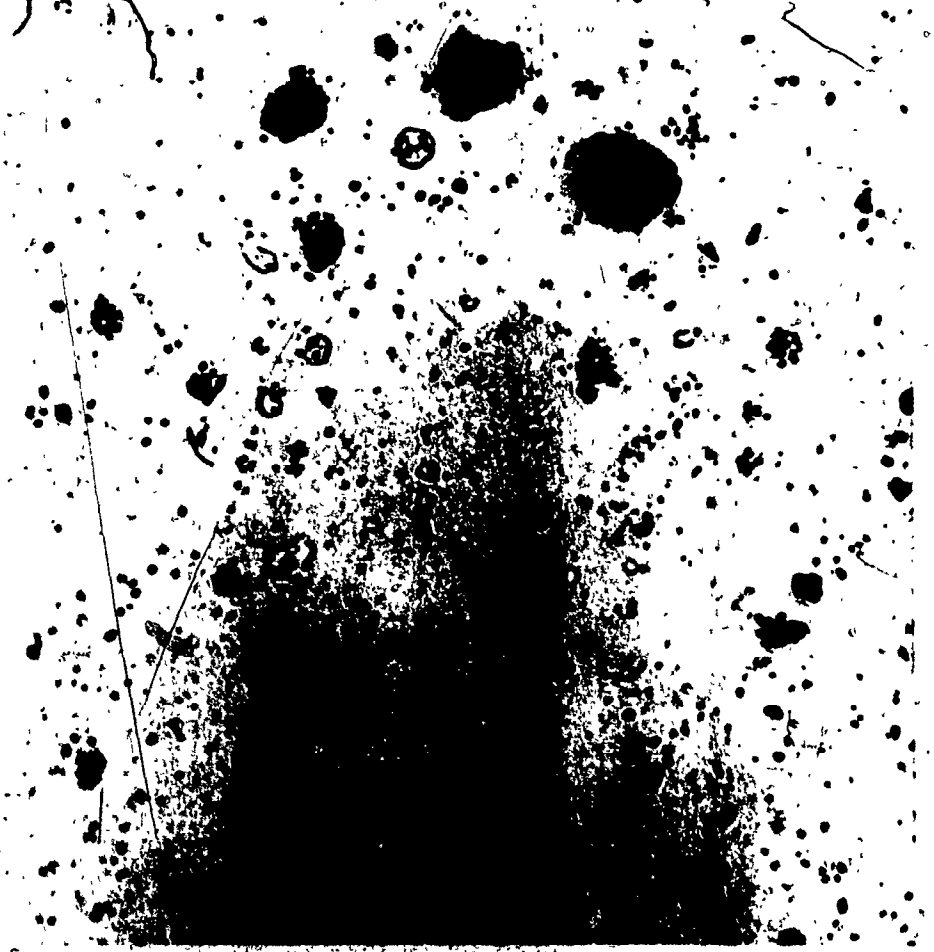

repeated to a total grinding time of 90 seconds. A final grinding to a total time of 300 seconds completed the process. The counting intensities are shown in APPENDIX B, TABLES B-1 to B-6.

The plots of counting intensities versus grinding time are shown in FIGURES 4-18 to 4-41. The following points should be noted:

(1) The Jamaican material ground in a manner such that, for each element, the counting intensity increased steadily to a plateau value with increasing grinding time.

(2) The Australian material gives a similar appearance, with some tendency to a high early intensity for silicon, followed by a decrease in intensity with grinding time.

(3) The Amazon material showed high early counting intensities for iron, silicon and titanium, with these intensities falling off with grinding time to a plateau value.

(4) Very generally the Boke and Demerara materials follow the same trend as that exhibited by the Amazon material.

(5) In general, for all materials, the counting intensity for aluminum increased to a plateau value.

(6) In general, for all elements in Amazon, Boke, Australian and Demerara bauxites, grinding beyond 90 seconds produces approximately plateau counting.

(7) For Jamaican bauxite, plateau counting is reached for all elements after 15 seconds of grinding.

It may be tentatively concluded from the above that the Jamaican

FIGURES 4-18 to 4-41

Variation of x-ray intensities (Al Kα,Si Kα,Ti Kα,Fe Kα) with respect to grinding time for six coarse bauxite samples from five different geographical regions.

FIGURE 4·18

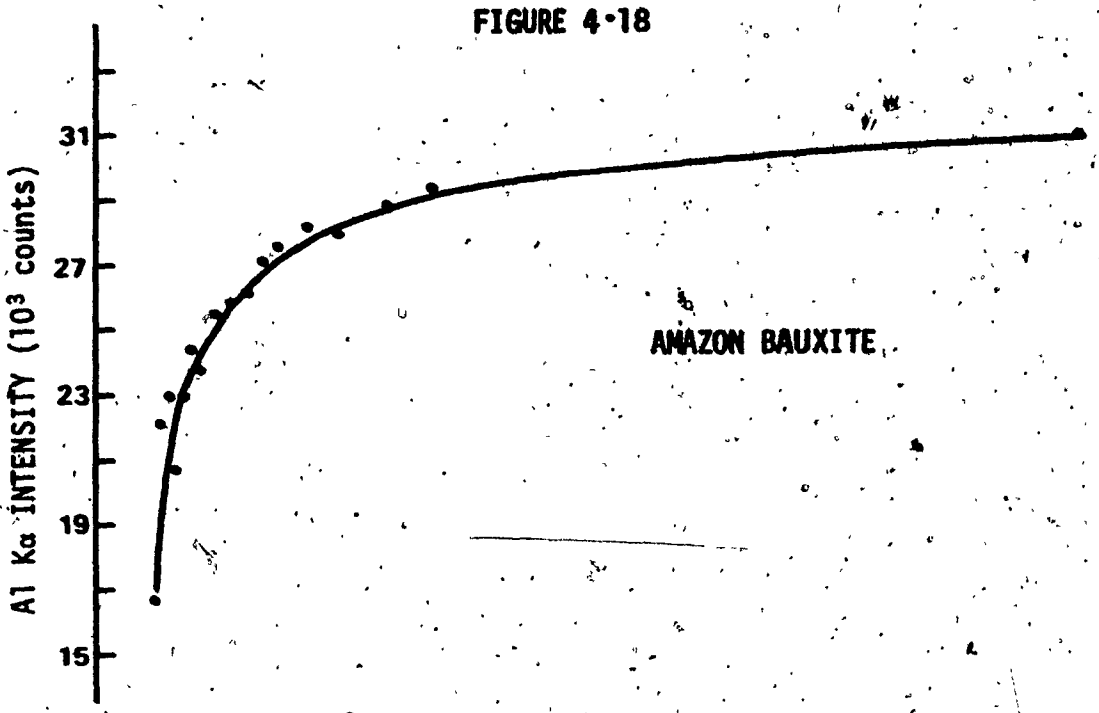

FIGURE 4·19

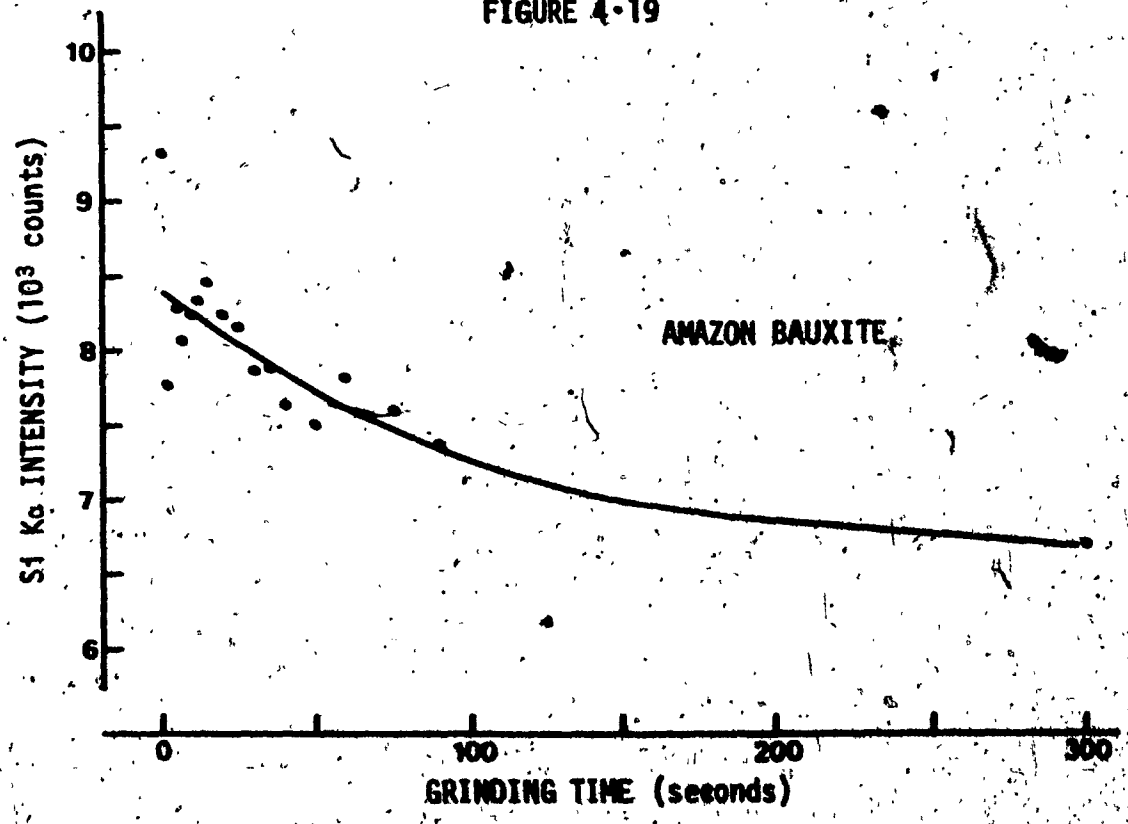

FIGURE 4-20

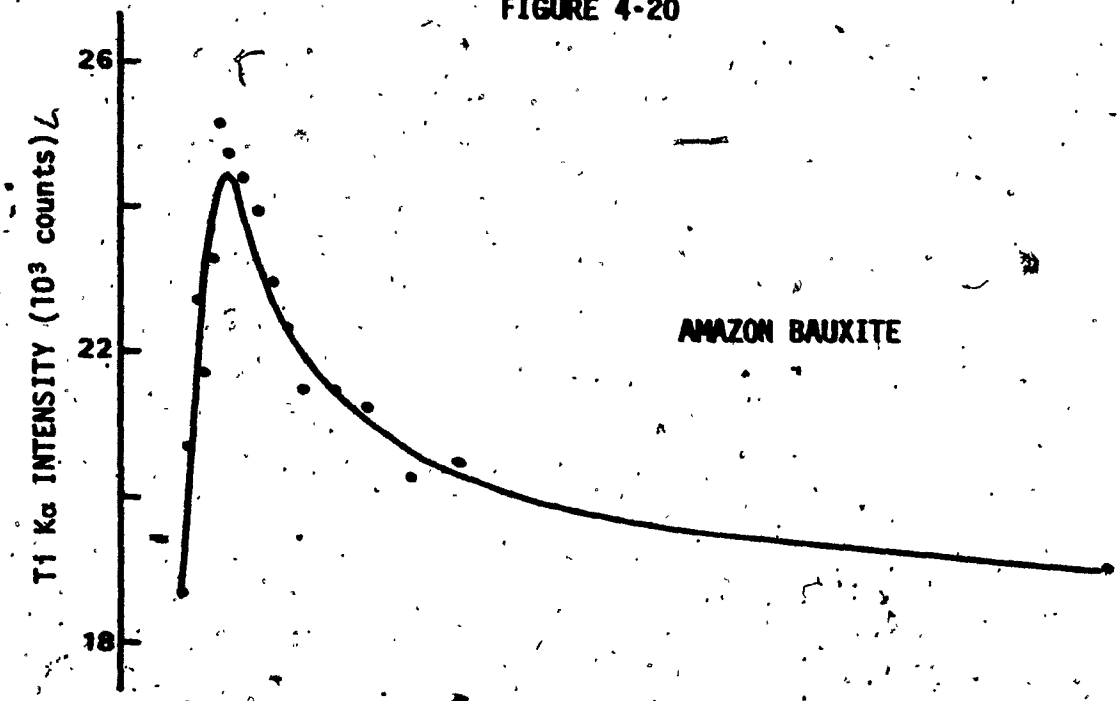

FIGURE 4-21

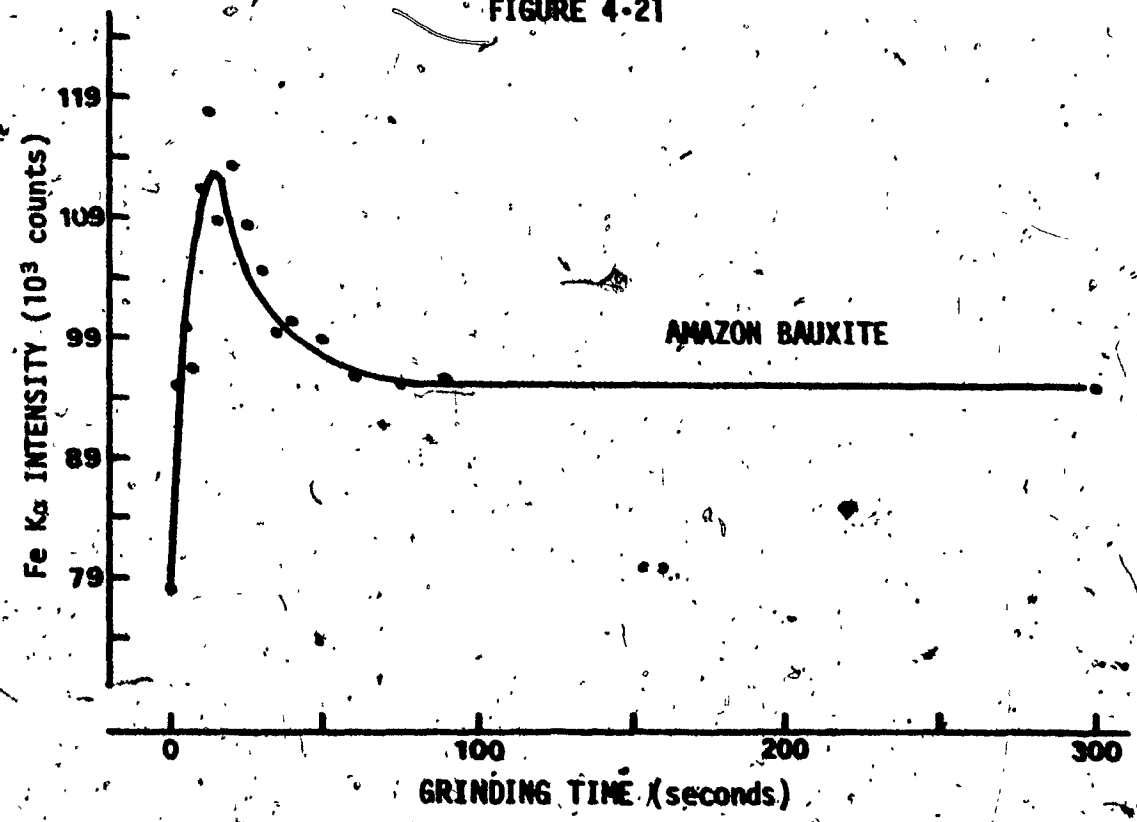

FIGURE 4·22

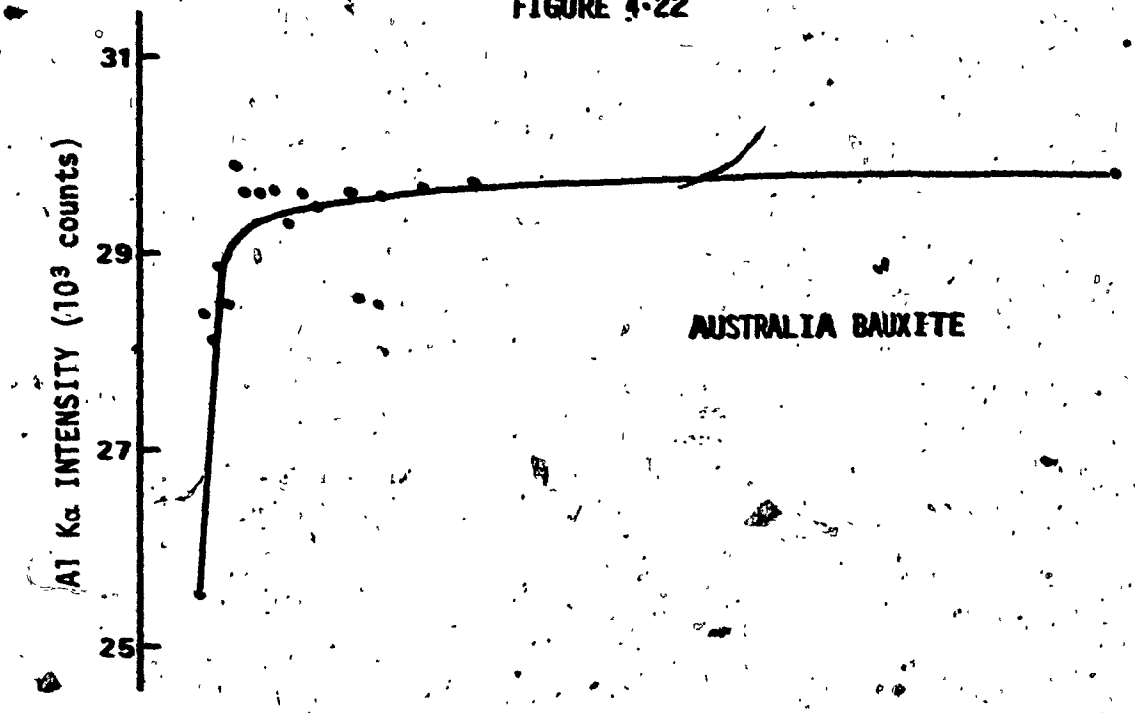

FIGURE 4·23

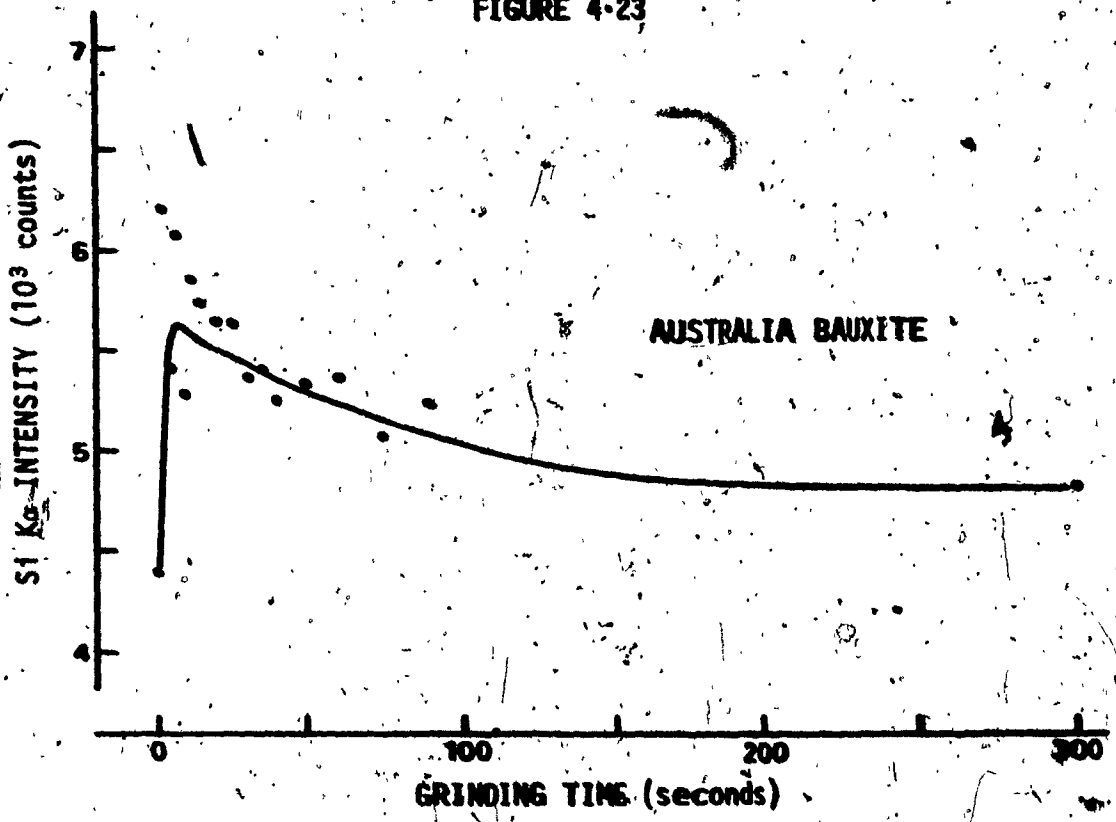

FIGURE 4-24

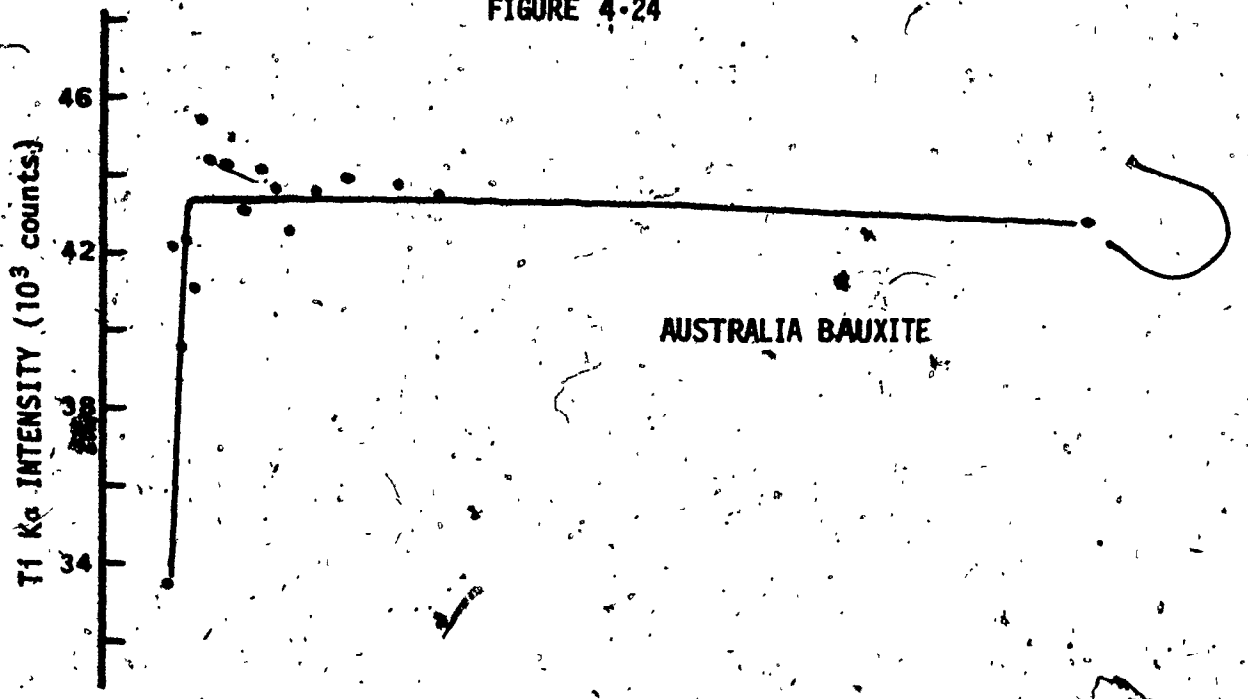

FIGURE 4-25

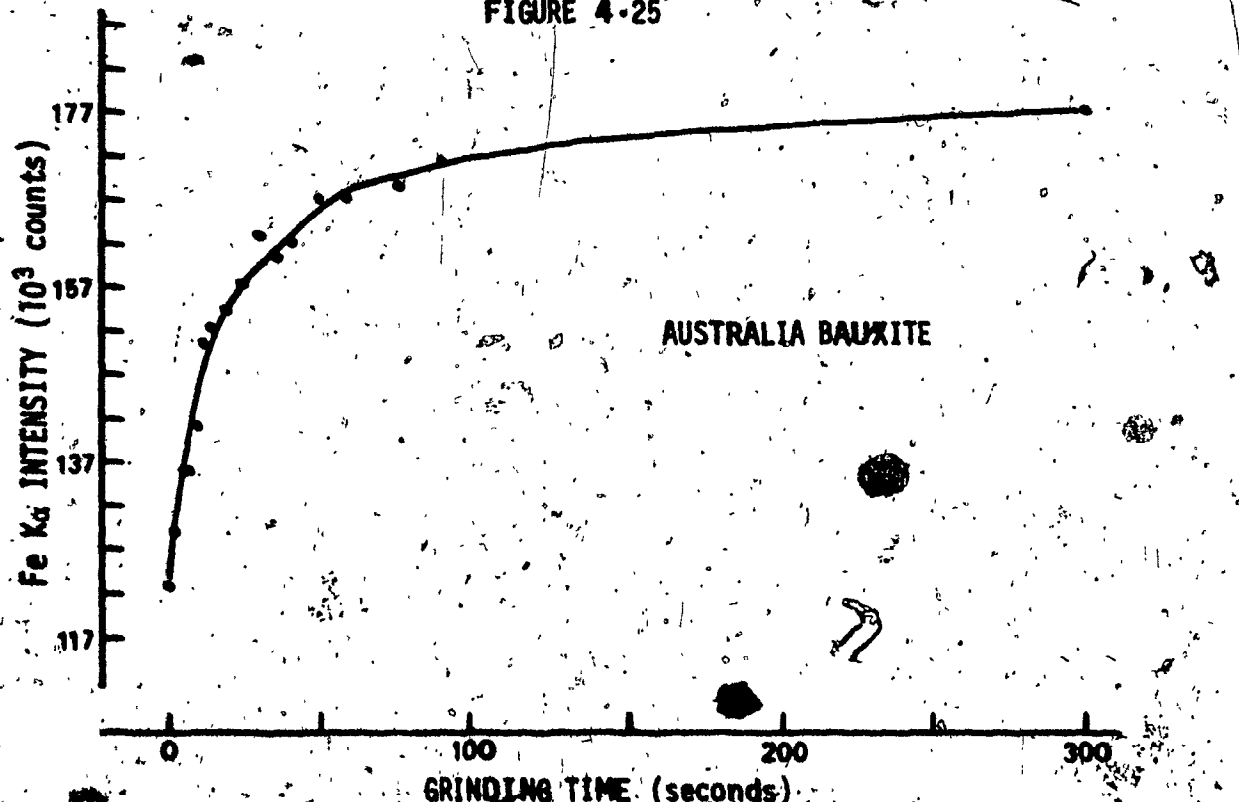

FIGURE 4·26

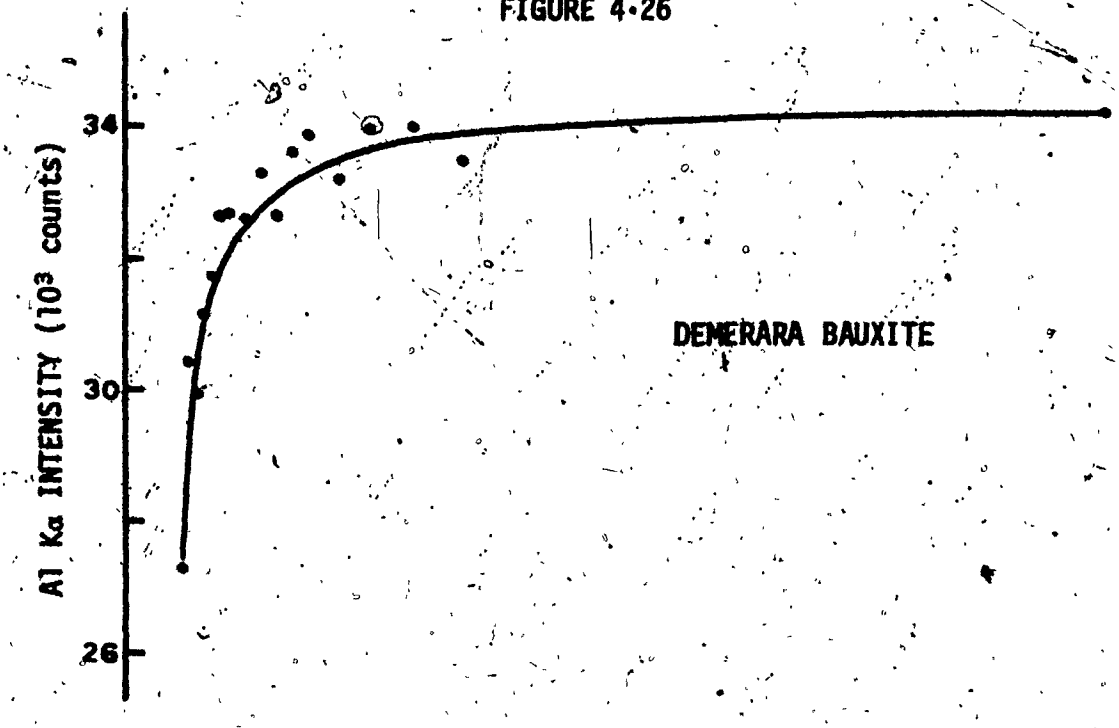

FIGURE 4·27

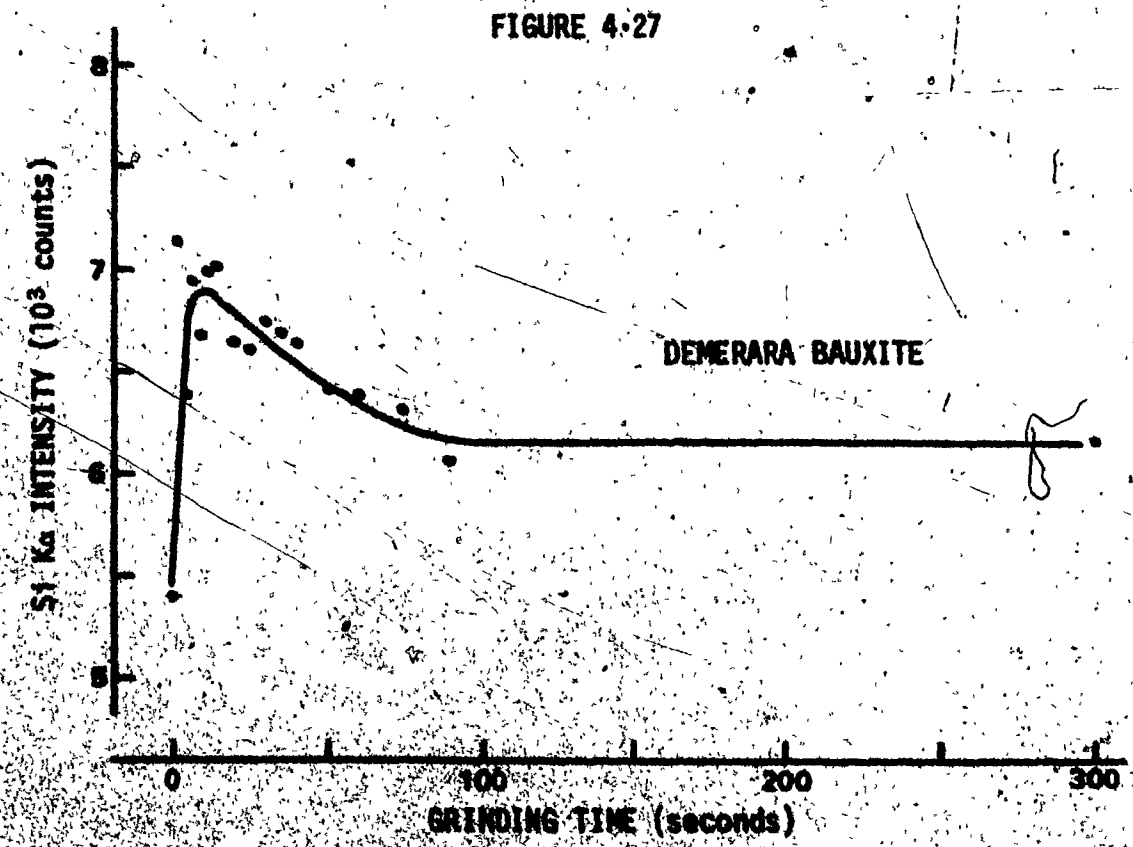

FIGURE 4-28

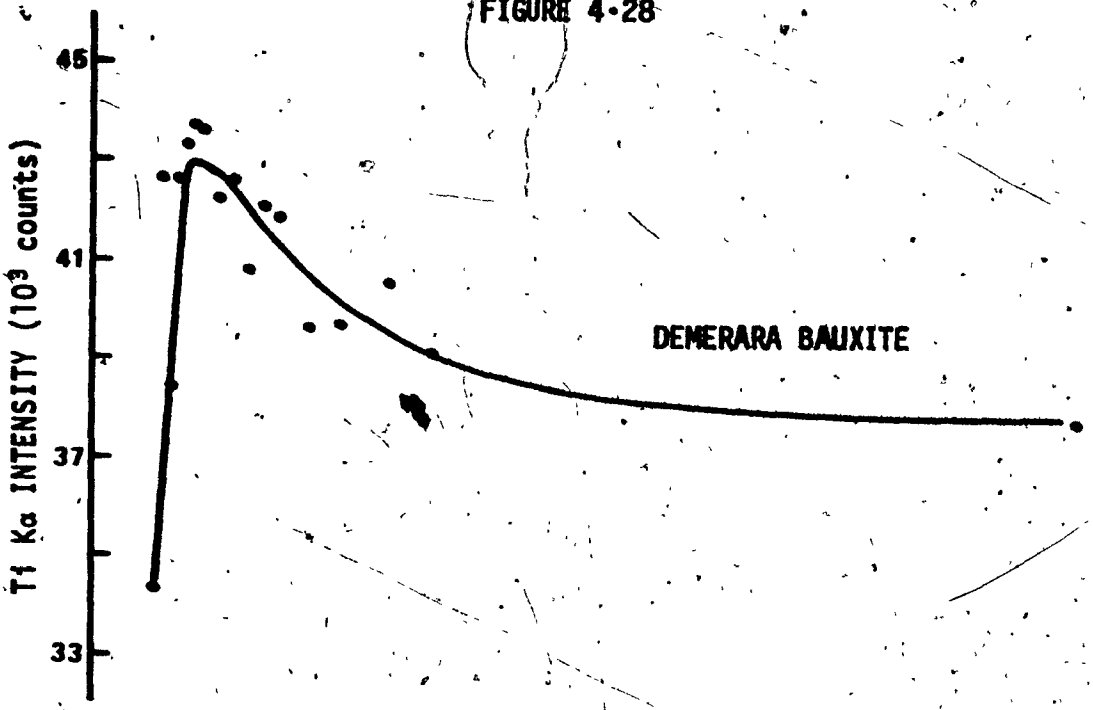

FIGURE 4-29

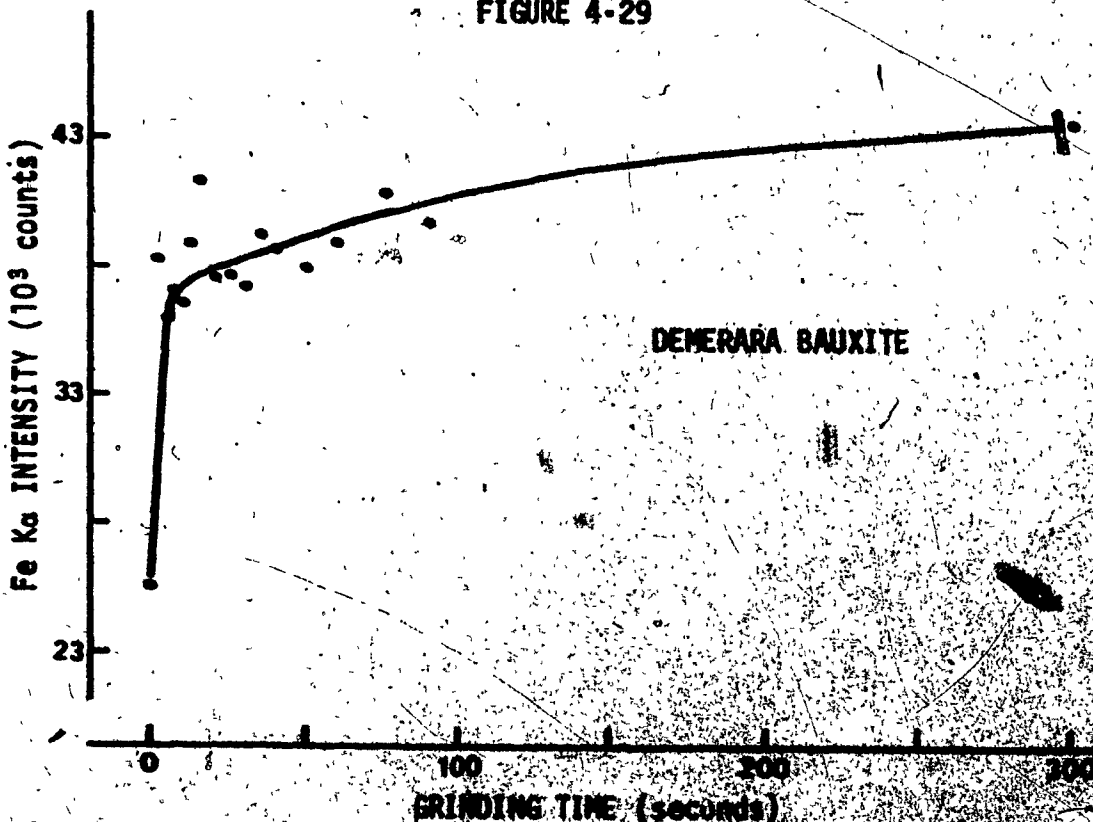

FIGURE 4-30

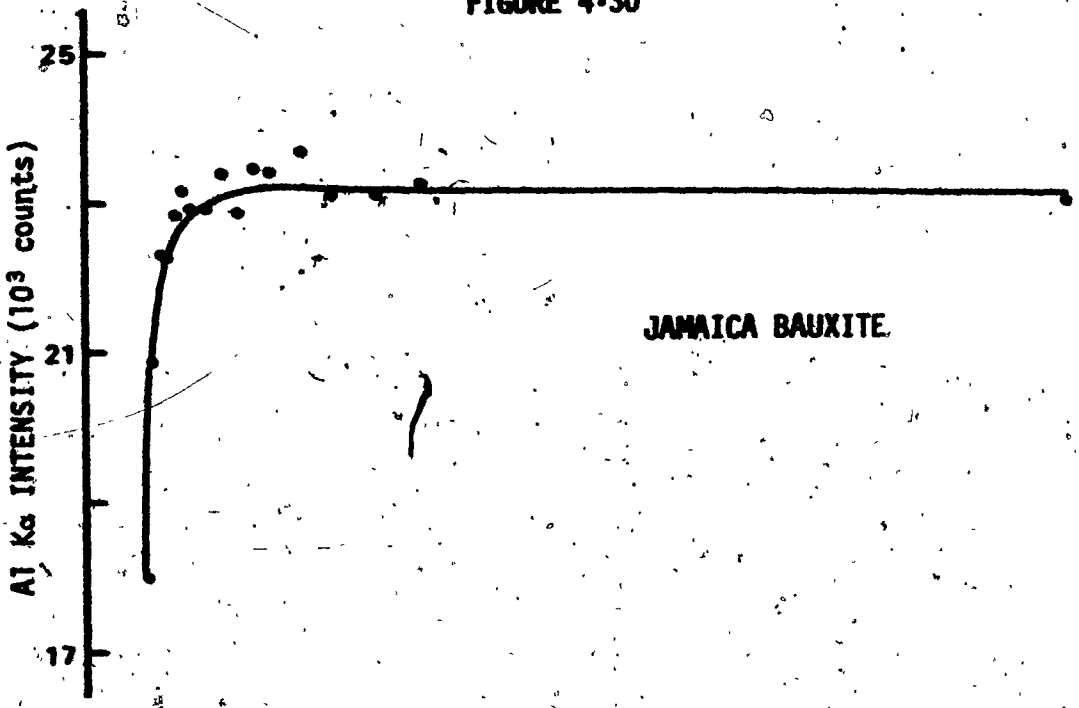

FIGURE 4-31

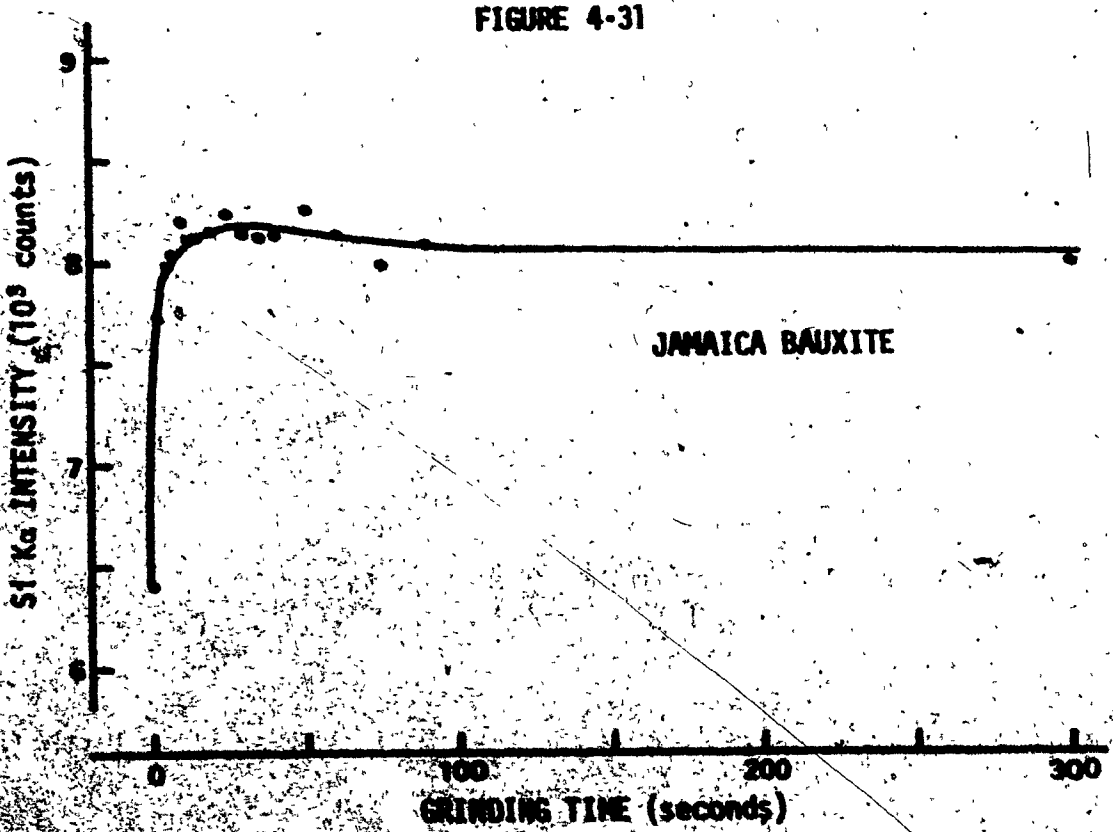

FIGURE 4·32

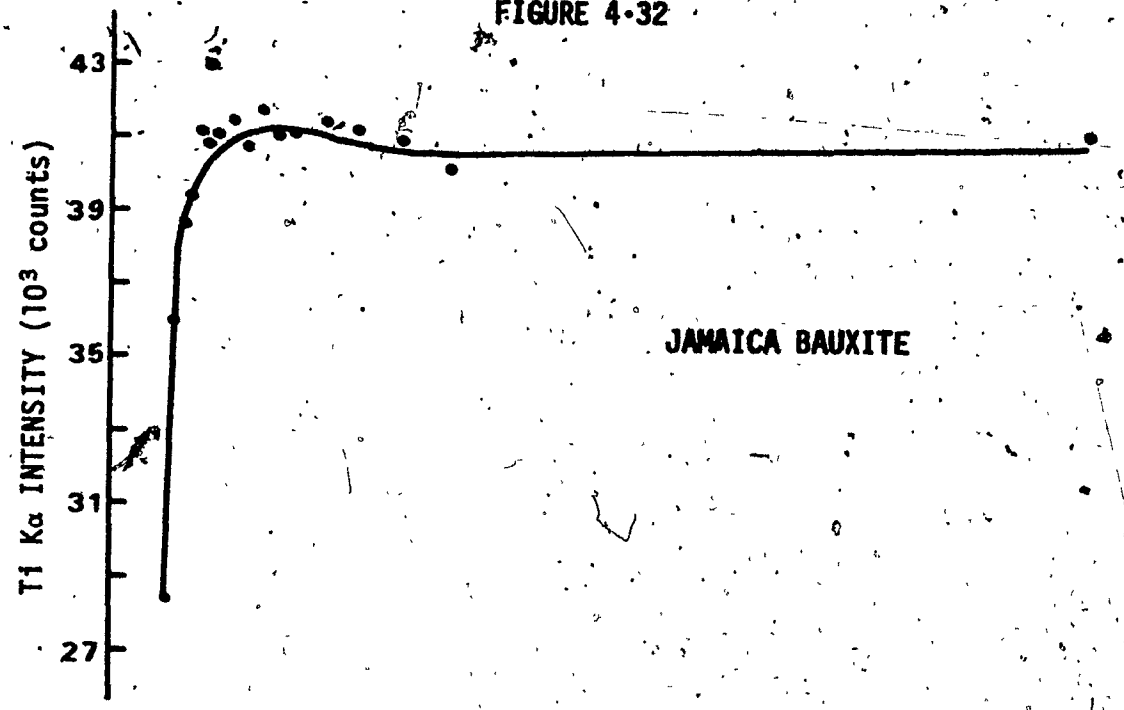

FIGURE 4·33

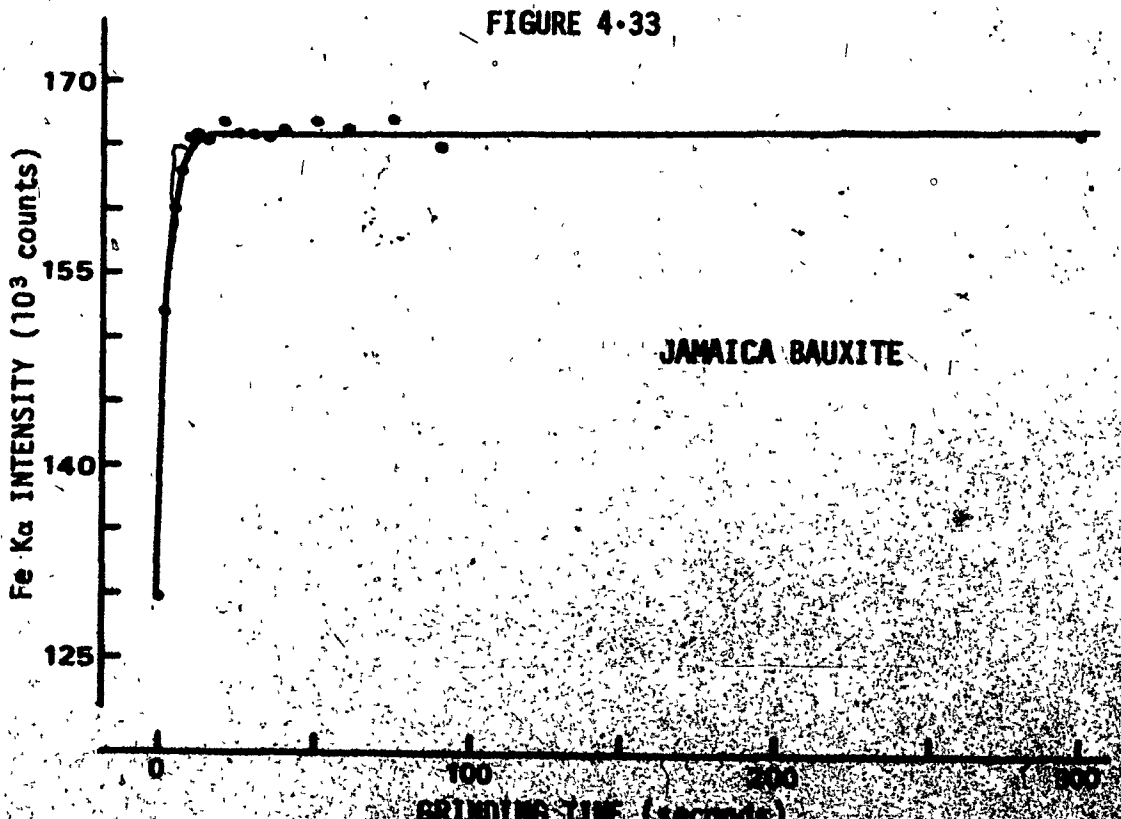

FIGURE 4-34

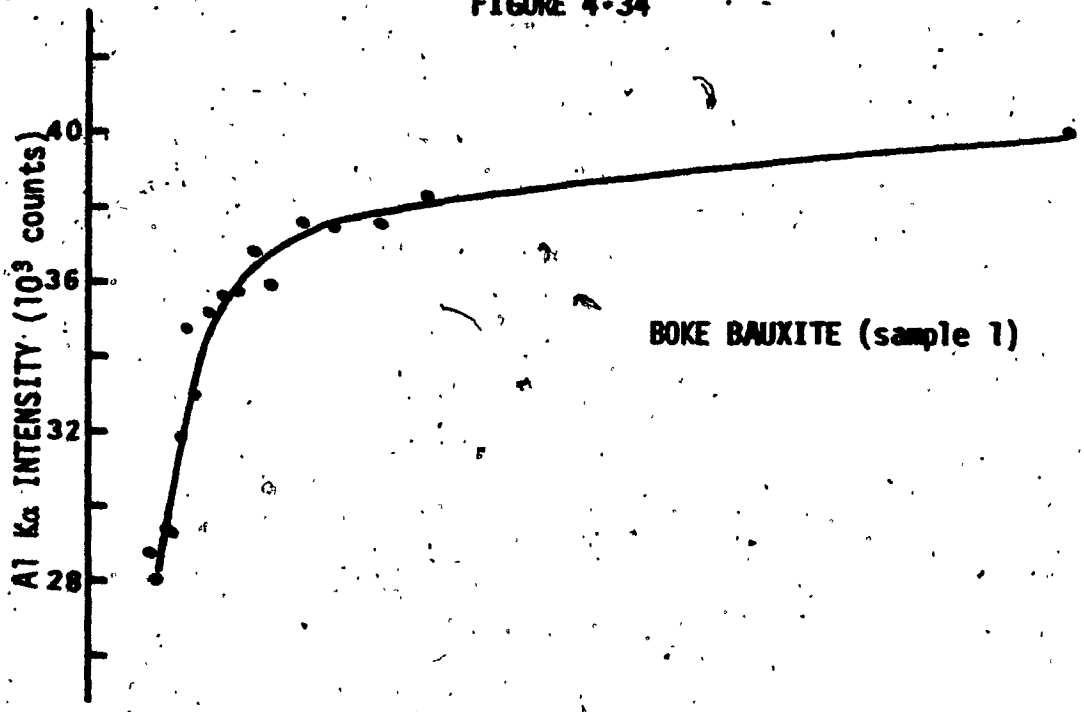

FIGURE 4-35

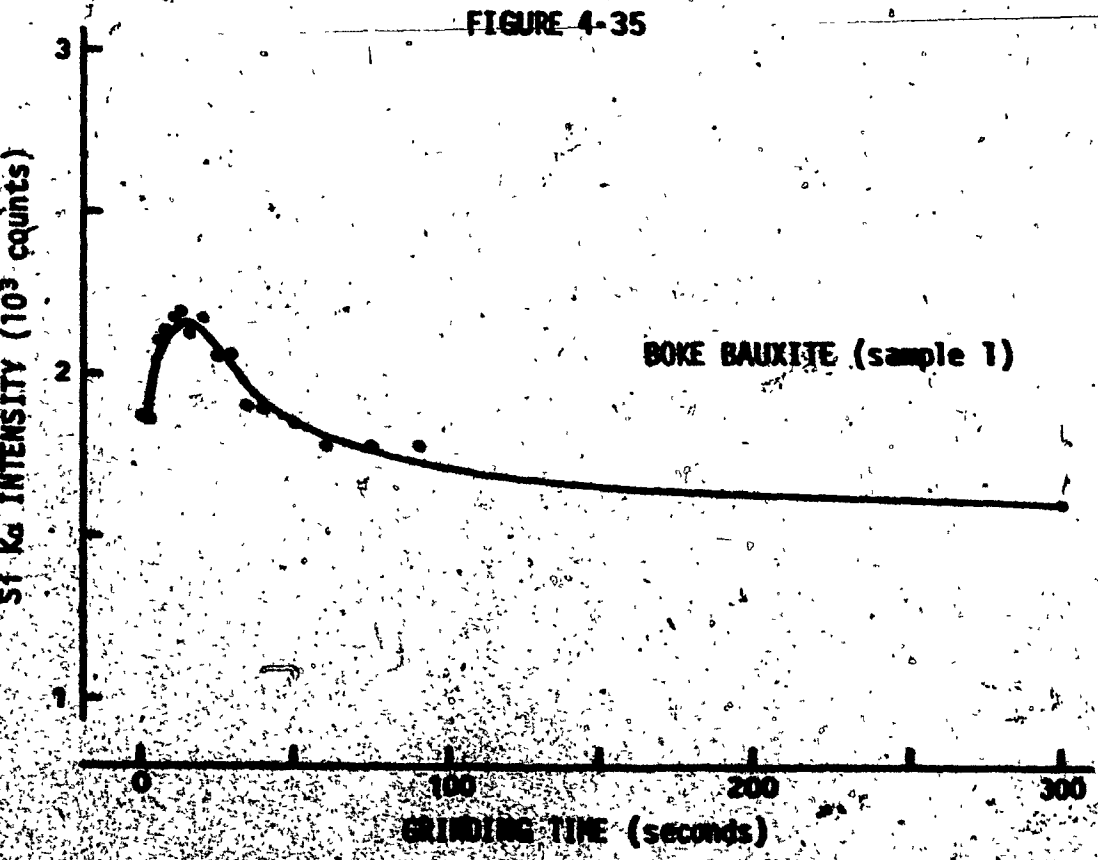

FIGURE 4-36

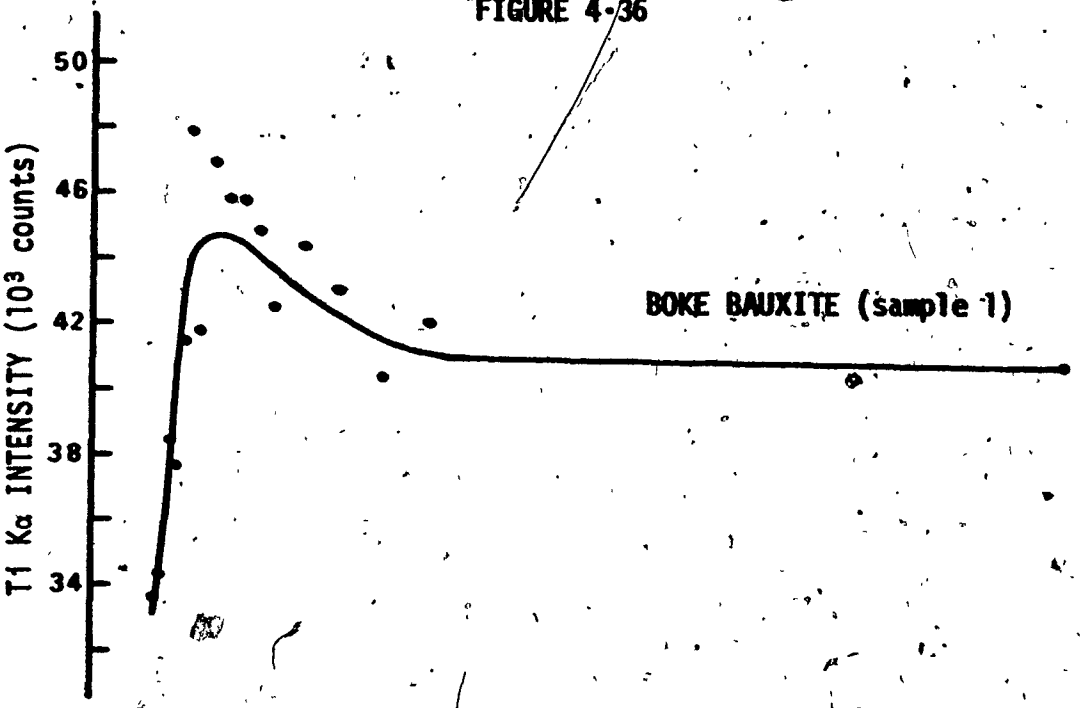

FIGURE 4-37

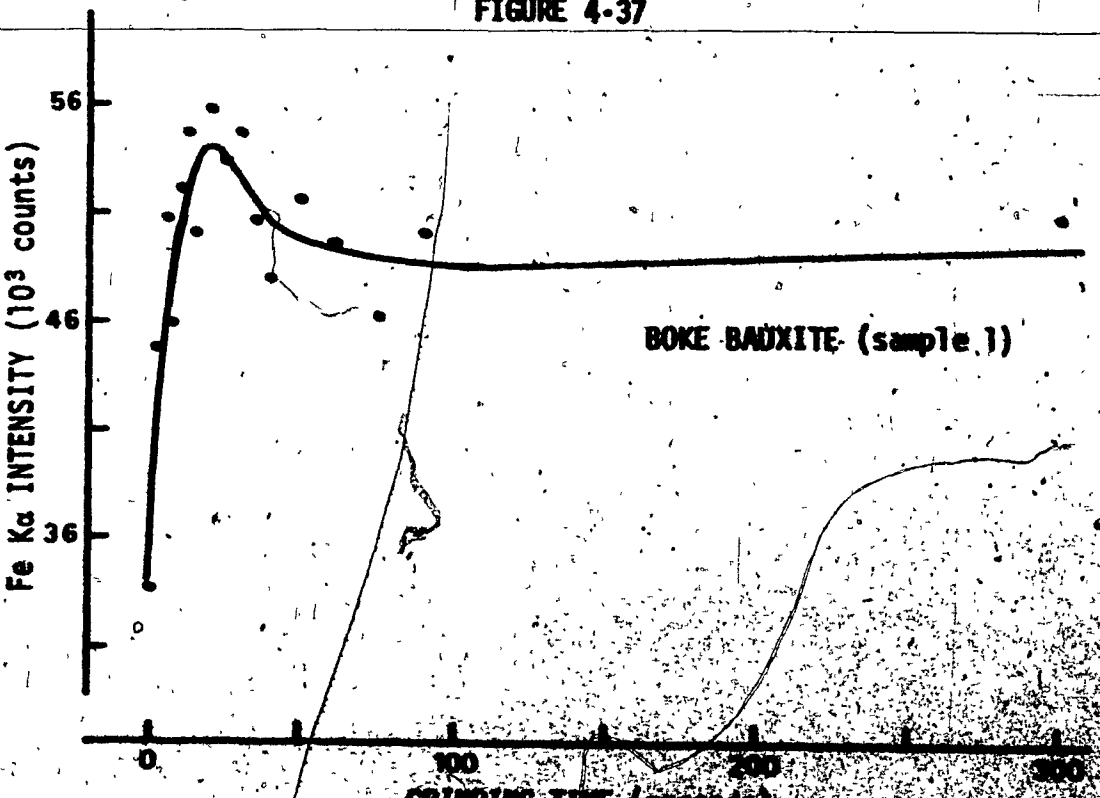

FIGURE 4·38

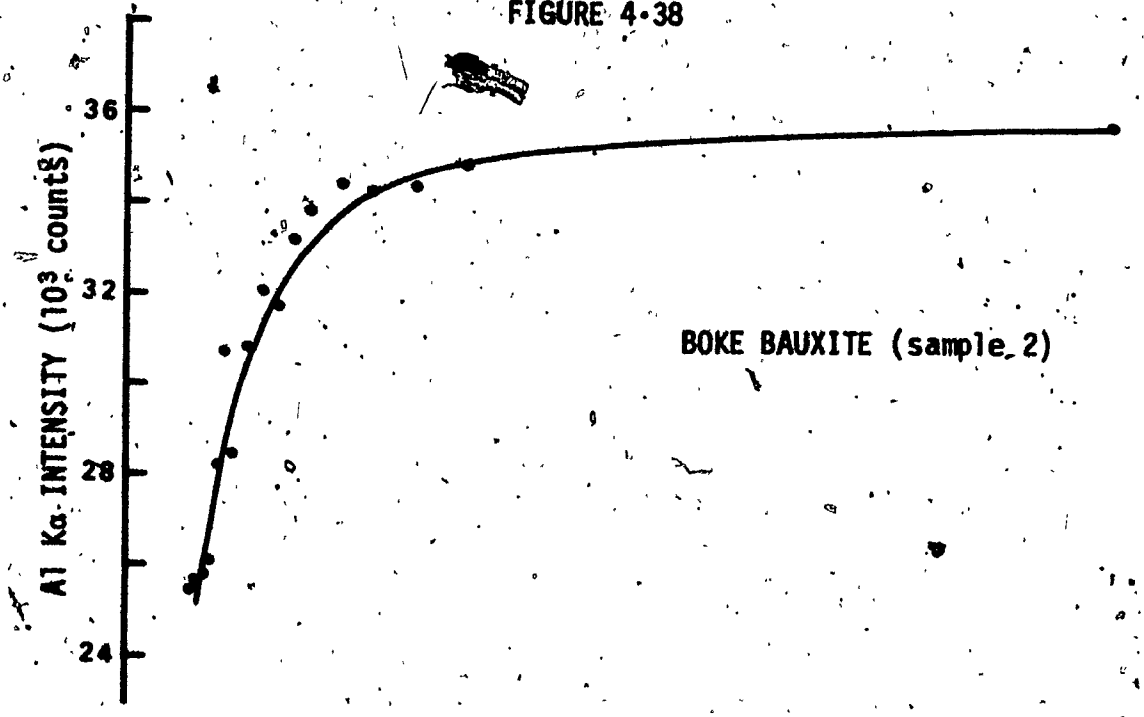

FIGURE 4·39

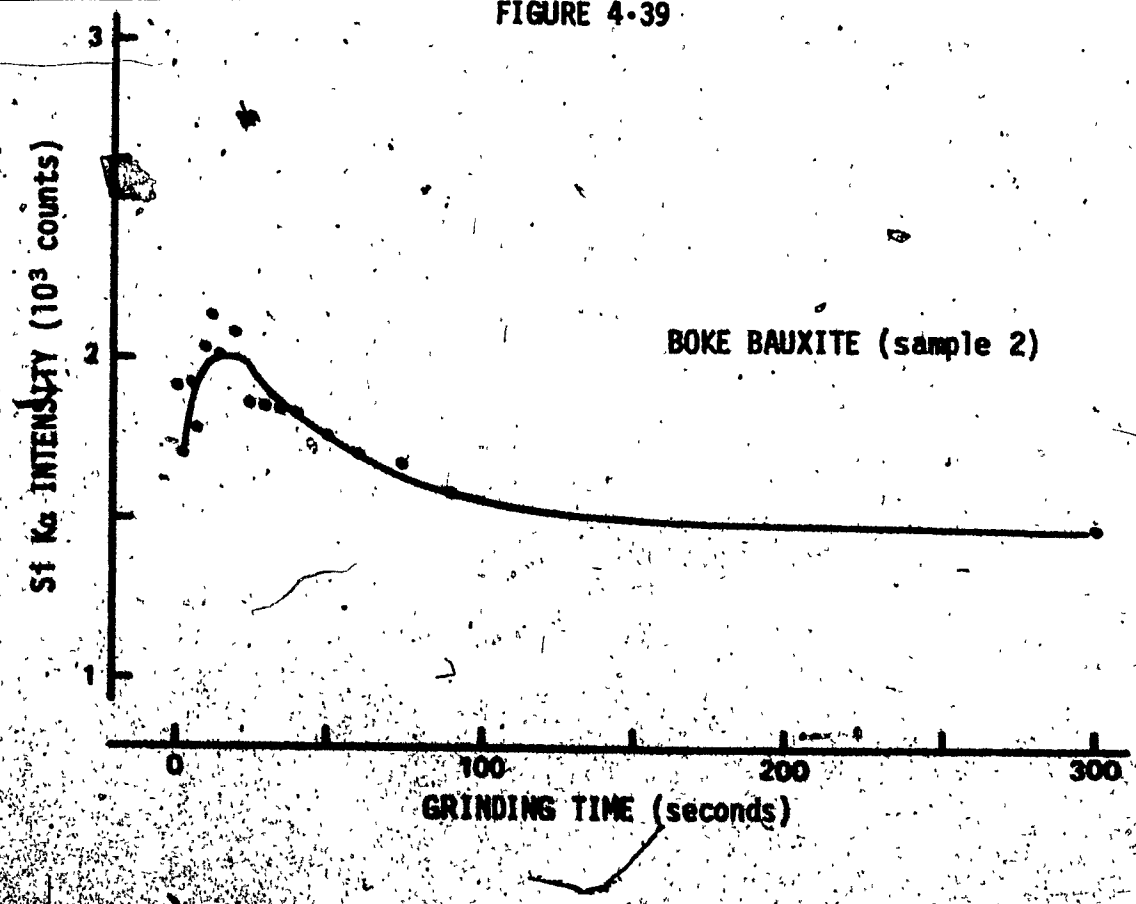

FIGURE 4-40

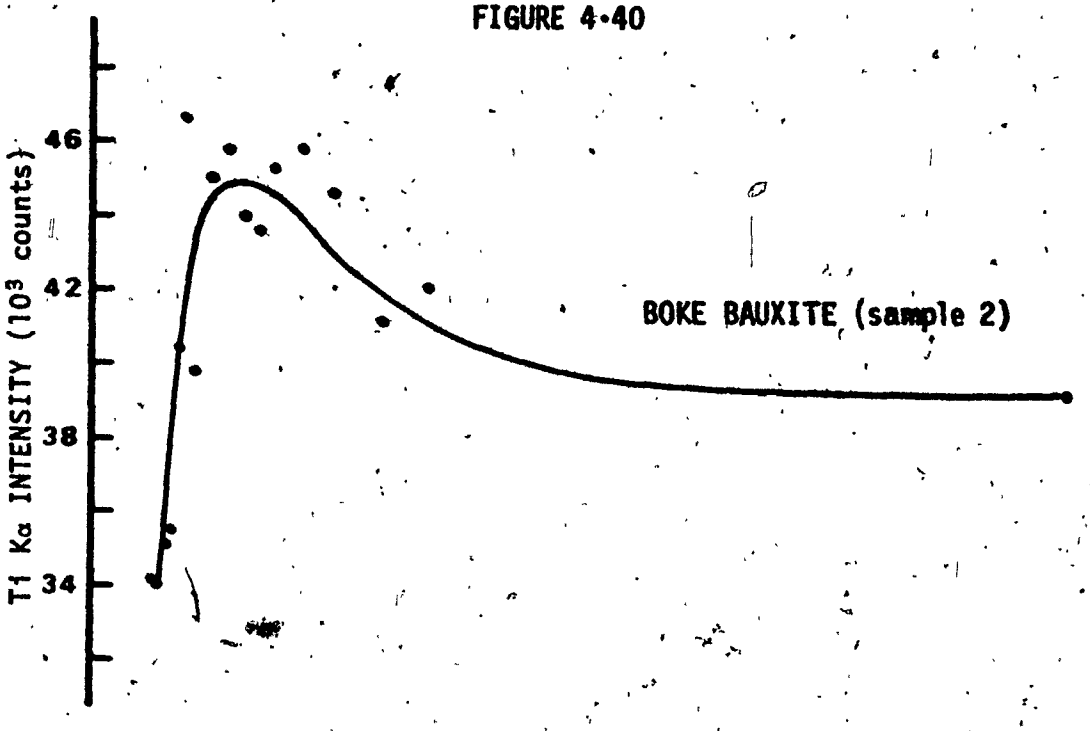

FIGURE 4-41

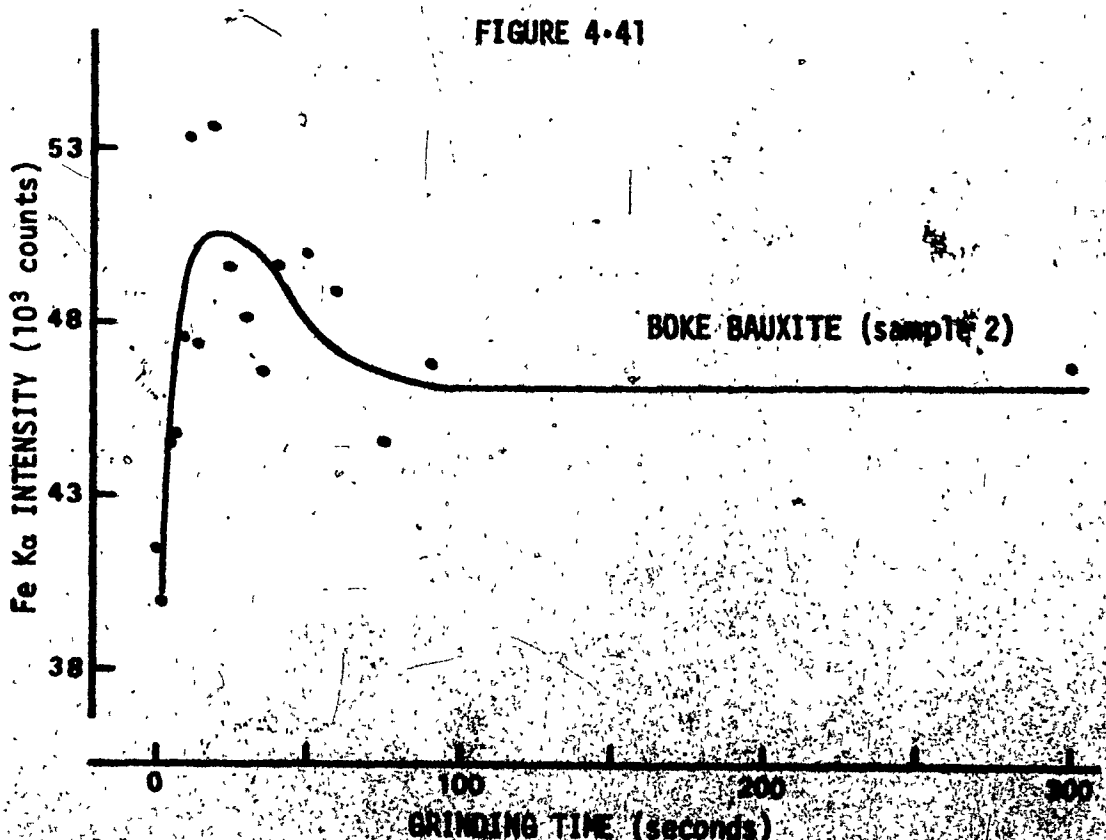

material shows either a uniform softness of components, permitting similar component particle size reduction with grinding time, or a high degree of compositional uniformity. In any case this material seems to more closely display a particle size effect than the others. Because of these results, the Jamaican bauxite is presently under investigation in an attempt to secure more specific information on the particle size effect.

The Australian material shows a somewhat similar trend, with the exception of the silicon counting intensity. While the counting intensity for this element is low, and therefore subject to a high relative counting error, it might be concluded, since small particles would envelop larger particles and produce a high counting rate, that the silicon component in the ore is reduced in size rapidly in the early grinding stages.

Where the remaining three materials are concerned, the high early intensities for iron, silicon and titanium might indicate rapid early size reduction with grinding for the ore components involving these elements. Such components, for example, may be significantly softer than those involving aluminum.

The general trend of the aluminum counting intensity to increase gradually with grinding time seems, where the Amazon, Boke and Demerara materials are concerned, to indicate a harder aluminum component, with size reduction progressing slowly with grinding time. Under such circumstances the softer iron, silicon and titanium components provide fine

particles in the early grinding stages. These finer particles fill the interstices between the larger aluminum component particles and provide high early intensities for these elements.

Finally, even if the bauxites ground homogeneously, it would be impossible to study particle size effects by grinding the bauxites for specific lengths of time. For any particular type of bauxite, particle size could be related to grinding time by the determination of particle size distributions. However, due to the apparent difference in total hardness of the various bauxites, the grinding time cannot be applied to determine any general particle size for different bauxites.

4.3 CONCLUSIONS

As far as the analysis of powdered bauxite is concerned, it is obvious that the composition of any sample varies with particle size. The results of this investigation indicate a disappearance of a particle size effect with decreasing particle size. This evidence of a variation of XRF counting intensity with particle size is almost totally masked by compositional variations.

In order to determine a particle size effect, a sample must be homogeneous. Also, most or all of the sample would have to be ground to the same particle size. Although difficult, the grinding to a uniform particle size could be possible; but bauxite ores are far from being homogeneous materials. It would thus seem impossible to establish

a definite relationship between XRF intensity and particle size that would be general for all kinds of bauxites. This results in the improbability of any accurate particle size effect correction in powdered bauxite analysis by x-ray fluorescence spectroscopy.

CHAPTER 5

MATRIX EFFECTS

5.1 INTRODUCTION

With the completion of the investigation of particle size effects, the second phase of the program could be attempted. This involved the examination of matrix absorption and enhancement effects and the correction of these effects in the XRF spectral analysis of bauxite material.

The matrix effect is the influence, as far as x-ray absorption or enhancement effects are concerned, that each element has with respect to each other element. The method of Lachance and Traill[31-37] was selected to establish and correct for these influences. In this method the matrix effects are represented by alpha coefficients in the Lachance and Traill expression (EQUATION 5.1) relating the measured x-ray intensity to elemental concentration for a binary sample.

$$C_A = R_A (1 + \alpha_{AB} C_B) \qquad 5.1$$

where R_A - the ratio of measured intensity for element A to the intensity of pure element A,

C_A - the concentration of A.

C_B = the concentration of the interfering element B,

α_{AB} = the alpha coefficient representing the effect of element B on the intensity of element A.

Using two samples containing different amounts of the two elements, the alpha coefficient (α_{AB}) is determined by the simultaneous solution of two Lachance and Traill expressions.

$$\alpha_{AB} = \frac{C_A I'_A - C'_A I_A}{C'_A I_A C_B - C_A I'_A C'_B} \qquad 5\text{-}2$$

where C_A and C'_A = two concentrations of element A,

I_A and I'_A = two measured intensities of element A,

C_B and C'_B = two concentrations of element B.

For multiple element systems the expression is extended by the addition of other terms giving EQUATION 5-3. Determination

$$C_A = R_A \left(1 + \alpha_{AB} C_B + \alpha_{AC} C_C + \alpha_{AD} C_D + - - - \right) \qquad 5\text{-}3$$

of the alpha coefficients requires the simultaneous solution of several such equations, one for each element in the system. Although possible, this multiple element method may produce large errors due to the number of variables involved, each with their own uncertainty.

In the analysis of bauxite ore, the alpha coefficients were determined through the preparation of a series of binary or

ternary samples. As described previously, the analysis only involved the four major elements (Al, Si, Ti, Fe). The balance of the sample is mostly oxygen (from the metal oxides and water) and some traces of other elements. This balance is henceforth referred to as the matrix. Thus, the sample is essentially a five element system. For each of the four analysed elements there are four alpha coefficients representing the influence of the matrix and the other three elements. In order to investigate the matrix effect in bauxite it was necessary to determine a total of 16 alpha coefficients.

The following sections describe the attempts to obtain a consistent set of alpha coefficients and their applicability to the analysis of bauxite ore.

5·2 EXPERIMENTAL RESULTS AND DISCUSSION

5·2·1 DETERMINATION OF ALPHA COEFFICIENTS FROM SYNTHETIC BINARY MIXTURES OF Al, Si, Ti AND Fe

To determine each alpha coefficient a series of binary samples was prepared and subjected to analysis by XRF using the parameters suitable for the determination of iron, titanium, silicon and aluminum. The samples consisted of the metal oxides and not the pure metals. In actual fact they were ternary systems. Only the

samples used to determine the alpha coefficients showing the effect of the matrix on each of the elements were truly binary systems. Since the other samples contained only two elements in addition to the matrix, they were considered as binary mixtures.

Initially, a complete set of 76 synthetic binary samples were prepared as outlined in SECTION 3·2. Since there was no fine quartz (SiO_2) available at this time, 320 grit silicon carbide (SiC) was used. The desired amounts of metallic oxides were weighed out and lithium carbonate (Li_2CO_3) was added as the balance of the matrix. It was noted that bauxite ore does not contain any significant amount of carbon. However, since carbon and oxygen are both very light elements, an assumption was made to the effect that their absorption properties would be basically similar. The replacement of carbon for oxygen was not expected to appreciably affect the results.

The observed spectral data for the 16 binary systems shows the effects of elemental interaction. This data is plotted in FIGURES 5·1 to 5·16.

The alpha coefficients were determined by the computer program AXMSD (for matrix interaction) and program AABSD (for elemental interaction). The detailed method of calculation and the program listings are described in APPENDIX C . Briefly, for each series of samples, the alpha coefficient so determined resulted

FIGURES 5-1 to 5-16

Binary system x-ray intensity data, measured and calculated, showing interelement effects and corrections for interelement effects by the method of Lachance and Traill.

FIGURE 5-1

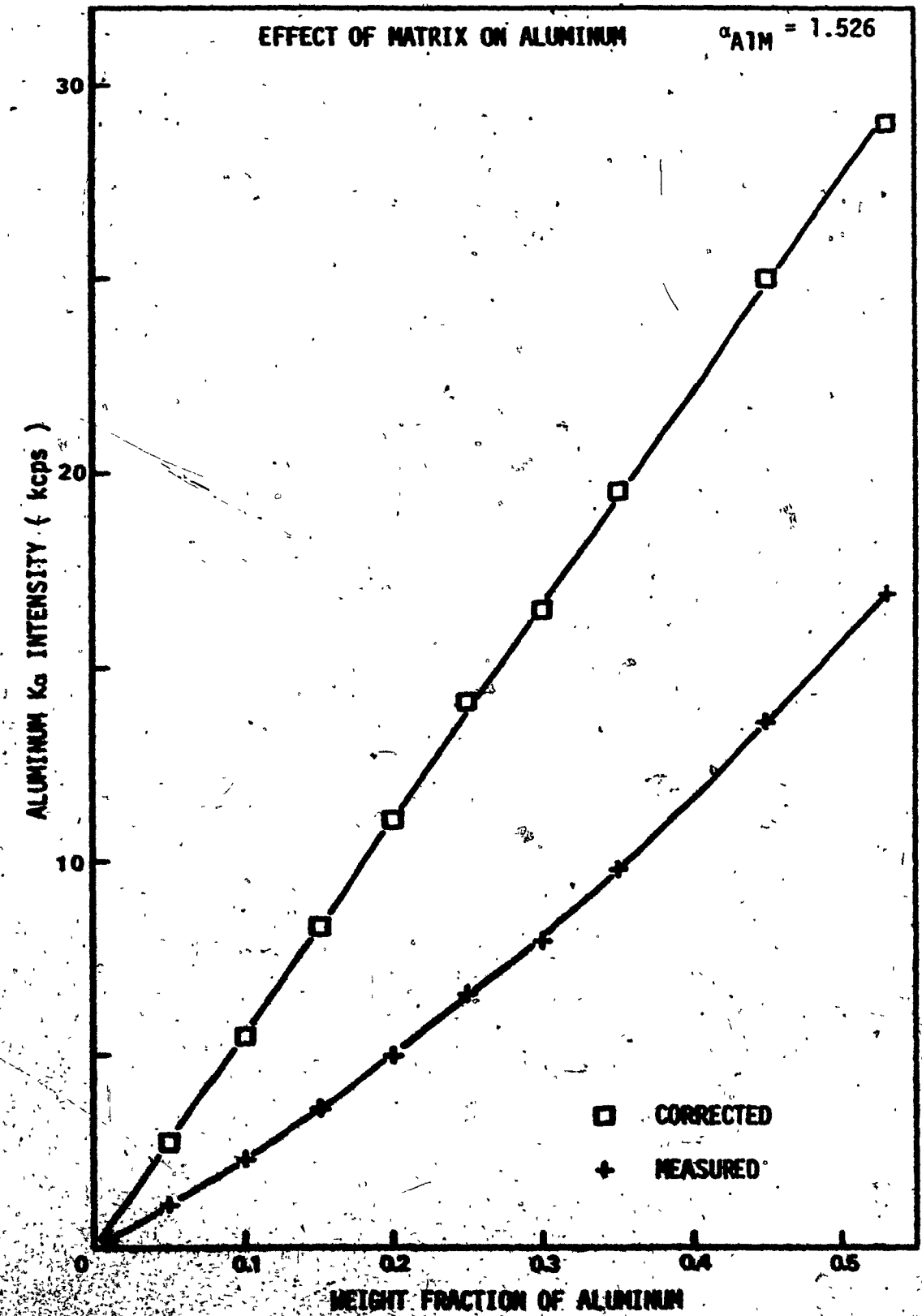
EFFECT OF MATRIX ON ALUMINUM
α_{AlM} = 1.526
ALUMINUM Kα INTENSITY (kcps)
30
20
10
0
0.1
0.2
0.3
0.4
0.5
WEIGHT FRACTION OF ALUMINUM
CORRECTED
MEASURED

FIGURE 5-2

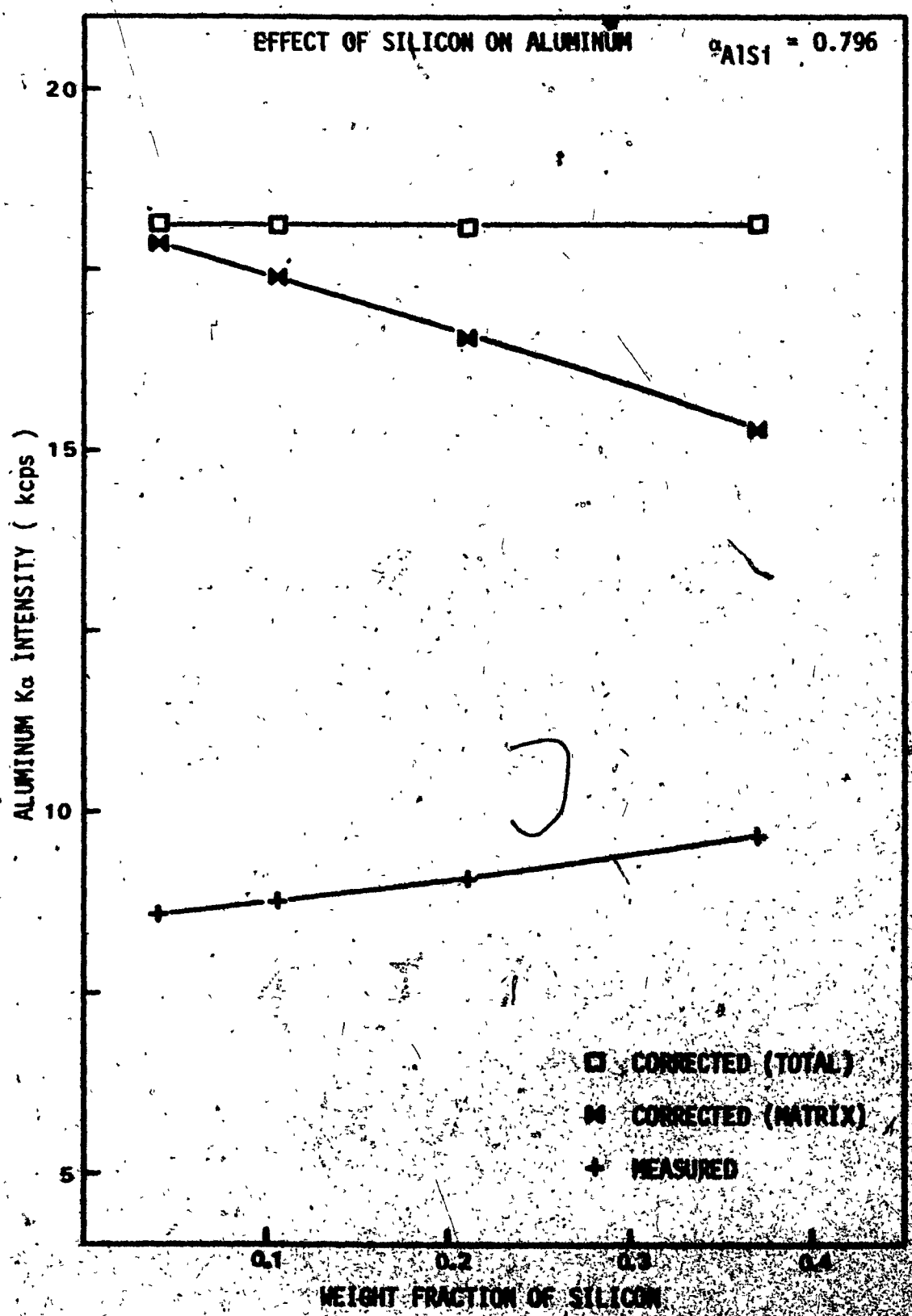
EFFECT OF SILICON ON ALUMINUM
α_{AlSi} = 0.796
ALUMINUM Kα INTENSITY (kcps)
20
15
10
5
0.1
0.2
0.3
0.4
WEIGHT FRACTION OF SILICON
CORRECTED (TOTAL)
CORRECTED (MATRIX)
MEASURED

FIGURE 5-3

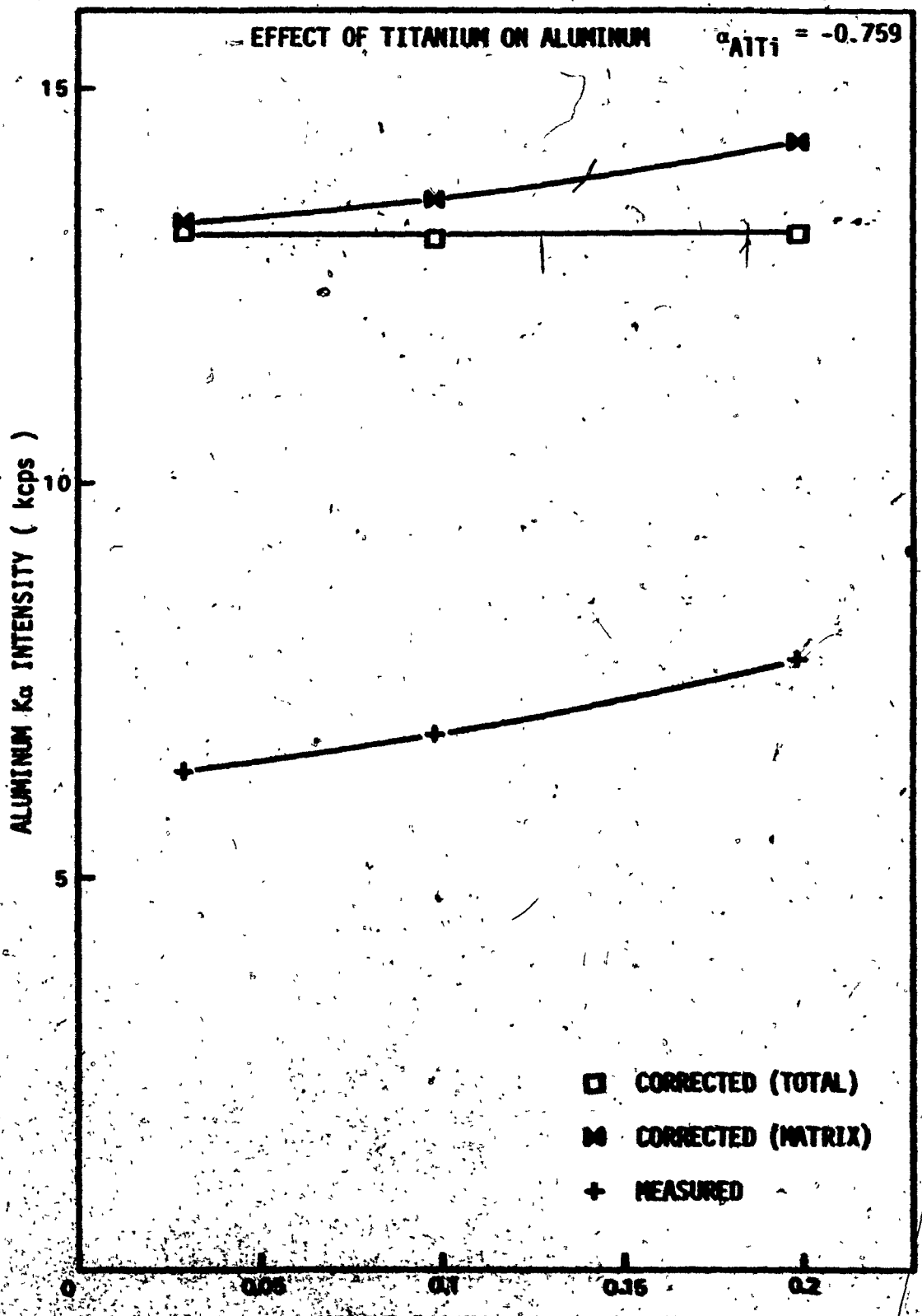
EFFECT OF TITANIUM ON ALUMINUM
α_{AlTi} = -0.759
15
10
5
ALUMINUM Kα INTENSITY (kcps)
CORRECTED (TOTAL)
CORRECTED (MATRIX)
MEASURED
0
0.05
0.1
0.15
0.2
WEIGHT FRACTION OF TITANIUM

FIGURE 5-4

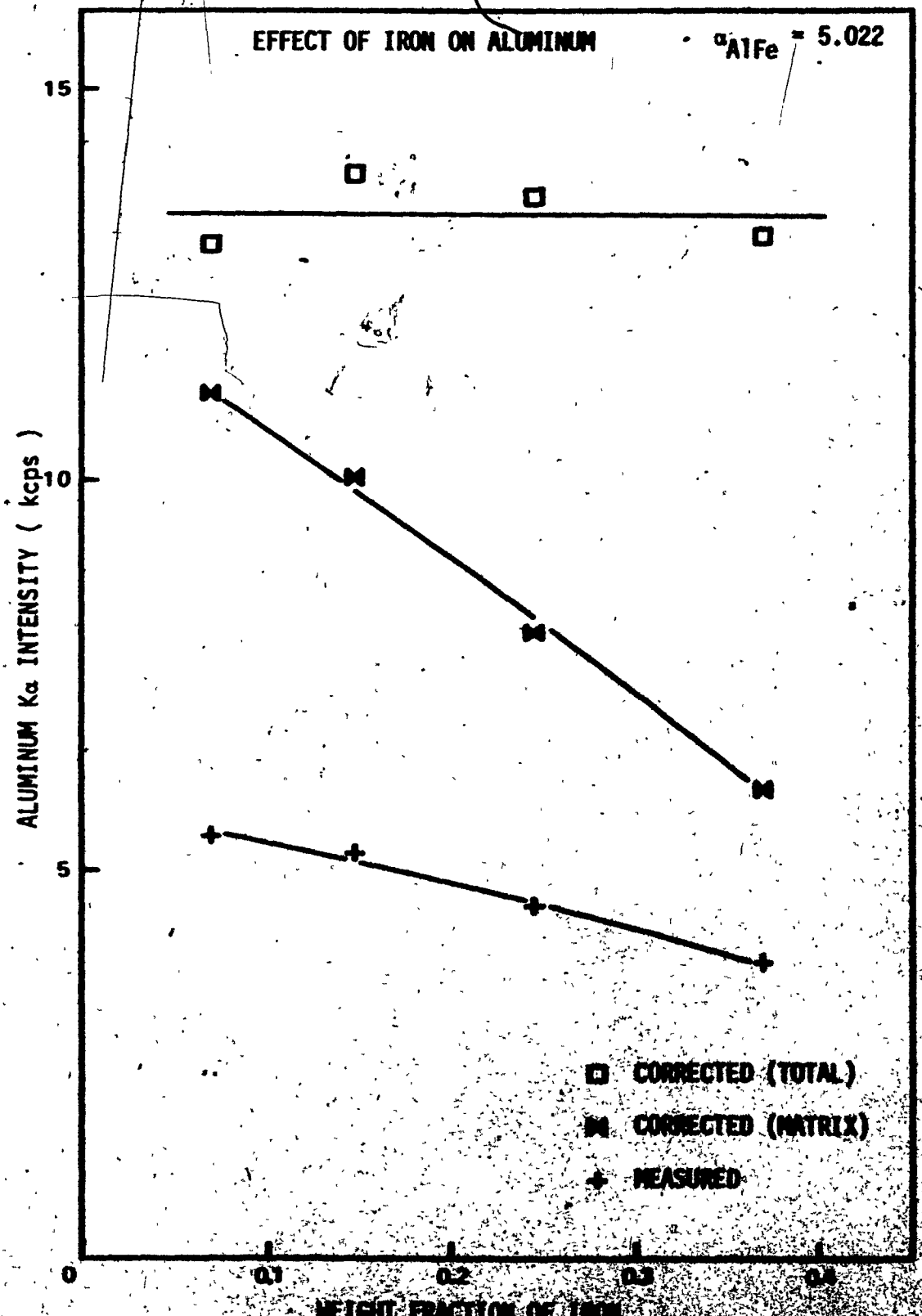
EFFECT OF IRON ON ALUMINUM
α_{AlFe} = 5.022
15
10
5
0
ALUMINUM Kα INTENSITY (kcps)
0.1
0.2
0.3
0.4
WEIGHT FRACTION OF IRON
CORRECTED (TOTAL)
CORRECTED (MATRIX)
MEASURED

FIGURE 5-5

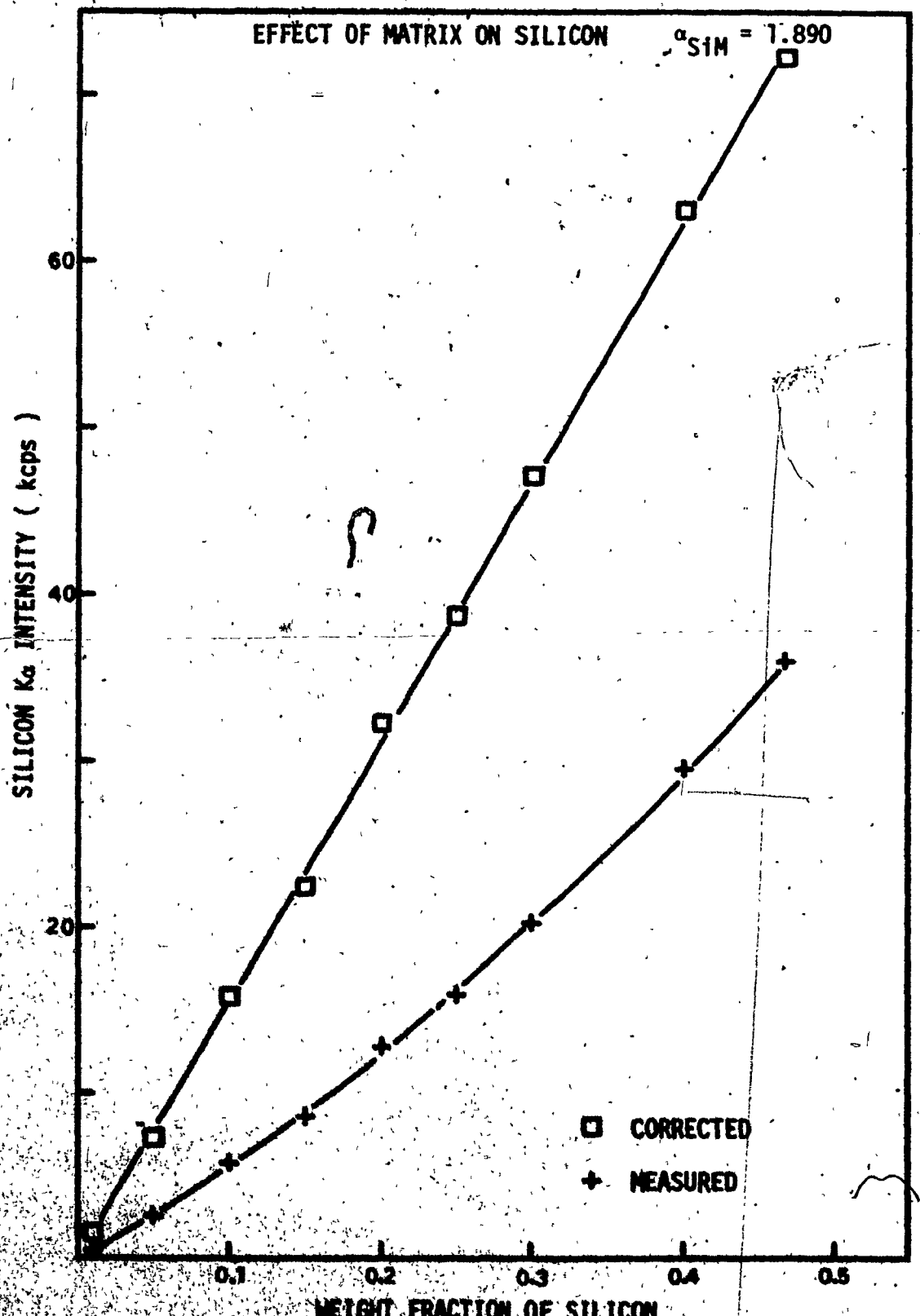
EFFECT OF MATRIX ON SILICON
α_{SiM} = 1.890
SILICON Kα INTENSITY (kcps)
60
40
20
0.1
0.2
0.3
0.4
0.5
WEIGHT FRACTION OF SILICON
CORRECTED
MEASURED

FIGURE 5-6

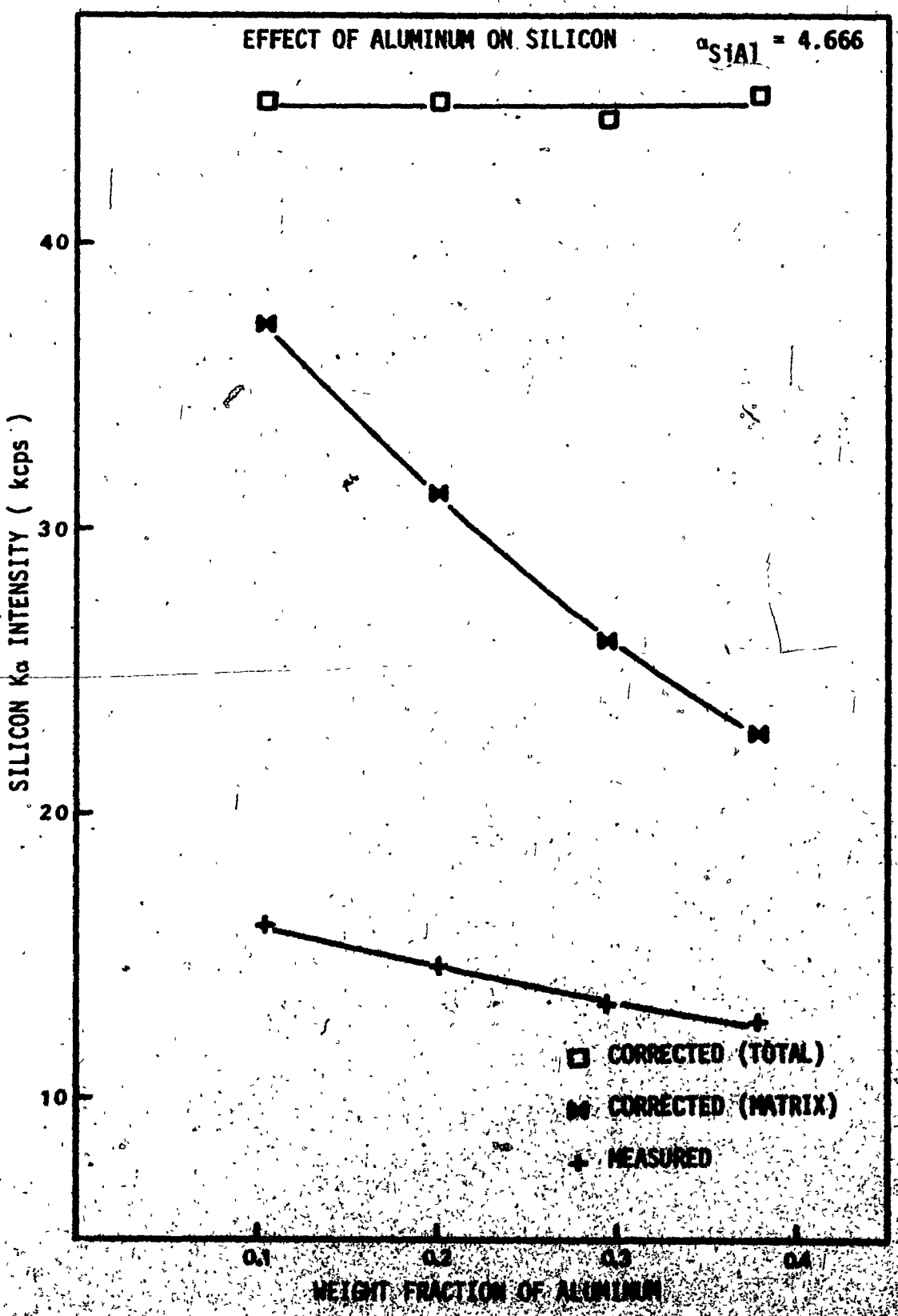
EFFECT OF ALUMINUM ON SILICON
α_{SiAl} = 4.666
SILICON Kα INTENSITY (kcps)
40
30
20
10
0.1
0.2
0.3
0.4
WEIGHT FRACTION OF ALUMINUM
CORRECTED (TOTAL)
CORRECTED (MATRIX)
MEASURED

FIGURE 5-7

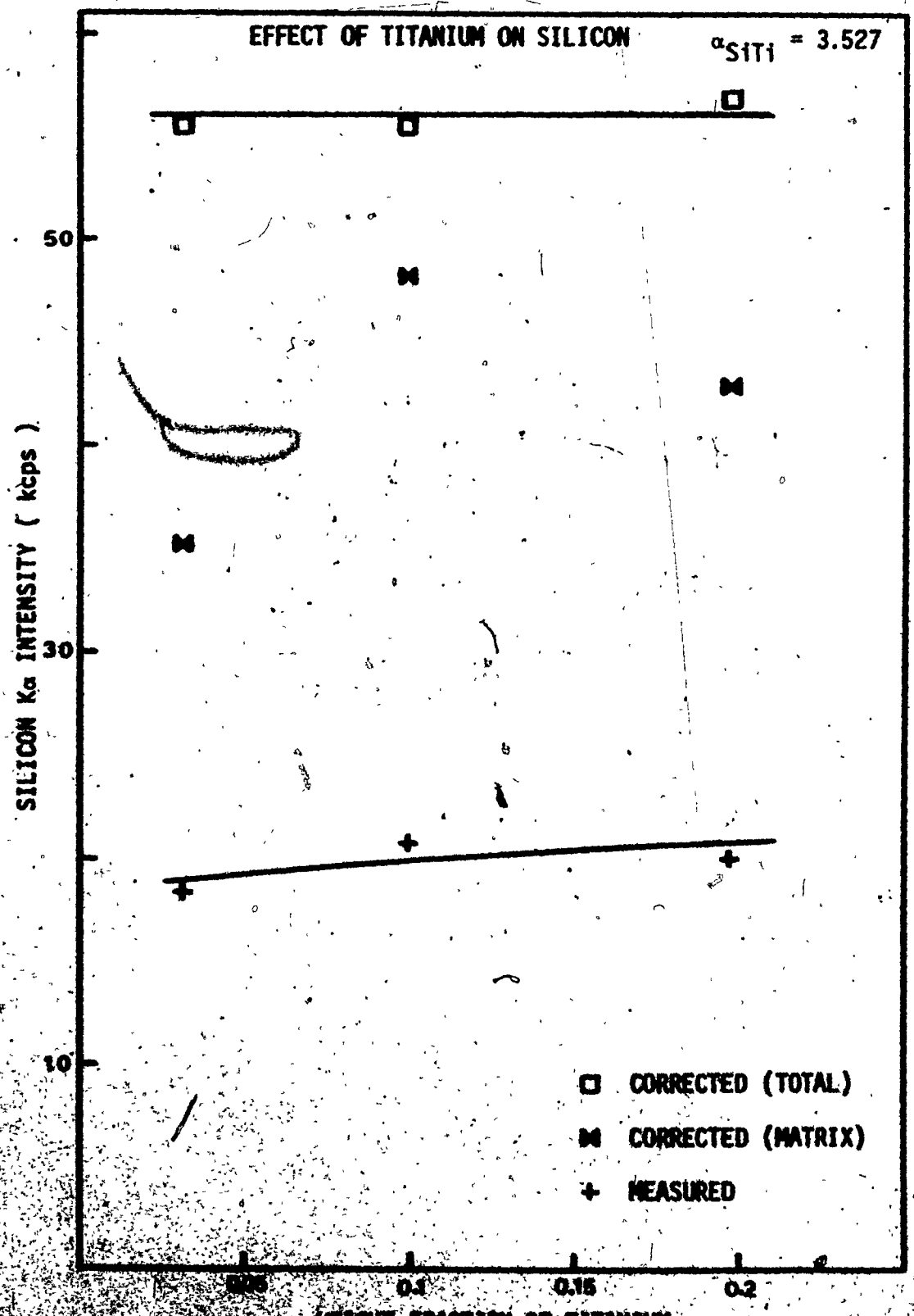
EFFECT OF TITANIUM ON SILICON
α_{SiTi} = 3.527
SILICON Ka INTENSITY (kcps)
50
30
10
CORRECTED (TOTAL)
CORRECTED (MATRIX)
MEASURED
0.1
0.15
0.2
WEIGHT FRACTION OF TITANIUM

FIGURE 5·8

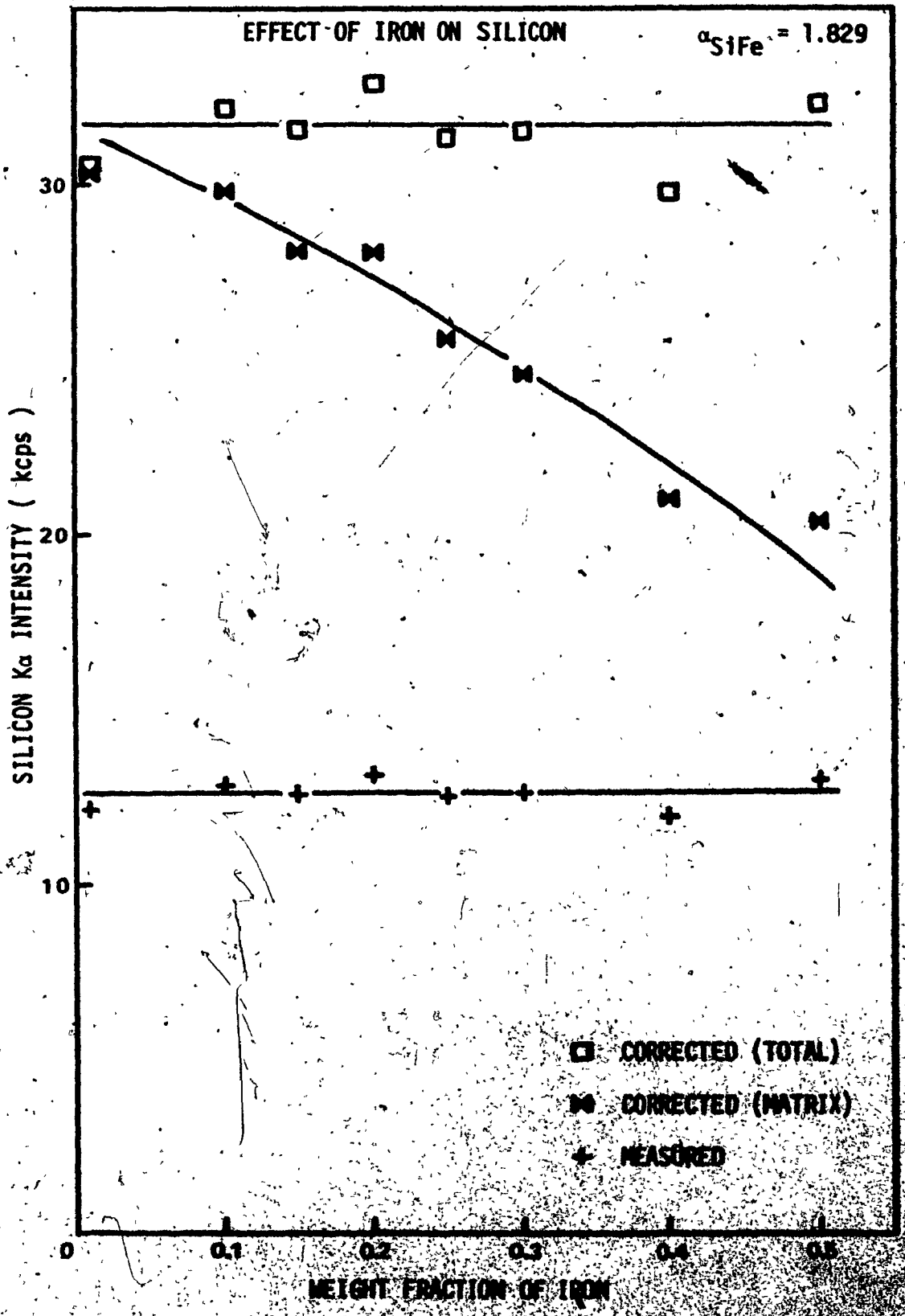
EFFECT OF IRON ON SILICON
α_{SiFe} = 1.829
SILICON Ka INTENSITY (kcps)
30
20
10
0
0.1
0.2
0.3
0.4
0.5
WEIGHT FRACTION OF IRON
CORRECTED (TOTAL)
CORRECTED (MATRIX)
MEASURED

FIGURE 5-9

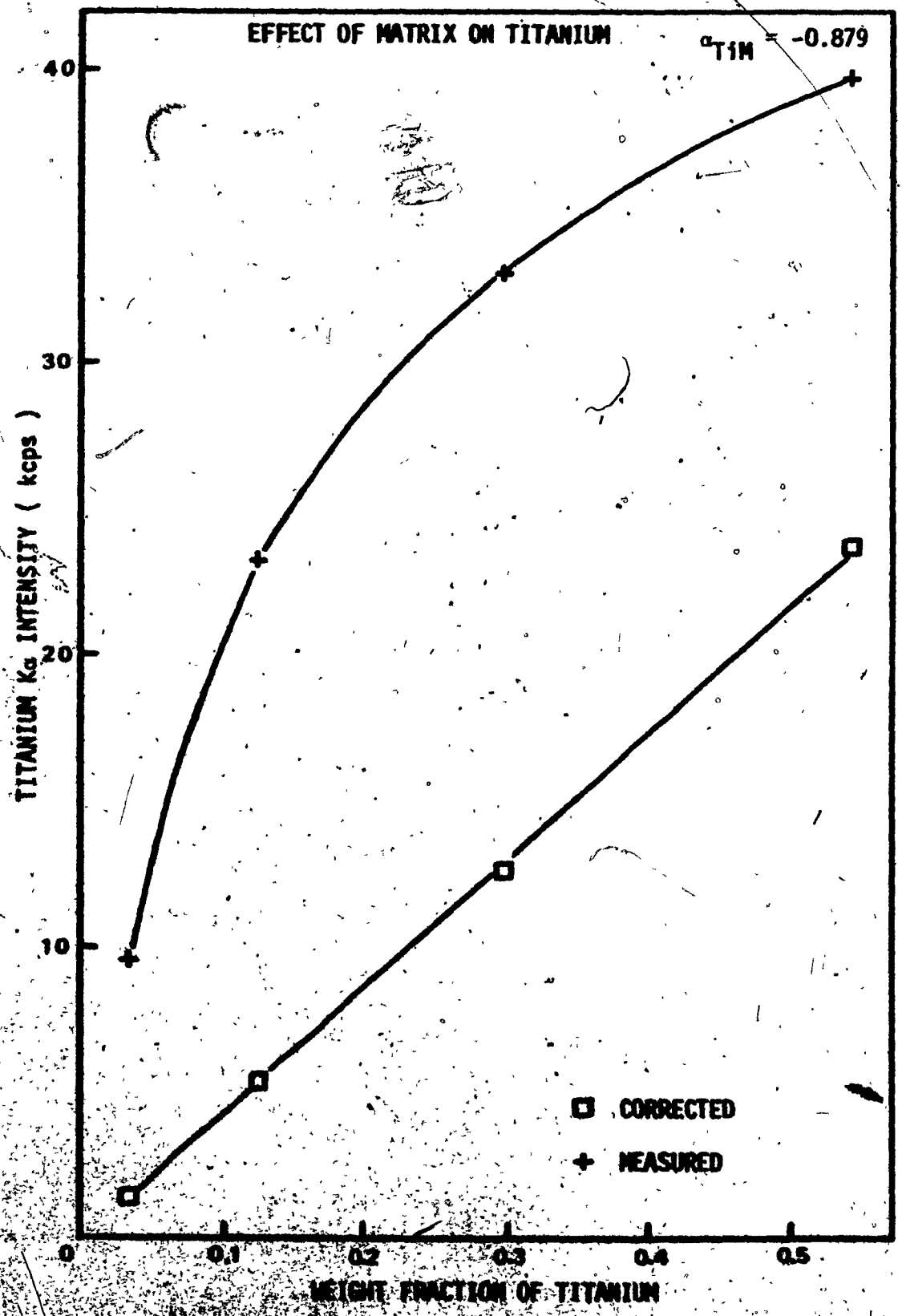
EFFECT OF MATRIX ON TITANIUM
α_{TiM} = -0.879
TITANIUM Kα INTENSITY (kcps)
40
30
20
10
0
0.1
0.2
0.3
0.4
0.5
WEIGHT FRACTION OF TITANIUM
CORRECTED
MEASURED

FIGURE 5-10

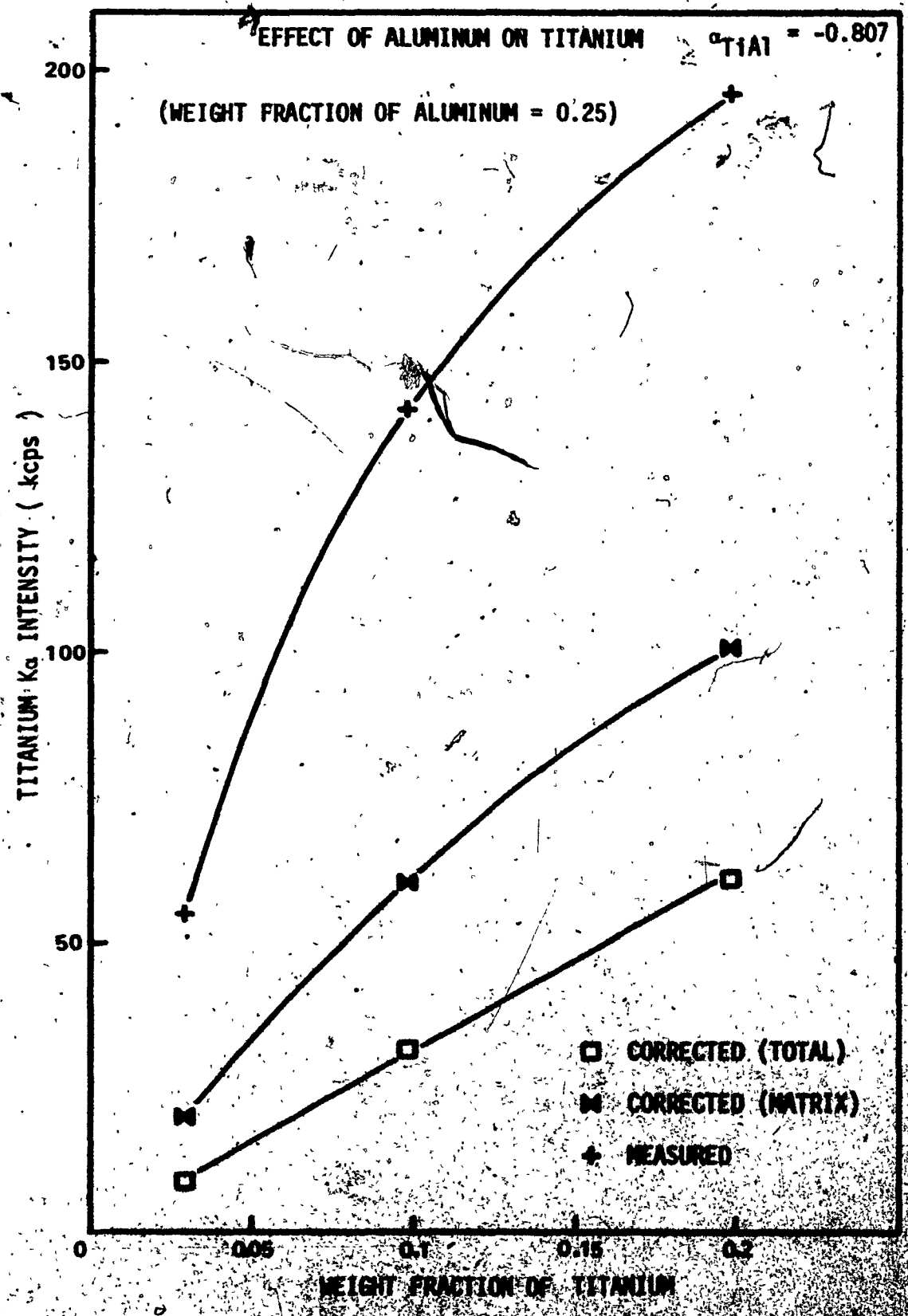
EFFECT OF ALUMINUM ON TITANIUM α_{TiAl} = -0.807
(WEIGHT FRACTION OF ALUMINUM = 0.25)
TITANIUM Kα INTENSITY (kcps)
200
150
100
50
0
0.05
0.1
0.15
0.2
WEIGHT FRACTION OF TITANIUM
CORRECTED (TOTAL)
CORRECTED (MATRIX)
MEASURED

FIGURE 5-11

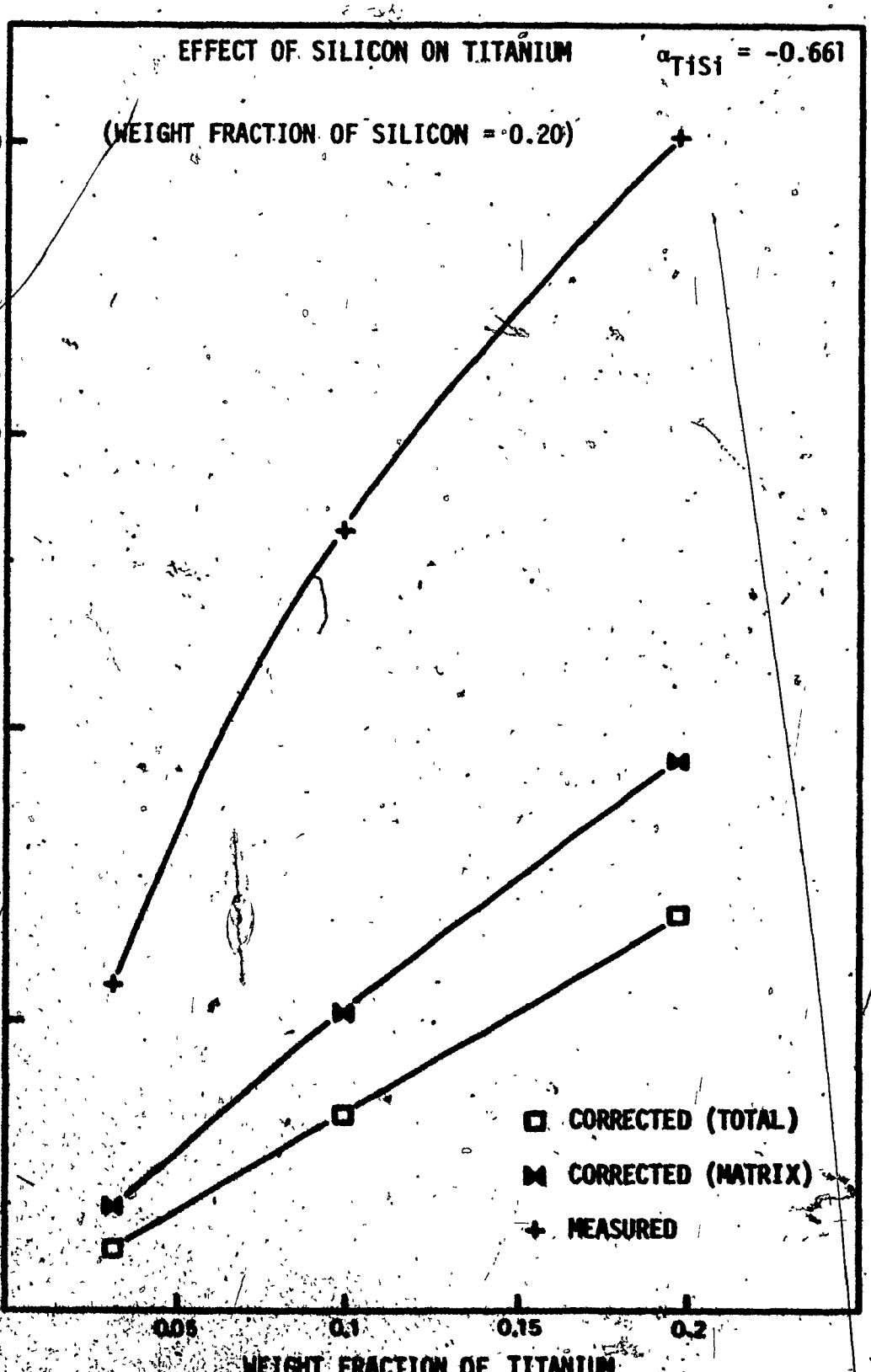
EFFECT OF SILICON ON TITANIUM
α_{TiSi} = -0.661
(WEIGHT FRACTION OF SILICON = 0.20)
TITANIUM Ka INTENSITY (kcps)
200
150
100
50
0
0.05
0.1
0.15
0.2
WEIGHT FRACTION OF TITANIUM
CORRECTED (TOTAL)
CORRECTED (MATRIX)
MEASURED

FIGURE 5-12

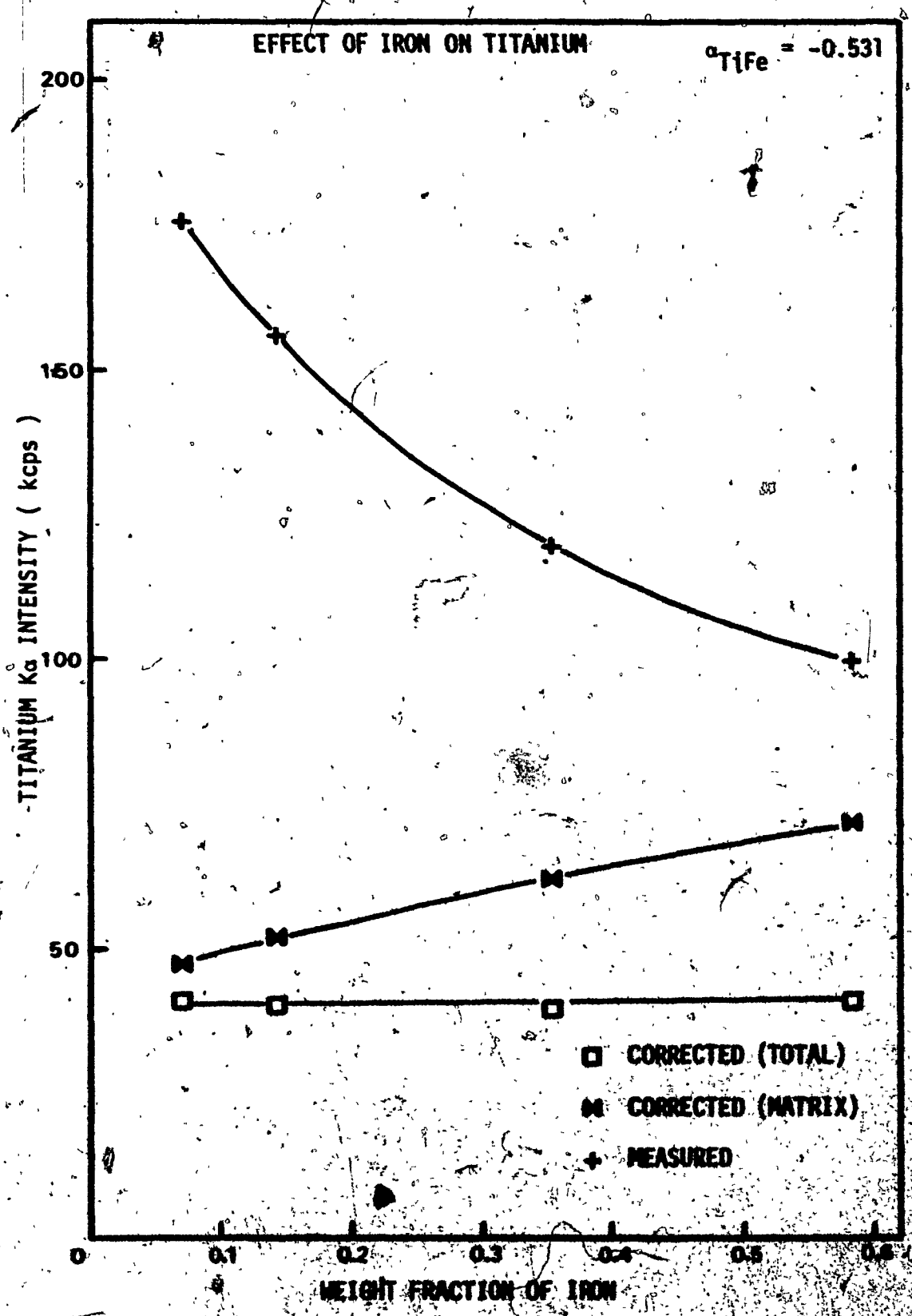
EFFECT OF IRON ON TITANIUM
α_{TiFe} = -0.531
200
150
100
50
0
-TITANIUM Ka INTENSITY (kcps)
0.1
0.2
0.3
0.4
0.5
0.6
WEIGHT FRACTION OF IRON
CORRECTED (TOTAL)
CORRECTED (MATRIX)
MEASURED

FIGURE 5-13

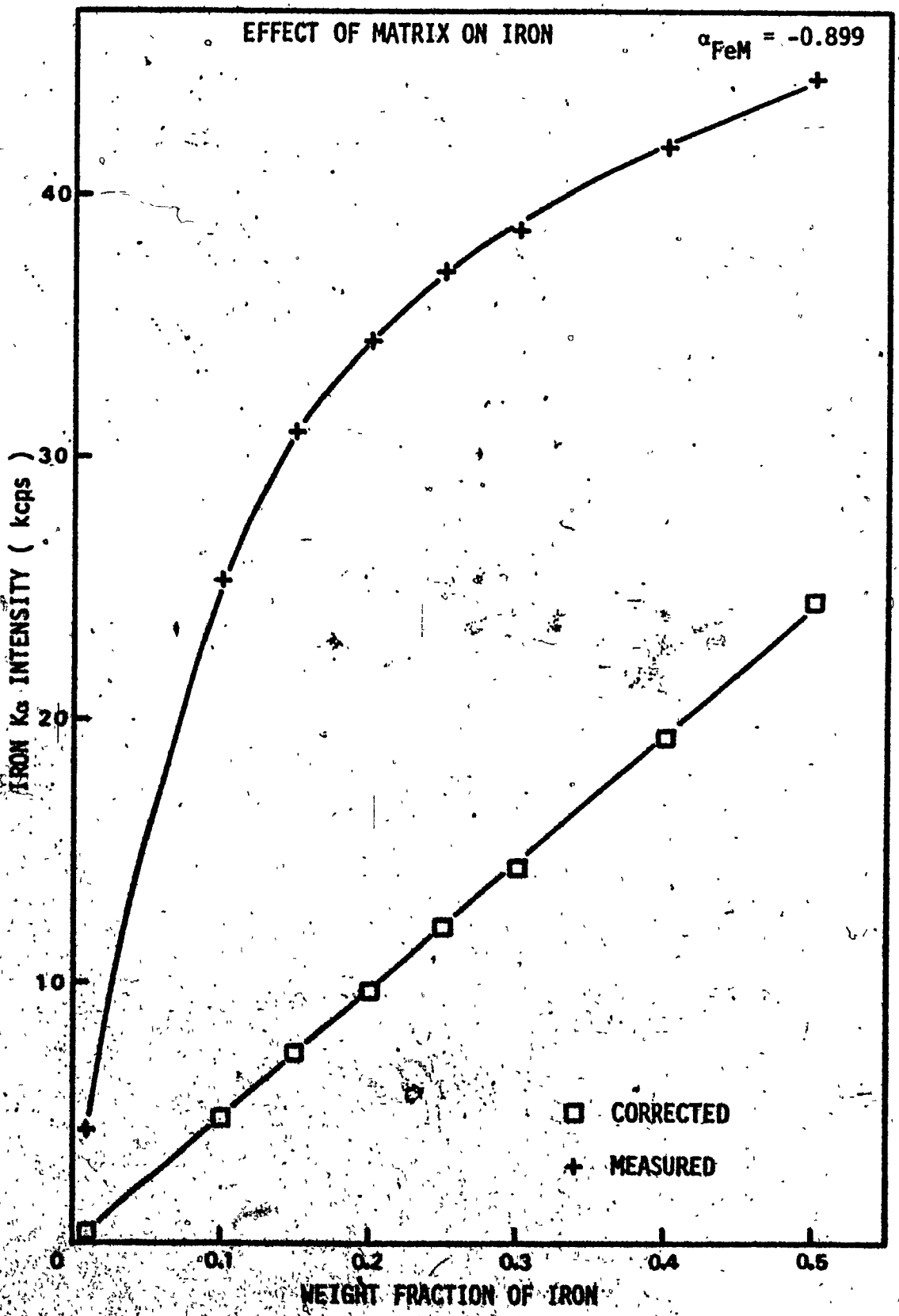
EFFECT OF MATRIX ON IRON
α_{FeM} = -0.899
IRON Kα INTENSITY (kcps)
40
30
20
10
0
0.1
0.2
0.3
0.4
0.5
WEIGHT FRACTION OF IRON
CORRECTED
MEASURED

FIGURE 5-14

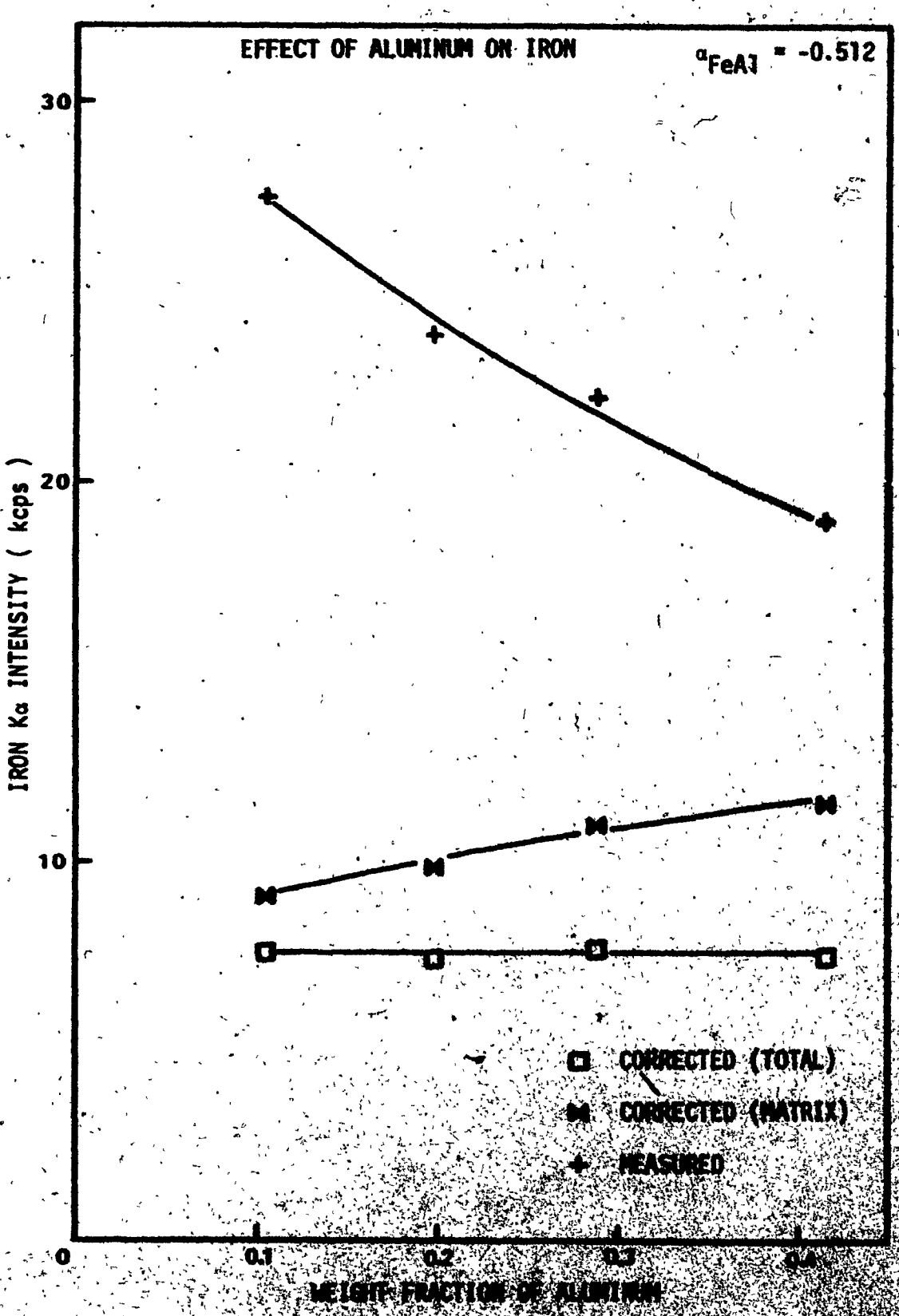
EFFECT OF ALUMINUM ON IRON
α_{FeAl} = -0.512
30
20
10
0
IRON Ka INTENSITY (kcps)
0.1
0.2
0.3
0.4
WEIGHT FRACTION OF ALUMINUM
CORRECTED (TOTAL)
CORRECTED (MATRIX)
MEASURED

FIGURE 5-15

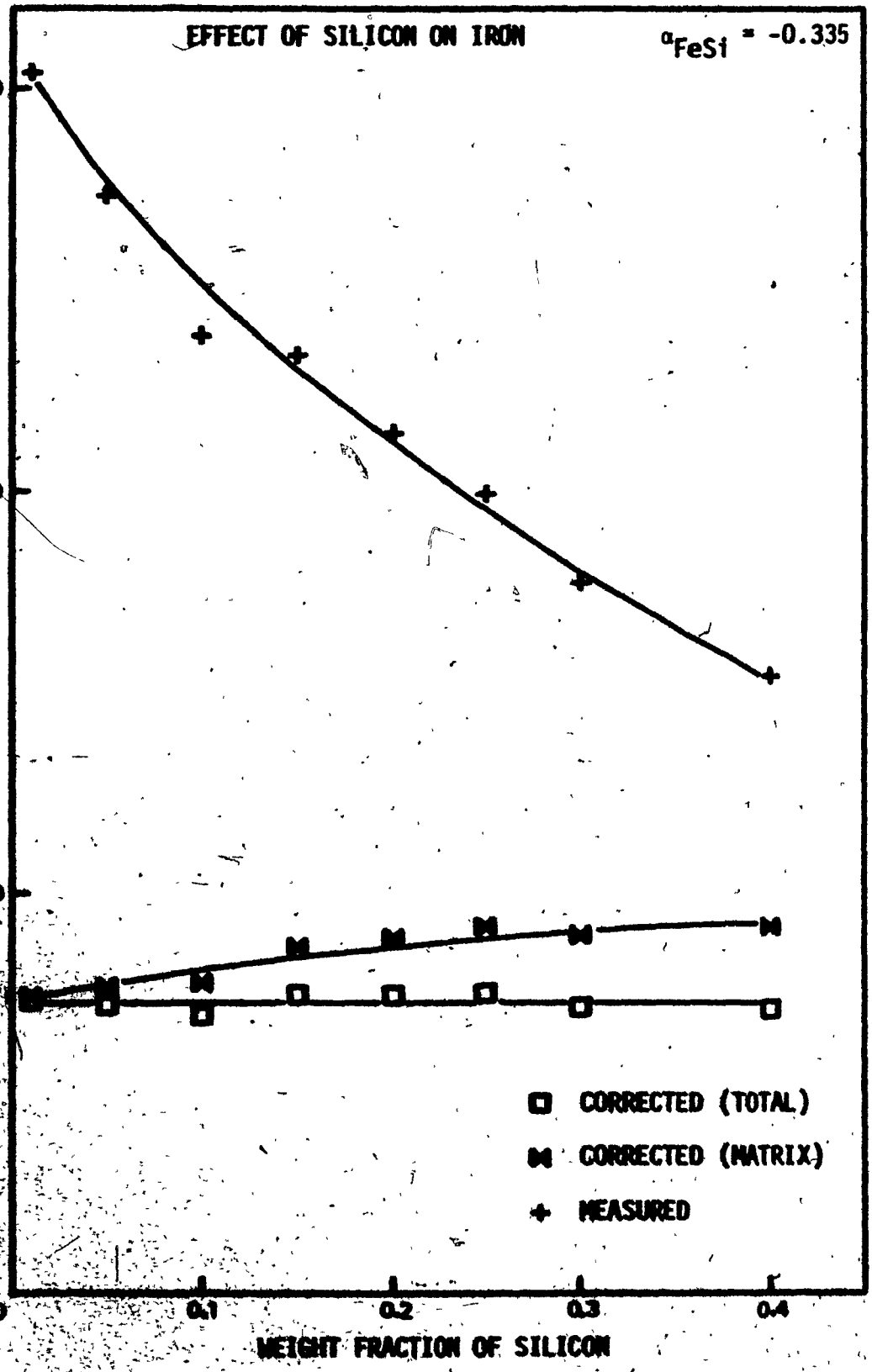
EFFECT OF SILICON ON IRON
α_{FeSi} = -0.335
IRON Ka INTENSITY (kcps)
30
20
10
0
0.1
0.2
0.3
0.4
WEIGHT FRACTION OF SILICON
CORRECTED (TOTAL)
CORRECTED (MATRIX)
MEASURED

FIGURE 5-16

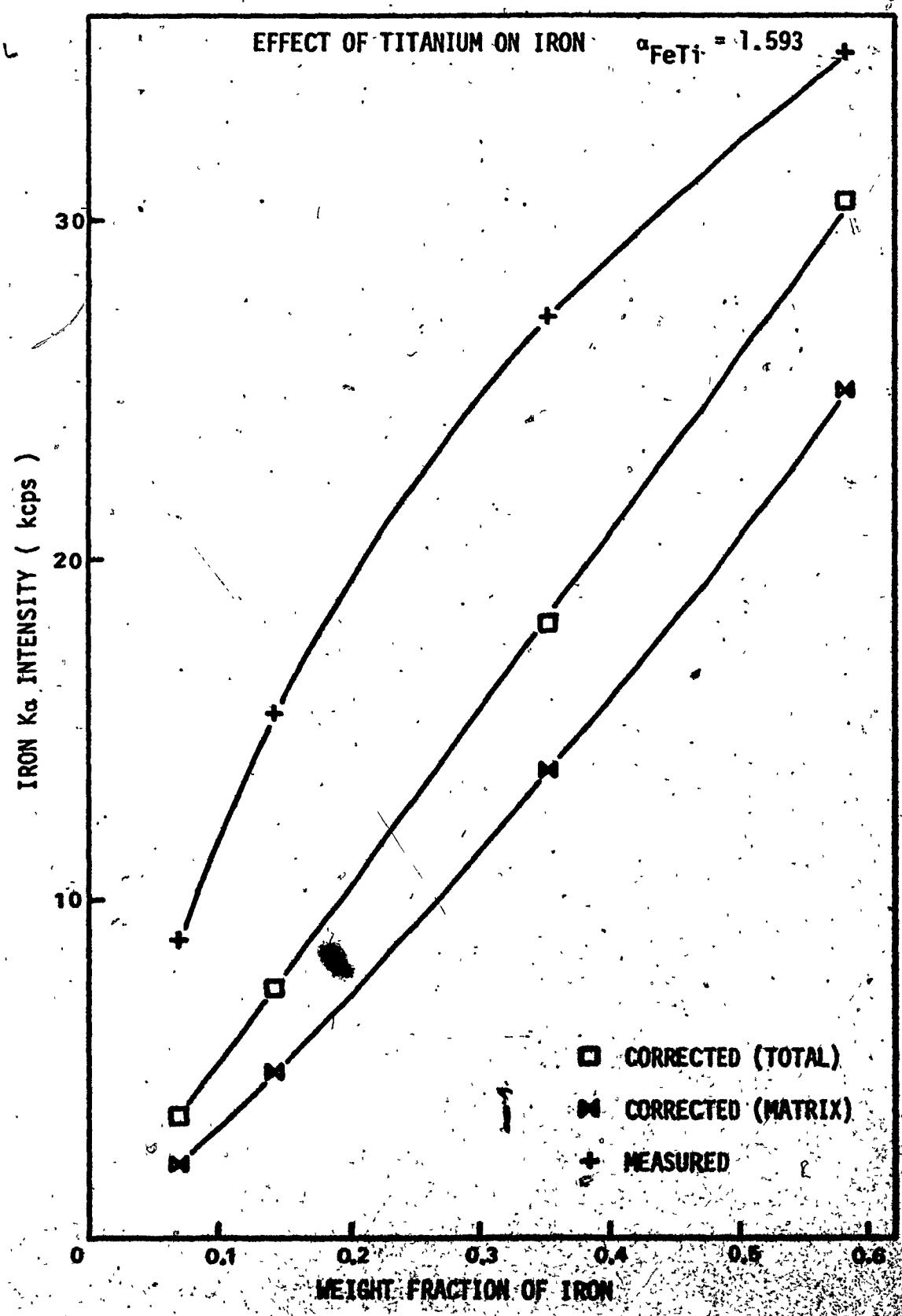
EFFECT OF TITANIUM ON IRON α_{FeTi} = 1.593
IRON Kα INTENSITY (kcps)
30
20
10
0
0.1
0.2
0.3
0.4
0.5
0.6
WEIGHT FRACTION OF IRON
CORRECTED (TOTAL)
CORRECTED (MATRIX)
MEASURED

in a minimum standard deviation for the calculated 100% intensity of the measured element. The intensity data, corrected for the interelement effects, are plotted with the measured data in FIGURES 5-1 to 5-16 . It may be seen from these curves that the Lachance and Traill method of matrix correction produces a linear relationship between the x-ray intensity and the elemental concentration.

Overall, the results appeared to be satisfactory especially for the heavy elements titanium and iron. However, certain discrepancies and large errors were observed in some matrix effect determinations where the light elements were involved. For example, the effect of titanium on aluminum (α_{AlTi}) was determined to be negative. At the same time, the effect of iron on aluminum (α_{AlFe}) had a large positive value. The result for α_{AlTi} was obviously in error. It is true that Ti Kα radiation will cause better excitation of Al Kα radiation than Fe Kα radiation. For this reason the α_{AlTi} was expected to have a lower value than the α_{AlFe} . However, the mass absorption coefficients of both Ti and Fe for Al Kα radiation are similar and very large. The Al Kα radiation should be absorbed more with a higher concentration of titanium giving a positive alpha coefficient.

Another particularly obvious error was detected in the effect of the matrix on silicon (α_{SiN}) . It was more positive than the coefficient for the effect of the matrix on aluminum (α_{AlN}) . The Si Kα radiation should not be absorbed more than the Al Kα radiation

in the same matrix. In general, poor precision appeared to be consistent where silicon was involved.

The cause of the errors was ascribed to the sample heterogeneity due to unsatisfactory mixing of the component materials. It was recalled that the TiO_2 tended to remain in small lumps and mixing of the 320 grit SiC was difficult. The grains of SiC appeared to settle to the bottom of the sample with just slight tapping. It was decided that additional samples were required taking greater care in the sample mixing. Finer (600 grit) SiC was used to facilitate sample homogeneity. A second set of 40 synthetic samples were prepared to represent the five binary systems Al and Ti, Al and Fe, Si and Ti, Si and Fe, Si and matrix. The appropriate alpha coefficients were computed as before.

The selected set of 16 alpha coefficients and the average calculated 100% intensity values were applied to the XRF intensity data for the 70 bauxite samples and the 280 concentrations were determined. This was achieved through the use of the computer program ANALY which is described in APPENDIX C. The absolute accuracy (difference between the known and the calculated values) was calculated for each sample for each element. The average absolute accuracy and average relative accuracy values are given below for the determination of the major element oxides.

	Average Absolute Accuracy	Average Relative Accuracy
Al_2O_3	24.8	63.8 %
SiO_2	2.2	21.2 %
TiO_2	0.35	14.7 %
Fe_2O_3	0.98	9.5 %

Accuracies of this nature were certainly not acceptable especially the large value for the alumina concentration. It was evident that the alpha coefficients determined from these binary mixtures were not applicable to the analysis of bauxite.

The presence of carbon in the synthetic samples was suspected to be the cause of the incompatability of the alpha coefficients. Looking at the different absorption properties of carbon and oxygen an answer to this problem was found. The mass absorption coefficients of carbon and oxygen for the four wavelengths involved in bauxite analysis are given below.

RADIATION	CARBON	OXYGEN	(diff.)
Al Kα	640	1520	880
Si Kα	400	965	565
Ti Kα	26	63	37
Fe Kα	9.0	21.5	12.5

The differences between these coefficients for the analysis of silicon and aluminum are significantly large.

It was decided, in view of the above results, that quartz (SiO_2) must be used in the synthetic samples. A matrix substance was chosen to be lithium hydroxide ($LiOH \cdot H_2O$). A completely new set of binary samples was prepared, XRF intensities were measured and alpha coefficients were determined. The calculated average absolute accuracy values for the 70 bauxite samples did not improve to any extent.

It was considered that errors may have been included as a result of too many variables, the alpha coefficients and the unknown 100% intensities. A decision was made to obtain the experimental x-ray intensities for the 100% samples of Al, Si, Ti and Fe. Pure metal standards of Al, Ti and Fe were available and the results from these samples were expected to be reliable. For the Si 100% x-ray intensity determination an estimation had to be made since pure Si was not available. In its place a sample of pure SiO_2 was used. The alpha coefficient for the effect of the matrix on silicon seemed to be reliable having a low standard deviation (for the calculated 100% intensity) of 0.09 percent. This alpha coefficient was applied to the Si Kα intensity for the pure SiO_2 sample and a 100% intensity was determined for silicon. Since the same 100% intensity values would be applied to the standards as well as the unknowns, a very accurate determination was deemed unnecessary. The final set of values was selected to be :-

100000 cps	for	100% Al
104000 cps	for	100% Si
413200 cps	for	100% Ti
49300 cps	for	100% Fe

These values were used throughout the remainder of this investigation.

The 16 alpha coefficients were recalculated using the selected 100% intensity values. TABLE 5-1 gives these alpha coefficients and their respective standard deviations. Unfortunately, when applied to the 70 bauxite samples the alpha coefficients were found to be still unsuitable. In fact the average absolute accuracy values for all elements were not as good as those obtained from the first set of alpha coefficients.

The known and calculated concentrations for the oxides (Fe_2O_3, TiO_2, SiO_2, Al_2O_3) of the 70 bauxite samples are shown in APPENDIX B , TABLE B-8 . It may be noted that there is a significant improvement in the accuracy when compared to the results that were obtained by a direct intensity ratio (no alpha coefficients) as shown in APPENDIX B , TABLE B-7 .

At this point the validity of the method was suspected. To clear up this matter a set of five synthetic bauxite samples were prepared in the same manner as the binary mixtures. The four metal oxides and lithium hydroxide were used to prepare the samples. Using the alpha coefficients (TABLE 5-1) and the selected 100% intensities

TABLE 5-1

ALPHA COEFFICIENTS DETERMINED FROM BINARY MIXTURES

ALPHA (α)	VALUE	STANDARD* DEVIATION (σ)
AlM	4.471	1.366 %
AlSi	1.357	6.123 %
AlTi	11.377	14.011 %
AlFe	5.955	2.755 %
SiM	1.162	0.087 %
SiAl	0.354	1.745 %
SiTi	1.351	11.468 %
SiFe	1.544	0.629 %
TiM	-0.892	3.697 %
TiAl	-0.503	4.612 %
TiSi	-0.251	7.701 %
TiFe	-0.470	4.843 %
FeM	-0.893	1.712 %
FeAl	-0.566	2.655 %
FeSi	-0.318	2.362 %
FeTi	1.270	1.740 %

* Standard deviation of calculated 100% intensity.

the elemental concentrations were calculated from the XRF data. A comparison of the known and calculated concentrations (for the oxides) is given in TABLE 5-2 . The average absolute accuracy values were determined to be

3.21 for percent Al_2O_3 ,

0.96 for percent SiO_2 ,

0.36 for percent TiO_2 ,

0.90 for percent Fe_2O_3 .

The average relative accuracy, calculated over all elements, was determined to be about 5 percent. For the 70 bauxite samples this value was greater than 35 percent.

It was thus obvious that the incompatability between binary alpha coefficients and bauxite material was due not to the method but the actual make-up of the bauxite samples. It was suspected that the chemical nature of the oxides in bauxite was significantly different from samples prepared from pure oxides. For example, Al_2O_3 in bauxite may occur as gibbsite ($Al_2O_3 \cdot 3H_2O$), boehmite ($Al_2O_3 \cdot H_2O$) or kaolinite ($Al_2O_3 \cdot 2SiO_2 \cdot 2H_2O$) . It became apparent that the determination of the alpha coefficients for bauxite analysis required actual bauxite samples and not synthetic samples.

TABLE 5-2

COMPARISON OF KNOWN (KWN) AND CALCULATED (CAL) CONCENTRATIONS FOR THE SYNTHETIC BAUXITE SAMPLES

SAMPLES		Al_2O_3	SiO_2	TiO_2	Fe_2O_3	TOTAL
1	KWN	37.62	11.56	16.59	34.14	99.91
	CAL	32.94	11.19	16.49	32.88	93.51
2	KWN	48.04	20.74	7.28	23.88	99.94
	CAL	43.05	19.44	6.92	22.15	91.56
3	KWN	50.99	27.86	9.44	11.71	100.00
	CAL	51.18	26.59	8.96	11.11	97.84
4	KWN	69.44	7.16	12.42	10.98	100.00
	CAL	69.97	6.92	11.98	10.80	99.66
5	KWN	57.40	16.63	8.10	17.83	99.96
	CAL	51.74	14.99	7.69	17.10	91.53

5·2·2 ALPHA COEFFICIENTS FROM BINARY MIXTURES APPLIED TO BAUXITE SAMPLES BY GEOGRAPHICAL REGION

The large errors encountered in the application of the binary alpha coefficients to the 70 bauxite samples (5 different geographical regions plus standards) was suspected to be due, at least partially, to the variation of the mineralogical constitution of the different bauxite ore types. To verify this, the binary alpha coefficients were applied to each of the five separate groups of samples representing the bauxite origins. The average absolute and relative accuracy values thus obtained are given in TABLE 5·3 . It may be noted that these binary alpha coefficients were not suitable for any of the regions. The Demerara bauxite analysis displayed very poor accuracy for the aluminum, titanium and iron determinations. This group of samples contained the greatest variation of chemical composition and was expected to produce the largest errors.

5·2·3 DETERMINATION OF THEORETICAL ALPHA COEFFICIENTS AND THEIR APPLICATION TO THE ANALYSIS OF BAUXITE ORE

In view of the disconcerting results that were obtained by using alpha coefficients determined from binary mixtures, an attempt was made to examine the applicability of theoretical alpha coefficients determined from elemental mass absorptions. The calculation of these alpha coefficients involved the use of EQUATION 5-4 .

TABLE 5-3

ABSOLUTE AND RELATIVE(%) ACCURACY OF ALPHA COEFFICIENTS FROM BINARY MIXTURES APPLIED TO REGIONS OF BAUXITE

		Al	Si	Ti	Fe	Average
ALL REGIONS	ABS.	27.863	4.816	0.420	1.506	8.651
	REL.	70.800	37.982	19.020	14.920	35.680
JAMAICA	ABS.	26.449	1.531	0.407	1.406	7.448
	REL.	56.898	46.618	15.558	7.490	31.641
DEMERARA	ABS.	27.545	6.185	0.475	3.151	9.339
	REL.	107.072	26.897	30.046	30.231	48.561
BRAZIL	ABS.	21.341	1.548	0.106	1.432	6.106
	REL.	44.796	44.832	5.755	6.418	25.450
BOKE	ABS.	35.263	0.223	0.764	0.698	9.237
	REL.	60.890	34.082	18.438	13.844	31.813
AUSTRALIA	ABS.	30.165	11.216	0.488	1.173	10.760
	REL.	85.380	37.763	25.721	13.193	40.514

$$\alpha_{AB} = \frac{[\ \mu_1 \cdot \mathrm{cosec}(\phi_1) + \mu_2 \cdot \mathrm{cosec}(\phi_2)\ ]_B}{[\ \mu_1 \cdot \mathrm{cosec}(\phi_1) + \mu_2 \cdot \mathrm{cosec}(\phi_2)\ ]_A} - 1 \qquad 5\cdot4$$

where $[\ \mu_1\ ]_A$ and $[\ \mu_1\ ]_B$ represent the mass absorption coefficients at the excitation wavelength for elements A and B respectively,

$[\ \mu_2\ ]_A$ and $[\ \mu_2\ ]_B$ represent the mass absorption coefficients at the wavelength of the measured radiation of element A for elements A and B respectively,

ϕ_1 represents the angle of incidence of the primary excitation radiation,

ϕ_2 represents the angle of emergence of the secondary emitted radiation.

The above equation is reduced to EQUATION 5·5 for a 45° spectrometer geometry where $\mathrm{cosec}(\phi_1) = \mathrm{cosec}(\phi_2) = 1$.

$$\alpha_{AB} = \frac{[\ \mu_1 + \mu_2\ ]_B}{[\ \mu_1 + \mu_2\ ]_A} - 1 \qquad 5\cdot5$$

The appropriate mass absorption coefficients were selected from the Table of Mass Absorption Coefficients[46]. The matrix was represented as oxygen. The 16 alpha coefficients were determined and are shown in TABLE 5·4. A quick comparison with the alpha coefficients determined from the binary mixtures (TABLE 5·1) shows

TABLE 5-4

THEORETICAL ALPHA COEFFICIENTS

α_{A10}	=	2.222
α_{A1Si}	=	0.393
α_{A1Ti}	=	4.311
α_{A1Fe}	=	5.263
α_{Si0}	=	0.970
α_{SiAl}	=	5.541
α_{SiTi}	=	2.671
α_{SiFe}	=	3.242
α_{Ti0}	=	-0.854
α_{TiAl}	=	-0.387
α_{TiSi}	=	-0.233
α_{TiFe}	=	-0.546
α_{Fe0}	=	-0.691
α_{FeAl}	=	0.328
α_{FeSi}	=	0.661
α_{FeTi}	=	4.064

some extreme differences. A close similarity between these two sets of alpha values was found only in the coefficients representing the elemental interactions on titanium radiation. With the exception of the two coefficients α_{AlTi} and α_{SiAl} (from the binary mixture set) the two sets of coefficients were comparable on a relative scale. The values of the coefficients concerning the effects on iron radiation may not appear to correlate. However, the expected trend of increased alpha coefficient value with increased atomic weight of the interfering element has been upheld in both sets of coefficients.

The theoretical alpha coefficients were applied to the 70 bauxite samples collectively and by region. The calculated oxide concentrations for all samples are compared to the known values in APPENDIX B , TABLE B-9 . The average absolute accuracies were determined and are given in TABLE 5-5 .

A significant improvement was observed in the analysis of aluminum. The accuracy in the analysis of silicon was not affected when all samples were considered but a large variation was observed between the five bauxite regions. For titanium, with the exception of the Brazil bauxite samples, some improvement was observed. On the other hand, the error in the analysis of iron had been magnified tremendously. Consequently, the set of theoretical alpha coefficients were found to be unsuitable to correct for matrix effects in bauxite ore analysis.

TABLE 5·5

ABSOLUTE ACCURACY OF THEORETICAL ALPHA COEFFICIENTS

	Al	Si	Ti	Fe	Average
ALL REGIONS	13.763	3.345	0.311	19.273	9.173
JAMAICA	16.444	0.712	0.253	26.295	10.926
DEMERARA	13.880	8.013	0.254	22.801	11.237
BRAZIL	12.433	0.881	0.502	29.950	10.941
BOKE	15.229	0.489	0.651	9.002	6.343
AUSTRALIA	14.285	5.259	0.098	14.178	8.455

5-2-4 DETERMINATION OF ALPHA COEFFICIENTS USING THE TRUE BAUXITE SAMPLES

The above excursion into the theoretical enhanced the idea that the alpha coefficients must be determined through the use of actual bauxite samples. To this end a coefficient refinement program was instituted with the aid of the computer program ANALY (see APPENDIX C). The initial alpha coefficient values were those obtained from the binary mixtures. In sequence, each alpha coefficient was revised until a minimum average absolute accuracy value was obtained.

The Australian bauxite samples were arbitrarily selected for the initial experiment. Variation of all 16 alpha coefficients constituted one complete revision cycle. The process was continued for 32 cycles. This was done in order to observe the degree of improvement with successive revision cycles. FIGURE 5-17 shows this relationship over the first 15 cycles. The improvement of the overall average absolute accuracy was about 0.04 for the fourth cycle, 0.01 for the eighth cycle and 0.003 for the thirty-second cycle. Due to the length of computing time required it was not feasible to carry out all revision attempts through such a large number of cycles. It was established that four cycles of revision yielded alpha coefficients that produced analytical results of reasonable accuracy. Coefficients from the eighth cycle gave results with good accuracy.

FIGURE 5-17

Improvement of average absolute accuracy as a function of the number of alpha coefficient revision cycles.

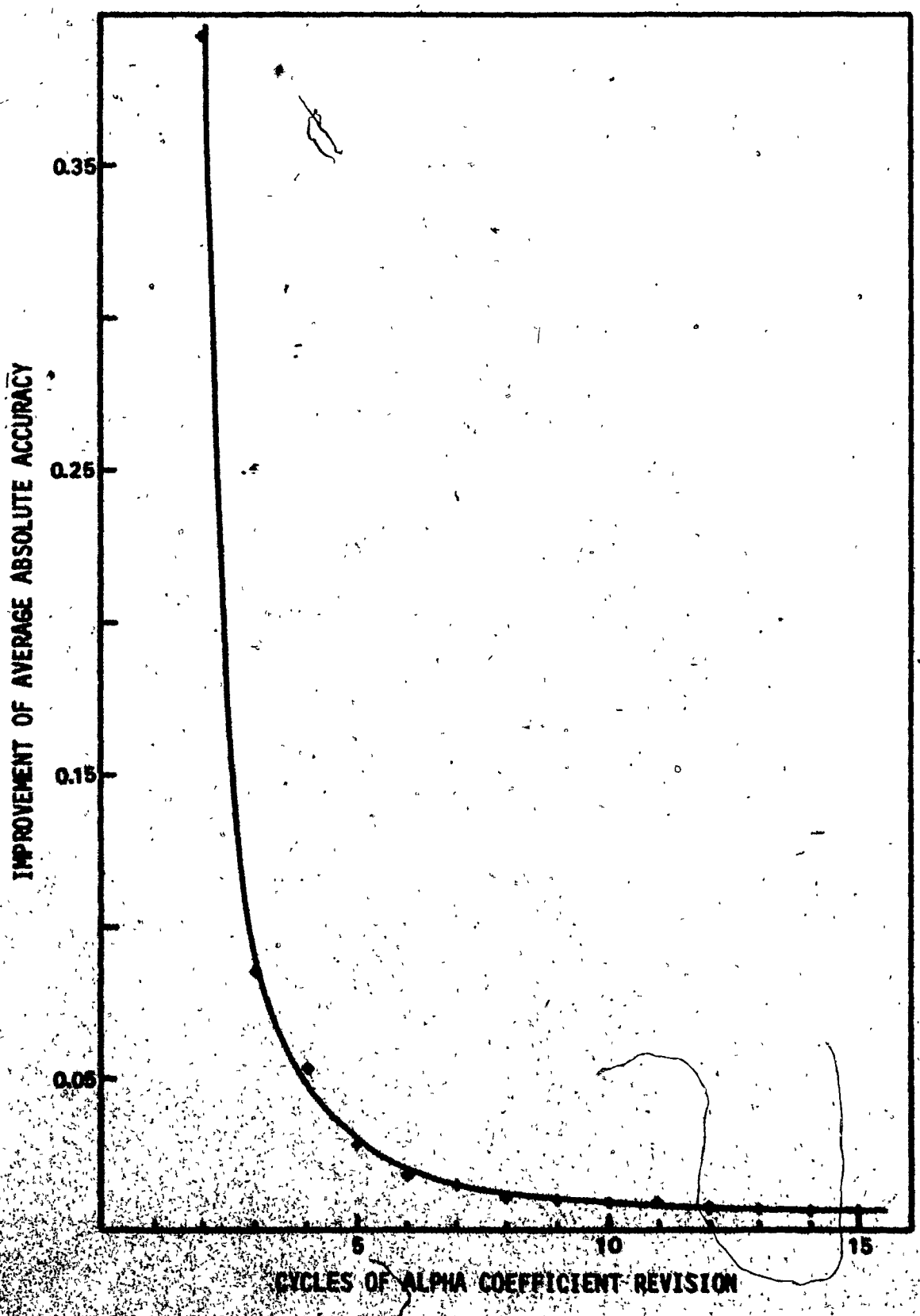
IMPROVEMENT OF AVERAGE ABSOLUTE ACCURACY
0.35
0.25
0.15
0.05
5
10
15
CYCLES OF ALPHA COEFFICIENT REVISION

The revision method was applied for four cycles to the 70 bauxite samples grouped by regions. The values of the resulting alpha coefficients are given in TABLE 5·6 . It was noted that within the collection of alpha coefficients there were some general peculiarities and some specific abnormal values.

Firstly, according to the theoretical definition described by EQUATION 5·4, the minimum allowable value of an alpha coefficient is -1.0 since mass absorption coefficients cannot be negative. The values of α_{TiSi} (-11.00) and α_{FeSi} (-2.694) for the Boke bauxite were obviously erroneous. At this point it must be kept in mind that the successful evaluation of a matrix effect and the corresponding correction coefficient is directly dependent on a large variation of elemental concentrations among the standard samples. Also, there are large errors inherent in small concentration values. A quick check of the concentration ranges of the Boke material revealed that the silicon content in these samples was very low.

Secondly, the values representing the effect of titanium on aluminum radiation were extremely high especially those values determined for the Australia and Demerara materials. The titanium concentration in all the bauxite samples was charactistically low. The maximum content was only 3.36 percent. The Australia and Demerara samples, on the average, contained the lowest concentration of titanium.

TABLE 5·6

ALPHA COEFFICIENTS DETERMINED FROM BAUXITE REGIONS

	JAMAICA	DEMERARA	BRAZIL	BOKE	AUSTRALIA
α_{AlM}	1.020	1.168	1.407	1.116	0.649
α_{AlSi}	1.383	1.024	7.658	-0.099	0.491
α_{AlTi}	8.581	19.459	6.337	10.703	27.02
α_{AlFe}	5.951	0.927	5.832	5.275	4.771
α_{SiM}	3.771	2.442	4.019	2.081	2.670
α_{SiAl}	0.352	1.819	0.308	0.397	0.982
α_{SiTi}	1.256	-0.150	5.135	1.423	4.908
α_{SiFe}	1.556	-0.099	0.473	-0.055	1.495
α_{TiM}	-0.711	-0.680	-0.790	-0.646	-0.640
α_{TiAl}	-0.503	-0.581	-0.503	-0.508	-0.437
α_{TiSi}	-0.163	-0.102	-0.620	-11.00	-0.879
α_{TiFe}	-0.474	-0.139	-0.458	-0.556	-0.132
α_{FeM}	-0.799	-0.799	-0.815	-0.824	-0.791
α_{FeAl}	-0.549	-0.444	-0.557	-0.566	-0.563
α_{FeSi}	-0.395	-0.327	-0.572	-2.694	-0.327
α_{FeTi}	1.269	0.893	1.533	2.573	1.423

The aim of this project was to attempt to determine a single set of matrix correction coefficients that would be applicable to the XRF analysis of any bauxite ore sample regardless of the geographical origin. The previous alpha coefficient determination by region explicitly showed significant differences attributable to sample origin. Consequently, the final set of alpha coefficients to be used for bauxite ore analysis were determined from all the bauxite samples available. The values were selected from the eighth revision cycle and are given in TABLE 5-7 . The calculated oxide concentrations are compared to the known concentrations in APPENDIX B , TABLE B-10 . The average absolute errors of 2.9% Al_2O_3, 1.3% SiO_2, 0.2% TiO_2 and 0.5% Fe_2O_3 were obtained. These accuracies compare favourably, with the exception of the value for Al_2O_3 , with those determined by a pellet spark technique of bauxite analysis[49] (1.4% Al_2O_3, 0.7% SiO_2, 0.3% TiO_2, 1.3% Fe_2O_3) and another x-ray fluorescence method[50] using matrix network charts (1.6% Al_2O_3, 1.1% SiO_2, 0.3% TiO_2, 0.7% Fe_2O_3) .

5-2-5 RELIABILITY OF ALPHA COEFFICIENT VALUES

In view of the questionable values that were obtained for some of the alpha coefficients it was uncertain whether any of the coefficients were reliable. All coefficients were generated by the same computational process and the error could possibly be systematic.

To investigate the degree of reliability of the coefficients a special computer program was designed to vary one alpha coefficient at a time, from a value of -1 to +10 in 0.1 intervals, while keeping all other alpha coefficients constant at the values given in TABLE 5-7 . At each step the 280 concentrations for the 70 bauxite samples were calculated and the average relative error (all elements combined) was determined. This resulted in a set of 16 plots (see FIGURES 5-18 to 5-33) each showing the average relative error in the bauxite analysis as a function of the value of one of the alpha coefficients.

It was clearly evident that some curves turned out to be very sharp (α_{TiM} , α_{TiAl} , α_{FeM} , α_{FeAl}) or moderately sharp (α_{AlM} , α_{SiM} , α_{TiSi} , α_{TiFe} , α_{FeSi}) indicating great reliability in the values of those alpha coefficients. On the other hand, a number of curves were very broad (α_{AlSi} , α_{AlFe} , α_{SiAl} , α_{SiFe} , α_{FeTi}) showing some flexability in these alpha coefficient values. Still other curves were essentially straight lines (α_{AlTi} , α_{SiTi}) indicating that any value could be selected for these alpha coefficients and there would be little or no effect on the average error in the analysis.

Unfortunately, the inability to obtain accurate values for all of the alpha coefficients had to be accepted for bauxite analysis of this nature. The reasons were clear. Primarily, true bauxite ore samples could not provide the complete concentration ranges required.

TABLE 5-7

FINAL SET OF ALPHA COEFFICIENTS

α_{AlM}	=	1.226
α_{AlSi}	=	-0.098
α_{AlTi}	=	9.959
α_{AlFe}	=	5.012
α_{SiM}	=	2.696
α_{SiAl}	=	0.862
α_{SiTi}	=	0.239
α_{SiFe}	=	1.025
α_{TiM}	=	-0.672
α_{TiAl}	=	-0.502
α_{TiSi}	=	-0.101
α_{TiFe}	=	-0.702
α_{FeM}	=	-0.799
α_{FeAl}	=	-0.565
α_{FeSi}	=	-0.329
α_{FeTi}	=	1.255

FIGURES 5-18 to 5-33

Effect of individual alpha coefficient values on the overall average relative error of analysis.

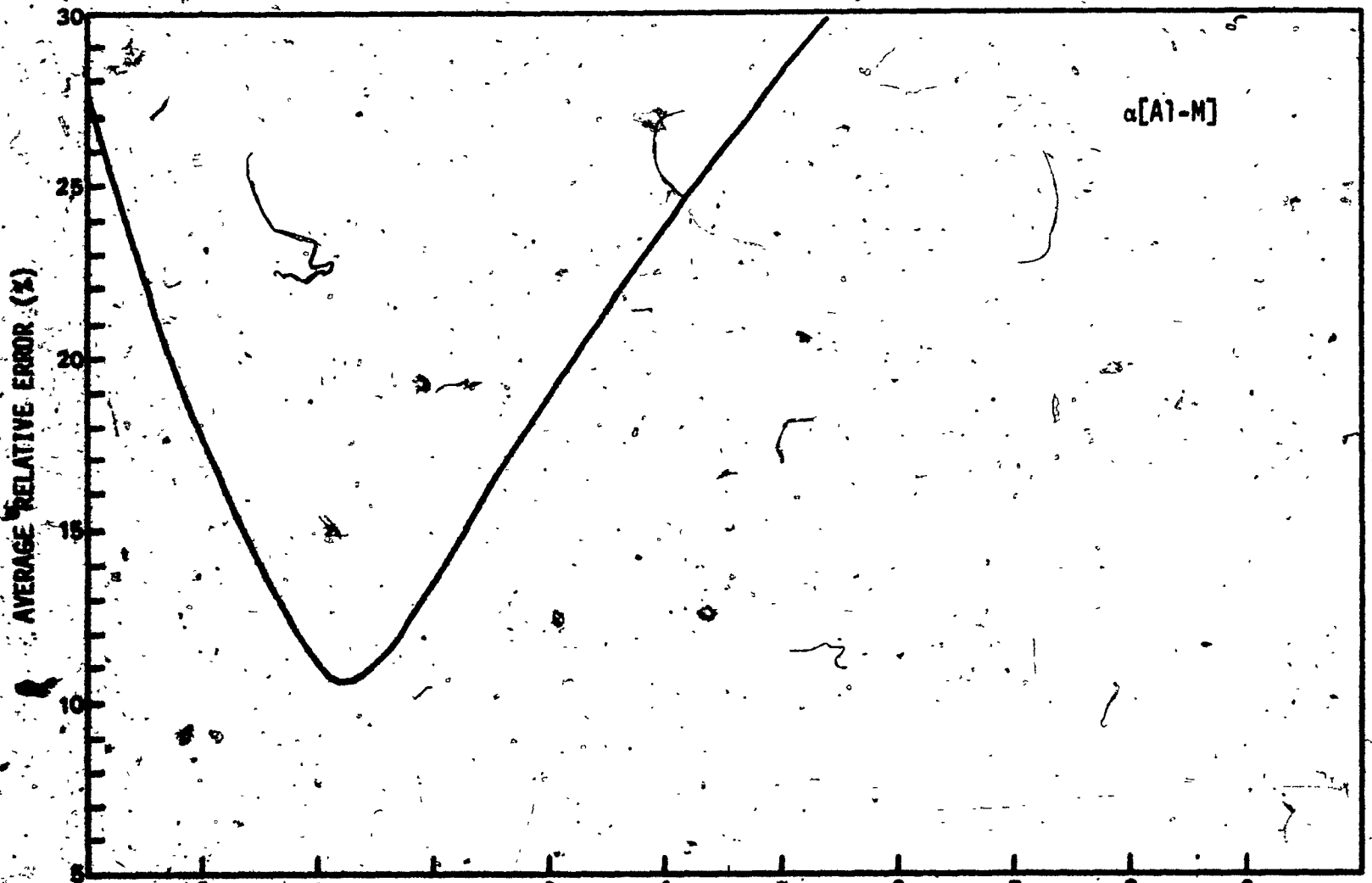
α[A1-M]
AVERAGE RELATIVE ERROR (%)
30
25
20
15
10
5
0
1
2
3
4
5
6
7
8
9
ALPHA COEFFICIENT VALUE

FIGURE 5-18

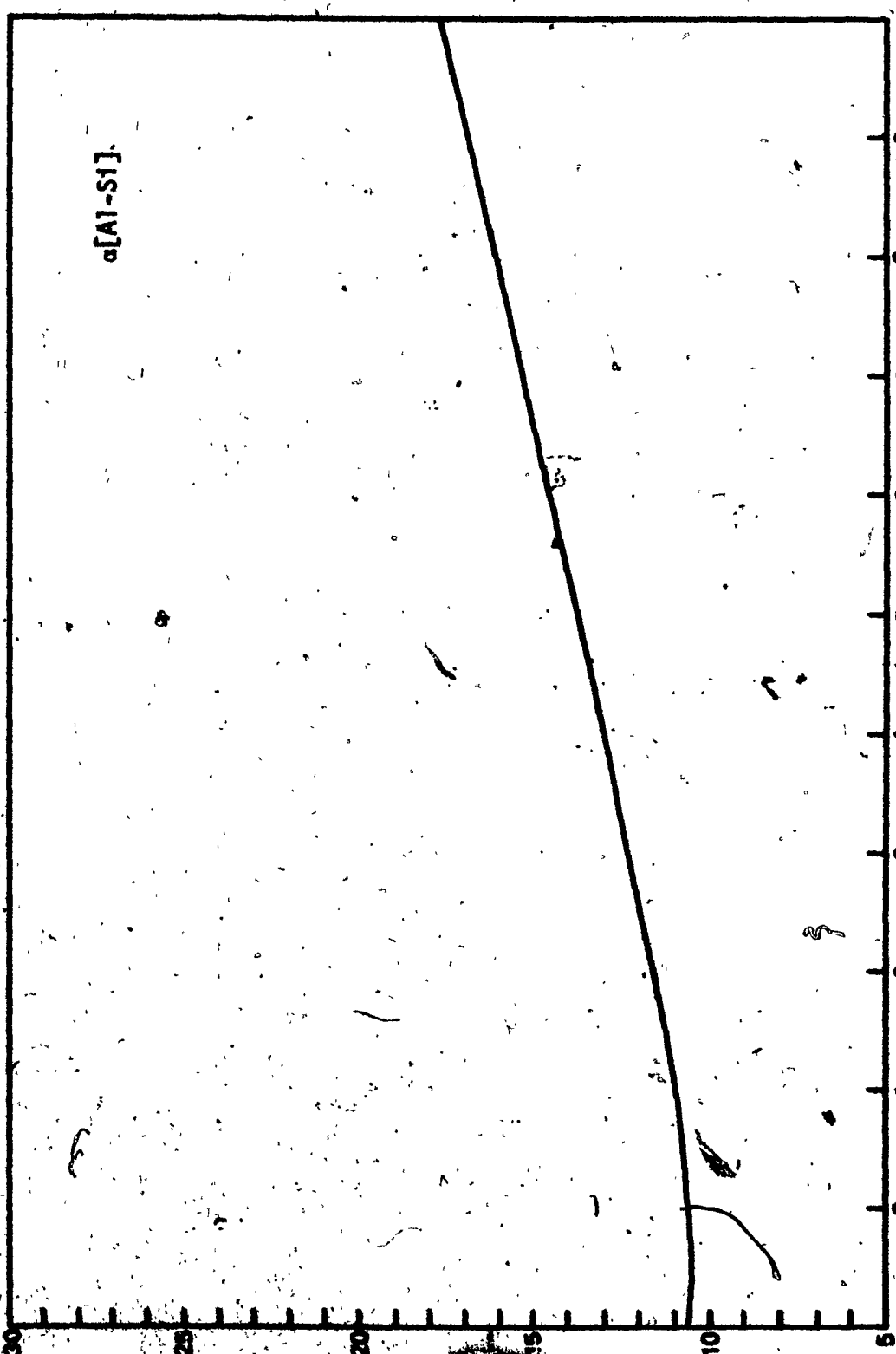
σ[A1-S1].
AVERAGE RELATIVE ERROR (%)
30
25
20
15
10
5
0
1
2
3
4
5
6
7
8
9
ALPHA COEFFICIENT VALUE

FIGURE 5.49

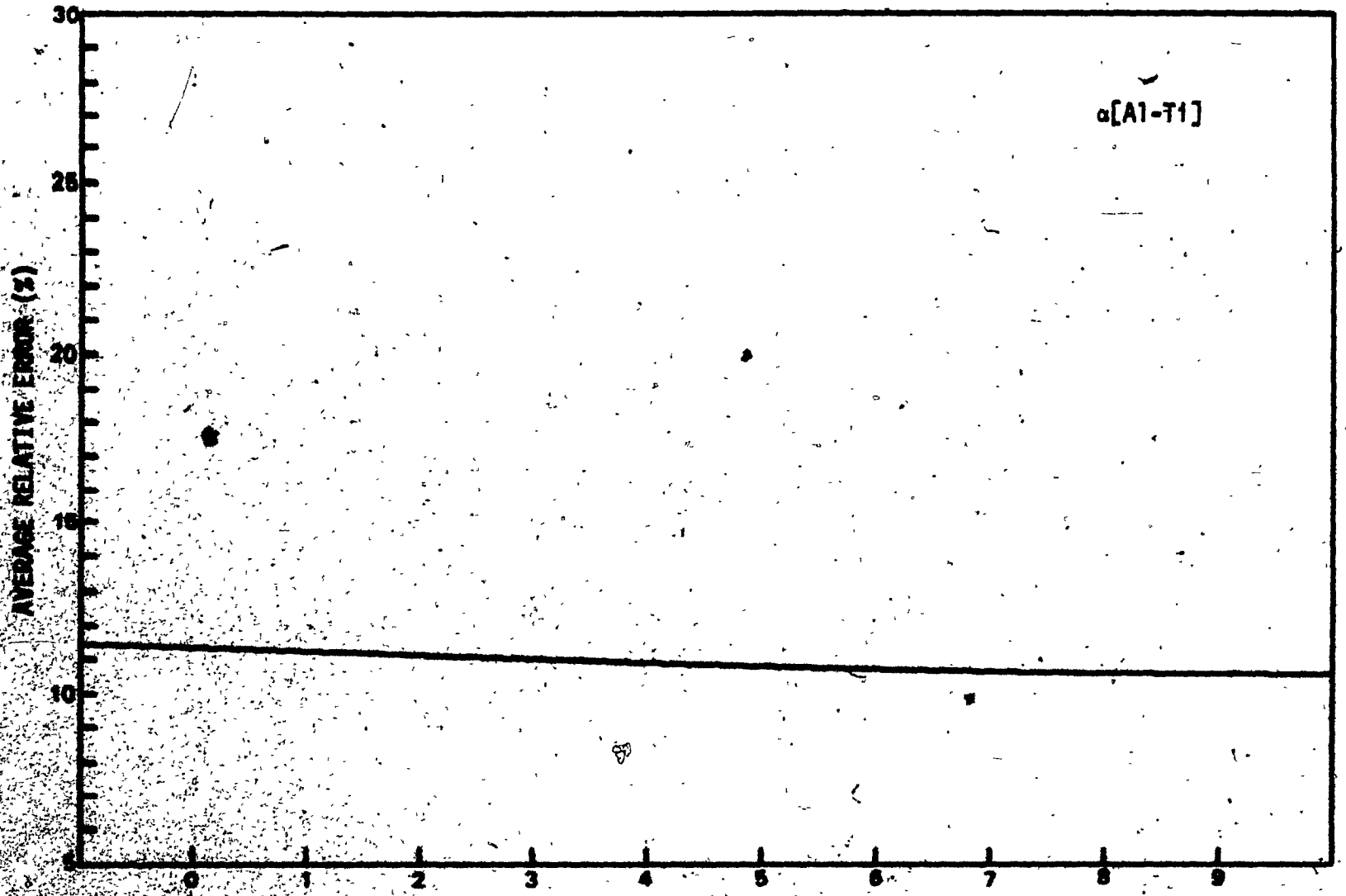
α[A1-T1]
AVERAGE RELATIVE ERROR (%)
30
25
20
15
10
0
1
2
3
4
5
6
7
8
9
ALPHA COEFFICIENT VALUE

FIGURE 5-20

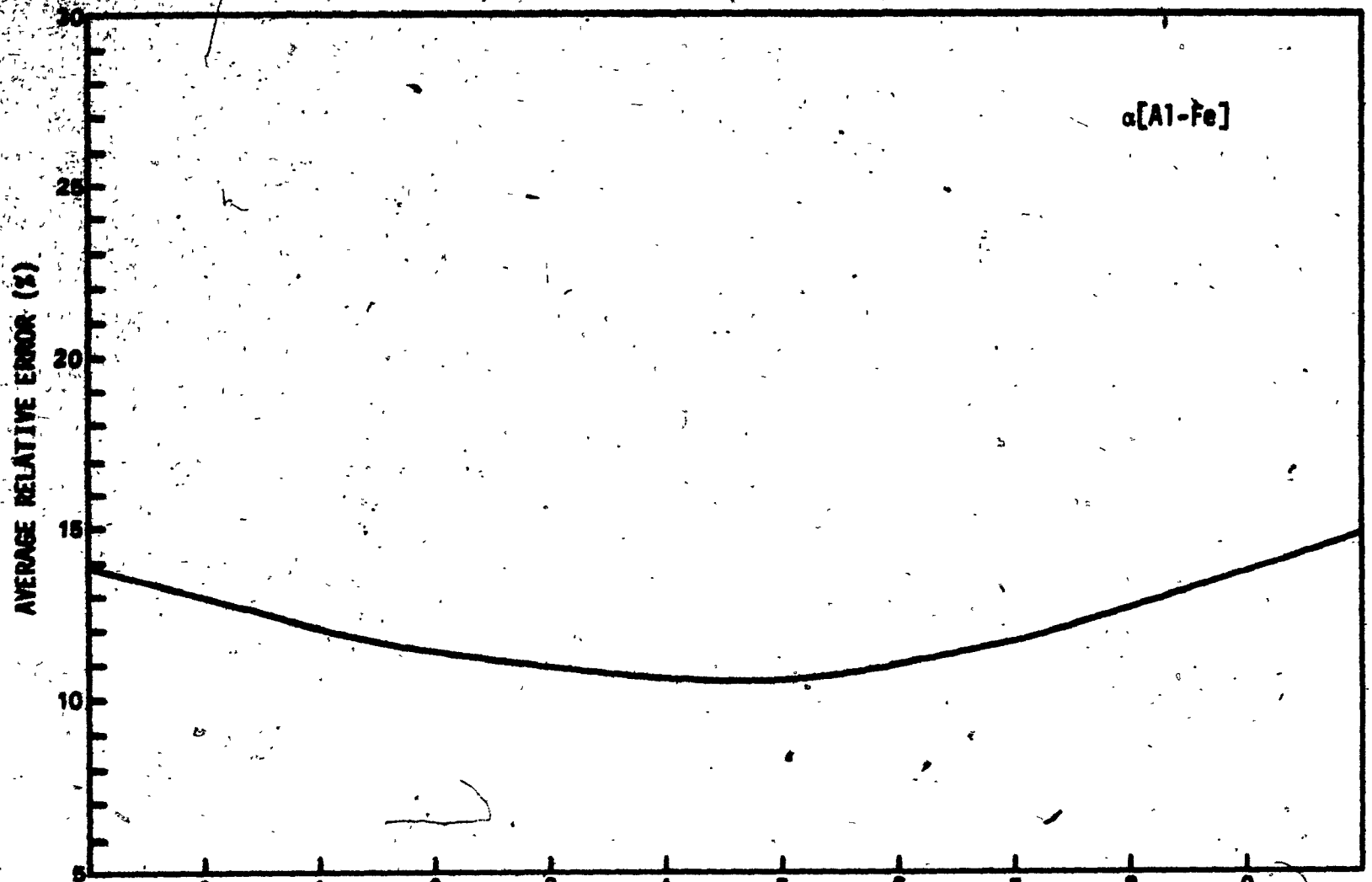
α[Al-Fe]
AVERAGE RELATIVE ERROR (%)
30
25
20
15
10
5
0
1
2
3
4
5
6
7
8
9
ALPHA COEFFICIENT VALUE

FIGURE 5-21

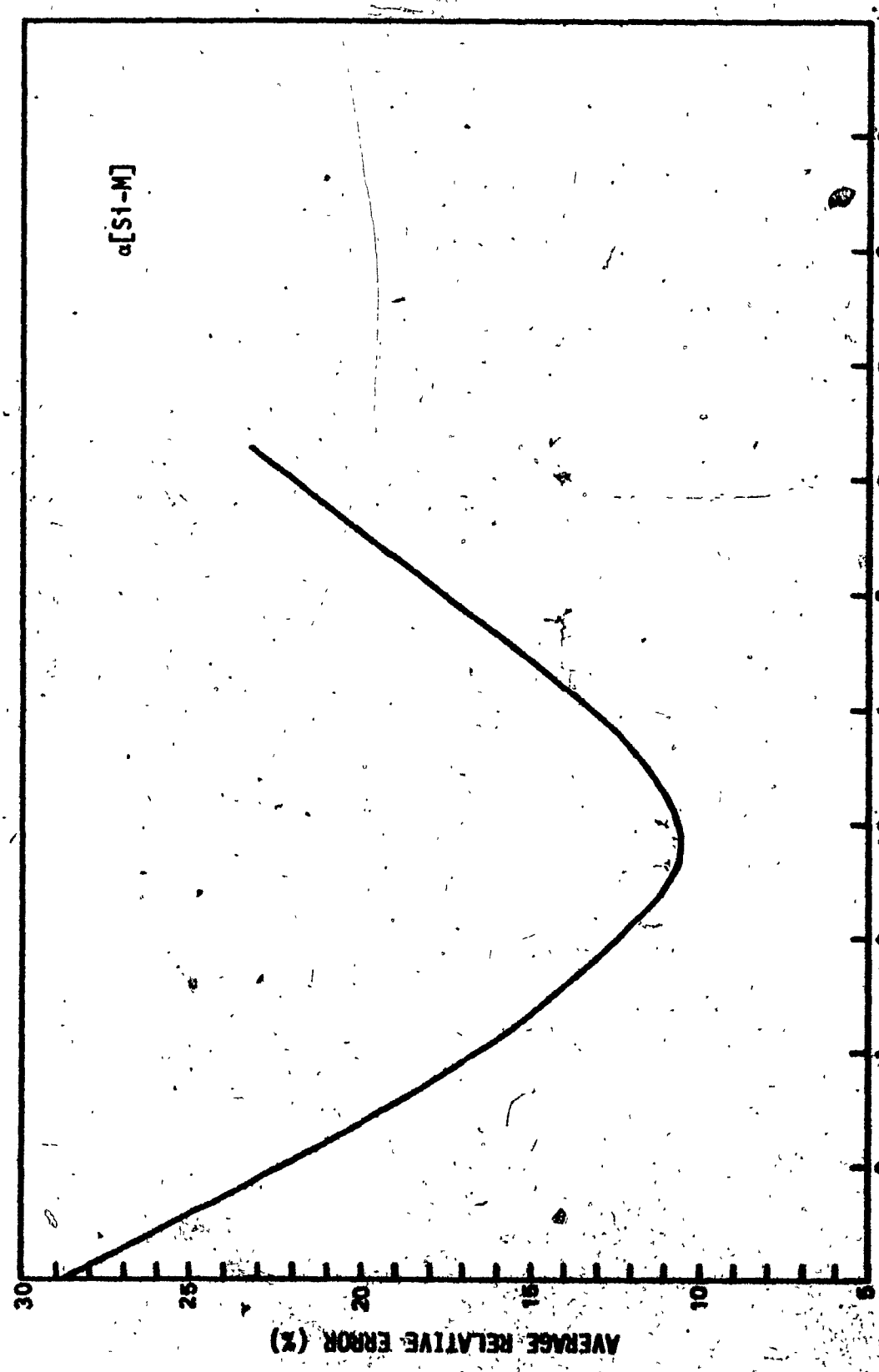
α[S1-M]
AVERAGE RELATIVE ERROR (%)
30
25
20
15
10
5
0
1
2
3
4
5
6
7
8
9
ALPHA COEFFICIENT VALUE

FIGURE 5·22

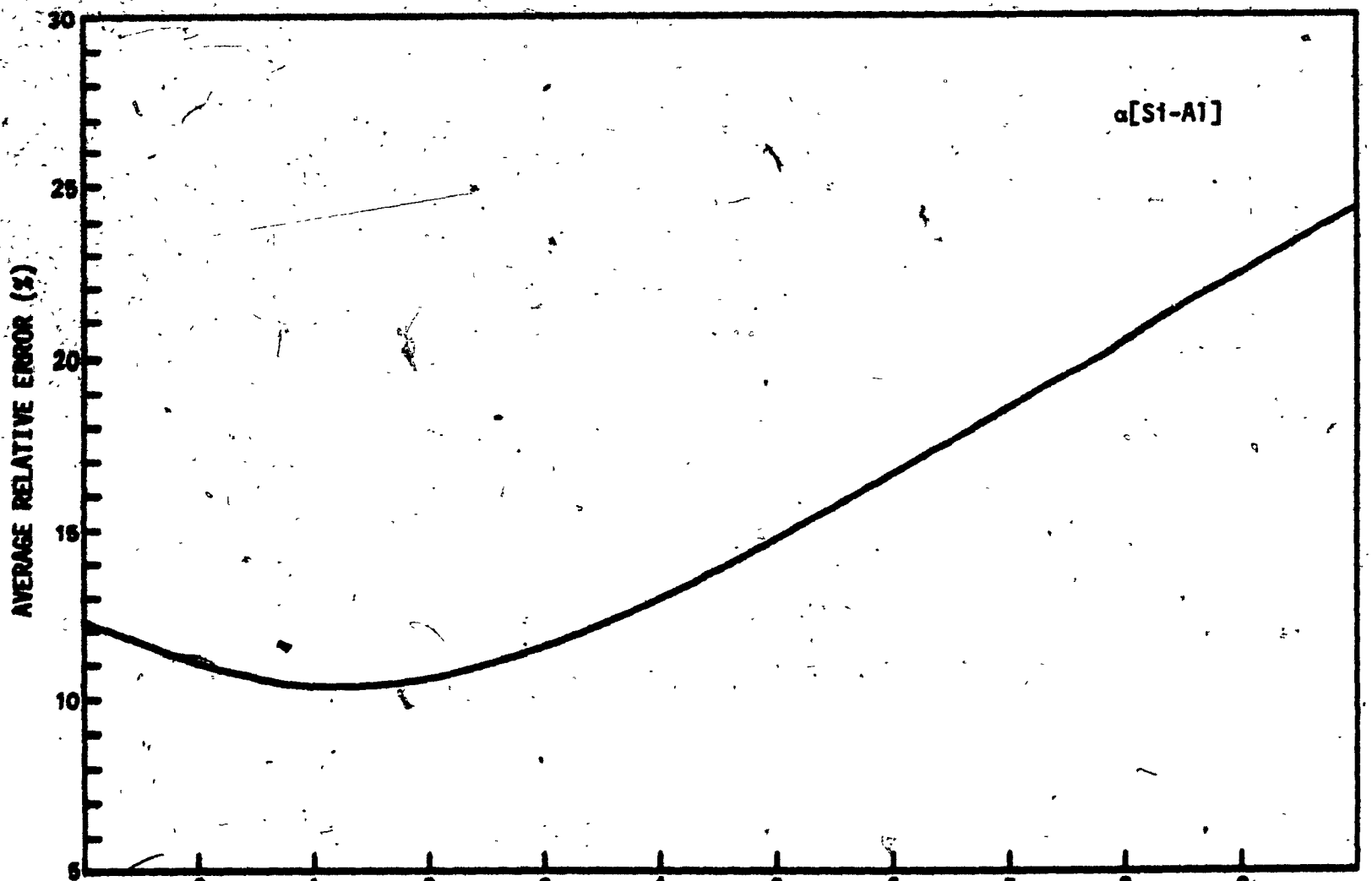
a[S1-A1]
AVERAGE RELATIVE ERROR (%)
30
25
20
15
10
5
0
1
2
3
4
5
6
7
8
9
ALPHA COEFFICIENT VALUE

FIGURE 5-23

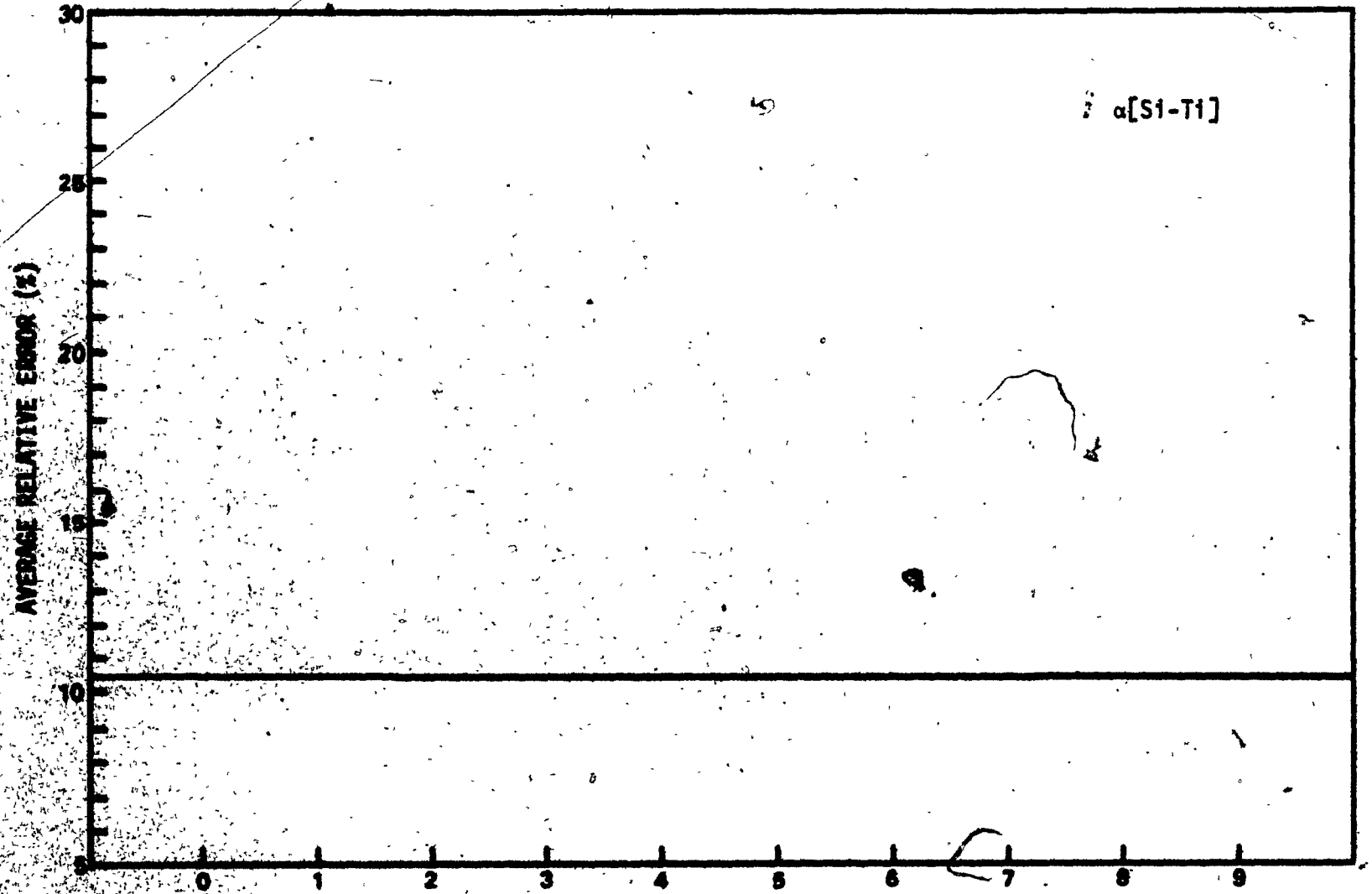
α[S1-T1]
AVERAGE RELATIVE ERROR (%)
30
25
20
15
10
5
0
1
2
3
4
5
6
7
8
9
ALPHA COEFFICIENT VALUE

FIGURE 5-24

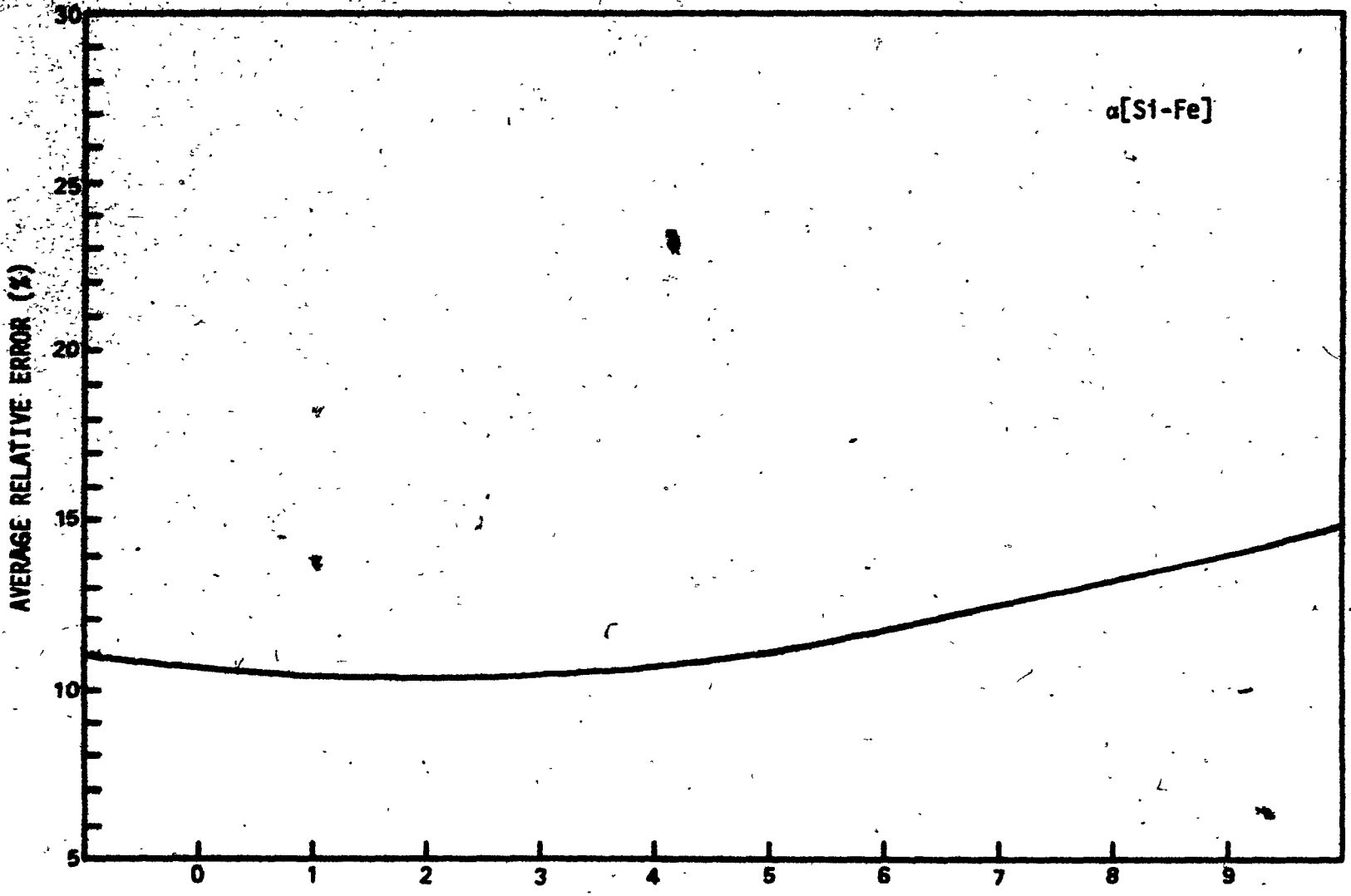
α[Si-Fe]
AVERAGE RELATIVE ERROR (%)
30
25
20
15
10
5
0
1
2
3
4
5
6
7
8
9
ALPHA COEFFICIENT VALUE

FIGURE 5·25

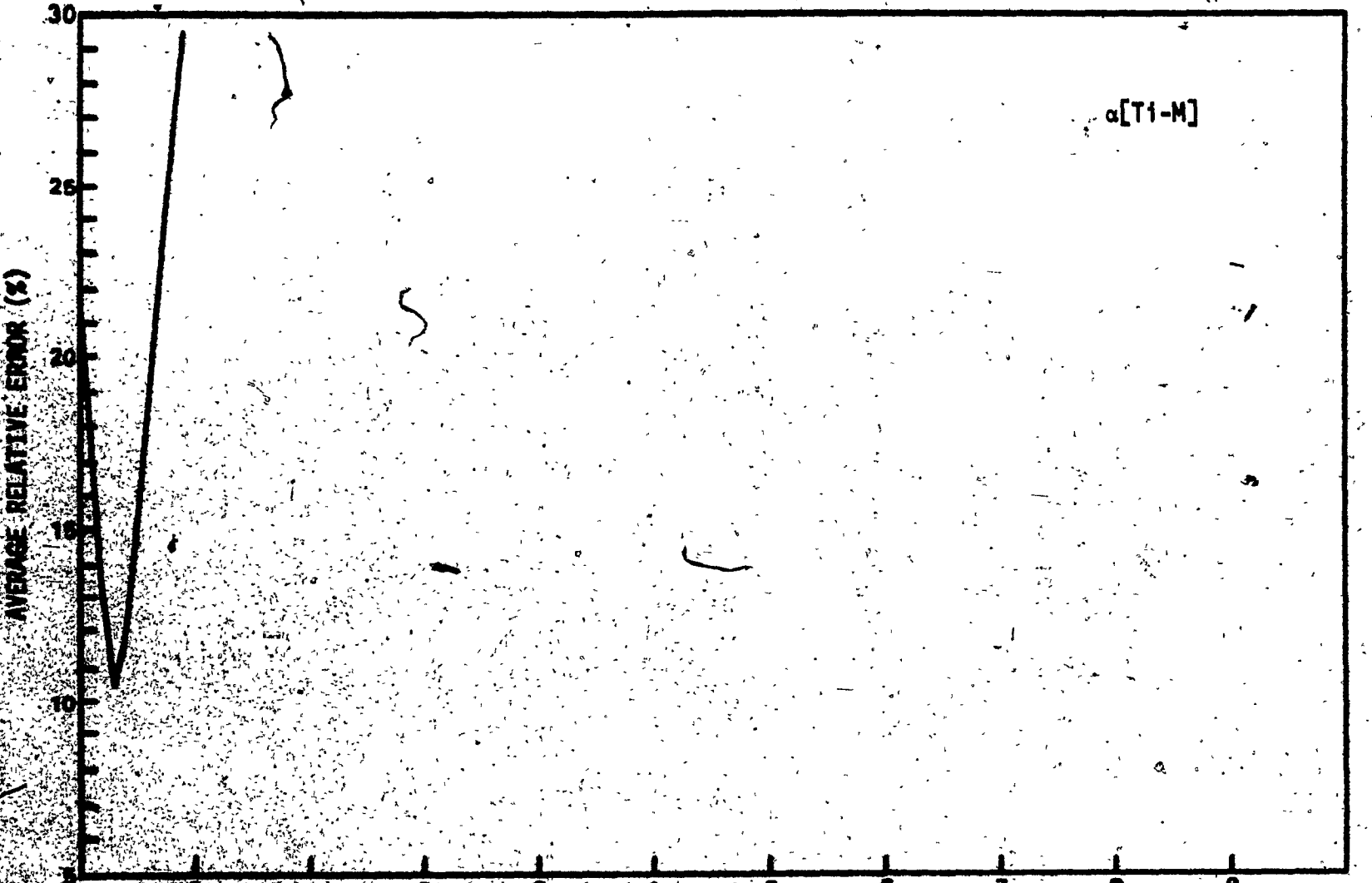
α[Ti-M]
AVERAGE RELATIVE ERROR (%)
30
25
20
15
10
5
0
1
2
3
4
5
6
7
8
9
ALPHA COEFFICIENT VALUE

FIGURE 5-26

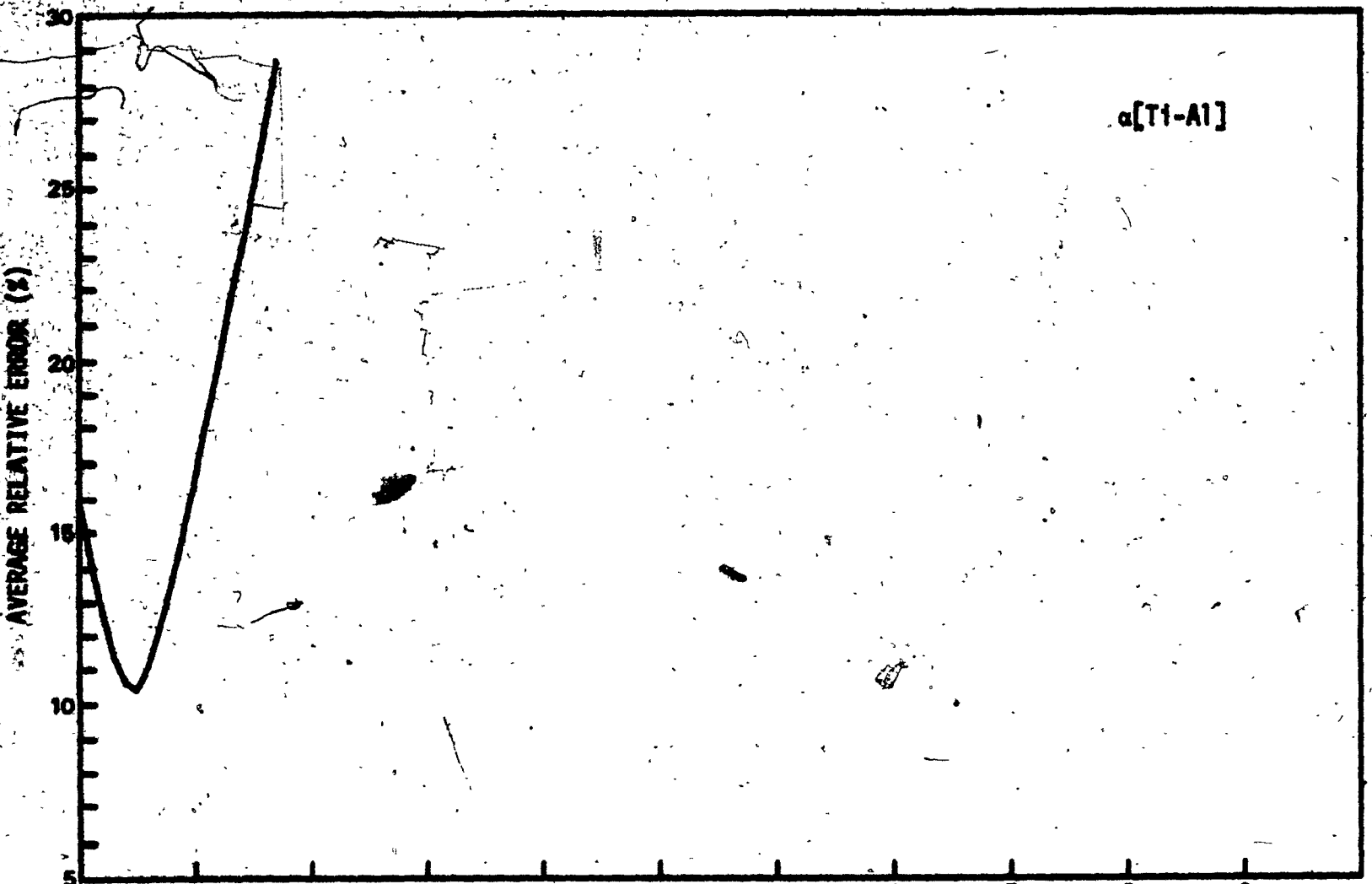
α[Ti-Al]
AVERAGE RELATIVE ERROR (%)
30
25
20
15
10
5
0
1
2
3
4
5
6
7
8
9
ALPHA COEFFICIENT VALUE

FIGURE 5·27


α[T1-S1]
AVERAGE RELATIVE ERROR (%)
30
25
20
15
10
5
0
1
2
3
4
5
6
7
8
9
ALPHA COEFFICIENT VALUE

FIGURE 5·28

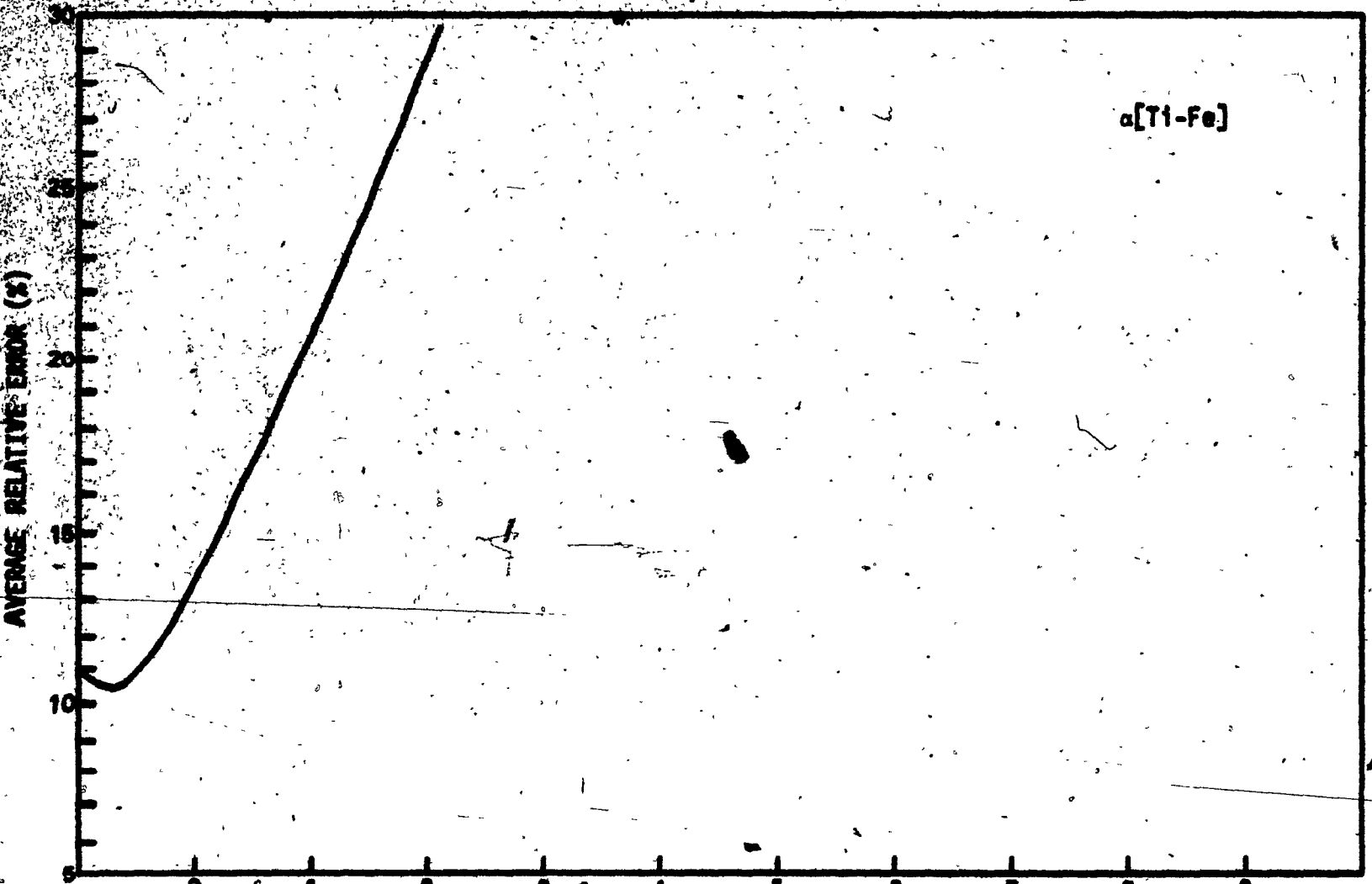
α[Ti-Fe]
AVERAGE RELATIVE ERROR (%)
30
25
20
15
10
5
0
1
2
3
4
5
6
7
8
9
ALPHA COEFFICIENT VALUE.

FIGURE 5·29

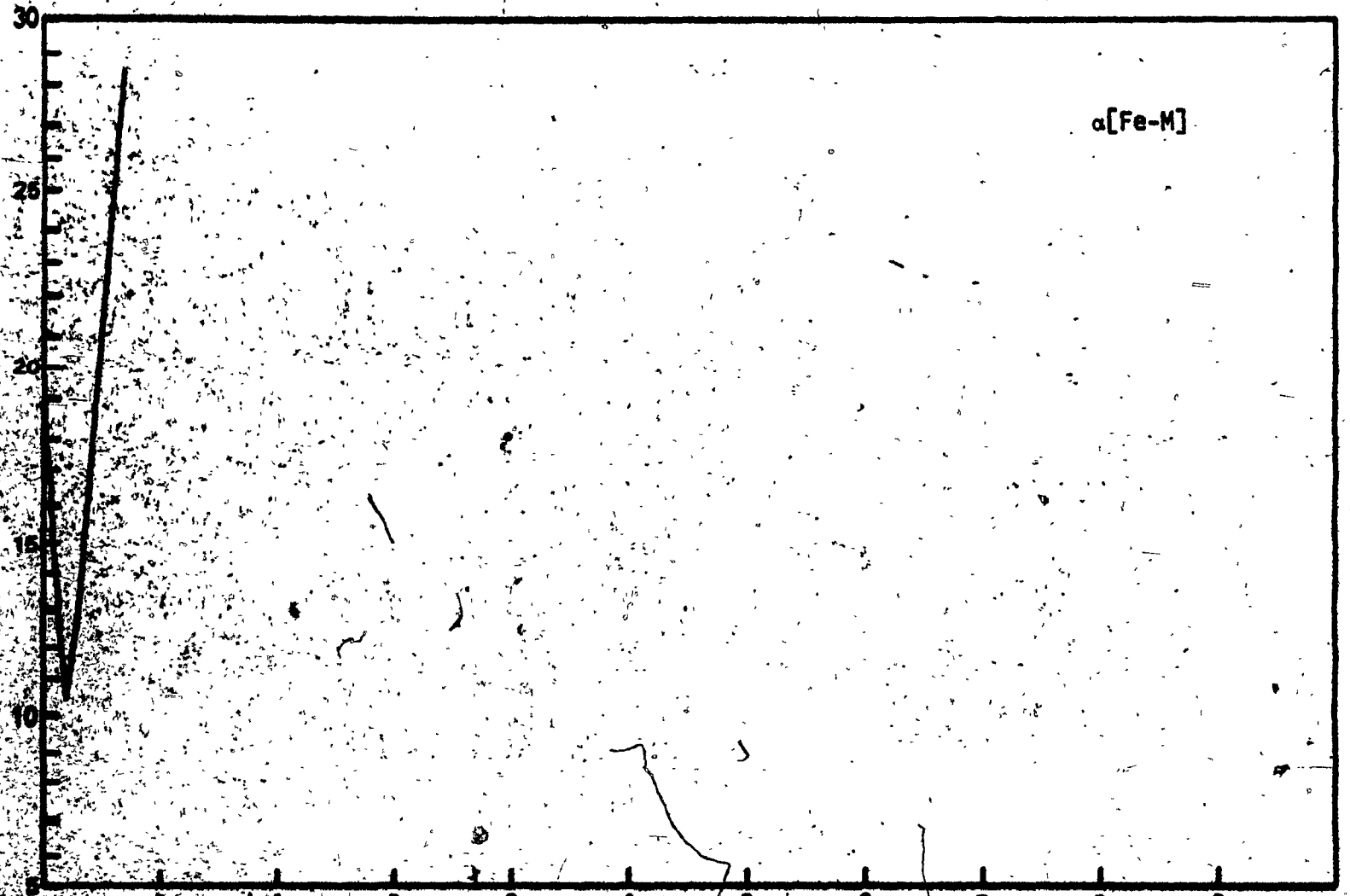
α[Fe-M]
AVERAGE RELATIVE ERROR (%)
30
25
20
15
10
5
0
1
2
3
4
5
6
7
8
9
ALPHA COEFFICIENT VALUE

FIGURE 5·30

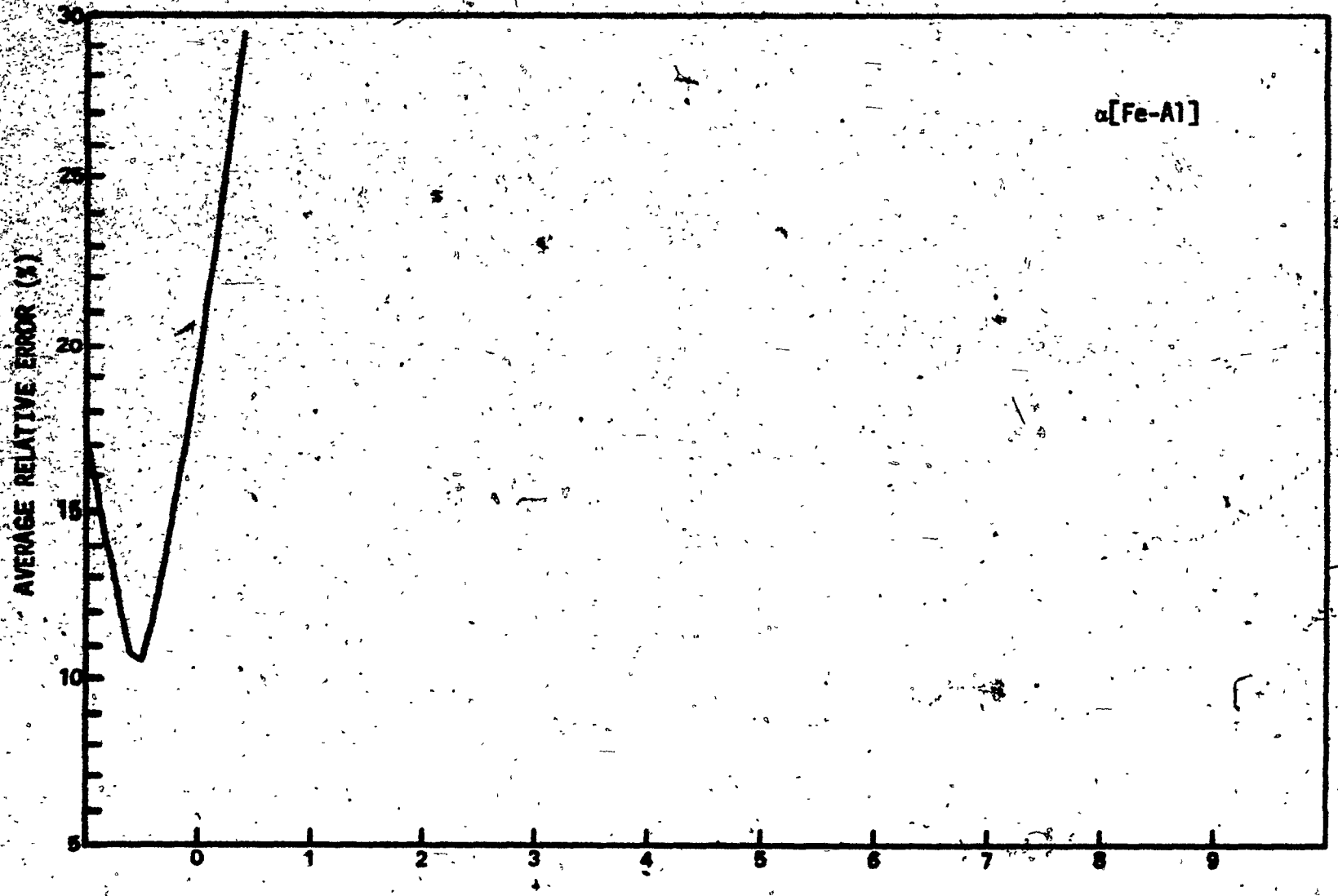
α[Fe-Al]
AVERAGE RELATIVE ERROR (%)
30
25
20
15
10
5
0
1
2
3
4
5
6
7
8
9
ALPHA COEFFICIENT VALUE

FIGURE 5-31

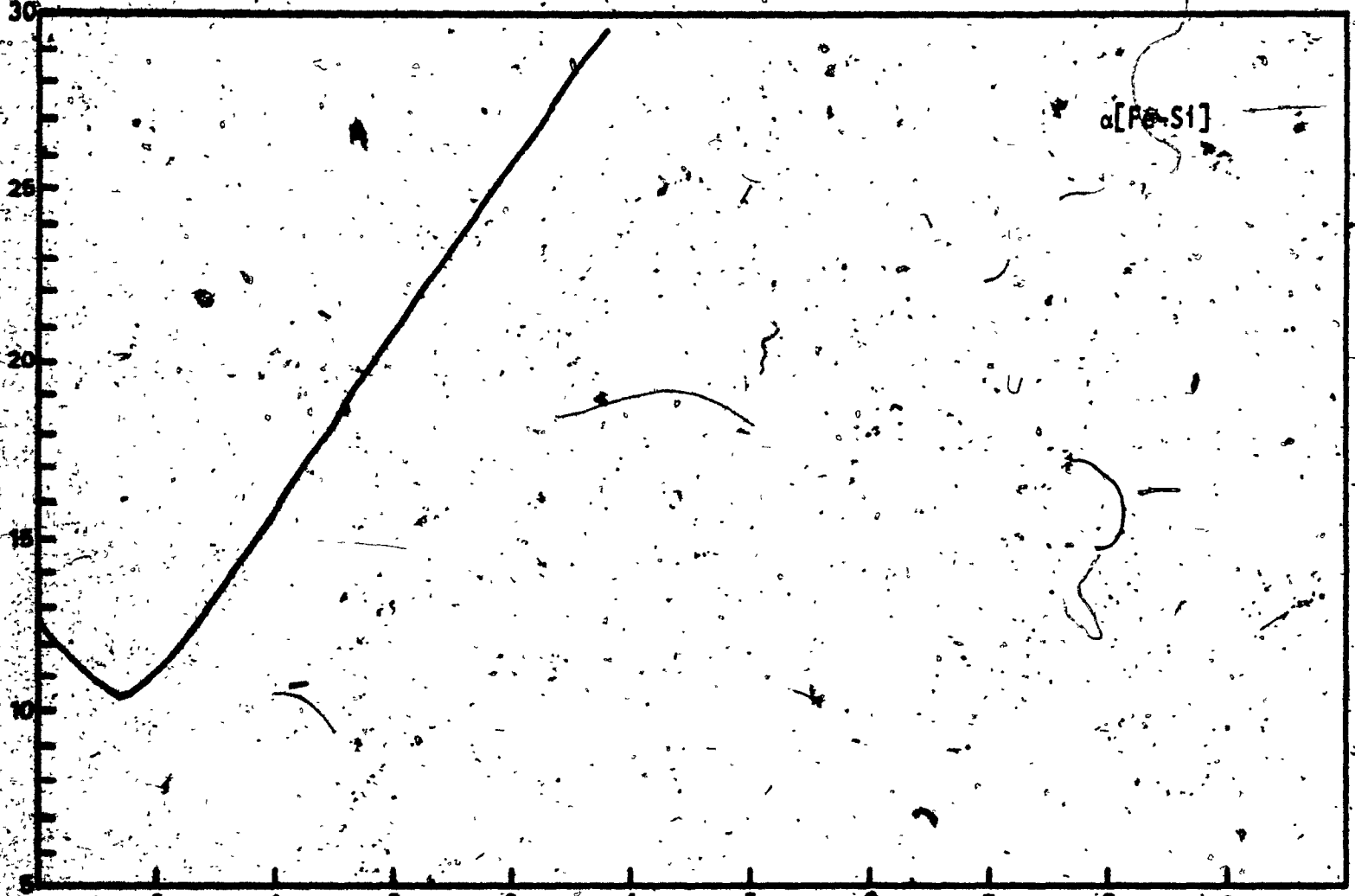
α[Fe-Si]
AVERAGE RELATIVE ERROR (%)
30
25
20
15
10
5
0
1
2
3
4
5
6
7
8
9
ALPHA COEFFICIENT VALUE

FIGURE 5-32.

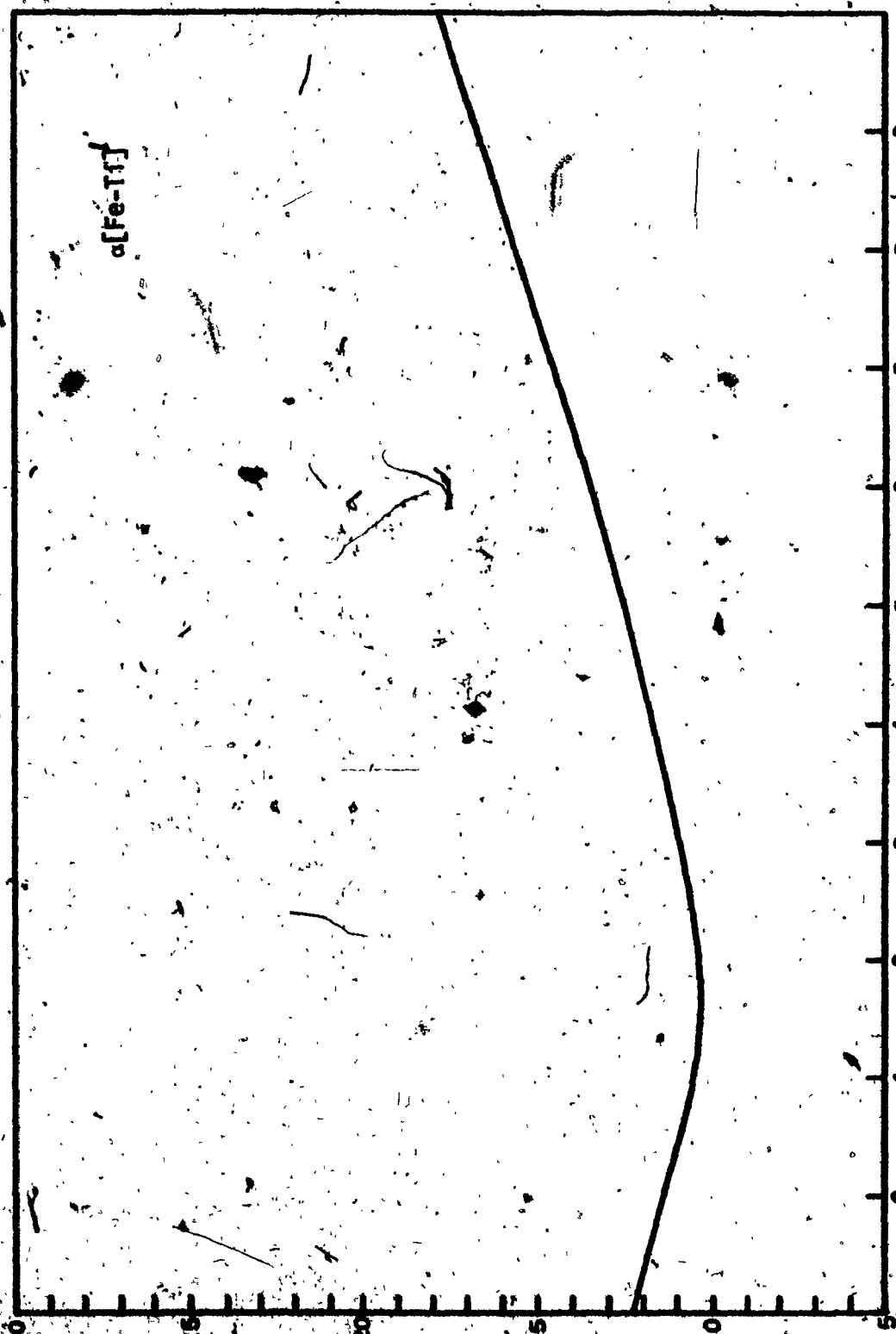
α[Fe-Ti]
AVERAGE RELATIVE ERROR (%)
30
25
20
15
10
5
0
1
2
3
4
5
6
7
8
9
ALPHA COEFFICIENT VALUE

FIGURE 5.33

The analytical results determined by wet chemical methods were, in themselves, not sufficiently accurate especially for the determination of aluminum which, in most cases, was a by-difference value. More precise alpha coefficients could only be obtained by using carefully prepared synthetic samples. However, this method has been shown to generate inaccurate alpha coefficients relative to the bauxite ore analysis.

5-2-6 XRF SPECTROCHEMICAL RESULTS FOR BAUXITE ORE SAMPLES

The determination of the matrix effect correction coefficients was completed using the x-ray line intensity and concentration data of the 70 bauxite samples which represented a cross section of bauxite material. The correction procedure modified the measured x-ray line intensities to give x-ray line intensities which were corrected for the matrix effects. The method produced a linear relationship between the corrected intensity data and the elemental concentration in the sample. It was expected that the correction procedure, if it was suitable for the analysis of this select group of samples, would be suitable to analyse any unknown bauxite sample to the same degree of accuracy.

The evaluation of the correction procedure involved treating the 70 bauxite samples as unknowns. A comparison was made between the

measured and the corrected data using both the direct ratio method (ratio of unknown sample intensity to intensity of a pure element) and the method of least squares for determining the elemental concentrations. The least squares straight line equations, determined by the use of the computer program LSERR (see APPENDIX C), are given in TABLE 5-8 . The final analytical results are given in TABLES 5-9 to 5-12 for aluminum, silicon, titanium and iron respectively. The calculated percentages are in terms of elemental percentage and not oxide percentage. The associated errors represent the differences between the calculated and the known values. The average absolute errors are shown at the bottom of each table.

The least squares treatment of the measured data for all four elements was shown to greatly improve the accuracy of the analytical determination compared to the direct ratio method. Application of the Lachance and Traill correction procedure for the x-ray intensity and the subsequent use of the direct ratio method produced results of even better accuracy. Plots of the relationship between corrected x-ray line intensity and the known concentration are shown in FIGURES 5-34 to 5-37 for aluminum, silicon, titanium and iron. The data for aluminum, although linear, was still very scattered. Of coarse this was not unexpected since the aluminum concentrations were mainly by-difference values. With the exception of one point, a very good relationship was achieved for silicon. The curvature seen for the element titanium was attributed to errors inherent in the small concentration range. Also, the expanded scale (factor of 10) makes the non-

TABLE 5-8

LEAST SQUARES EQUATIONS

ALUMINUM

I(MEAS) = 419.732 (% Al) + 411.998

I(CORR) = 818.055 (% Al) + 4123.27

SILICON

I(MEAS) = 426.077 (% Si) - 237.127

I(CORR) = 1151.98 (% Si) - 466.390

TITANIUM

I(MEAS) = 9963.81 (% Ti) + 362.338

I(CORR) = 3912.82 (% Ti) + 336.148

IRON

I(MEAS) = 1030.33 (% Fe) + 1270.91

I(CORR) = 510.254 (% Fe) - 190.087

TABLE 5-9

I((BOX AL.)= 100000

SAMPLE	AL.	I(MEAS)	MEASURED DATA RATIO AL.	MEASURED DATA METHOD ERROR	MEASURED DATA LEAST SQUARES AL.	MEASURED DATA LEAST SQUARES ERROR	I(CORR)	CORRECTED DATA RATIO AL.	CORRECTED DATA METHOD ERROR	CORRECTED DATA LEAST SQUARES AL.	CORRECTED DATA LEAST SQUARES ERROR
# 1	25.72	18311.	18.31	-15.41	23.58	-2.14	26658.	26.65	.93	27.54	1.81
# 2	24.98	18081.	18.08	-14.98	22.85	-2.14	25316.	25.32	.33	25.91	.93
# 3	23.39	9215.	9.22	-14.18	20.97	-2.42	23186.	23.11	-.29	23.20	-.19
# 4	24.82	18233.	18.23	-14.59	23.40	-1.42	25714.	25.71	.89	26.39	1.57
# 5	24.61	9764.	9.77	-14.84	22.29	-2.32	24571.	24.37	-.24	24.75	.14
# 6	24.24	9587.	9.51	-14.73	21.67	-2.57	24151.	24.15	-.09	24.48	.24
# 7	24.98	9578.	9.58	-15.40	21.84	-3.14	25822.	25.82	.84	25.55	.57
# 8	26.28	9998.	9.99	-16.21	22.82	-3.37	25126.	25.13	-1.07	25.68	-.52
# 9	23.23	8957.	8.96	-14.28	20.36	-2.86	22711.	22.71	-.52	22.72	-.51
#10	24.03	9458.	9.45	-14.58	21.53	-2.50	23528.	23.53	-.50	23.72	-.31
#11	24.93	9598.	9.60	-15.33	21.89	-3.04	24384.	24.38	-.54	24.77	-.16
#12	24.84	9548.	9.55	-14.69	21.77	-2.47	24758.	24.75	.51	25.22	.98
#13	29.11	13321.	13.32	-15.59	31.23	2.12	28819.	28.82	-.29	30.19	1.08
#14	31.60	15041.	15.04	-16.54	34.85	3.26	29912.	29.91	-1.68	31.52	-.07
#15	31.38	15078.	15.07	-16.31	34.92	3.54	30817.	30.82	-1.37	31.65	.27
#16	29.74	13085.	13.08	-16.64	30.19	.45	28968.	28.97	-2.78	27.92	-1.82
#17	31.91	15463.	15.46	-16.45	35.86	3.94	31131.	31.13	-.78	33.01	1.10
#18	27.37	13096.	13.10	-14.48	30.82	3.45	24768.	24.77	-2.81	25.24	-2.34
#19	25.24	11651.	11.65	-13.59	26.78	1.53	22547.	22.55	-2.70	22.52	-2.72
#20	23.50	10944.	10.94	-12.56	25.09	1.59	22679.	22.68	-.82	22.68	-.82
#21	22.60	11063.	11.06	-11.54	25.38	2.78	20982.	20.98	-1.70	20.51	-2.09
#22	22.12	10955.	10.95	-11.17	25.12	3.00	19498.	19.49	-2.63	18.78	-3.34
#23	1.75	1861.	1.84	.11	3.45	1.71	4196.	4.20	8.45	.07	-1.66
#24	31.76	15379.	15.38	-16.38	35.66	3.90	29572.	29.57	-2.18	31.11	-.65
#25	13.64	6789.	6.71	-6.95	15.00	1.35	17226.	17.23	3.57	16.02	2.36
#26	19.26	9431.	9.43	-9.83	21.49	2.22	26818.	26.81	6.74	26.73	7.47
#27	18.28	5814.	5.81	-6.46	12.87	-.59	17454.	17.45	5.17	16.38	4.82
#28	9.68	4895.	4.90	-4.79	10.68	1.00	16619.	16.62	6.93	15.27	5.59
#29	4.71	2869.	2.87	-2.64	3.95	-.76	7499.	7.50	2.79	4.13	-.58
#30	26.67	10141.	10.14	-16.53	23.18	-3.49	25481.	25.48	-1.19	26.11	-.57
#31	30.86	12487.	12.49	-17.37	28.77	-1.29	27717.	27.72	-2.34	28.84	-1.22
#32	21.84	6767.	6.77	-15.09	15.14	-6.70	18[illegible]	18.09	-3.17	17.88	-4.06
#33	21.38	6448.	6.45	-14.93	14.38	-7.00	[illegible]118.	17.11	-4.27	15.88	-5.50
#34	23.13	7748.	7.74	-15.39	17.44	-5.67	20804.	20.80	-2.34	19.51	-3.62
#35	28.11	6761.	6.76	-13.35	15.13	-4.99	28687.	28.61	.49	28.15	.04
#36	26.46	9581.	9.58	-16.88	21.84	-4.62	27979.	27.98	1.52	26.27	-.19
#37	28.12	7136.	7.14	-14.99	16.98	-6.10	28684.	28.68	.56	28.24	.11
#38	31.82	13483.	13.48	-17.77	31.67	-.16	28832.	28.83	-2.99	30.28	-1.52
#39	24.19	7948.	7.97	-16.88	18.98	-5.19	20944.	20.94	-3.24	20.56	-3.63
#40	26.61	8881.	8.88	-15.81	19.99	-6.62	21918.	21.91	-4.70	21.74	-4.87
#41	24.98	9818.	9.81	-15.97	20.48	-4.50	23718.	23.71	-1.27	23.94	-1.04
#42	25.40	8868.	8.86	-16.34	20.13	-5.28	22998.	22.99	-2.41	22.57	-2.83
#43	27.79	10624.	10.62	-17.16	24.33	-3.45	25118.	25.12	-2.67	25.66	-2.12
#44	27.53	11612.	11.61	-15.91	24.69	-.84	27787.	27.79	.26	28.93	1.40
#45	28.19	12098.	12.09	-16.08	27.85	-.31	28116.	28.11	-.83	29.33	1.18
#46	29.76	14438.	14.04	-15.72	32.46	2.70	32268.	32.27	2.68	34.53	4.76
#47	32.41	15344.	15.34	-17.06	35.58	3.17	33398.	33.40	.99	35.79	3.38
#48	30.43	14235.	14.23	-16.28	32.98	2.53	31346.	31.37	.91	33.38	2.85
#49	30.09	14468.	14.47	-16.12	33.49	2.90	32748.	32.74	2.15	34.98	4.39
#50	33.71	16748.	16.72	-16.96	38.92	5.21	33989.	33.93	.22	36.43	2.72
#51	31.69	13838.	13.83	-15.84	36.02	4.33	33888.	33.89	1.71	35.35	4.06
#52	31.76	15819.	15.82	-16.84	35.50	3.58	32145.	32.14	.39	34.23	2.36
#53	27.83	12408.	12.38	-16.80	25.04	-1.09	28833.	28.83	-2.38	29.84	-1.19
#54	20.12	9988.	9.91	-15.63	22.68	2.18	18483.	18.48	-9.18	17.48	-3.84
#55	13.38	6841.	6.85	-16.68	15.32	1.88	12473.	12.47	-1.04	10.21	-3.31
#56	21.86	11421.	11.47	-9.89	26.35	5.28	24129.	24.13	2.07	24.46	2.39
#57	18.47	9471.	9.48	-8.88	21.94	3.47	20891.	20.89	2.42	20.58	2.11
#58	21.38	9469.	9.46	-11.73	22.81	.68	21988.	21.99	.31	21.47	.09
#59	19.21	8878.	8.88	-10.64	19.48	.26	20489.	20.41	1.20	19.91	.70
#60	24.48	11328.	11.33	-13.87	26.01	1.53	24737.	24.74	.26	25.22	.82
#61	16.72	7867.	7.87	-8.86	17.76	1.04	17988.	17.99	1.26	16.95	.22
#62	14.39	6134.	6.13	-6.25	13.45	-.94	15388.	15.38	.98	13.76	-.63
#63	16.19	8090.	8.08	-7.30	16.82	.63	17149.	17.15	.95	15.98	-.21
#64	13.76	7280.	7.28	-6.28	14.60	.84	15[illegible]	15.28	.68	13.83	[illegible]
#65	[illegible]	[illegible]	[illegible]	[illegible]	[illegible]	[illegible]	[illegible]	13.34	[illegible]	11.82	-.97
#66	[illegible]	[illegible]	[illegible]	[illegible]	[illegible]	[illegible]	[illegible]	[illegible]	.67	[illegible]	.09
#67	[illegible]	[illegible]	[illegible]	[illegible]	[illegible]	[illegible]	[illegible]	[illegible]	[illegible]	[illegible]	.96
#68	[illegible]	[illegible]	[illegible]	[illegible]	[illegible]	[illegible]	[illegible]	[illegible]	[illegible]	[illegible]	[illegible]
#69	[illegible]	[illegible]	[illegible]	[illegible]	[illegible]	[illegible]	[illegible]	[illegible]	[illegible]	[illegible]	[illegible]
#70	[illegible]	[illegible]	[illegible]	[illegible]	[illegible]	[illegible]	[illegible]	[illegible]	[illegible]	[illegible]	[illegible]
AVG.	[illegible]	[illegible]	10.27		8.79			4.77		4.98	

TABLE 5-10

I(100% SI)= 184000

SAMPLE	%SI	I(MEAS)	MEASURED DATA RATIO METHOD %SI	MEASURED DATA RATIO METHOD ERROR	MEASURED DATA LEAST SQUARES %SI	MEASURED DATA LEAST SQUARES ERROR	I(CORR)	CORRECTED DATA RATIO METHOD %SI	CORRECTED DATA RATIO METHOD ERROR	CORRECTED DATA LEAST SQUARES %SI	CORRECTED DATA LEAST SQUARES ERROR
# 1	.15	58.	.86	-.18	.69	.34	171.	.16	.01	.55	.48
# 2	.47	219.	.21	-.46	1.07	.48	656.	.63	-.05	.97	.38
# 3	2.67	836.	.88	-1.87	2.52	-.16	2466.	2.37	-.38	2.55	-.13
# 4	1.67	497.	.48	-1.19	1.72	.05	1464.	1.41	-.26	1.68	.01
# 5	2.65	791.	.76	-1.89	2.41	-.24	2314.	2.22	-.43	2.41	-.24
# 6	.38	97.	.09	-.21	.78	.49	298.	.28	-.02	.66	.36
# 7	.16	56.	.05	-.11	.69	.53	165.	.16	-.00	.55	.39
# 8	.38	23.	.02	-.28	.61	.31	68.	.07	-.23	.46	.16
# 9	3.11	918.	.88	-2.23	2.71	-.48	2685.	2.58	-.53	2.74	-.37
#10	4.18	1261.	1.21	-2.97	3.58	-.66	3649.	3.51	-.67	3.57	-.61
#11	1.46	444.	.43	-1.04	1.48	.14	1305.	1.25	-.21	1.34	.07
#12	1.33	348.	.33	-.99	1.37	.05	1002.	.98	-.34	1.29	-.04
#13	2.81	776.	.75	-2.06	2.38	-.43	2217.	2.23	-.58	2.42	-.39
#14	2.45	856.	.82	-1.63	2.57	.11	2561.	2.46	-.01	2.63	.17
#15	2.33	828.	.80	-1.54	2.50	.17	2483.	2.39	.05	2.56	.23
#16	4.15	1762.	1.69	-2.45	4.69	.55	5175.	4.98	.83	4.98	.75
#17	.96	341.	.33	-.65	1.06	.37	1030.	.99	.01	1.30	.32
#18	9.25	3499.	3.36	-5.89	8.77	-.49	10146.	9.76	.50	9.21	-.04
#19	12.86	4388.	4.22	-7.84	10.86	-1.28	12583.	12.02	-.84	11.26	-.88
#20	13.46	5278.	5.07	-8.39	12.94	-.52	14758.	14.19	.73	13.22	-.25
#21	14.59	6883.	5.85	-10.74	14.83	-1.76	16908.	16.26	-.34	15.08	-1.51
#22	18.79	6859.	6.60	-12.28	16.65	-2.14	18947.	18.22	-.57	16.65	-1.94
#23	28.28	15853.	15.24	-13.84	37.76	9.48	43128.	41.47	13.19	37.84	9.56
#24	3.18	1086.	.97	-2.21	2.92	-.26	3007.	2.89	-.29	3.08	-.10
#25	16.69	6527.	6.28	-10.41	15.68	-.81	17518.	16.84	.15	15.68	-1.00
#26	3.13	1648.	1.58	-1.56	4.41	1.27	4771.	4.59	1.46	4.35	1.41
#27	11.55	4889.	4.70	-6.85	12.03	.48	13175.	12.67	1.12	11.84	.30
#28	3.09	1621.	1.56	-1.53	4.36	1.28	4630.	4.45	1.37	4.42	1.34
#29	4.11	2191.	2.11	-2.01	5.78	1.59	6236.	6.00	1.88	5.82	1.71
#30	.51	144.	.14	-.38	.89	.38	424.	.41	-.11	.77	.26
#31	.51	132.	.13	-.39	.87	.35	395.	.38	-.13	.75	.23
#32	3.23	987.	.87	-2.35	2.69	-.54	2589.	2.49	-.74	2.65	-.57
#33	5.00	1648.	1.56	-3.42	4.42	-.58	4695.	4.51	-.49	4.48	-.52
#34	3.83	1344.	1.29	-2.54	3.71	-.12	3863.	3.71	-.12	3.76	-.07
#35	.88	235.	.23	-.57	1.11	.31	669.	.64	-.15	.99	.19
#36	1.06	318.	.30	-.78	1.28	.21	988.	.87	-.28	1.19	.12
#37	.42	124.	.12	-.30	.85	.43	357.	.34	-.08	.71	.29
#38	.42	117.	.11	-.31	.83	.41	351.	.34	-.08	.71	.29
#39	2.18	689.	.59	-1.52	1.99	-.12	1761.	1.69	-.41	1.93	-.17
#40	3.84	841.	.81	-2.23	2.53	-.51	2444.	2.35	-.69	2.53	-.51
#41	.33	108.	.10	-.23	.79	.46	293.	.28	-.05	.64	.33
#42	1.36	482.	.46	-.89	1.69	.33	1484.	1.35	-.00	1.63	.27
#43	1.17	385.	.35	-.82	1.41	.24	1077.	1.04	-.13	1.34	.17
#44	.56	327.	.31	-.25	1.32	.76	972.	.93	.37	1.25	.69
#45	.38	258.	.24	-.14	1.14	.76	748.	.72	.34	1.05	.68
#46	.37	135.	.13	-.24	.87	.50	403.	.39	.01	.75	.38
#47	.19	79.	.08	-.11	.74	.55	236.	.23	.04	.61	.42
#48	.52	163.	.16	-.37	.94	.42	488.	.47	-.05	.83	.30
#49	.25	84.	.08	-.17	.75	.51	251.	.24	-.01	.62	.37
#50	.21	59.	.06	-.15	.78	.49	177.	.17	-.04	.56	.35
#51	.25	94.	.09	-.16	.78	.53	283.	.27	.02	.65	.40
#52	.27	91.	.09	-.18	.77	.50	274.	.26	-.00	.64	.38
#53	9.67	4497.	4.32	-5.35	11.11	1.44	12138.	11.66	1.99	10.93	1.26
#54	28.04	7985.	7.68	-12.36	19.38	-.74	21824.	20.98	.95	19.35	-.69
#55	27.63	11814.	11.36	-16.27	28.28	.65	31486.	30.20	2.57	27.67	.04
#56	10.38	3466.	3.33	-7.04	8.69	-1.69	10158.	9.77	-.61	9.22	-1.15
#57	15.15	5376.	5.17	-9.98	13.17	-1.97	15868.	14.49	-.66	12.48	-1.66
#58	10.64	3729.	3.59	-7.87	9.31	-1.33	10612.	10.20	-.45	9.62	-1.02
#59	11.92	4171.	4.01	-7.91	10.35	-1.57	11668.	11.21	-.71	10.53	-1.39
#60	8.18	2895.	2.79	-5.39	6.86	-1.32	7779.	7.48	-.70	7.16	-1.02
#61	16.69	6815.	5.98	-10.71	15.14	-1.54	17826.	15.37	-.32	15.15	-1.54
#62	24.92	10287.	9.89	-15.02	24.78	-.21	27768.	26.78	1.88	24.36	-.41
#63	22.44	8687.	8.28	-14.16	20.76	-1.68	23431.	22.53	.09	20.74	-1.69
#64	25.85	10687.	10.28	-14.86	25.45	-.40	28429.	27.34	2.88	25.98	.13
#65	27.16	11022.	11.37	-15.79	26.38	1.14	31501.	30.35	3.14	27.75	.60
#66	11.58	3878.	3.73	-7.77	9.46	-1.84	11017.	10.60	-.85	10.02	-1.40
#67	4.21	1284.	1.23	-2.91	3.07	-.64	3779.	3.63	-.57	3.60	-.58
#68	7.98	2272.	2.17	-5.43	6.99	-1.31	7266.	7.00	-.82	6.80	-1.18
#69	10.10	3548.	3.41	-6.69	8.88	-1.22	10028.	9.70	-.68	9.16	-.94
#70	15.75	5794.	5.57	-10.18	14.16	-1.60	16958.	15.30	-.45	14.59	-1.16
AVG. ABS. ERROR =			4.86		.88			.71		.73	

TABLE 5-11

I(100% TI)= 413280

SAMPLE	%TI	I(MEAS)	MEASURED DATA RATIO %TI	METHOD ERROR	LEAST SQUARES %TI	ERROR	I(CORR)	CORRECTED DATA RATIO %TI	METHOD ERROR	LEAST SQUARES %TI	ERROR
#1	1.68	19148.	4.63	2.95	1.68	.21	7263.	1.76	.08	1.77	.09
#2	1.62	17536.	4.24	2.62	1.72	.10	6684.	1.62	-.00	1.62	.00
#3	1.49	15785.	3.82	2.33	1.55	.06	6141.	1.49	-.00	1.48	-.00
#4	1.45	15960.	3.86	2.42	1.57	.12	6158.	1.49	.04	1.49	.04
#5	1.46	15876.	3.84	2.39	1.56	.10	6203.	1.50	.04	1.50	.04
#6	1.35	15161.	3.67	2.32	1.49	.14	5698.	1.38	.03	1.37	.02
#7	1.98	20973.	5.08	3.09	2.07	.08	7977.	1.93	-.05	1.95	-.03
#8	1.61	17258.	4.18	2.57	1.70	.09	6576.	1.59	-.02	1.59	-.01
#9	1.34	14818.	3.59	2.06	1.37	.03	5466.	1.32	-.01	1.31	-.03
#10	1.54	15868.	3.64	2.10	1.48	-.07	6010.	1.45	-.09	1.45	-.09
#11	1.62	16710.	4.04	2.42	1.64	.02	6441.	1.56	-.07	1.56	-.06
#12	1.68	17203.	4.16	2.48	1.69	.01	6599.	1.60	-.08	1.60	-.08
#13	1.67	19488.	4.71	3.05	1.92	.25	7855.	1.90	.23	1.92	.25
#14	1.53	17488.	4.21	2.68	1.71	.17	7053.	1.71	.17	1.72	.18
#15	1.52	17294.	4.19	2.66	1.70	.16	6998.	1.69	.17	1.70	.18
#16	.73	7283.	1.75	1.02	.69	-.04	2928.	.71	-.02	.66	-.07
#17	1.56	17413.	4.21	2.66	1.71	.15	6923.	1.68	.12	1.68	.12
#18	1.02	9919.	2.40	1.38	.96	-.06	4385.	1.06	.02	1.01	-.00
#19	1.44	14657.	3.55	2.11	1.43	-.00	6577.	1.59	.15	1.59	.16
#20	2.28	17429.	4.22	1.94	1.71	-.57	7999.	1.94	-.34	1.96	-.32
#21	1.14	8715.	2.11	.97	.84	-.30	4879.	.99	-.15	.96	-.18
#22	.78	6835.	1.65	.88	.65	-.13	3266.	.79	.01	.75	-.03
#23	.48	1341.	.32	-.16	.10	-.38	660.	.16	-.32	.08	-.40
#24	1.26	15328.	3.71	2.45	1.50	.24	6256.	1.51	.26	1.51	.25
#25	.66	4894.	1.18	.53	.45	-.20	2188.	.53	-.13	.47	-.19
#26	.60	5267.	1.27	.67	.49	-.11	1983.	.48	-.12	.42	-.18
#27	.84	5819.	1.41	.57	.55	-.29	2488.	.56	-.26	.53	-.31
#28	.34	4218.	1.02	.48	.39	-.15	1497.	.36	-.18	.30	-.24
#29	1.02	10537.	2.55	1.53	1.02	.00	3741.	.91	-.11	.87	-.15
#30	1.62	19433.	4.70	3.05	1.91	.29	7446.	1.80	.18	1.82	.20
#31	1.58	19252.	4.66	3.16	1.90	.40	7507.	1.82	.32	1.83	.33
#32	1.36	16367.	3.96	2.58	1.61	.25	6333.	1.53	.15	1.53	.15
#33	.96	11457.	2.77	1.81	1.11	.15	4512.	1.09	.13	1.07	.11
#34	1.14	13765.	3.33	2.19	1.35	.21	5394.	1.31	.17	1.29	.15
#35	1.20	13526.	3.27	2.07	1.32	.12	4963.	1.20	.00	1.18	-.02
#36	1.44	18094.	4.38	2.94	1.78	.34	6961.	1.68	.25	1.69	.25
#37	1.20	13711.	3.32	2.12	1.34	.14	5062.	1.23	.03	1.21	.01
#38	1.38	16482.	3.99	2.61	1.62	.24	6444.	1.56	.18	1.56	.18
#39	1.14	13956.	3.38	2.24	1.36	.23	5354.	1.30	.16	1.28	.14
#40	.78	8293.	2.01	1.23	.88	.02	3217.	.78	-.00	.74	-.04
#41	1.32	16360.	3.91	2.69	1.63	.31	6238.	1.51	.19	1.51	.19
#42	.98	10738.	2.60	1.78	1.04	.06	4088.	.99	.00	.96	-.02
#43	1.82	18981.	3.13	2.11	1.26	-.56	4979.	1.20	.38	1.19	-.63
#44	1.66	19833.	4.80	3.28	1.95	.29	7647.	1.85	.19	1.87	.21
#45	1.47	19879.	4.82	3.14	1.88	.40	7348.	1.78	.30	1.79	.32
#46	2.88	23888.	5.76	3.88	2.35	-.53	9482.	2.29	-.59	2.34	-.55
#47	2.92	30578.	7.40	4.48	3.02	.11	12311.	2.98	.06	3.06	.14
#48	2.12	21965.	5.10	2.98	2.08	-.04	8329.	2.02	-.11	2.04	-.08
#49	3.36	33358.	8.07	4.71	3.31	-.05	13433.	3.25	-.11	3.35	-.02
#50	2.03	20138.	4.87	2.85	1.98	-.04	8045.	1.95	-.08	1.97	-.06
#51	2.24	19279.	4.67	2.42	1.90	-.34	7651.	1.85	-.39	1.87	-.37
#52	2.23	21864.	5.29	3.06	2.16	-.07	8691.	2.10	-.13	2.14	-.09
#53	2.02	17673.	4.28	2.26	1.74	-.28	8118.	1.96	-.06	1.99	-.03
#54	1.43	13698.	3.32	1.89	1.34	-.09	6663.	1.61	.19	1.62	.19
#55	.66	7345.	1.78	.92	.78	-.16	3774.	.91	.06	.88	.02
#56	1.52	15854.	3.84	2.11	1.47	-.05	6489.	1.57	.05	1.57	.05
#57	1.89	18800.	4.55	1.66	1.19	-.11	5518.	1.34	.04	1.32	.03
#58	1.28	11975.	2.65	1.48	1.08	-.12	4768.	1.15	-.05	1.13	-.07
#59	1.06	9850.	2.34	1.28	.93	-.12	4169.	1.01	-.05	.98	-.08
#60	1.45	13897.	3.36	1.92	1.36	-.09	5889.	1.42	-.02	1.42	-.03
#61	1.06	8599.	2.08	1.03	.83	-.23	3917.	.95	-.11	.92	-.14
#62	1.06	8831.	2.15	1.07	.85	-.21	4448.	1.08	.02	1.05	-.01
#63	1.18	9864.	2.20	1.18	.89	-.29	4542.	1.10	-.08	1.07	-.11
#64	.73	6374.	1.54	.81	.60	-.13	3174.	.77	.04	.73	-.01
#65	.78	8964.	1.44	.74	.56	-.14	3889.	.73	.03	.69	-.01
#66	1.33	13843.	3.20	1.88	1.29	-.03	5881.	1.40	.08	1.40	.07
#67	1.39	13897.	3.36	1.97	1.36	-.03	5648.	1.37	-.02	1.36	-.03
#68	1.17	11284.	2.72	1.55	1.09	-.08	4692.	1.14	-.04	1.11	-.06
#69	1.26	11166.	2.70	1.44	1.08	-.17	4798.	1.16	-.10	1.14	-.12
#70	1.01	8488.	2.05	1.02	.81	-.21	3787.	.98	-.10	.88	-.13
AVG. ABS. ERROR =				2.06		.17			.10		.12

TABLE 5-12

I((100% FE)= 49388

SAMPLE	%FE	I(MEAS)	MEASURED DATA RATIO %FE	METHOD ERROR	LEAST SQUARES %FE	ERROR	I(CORR)	CORRECTED DATA RATIO %FE	METHOD ERROR	LEAST SQUARES %FE	ERROR
# 1	13.99	16466.	33.48	19.41	14.75	.76	6724.	13.64	-.35	13.55	-.44
# 2	12.66	14782.	29.82	17.16	13.84	.38	5848.	11.85	-.81	11.82	-.84
# 3	12.52	15288.	31.81	18.49	13.68	1.88	6181.	12.38	-.14	12.83	-.19
# 4	12.87	15616.	31.68	18.81	13.92	1.85	6241.	12.66	-.21	12.68	-.27
# 5	12.66	15617.	31.68	19.82	13.92	1.26	6283.	12.74	.08	12.69	.03
# 6	13.15	16236.	32.93	19.78	14.52	1.38	6366.	12.91	-.24	12.85	-.30
# 7	13.78	16396.	33.66	19.88	14.87	1.89	6825.	13.84	.86	13.75	-.93
# 8	12.52	16151.	32.76	20.24	14.44	1.92	6411.	13.00	.48	12.94	.42
# 9	13.71	17089.	34.66	20.95	15.35	1.64	6958.	14.11	.48	14.01	.30
#10	12.66	15259.	30.95	18.29	13.58	.92	6254.	12.69	.03	12.63	-.03
#11	13.15	16118.	32.69	19.54	14.41	1.26	6525.	13.24	.09	13.16	.01
#12	14.13	16511.	33.49	19.36	14.79	.66	6795.	13.78	-.35	13.69	-.44
#13	4.87	5516.	11.19	7.12	4.12	.85	1927.	3.91	-.16	4.15	.08
#14	1.29	1783.	3.45	2.17	.42	-.87	559.	1.13	-.15	1.47	.18
#15	1.29	1784.	3.46	2.17	.42	-.87	557.	1.13	-.16	1.46	.18
#16	5.84	6879.	12.33	7.29	4.67	-.37	2181.	4.26	-.77	4.49	-.55
#17	1.47	1798.	3.65	2.18	.51	-.96	583.	1.18	-.29	1.52	.05
#18	.98	1267.	2.57	1.59	-.88	-.98	428.	.87	-.11	1.21	.23
#19	1.48	1559.	3.16	1.76	.28	-1.12	556.	1.13	-.27	1.47	.87
#20	3.81	3852.	6.19	3.18	1.73	-1.28	1191.	2.42	-.59	2.71	-.38
#21	1.61	1733.	3.52	1.91	.45	-1.16	638.	1.29	-.31	1.62	.01
#22	.14	381.	.77	.63	-.86	-1.88	137.	.28	.14	.64	.50
#23	10.14	11415.	23.15	13.81	9.85	-.38	4899.	9.94	-.28	9.97	-.17
#24	.49	512.	1.04	.55	-.74	-1.23	164.	.33	-.16	.69	.20
#25	17.77	17457.	35.41	17.64	15.71	-2.06	8154.	16.54	-1.23	16.35	-1.41
#26	20.88	20959.	42.51	22.51	19.11	-.98	9878.	18.41	-1.59	18.16	-1.84
#27	26.58	25865.	52.84	24.26	23.89	-3.48	12878.	26.12	-.46	25.61	-.97
#28	33.85	33135.	67.21	33.36	30.93	-2.93	17226.	34.95	1.09	34.14	.28
#29	37.56	36418.	73.87	36.31	34.11	-3.45	20125.	40.82	3.26	39.81	2.25
#30	12.66	15547.	31.54	18.88	13.86	1.20	6225.	12.63	-.03	12.57	-.09
#31	6.38	8558.	17.36	11.06	7.87	.78	3838.	6.16	-.13	6.33	.03
#32	19.16	21767.	44.15	24.99	19.89	.73	9772.	19.82	.66	19.52	.36
#33	17.77	20859.	42.31	24.54	19.01	1.25	9182.	18.46	.70	18.21	.44
#34	16.95	18976.	38.49	22.54	17.18	1.24	8848.	16.32	.38	16.15	.20
#35	23.74	26262.	53.27	27.53	24.26	-1.48	12645.	25.69	-.05	25.19	-.55
#36	12.94	16149.	32.76	19.82	14.44	1.58	6477.	13.14	.20	13.07	.13
#37	22.31	24437.	49.57	27.26	22.48	.17	11188.	22.69	.38	22.38	-.81
#38	4.98	6866.	13.91	9.82	5.42	.53	2358.	4.78	-.11	4.99	.10
#39	16.58	19764.	40.09	23.51	17.95	1.37	8378.	16.98	.40	16.78	.20
#40	14.28	17929.	36.37	22.17	16.17	1.97	7217.	14.64	.44	14.52	.32
#41	13.88	18853.	38.24	22.36	17.06	1.19	7826.	15.87	-.00	15.71	-.17
#42	15.18	18726.	37.98	22.81	16.94	1.76	7617.	15.45	.27	15.38	.12
#43	10.70	13991.	28.38	17.68	12.35	1.64	5291.	10.73	.03	10.74	.04
#44	9.83	13143.	26.66	16.83	11.52	1.70	4998.	10.12	.29	10.15	.32
#45	6.45	12247.	24.84	16.39	10.65	2.20	4498.	9.11	.66	9.17	.72
#46	5.22	6520.	13.23	7.99	5.09	-.14	2436.	4.94	-.29	5.15	-.09
#47	2.53	3891.	6.27	3.74	1.77	-.76	1187.	2.25	-.28	2.54	.02
#48	4.48	5836.	11.84	7.36	4.43	-.05	2068.	4.19	-.28	4.43	-.05
#49	3.21	4882.	8.28	5.87	2.73	-.48	1585.	3.05	-.16	3.32	.11
#50	1.84	1436.	2.91	1.66	.16	-.87	475.	.96	-.87	1.30	.27
#51	2.79	2334.	4.73	1.94	1.83	-1.76	884.	1.63	-1.16	1.95	-.84
#52	2.23	2766.	5.61	3.38	1.45	-.78	942.	1.91	-.32	2.22	-.01
#53	.55	512.	1.04	.49	-.74	-1.29	194.	.39	-.16	.75	.20
#54	.46	755.	1.53	.85	-.56	-1.19	286.	.58	-.10	.93	.25
#55	1.43	1546.	3.14	1.78	.27	-1.17	686.	1.23	-.20	1.56	.13
#56	3.71	4992.	10.13	6.42	3.61	-.10	1798.	3.65	-.06	3.98	.27
#57	6.85	8249.	16.73	9.88	6.77	-.08	3275.	6.64	-.21	6.79	-.06
#58	8.46	11334.	22.99	14.53	9.77	1.30	4461.	9.05	.59	9.12	.65
#59	12.83	13941.	28.28	16.25	12.38	.27	5855.	11.88	-.15	11.85	-.18
#60	6.36	8185.	16.60	10.24	6.71	.35	3088.	6.26	-.10	6.42	.06
#61	10.42	11804.	23.94	13.52	10.22	-.20	5062.	10.15	-.26	10.18	-.23
#62	1.96	2287.	4.64	2.68	.99	-.97	892.	1.81	-.15	2.12	.16
#63	2.66	3162.	6.41	3.76	1.84	-.82	1238.	2.49	-.16	2.78	.12
#64	4.28	4837.	9.81	5.61	3.46	-.82	1924.	3.92	-.37	4.16	-.13
#65	3.15	3774.	7.66	4.51	2.43	-.72	1481.	3.04	-.10	3.21	.17
#66	5.68	7181.	14.48	8.81	5.66	.00	2689.	5.45	-.14	5.64	-.05
#67	6.89	8234.	16.78	10.62	6.76	-.07	3284.	6.68	-.08	6.82	-.14
#68	10.07	12203.	24.75	14.68	10.61	.54	4548.	9.82	-.25	9.86	-.21
#69	8.11	10176.	20.64	12.52	8.64	.53	3909.	8.02	-.08	8.19	.08
#70	10.92	12641.	25.60	14.73	11.04	.12	5388.	10.86	-.06	10.86	-.06
AVE. ABS. ERROR =				13.13		1.04			.35		.30

FIGURES 5·34 to 5·37

Relationship of x-ray intensity (corrected) and the known concentrations for the determination of the principal elements in bauxite (Al, Si, Ti and Fe).

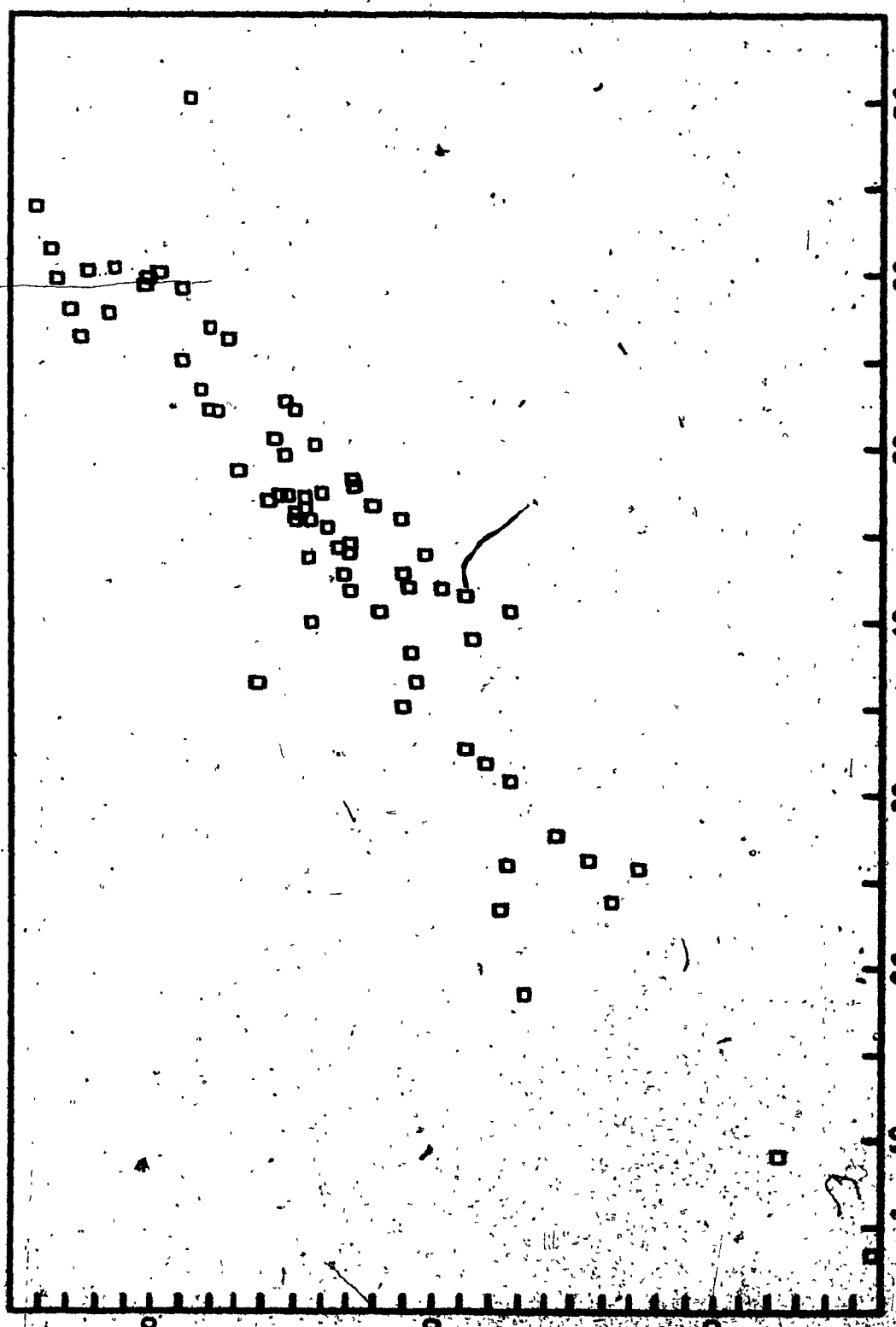
CORRECTED Al Kα INTENSITY (kcps)
30
20
10
0
10
20
30
40
50
60
70
KNOWN CONCENTRATION OF Al_2O_3 (%)

FIGURE 5-34

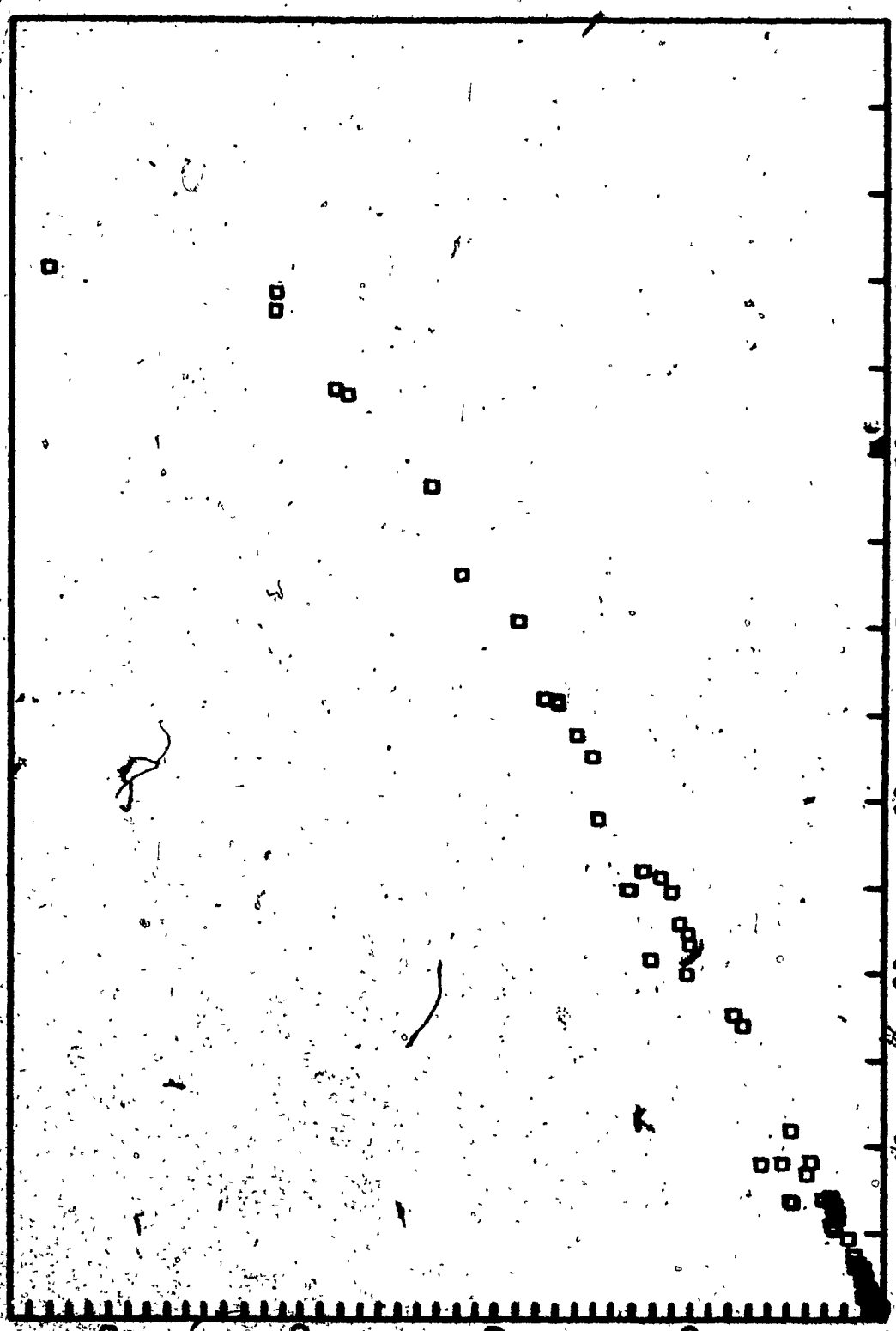
CORRECTED Si Kα INTENSITY (KCPS)
10
20
30
40
KNOWN CONCENTRATION OF SiO_2 (%)
10
20
30
40
50
60
70

FIGURE 5.35

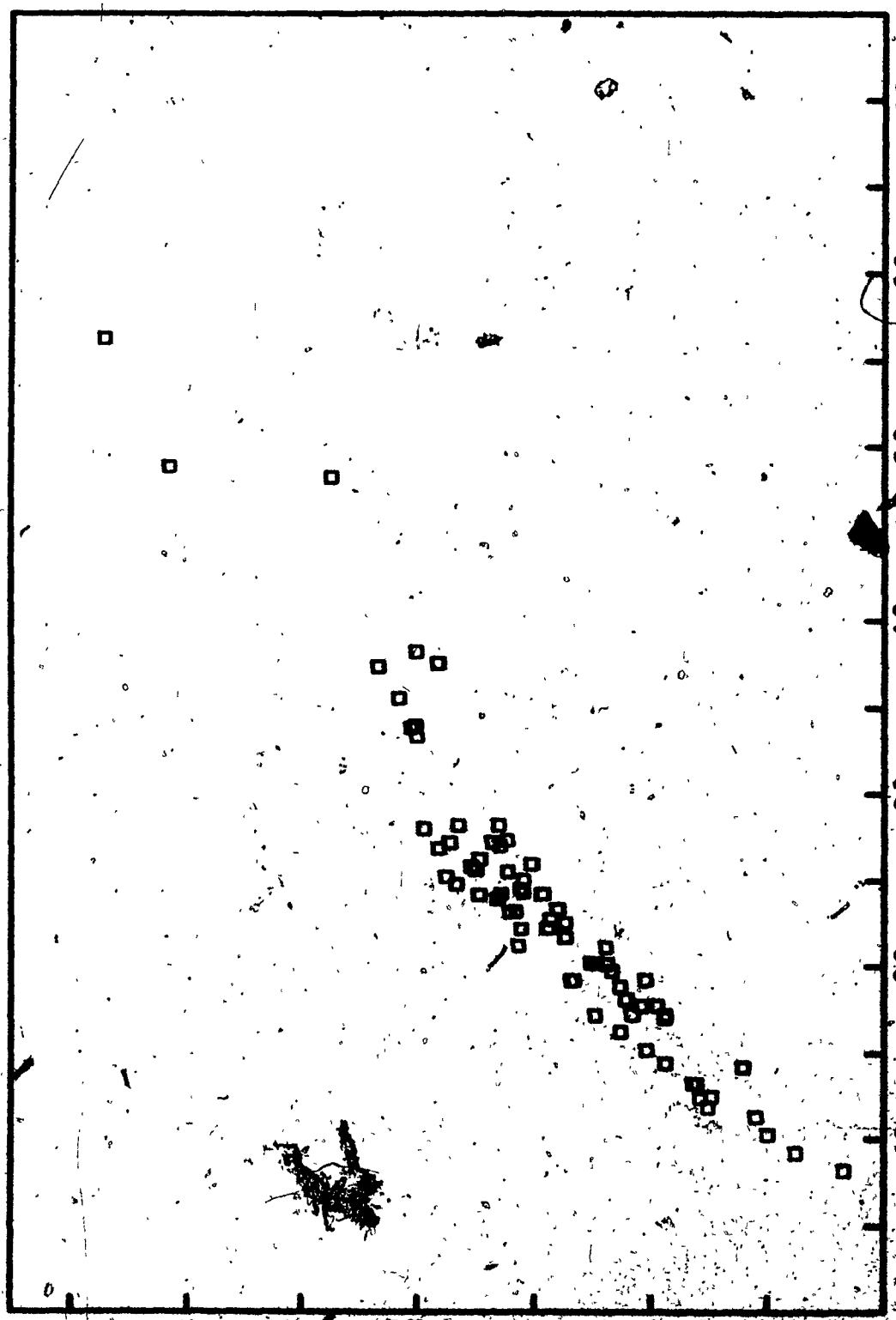
CORRECTED Ti Kα INTENSITY (kcps)
0
12
KNOWN CONCENTRATION OF TiO2 (%)
1.0
2.0
3.0
4.0
5.0
6.0
7.0

FIGURE 5-36

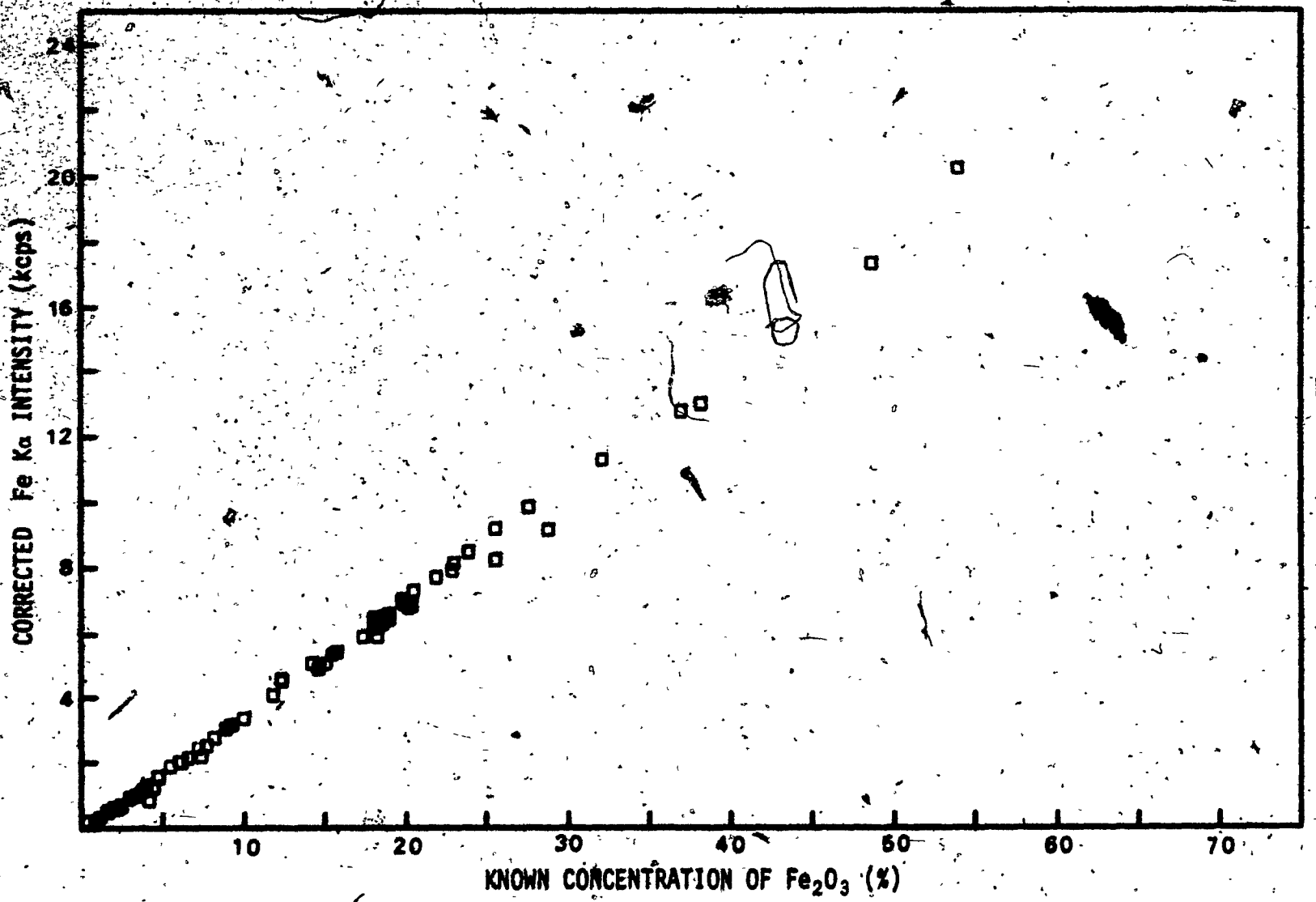
CORRECTED Fe Kα INTENSITY (kcps)
24
20
16
12
8
4
10
20
30
40
50
60
70
KNOWN CONCENTRATION OF Fe_2O_3 (%)

FIGURE 5·37

linearity and the scatter appear a lot greater than they really are when compared to the results obtained for the other elements. An excellent relationship was obtained for the analysis of iron. The average absolute errors of 1.77% Al, 0.71% Si, 0.12% Ti and 0.35% Fe would seem to be adequate for a routine analytical determination. There was no advantage to performing a least squares treatment of the corrected intensity data.

One final investigation was carried out in order to determine the degree of improvement in the accuracy if a number of the bauxite samples (high analytical error or extreme concentration values) were rejected. Initially, only five samples (#23, #26, #27, #29, #53) were removed from the total sample lot. Subsequently, an additional fifteen samples were discarded. The main criterion for rejection was that the absolute error was greater than twice the average absolute error (corrected data - ratio method) for a particular element.

A comparison of the average absolute errors for 70 samples, 65 samples and 50 samples follows :

ALUMINUM	AVE. ASB. ERROR
70 samples	1.77 %
65 samples	1.51 %
50 samples	1.38 %

	AVE. ABS. ERROR
SILICON	
70 samples	0.71 %
65 samples	0.46 %
50 samples	0.31 %
TITANIUM	
70 samples	0.12 %
65 samples	0.12 %
50 samples	0.09 %
IRON	
70 samples	0.35 %
65 samples	0.28 %
50 samples	0.22 %

It was noted that sample rejection improved the overall accuracy but there was a significant improvement for the silicon and iron determinations. As far as the aluminum and titanium results are concerned, it seemed that the inherent error was spread over all samples. For the silicon and iron results there were definite peculiarities with certain samples affecting the error. However, the source of the errors in these samples was not determinable.

5-3 CONCLUSIONS

Elemental interactions present severe problems in the XRF spectrochemical analysis of bauxite material. The Lachance and Traill method of correction for such interferences is relatively simple and is effective when dealing with simple well-defined systems. Most significantly, matrix effect correction coefficients, obtained through the use of ideal standard samples, cannot be applied to the practical problem of bauxite analysis. Similarly, theoretically determined coefficients cannot be applied in bauxite analysis with any degree of accuracy. There are too many undefined extraneous factors (particle size heterogeneity, compositional heterogeneity, chemical combination effects, mineralogical variations, impurities) which influence the measured x-ray line intensities. It is necessary to use standard samples that contain any abnormalities that may occur in the unknown samples to be analysed. Matrix effect correction coefficients, if determined by any means other than that involving actual bauxite samples, would not be applicable to the analysis of bauxite material.

The interelement effect correction coefficients incorporate any peculiarities or errors inherent in the standard samples from which they are determined. The values of these coefficients are dependent on the geographical origin of the standard bauxite samples. To overcome such variance, in order to employ a general analysis

program (i.e. samples from any source) , the selection of standards must include numerous samples from all possible regions. Naturally, a certain amount of accuracy is lost by the process but this is unavoidable.

The influence of the coefficient values on the accuracy of the analysis shows the extreme dependence on the nature of the standard samples. For accurate coefficients a wide range of concentrations is necessary for each element under investigation. Using actual bauxite samples as standards, with their restricted concentration ranges, prohibits the determination of accurate coefficients. A certain degree of uncertainty must be accepted in this type of analysis where non-ideal standards are being used.

The analytical accuracy (2.8% Al_2O_3 , 1.3% SiO_2 , 0.2% TiO_2 , 0.5% Fe_2O_3) of the Lachance and Traill treatment for matrix effect correction in bauxite analysis is adequate for general applications. Once the correction coefficients are determined the analytical procedure is extremely simple. There is no necessity for any sort of calibration curves or network charts. Measured x-ray line intensities are entered into a computer and a short calculation yields elemental concentrations. Analysis of an unknown bauxite sample (regardless of origin) is easily performed with reasonable accuracy by the x-ray fluorescence spectrochemical technique.

REFERENCES

1. R.H. Black, Anal. Chem., 25, 743 (1953).
2. S. Ostap, ALCAN, Report A-RR-1458-70-03 (April, 1970).
3. J. VanEs and W.D. Lamb, ALCAN, Report A-RR-1396-69-09, Progress Report 3 (October, 1959).
4. E.P. Bertin, Principles and Practice of X-Ray Spectrometric Analysis, Plenum, N.Y., (1970).
5. J.A. Victoreen, J. Appl. Phys., 20, 1141 (1949).
6. B.L. Henke, Advan. X-Ray Anal., 5, 285 (1962).
7. L.S. Birks, E.J. Brooks and H. Friedman, Anal. Chem., 25, 692 (1953).
8. W. Krawciw, ALCAN, Report A-RR-993-65-21, Progress Report 11 (February, 1965).
9. F. Claisse, Quebec Dept. of Mines, Progress Report 327 (1956).
10. F. Claisse, Norelco Reporter IV(4), 95 (1957).
11. F. Claisse, Quebec Dept. of Mines, Progress Report 402 (1960).
12. F. Claisse, Can. Spectrosc., 12, 20 (1967).
13. F. Claisse and C. Samson, Advan. X-Ray Anal., 5, 335 (1962).
14. E.L. Gunn, Advan. X-Ray Anal., 4, 382 (1961).
15. K.W. Madlem, Advan. X-Ray Anal., 9, 441 (1966).
16. I. Adler and J.M. Axelrod, Specrochim. Acta, 7, 91 (1955).
17. M. Siegbahn and T. Magnusson, Nature, 132, 895 (1933).
18. M. Siegbahn and H. Karlsson, Nature, 132, 895 (1933).
19. M. Siegbahn and T. Magnusson, Nature, 133, 257 (1934).
20. D.M. Koffman and S.H. Moll, Advan. X-Ray Anal., 9, 323 (1966).

21. P.D. Zemany, Anal. Chem., 32, 595 (1960).

22. D.W. Fischer and W.L. Baun, Advan. X-Ray Anal., 10, 374 (1967).

23. A.D. Ambrose, R. Rutherford and S. Muir, Metallurgia, 82, 119 (1970).

24. H.J. Rose Jr., I. Adler adn F.J. Flanagan, Appl. Spectrosc., 17, 81 (1963).

25. B.M. Gunn, Can. Spectrosc., 12, 36 (1967).

26. J. Sherman, Spectrochim. Acta, 7, 283 (1955).

27. J. Lucas-Tooth and B.J. Price, Metallurgia, 64, 149 (1961).

28. J. Lucas-Tooth and C. Pyne, Advan. X-Ray Anal., 7, 523 (1964).

29. B.S. Sanderson and J.A. Yeck, Advan. X-Ray Anal., 10, 474 (1967).

30. H.J. Beattie and R.M. Brissey, Anal. Chem., 26, 980 (1954).

31. G.R. Lachance, Geol. Survey of Can., Paper 64-50 (1964).

32. R.J. Traill and G.R. Lachance, ibid, Paper 64-57 (1965).

33. G.R. Lachance, Can. Spectrosc., 10, 38 (1965).

34. G.R. Lachance and R.J. Traill, Can. Spectrosc., 11, 43 (1966).

35. R.J. Traill and G.R. Lachance, Can. Spectrosc., 11, 63 (1966).

36. F. Claisse and M. Quintin, Can. Spectrosc., 12, 129 (1967).

37. G.R. Lachance, Can. Spectrosc., 15, 64 (1970).

38. B.J. Mitchell, Advan. X-Ray Anal., 11, 129 (1968).

39. H. Hughes, Analyst, 97, 161 (1972).

40. R. Jenkins and A. Campbell-Whitelaw, Can. Spectrosc., 15, 32 (1970).

41. J.W. Criss and L.S. Birks, Anal. Chem., 40, 1080 (1968).

42. D.A. Stephenson, Anal. Chem., 43, 310 (1971).

43. A.B. Poole and S.M. Holloway, Advan. X-Ray Anal., 12, 534 (1969).

44. C.N. McKinney and A.S. Rosenberg, Advan. X-Ray Anal., 13, 125 (1970).

45. J.J. Renton and W.L. Baun, Appl. Spectrosc., 18, 93 (1964).

46. R. Jenkins and J.L. DeVries, Practical X-Ray Spectrometry, Philips Technical Library, Eindhoven, Netherlands (1967).

47. N. Spielberg, Advan. X-Ray Anal., 10, 534 (1967).

48. J.G. Dick and A.R. Fraser, Can. J. Spectrosc., 17, 135 (1972).

49. M.B. Fletcher, ALCAN, Report A-RR-596-58-21, Progress Report 14 (October, 1958).

50. W.J. Forsyth, ALCAN, Report A-RR-360-59-21, Progress Report 3 (October, 1959).

BIBLIOGRAPHY

ADVANCES IN X-RAY ANALYSIS; Proceedings for Conference on Applications of X-Ray Analysis; Plenum Press, N.Y., 1957— .

ASTM Special Technical Publication No. 292 ; INDEX TO THE LITERATURE ON X-RAY SPECTROGRAPHIC ANALYSIS, Part I (1913-1957), Committee E-2 on Emission Spectroscopy; ASTM, Phil., Pa., 1960.

ASTM Special Technical Publication No. 349 ; SYMPOSIUM ON X-RAY AND ELECTRON PROBE ANALYSIS, 66th Annual Meeting of ASTM, Atlantic City, June 1963; ASTM, Phil., Pa., 1964.

A.K. Baird; LIGHT ELEMENT ANALYSIS, Advan. X-Ray Anal., 13, 26 (1969).

P.F. Berry, T. Furuta and J.R. Rhodes; PARTICLE SIZE EFFECTS IN RADIOISOTOPE X-RAY SPECTROMETRY, Advan. X-Ray Anal., 12, 612 (1968).

E.P. Bertin ; PRINCIPLES AND PRACTICE OF X-RAY SPECTROMETRIC ANALYSIS; Plenum Press, N.Y., 1970.

E.P. Bertin and R.J. Longobucco; SPECTRAL LINE INTERFERENCE IN X-RAY FLUORESCENCE SPECTROMETRY, Norelco Reporter IX(3), 64 (1962).

R. Jenkins and J.L. DeVries; PRACTICAL X-RAY SPECTROMETRY, Philips Technical Library, Eindhoven, Netherlands, (1967.

H.A. Liebhafsky, H.G. Pfeiffer, E.H. Winslow and P.D. Zemany; X-RAY ABSORPTION AND EMISSION IN ANALYTICAL CHEMISTRY, Wiley, N.Y., 1960.

APPENDIX A

CHEMICAL AND X-RAY SPECTRAL DATA

SAMPLE IDENTIFICATION		% Fe_2O_3	TOL.*	REL. CONC. ERROR	NET† Fe Kα XRF INT. (cps)	REL. COUNTING ERROR
# 1	JM 453	20.0	.7	3.50%	16466.	.97%
# 2	JM 454	16.1	.7	3.87%	14702.	.83%
# 3	JM 634	17.9	.7	3.91%	15288.	1.01%
# 4	JM 635	18.4	.7	3.80%	15616.	.49%
# 5	JM 661	18.1	.7	3.87%	15617.	.76%
# 6	JM 662	18.8	.7	3.72%	16236.	.78%
# 7	JM 917	19.7	.7	3.55%	16596.	.72%
# 8	JM 918	17.9	.7	3.91%	16151.	.57%
# 9	JM 919	19.6	.7	3.57%	17089.	.95%
#10	JM 920	18.1	.7	3.87%	15259.	.90%
#11	JM 921	18.8	.7	3.72%	16118.	1.04%
#12	JM 922	20.2	.7	3.47%	16511.	.73%
#13	NBS 69A	5.82	.22	3.78%	5516.	1.03%
#14	AP CAA	1.84	.11	5.98%	1703.	2.50%
#15	AP CAB	1.84	.11	5.98%	1704.	1.67%
#16	AP CAC	7.20	.25	3.47%	6079.	.87%
#17	DM CAA	2.1	.3	14.29%	1798.	2.48%
#18	DM CAE	1.4	.2	14.29%	1267.	3.98%
#19	DM CAF	2.0	.3	15.00%	1559.	2.52%
#20	DM CAG	4.3	.4	9.30%	3052.	2.15%
#21	DM CAH	2.3	.3	13.04%	1733.	2.80%
#22	DM CAI	.2	.1	50.00%	381.	3.35%
#23	DM CAJ	14.5	.6	4.14%	1141.	1.49%
#24	DM CAK	.7	.2	28.57%	512.	3.34%
#25	DM CAM	25.4	.8	3.15%	17457.	1.25%
#26	DM CAN	28.6	.8	2.80%	20959.	.48%
#27	DM CAO	38.0	.9	2.37%	25065.	.63%
#28	DM CAQ	48.4	1.0	2.07%	32767.	.69%
#29	DM CAR	53.7	1.0	1.86%	32767.	.29%
#30	BZ 30A-S	18.1	.7	3.87%	15547.	.93%
#31	BZ 30B-S	9.0	.5	5.56%	8558.	.52%
#32	BZ 61A-S	27.4	.8	2.92%	21767.	.61%
#33	BZ 62A-S	25.4	.8	3.15%	20859.	.39%
#34	BZ 67A-S	22.8	.7	3.07%	18976.	.63%
#35	BZ 128A-S	36.8	.9	2.45%	26262.	.24%

* TOLERANCE LIMITS. (Alcan 85% confidence level)

† corrected for instrumental drift and background intensity

SAMPLE IDENTIFICATION	% Fe_2O_3	TOL.*	REL. CONC. ERROR	NET† Fe Kα XRF INT. (cps)	REL. COUNTING ERROR
#36 BZ 140A-S	18.5	.7	3.78%	16149.	.81%
#37 BZ 19A-M	31.9	.8	2.51%	24437.	.72%
#38 BZ 30B-M	7.0	.5	7.14%	6860.	1.97%
#39 BZ 61A-M	23.7	.8	3.38%	19764.	.79%
#40 BZ 74A-M	20.3	.7	3.45%	17929.	.66%
#41 BZ 93B-M	22.7	.7	3.08%	18853.	.30%
#42 BZ 121A-M	21.7	.7	3.23%	18726.	.82%
#43 BZ 138A-M	15.3	.6	3.92%	13991.	.27%
#44 BK 14134	14.05	.38	2.70%	13143.	.68%
#45 BK 14135	12.08	.34	2.81%	12247.	1.13%
#46 BK 16726	7.48	.26	3.48%	6520.	1.02%
#47 BK 19356	3.61	.17	4.71%	3091.	2.01%
#48 BK 19987	6.40	.23	3.59%	5836.	.79%
#49 BK 20497	4.59	.19	4.14%	4082.	1.78%
#50 BK 38741	1.48	.10	6.76%	1436.	1.71%
#51 BK 38742	3.99	.18	4.51%	2334.	1.86%
#52 BK 38743	3.19	.15	4.70%	2766.	2.39%
#53 NBS 78	.79	.07	8.86%	512.	2.79%
#54 NBS 97	.98	.08	8.16%	755.	2.72%
#55 NBS 98	2.05	.12	5.85%	1546.	1.63%
#56 AU TH1A	5.3	.4	7.55%	4992.	1.56%
#57 AU TH1E	9.8	.5	5.10%	8249.	1.52%
#58 AU TH3B	12.1	.6	4.96%	11334.	1.37%
#59 AU TH3C	17.2	.7	4.07%	13941.	.55%
#60 AU TH5B	9.1	.5	5.49%	8185.	.74%
#61 AU TH5E	14.9	.6	4.03%	11804.	.70%
#62 AU TH5G	2.8	.3	10.71%	2287.	1.33%
#63 AU TH5H	3.8	.4	10.53%	3162.	2.04%
#64 AU TH6G	6.0	.4	6.67%	4837.	.33%
#65 AU TH6H	4.5	.4	8.89%	3774.	1.26%
#66 AU TH7A	8.0	.5	6.25%	7101.	2.02%
#67 AU TH7C	8.7	.5	5.75%	8234.	1.30%
#68 AU TH7E	14.4	.6	4.17%	12203.	.45%
#69 AU TH7F	11.6	.6	5.17%	10176.	1.09%
#70 AU TH7G	15.6	.6	3.85%	12641.	.68%

* TOLERANCE LIMITS (ATcan 85% confidence level)

† corrected for instrumental drift and background intensity

SAMPLE IDENTIFICATION	% TiO_2	TOL.*	REL. CONC. ERROR	NET† Ti Kα XRF INT. (cps)	REL. COUNTING ERROR
# 1 JM 453	2.80	.14	5.00%	19140.	.41%
# 2 JM 454	2.70	.14	5.19%	17536.	.58%
# 3 JM 634	2.48	.14	5.65%	15785.	.61%
# 4 JM 635	2.41	.14	5.81%	15960.	.43%
# 5 JM 661	2.43	.14	5.76%	15876.	.63%
# 6 JM 662	2.25	.12	5.33%	15161.	.53%
# 7 JM 917	3.31	.16	4.83%	20973.	.41%
# 8 JM 918	2.68	.14	5.22%	17258.	.33%
# 9 JM 919	2.23	.12	5.38%	14018.	.39%
#10 JM 920	2.57	.14	5.45%	15060.	.57%
#11 JM 921	2.71	.14	5.17%	16710.	.55%
#12 JM 922	2.80	.14	5.00%	17203.	.43%
#13 NBS 69A	2.78	.14	5.04%	19480.	.72%
#14 AP CAA	2.56	.14	5.47%	17400.	.68%
#15 AP CAB	2.54	.14	5.51%	17294.	.60%
#16 AP CAC	1.22	.09	7.38%	7223.	1.86%
#17 DM CAA	2.6	.3	11.54%	17413.	1.88%
#18 DM CAE	1.7	.3	17.65%	9919.	.49%
#19 DM CAF	2.4	.3	12.50%	14657.	.43%
#20 DM CAG	3.8	.4	10.53%	17429.	1.29%
#21 DM CAH	1.9	.3	15.79%	8715.	1.68%
#22 DM CAI	1.3	.2	15.38%	6835.	1.74%
#23 DM CAJ	.8	.2	25.00%	1341.	2.40%
#24 DM CAK	2.1	.3	14.29%	15328.	.38%
#25 DM CAM	1.1	.2	18.18%	4894.	2.09%
#26 DM CAN	1.0	.2	20.00%	5267.	2.23%
#27 DM CAO	1.4	.2	14.29%	5819.	1.38%
#28 DM CAQ	.9	.2	22.22%	4210.	1.12%
#29 DM CAR	1.7	.3	17.65%	18537.	1.79%
#30 BZ 30A-S	2.7	.3	11.11%	19433.	.94%
#31 BZ 30B-S	2.5	.3	12.00%	19252.	.71%
#32 BZ 61A-S	2.3	.3	13.04%	16367.	1.62%
#33 BZ 62A-S	1.6	.3	18.75%	11457.	1.86%
#34 BZ 67A-S	1.9	.3	15.79%	13765.	1.42%
#35 BZ 128A-S	2.0	.3	15.00%	13526.	1.83%

* TOLERANCE LIMITS (Alcan 85% confidence level)

† corrected for instrumental drift and background intensity

SAMPLE IDENTIFICATION	% TiO_2	TOL.*	REL. CONC. ERROR	NET† Ti Kα XRF INT. (cps)	REL. COUNTING ERROR
#36 BZ 140A-S	2.4	.3	12.50%	18094.	.34%
#37 BZ 19A-M	2.0	.3	15.00%	13711.	.69%
#38 BZ 30B-M	2.3	.3	13.04%	16482.	1.95%
#39 BZ 61A-M	1.9	.3	15.79%	13956.	1.06%
#40 BZ 74A-M	1.3	.2	15.38%	8293.	1.99%
#41 BZ 93B-M	2.2	.3	13.64%	16560.	1.78%
#42 BZ 121A-M	1.5	.2	13.33%	10730.	.49%
#43 BZ 138A-M	1.7	.3	17.65%	12921.	.71%
#44 BK 14134	2.67	.14	5.24%	19883.	.87%
#45 BK 14135	2.46	.13	5.28%	19079.	.63%
#46 BK 16726	4.81	.20	4.16%	23808.	.17%
#47 BK 19356	4.87	.20	4.11%	30570.	.52%
#48 BK 19987	3.54	.16	4.52%	21065.	.60%
#49 BK 20497	5.61	.22	3.92%	32767.	.71%
#50 BK 38741	3.38	.16	4.73%	20138.	.32%
#51 BK 38742	3.74	.17	4.55%	19279.	.39%
#52 BK 38743	3.72	.17	4.57%	21864.	1.14%
#53 NBS 78	3.37	.16	4.75%	17673.	.39%
#54 NBS 97	2.38	.13	5.46%	13698.	.91%
#55 NBS 98	1.43	.09	6.29%	7345.	1.51%
#56 AU TH1A	2.54	.13	5.12%	15024.	1.26%
#57 AU TH1E	2.16	.12	5.66%	12200.	.94%
#58 AU TH3B	2.00	.12	6.00%	11075.	1.44%
#59 AU TH3C	1.76	.11	6.25%	9650.	1.21%
#60 AU TH5B	2.41	.13	5.39%	13897.	1.05%
#61 AU TH5E	1.76	.11	6.25%	8529.	2.14%
#62 AU TH5G	1.80	.11	6.11%	8871.	.62%
#63 AU TH5H	1.87	.11	5.88%	9266.	1.22%
#64 AU TH6G	1.22	.09	7.38%	6374.	2.23%
#65 AU TH6H	1.17	.08	6.84%	5964.	1.39%
#66 AU TH7A	2.21	.12	5.43%	13243.	2.62%
#67 AU TH7C	2.32	.13	5.60%	13897.	.52%
#68 AU TH7E	1.96	.11	5.61%	11254.	.89%
#69 AU TH7F	2.10	.12	5.71%	11166.	2.12%
#70 AU TH7G	1.69	.10	5.92%	8408.	1.73%

** TOLERANCE LIMITS (Alcan 85% confidence level)

† corrected for instrumental drift and background intensity

SAMPLE IDENTIFICATION	% SiO_2	TOL*	REL. CONC. ERROR	NET† Si Kα XRF INT. (cps)	REL. COUNTING ERROR
# 1 JM 453	.33	.04	12.12%	58.	5.50%
# 2 JM 454	1.44	.10	6.94%	219.	3.15%
# 3 JM 634	5.72	.22	3.85%	836.	1.48%
# 4 JM 635	3.57	.16	4.48%	497.	2.18%
# 5 JM 636	5.67	.22	3.88%	791.	1.27%
# 6 JM 637	.64	.06	9.37%	97.	3.15%
# 7 JM 917	.34	.04	11.76%	56.	5.68%
# 8 JM 918	.64	.06	9.37%	23.	9.12%
# 9 JM 919	6.65	.24	3.61%	918.	1.19%
#10 JM 920	8.94	.29	3.24%	1261.	1.21%
#11 JM 921	3.13	.15	4.79%	444.	2.09%
#12 JM 922	2.84	.14	4.93%	348.	1.44%
#13 NBS 69A	6.01	.23	3.83%	778.	4.02%
#14 AP CAA	5.25	.21	4.00%	856.	2.10%
#15 AP CAB	4.99	.20	4.01%	828.	1.28%
#16 AP CAC	8.87	.29	3.27%	1762.	1.06%
#17 DM CAA	2.1	.3	14.29%	341.	2.11%
#18 DM CAE	19.8	.7	3.54%	3499.	1.69%
#19 DM CAF	25.6	.8	3.10%	4388.	1.29%
#20 DM CAG	28.8	.8	2.78%	5278.	.66%
#21 DM CAH	35.5	.9	2.54%	6083.	2.89%
#22 DM CAI	40.2	.9	2.24%	6859.	1.46%
#23 DM CAJ	60.5	1.1	1.82%	15853.	.63%
#24 DM CAK	6.8	.4	5.88%	1006.	2.76%
#25 DM CAM	35.7	.9	2.52%	6527.	.95%
#26 DM CAN	6.7	.4	5.97%	1640.	.73%
#27 DM CAO	24.7	.8	3.24%	4889.	2.24%
#28 DM CAQ	6.6	.4	6.06%	1621.	.65%
#29 DM CAR	8.8	.5	5.68%	2191.	1.72%
#30 BZ 30A-S	1.1	.2	18.18%	144.	6.06%
#31 BZ 30B-S	1.1	.2	18.18%	132.	6.32%
#32 BZ 61A-S	6.9	.5	7.25%	907.	1.53%
#33 BZ 62A-S	10.7	.5	4.67%	1648.	.72%
#34 BZ 67A-S	8.2	.5	6.10%	1344.	1.28%
#35 BZ 128A-S	1.7	.3	17.65%	235.	.44%

* TOLERANCE LIMITS (Alcan 85% confidence level)

† corrected for instrumental drift and background intensity

SAMPLE IDENTIFICATION	% SiO_2	TOL.*	REL. CONC. ERROR	NET† Si Kα XRF INT. (cps)	REL. COUNTING ERROR
#36 BZ 140A-S	2.3	.3	13.04%	310.	2.18%
#37 BZ 19A-M	.9	.2	22.22%	124.	1.47%
#38 BZ 30B-M	.9	.2	22.22%	117.	5.14%
#39 BZ 61A-M	4.5	.4	8.89%	609.	1.48%
#40 BZ 74A-M	6.5	.4	6.15%	841.	3.52%
#41 BZ 93B-M	.7	.2	28.57%	100.	5.02%
#42 BZ 121A-M	2.9	.3	10.34%	482.	.15%
#43 BZ 138A-M	2.5	.3	12.00%	365.	1.78%
#44 BK 14134	1.20	.09	7.50%	327.	2.01%
#45 BK 14135	.81	.07	8.64%	250.	2.43%
#46 BK 16726	.80	.07	8.75%	135.	3.91%
#47 BK 19356	.40	.04	10.00%	79.	5.89%
#48 BK 19987	1.12	.08	7.14%	163.	3.05%
#49 BK 20497	.53	.05	9.43%	84.	2.52%
#50 BK 38741	.45	.05	11.11%	59.	3.40%
#51 BK 38742	.53	.05	9.43%	94.	3.81%
#52 BK 38743	.57	.05	8.77%	91.	4.23%
#53 NBS 78	20.69	.48	2.32%	4497.	1.06%
#54 NBS 97	42.87	.74	1.73%	7985.	.62%
#55 NBS 98	59.11	.90	1.52%	11814.	.85%
#56 AU TH1A	22.2	.7	3.15%	3466.	1.13%
#57 AU TH1E	32.4	.8	2.47%	5376.	1.97%
#58 AU TH3B	22.8	.7	3.07%	3729.	.52%
#59 AU TH3C	25.5	.8	3.14%	4171.	2.47%
#60 AU TH5B	17.5	.7	4.00%	2695.	1.82%
#61 AU TH5E	35.7	.9	2.52%	6215.	1.74%
#62 AU TH5G	53.3	1.0	1.88%	10287.	.53%
#63 AU TH5H	48.0	1.0	2.08%	8607.	1.23%
#64 AU TH6G	53.6	1.0	1.87%	10607.	1.45%
#65 AU TH6H	58.1	1.1	1.89%	11822.	.51%
#66 AU TH7A	24.6	.8	3.25%	3878.	.88%
#67 AU TH7C	9.0	.5	5.56%	1284.	2.82%
#68 AU TH7E	16.9	.6	3.55%	2572.	1.56%
#69 AU TH7F	21.6	.7	3.24%	3545.	1.21%
#70 AU TH7G	33.7	.9	2.67%	5794.	1.98%

* TOLERANCE LIMITS (Alcan 85% confidence level)

† corrected for instrumental drift and background intensity

SAMPLE IDENTIFICATION	% Al_2O_3	TOL.*	REL. CONC. ERROR	NET† Al Kα XRF INT. (cps)	REL. COUNTING ERROR
# 1 JM 453	48.6	1.0	2.06%	10311.	.90%
# 2 JM 454	47.2	1.0	2.12%	10001.	1.20%
# 3 JM 634	44.2	1.0	2.26%	9215.	1.24%
# 4 JM 635	46.9	1.0	2.13%	10233.	1.24%
# 5 JM 661	46.5	1.0	2.15%	9766.	1.51%
# 6 JM 662	45.8	1.0	2.18%	9507.	.69%
# 7 JM 917	47.2	1.0	2.12%	9578.	.91%
# 8 JM 918	49.5	1.0	2.02%	9992.	.85%
# 9 JM 919	43.9	1.0	2.28%	8957.	1.08%
#10 JM 920	45.4	1.0	2.20%	9450.	1.25%
#11 JM 921	47.1	1.0	2.12%	9598.	.64%
#12 JM 922	45.8	1.0	2.18%	9548.	1.30%
#13 NBS 69A	55.0	1.1	2.00%	13521.	.63%
#14 AP CAA	59.7	1.1	1.84%	15041.	.86%
#15 AP CAB	59.3	1.1	1.85%	15070.	.62%
#16 AP CAC	56.2	1.1	1.96%	13885.	.47%
#17 DM CAA	60.3	1.1	1.82%	15463.	1.06%
#18 DM CAE	52.1	1.0	1.92%	13096.	1.21%
#19 DM CAF	47.7	1.0	2.10%	11651.	1.53%
#20 DM CAG	44.4	1.0	2.25%	10944.	.99%
#21 DM CAH	42.7	1.0	2.34%	11063.	.65%
#22 DM CAI	41.8	.9	2.15%	10955.	.98%
#23 DM CAJ	3.3	.3	9.09%	1861.	5.63%
#24 DM CAK	60.0	1.1	1.83%	15379.	.33%
#25 DM CAM	25.8	.8	3.10%	6709.	1.56%
#26 DM CAN	36.4	.9	2.47%	9431.	.96%
#27 DM CAO	23.2	.8	3.45%	5814.	1.39%
#28 DM CAQ	18.3	.7	3.83%	4895.	.49%
#29 DM CAR	8.9	.5	5.62%	2069.	1.61%
#30 BZ 30A-S	58.4	1.0	1.98%	18141.	1.05%
#31 BZ 30B-S	56.8	1.1	1.94%	12487.	.92%
#32 BZ 61A-S	41.3	.9	2.18%	6767.	.96%
#33 BZ 62A-S	48.4	.9	2.23%	6448.	1.20%
#34 BZ 67A-S	43.7	1.0	2.29%	7748.	1.00%
#35 BZ 128A-S	38.0	.9	2.37%	6767.	1.27%

* TOLERANCE LIMITS (Alcan 95% confidence level)

† corrected for instrumental drift and background intensity

SAMPLE IDENTIFICATION	% Al_2O_3	TOL.*	REL. CONC. ERROR	NET† Al Kα XRF INT. (cps)	REL. COUNTING ERROR
#36 BZ 148A-S	50.0	1.0	2.00%	9581.	.68%
#37 BZ 19A-M	41.8	.9	2.15%	7136.	.74%
#38 BZ 38B-M	59.0	1.1	1.86%	13453.	.68%
#39 BZ 61A-M	45.7	1.0	2.19%	7968.	1.41%
#40 BZ 74A-M	46.5	1.0	2.15%	8801.	.40%
#41 BZ 93B-M	47.2	1.0	2.12%	9010.	1.50%
#42 BZ 121A-M	48.0	1.0	2.08%	8860.	.75%
#43 BZ 136A-M	52.5	1.0	1.90%	10626.	1.16%
#44 BK 14134	52.01	.84	1.62%	11613.	.70%
#45 BK 14135	53.18	.84	1.58%	12095.	1.26%
#46 BK 16726	56.24	.88	1.56%	14038.	1.06%
#47 BK 19356	61.23	.92	1.50%	15344.	1.31%
#48 BK 19987	57.54	.88	1.53%	14255.	.57%
#49 BK 20497	57.8	1.1	1.90%	14469.	.95%
#50 BK 38741	63.7	1.1	1.73%	16748.	.82%
#51 BK 38742	59.5	1.1	1.85%	15530.	.98%
#52 BK 38743	60.0	1.1	1.83%	15219.	.76%
#53 NBS 78	69.97	1.00	1.43%	15498.	.43%
#54 NBS 97	38.77	.70	1.81%	9908.	1.55%
#55 NBS 98	25.54	.54	2.11%	6841.	.96%
#56 AU TH1A	39.8	.9	2.26%	11471.	.55%
#57 AU TH1E	34.9	.9	2.58%	9621.	.90%
#58 AU TH3B	40.4	.9	2.23%	9649.	.88%
#59 AU TH3C	36.3	.9	2.48%	8575.	.98%
#60 AU TH5B	46.1	1.0	2.17%	11328.	.60%
#61 AU TH5E	31.6	.8	2.53%	7867.	1.61%
#62 AU TH5G	27.4	.8	2.92%	8154.	1.10%
#63 AU TH5H	38.6	.8	2.61%	8892.	.46%
#64 AU TH6G	26.0	.8	3.08%	7380.	1.49%
#65 AU TH6H	23.6	.8	3.39%	7153.	.70%
#66 AU TH7A	41.6	.9	2.16%	10650.	1.48%
#67 AU TH7C	51.9	1.0	1.93%	12531.	.29%
#68 AU TH7E	43.5	1.0	2.30%	10444.	.61%
#69 AU TH7F	42.5	1.0	2.35%	10269.	.64%
#70 AU TH7G	32.4	.9	2.78%	8090.	.42%

* TOLERANCE LIMITS (Alcan 85% confidence level)

† corrected for instrumental drift and background intensity

APPENDIX B

XRF INTENSITY vs GRINDING TIME DATA
TABLES B-1 to B-6

CALCULATED CONCENTRATIONS OF 70 BAUXITE SAMPLES
TABLES B-7 to B-10

TABLE B-1

XRF INTENSITY* FOR COARSE AMAZON BAUXITE

Total time of grinding (seconds)	Fe Kα	Ti Kα	Si Kα	Al Kα
0	78.03	18.66	9.31	16.63
2	94.95	20.67	7.76	22.09
5	99.77	22.69	8.27	22.93
7	96.33	21.69	8.06	20.65
10	111.26	23.27	8.23	22.94
12	117.69	25.12	8.33	24.37
15	108.62	24.71	8.45	23.74
20	113.17	24.38	8.23	25.45
25	108.33	23.93	8.15	25.81
30	104.45	22.93	7.86	26.12
35	99.27	22.38	7.88	27.09
40	100.20	21.45	7.63	27.56
50	98.73	21.45	7.58	28.18
60	95.65	21.22	7.81	27.92
75	95.83	20.25	7.59	28.83
90	95.55	20.46	7.37	29.33
300	94.75	19.80	6.69	30.98
Counting time	10 sec.	10 sec.	40 sec.	20 sec.

* Intensity in kilo counts

TABLE B-2

XRF INTENSITY* FOR COARSE AUSTRALIA BAUXITE

Total time of grinding (seconds)	Fe Kα	Ti Kα	Si Kα	Al Kα
0	122.88	33.44	4.39	25.51
2	129.85	42.13	6.28	28.36
5	135.82	39.52	5.41	28.18
7	135.93	42.28	6.87	28.85
10	141.13	41.85	5.28	28.46
12	150.53	45.38	5.85	29.87
15	152.26	44.33	5.73	29.68
20	154.23	44.24	5.64	29.59
25	157.31	43.87	5.63	29.62
30	162.93	44.13	5.36	29.29
35	160.41	43.61	5.48	29.59
40	162.23	42.52	5.25	29.45
50	167.12	43.55	5.33	29.68
60	167.29	43.98	5.36	29.56
75	168.57	43.72	5.07	29.64
90	171.36	43.46	5.23	29.78
300	177.28	48.76	4.88	29.76
Counting time	10 sec.	10 sec.	40 sec.	20 sec.

* - intensity in kilo counts

TABLE B-3

XRF INTENSITY* FOR COARSE DEMERARA BAUXITE

Total time of grinding (seconds)	Fe Kα	Ti Kα	Si Kα	Al Kα
0	25.54	34.33	5.40	27.26
2	38.28	42.60	7.13	30.39
5	35.94	38.38	6.38	29.92
7	37.00	42.59	6.94	31.13
10	36.51	43.27	6.67	31.71
12	38.88	43.67	6.98	32.63
15	41.31	43.56	7.01	32.67
20	37.50	42.18	6.64	32.58
25	37.61	42.56	6.60	33.27
30	37.17	40.75	6.74	32.62
35	39.22	42.03	6.68	33.57
40	38.64	41.81	6.63	33.84
50	37.91	39.57	6.41	33.18
60	38.91	39.64	6.38	33.94
75	40.83	40.49	6.31	33.98
90	39.70	39.86	6.86	33.46
300	43.53	37.66	6.16	34.82
Counting time	10 sec.	10 sec.	40 sec.	20 sec.

* Intensity in kilo counts

TABLE B-4

XRF INTENSITY* FOR COARSE JAMAICA BAUXITE

Total time of grinding (seconds)	Fe Kα	Ti Kα	Si Kα	Al Kα
0	129.67	28.48	6.48	17.99
2	151.88	35.93	7.72	20.85
5	159.96	38.61	7.98	22.38
7	162.88	39.34	8.04	22.25
10	165.41	41.11	8.28	22.83
12	165.71	40.76	8.11	23.14
15	165.24	41.02	8.12	22.91
20	166.69	41.41	8.15	22.98
25	165.77	40.68	8.23	23.36
30	165.78	41.67	8.14	22.86
35	165.47	40.98	8.12	23.43
40	166.10	41.04	8.13	23.38
50	166.75	41.37	8.25	23.65
60	166.18	41.12	8.13	23.06
75	166.98	40.86	7.98	23.08
90	164.91	40.10	8.05	23.22
300	166.83	41.09	7.99	22.95
Counting time	10 sec.	10 sec.	40 sec.	20 sec.

* intensity in kilo counts

TABLE B-5

XRF INTENSITY* FOR COARSE BOKE BAUXITE (sample 1)

Total time of grinding (seconds)	Fe Kα	Ti Kα	Si Kα	Al Kα
0	33.69	33.69	1.87	28.70
2	44.71	34.31	1.86	28.00
5	50.75	38.41	2.10	29.33
7	45.90	37.65	2.13	29.25
10	52.07	41.42	2.17	31.82
12	54.62	47.81	2.19	34.71
15	50.00	41.72	2.12	32.94
20	55.70	46.86	2.17	35.13
25	53.34	45.77	2.05	35.61
30	54.65	45.72	2.06	35.71
35	50.66	44.82	1.90	36.79
40	47.94	42.47	1.89	35.90
50	51.57	44.34	1.85	37.58
60	49.62	42.98	1.78	37.44
75	46.22	40.34	1.78	37.54
90	50.10	42.81	1.76	38.30
300	50.90	40.80	1.60	40.05
Counting time	10 sec.	10 sec.	40 sec.	20 sec.

* Intensity in kilo counts

TABLE B-6

XRF INTENSITY* FOR COARSE BOKE BAUXITE (sample 2)

Total time of grinding (seconds)	Fe Kα	Ti Kα	Si Kα	Al Kα
0	41.47	34.13	1.91	25.44
2	39.94	34.80	1.70	25.67
5	44.49	35.86	1.92	25.79
7	44.78	35.44	1.78	26.86
10	47.53	40.38	2.03	28.19
12	53.30	46.59	2.13	30.70
15	47.35	39.74	2.01	28.45
20	53.59	44.98	2.08	30.81
25	49.58	45.75	1.86	32.05
30	48.10	43.95	1.85	31.71
35	46.56	43.57	1.84	33.20
40	49.63	45.21	1.83	33.61
50	49.97	45.75	1.76	34.39
60	48.86	44.55	1.70	34.24
75	48.56	41.86	1.67	34.35
90	46.79	42.80	1.58	34.82
300	46.77	39.15	1.47	35.72
Counting time	10 sec.	10 sec.	40 sec.	20 sec.

* intensity in kilo counts

TABLE B-7.

CONCENTRATIONS OF 70 BAUXITE SAMPLES (DIRECT INTENSITY RATIO)

SAMPLE		AL	SI	TI	FE	TOTAL
1	KNN	65.60	.53	5.00	00.00	71.73
	CAL	70.00	.18	7.73	07.75	75.00
2	KNN	63.20	1.00	3.20	10.10	00.00
	CAL	10.00	.00	7.00	00.00	00.00
3	KNN	00.20	5.72	3.00	17.00	70.30
	CAL	17.01	1.70	6.27	00.00	00.00
4	KNN	00.00	3.07	5.01	10.00	71.00
	CAL	10.00	1.00	6.04	05.07	70.00
5	KNN	00.00	5.07	3.03	10.10	70.70
	CAL	10.00	1.00	6.01	05.00	71.70
6	KNN	00.00	.00	0.00	10.00	07.00
	CAL	13.00	.00	6.12	07.00	71.37
7	KNN	07.20	.30	3.31	10.70	70.01
	CAL	10.10	.10	6.07	00.13	70.01
8	KNN	00.00	.00	0.00	17.00	70.70
	CAL	10.00	.00	6.07	00.04	70.72
9	KNN	02.00	0.00	0.03	12.00	70.20
	CAL	10.00	1.00	0.00	00.00	70.03
10	KNN	00.00	0.00	0.07	10.10	70.01
	CAL	17.00	0.00	0.00	00.23	70.70
11	KNN	07.10	3.13	3.71	10.00	71.70
	CAL	10.10	.01	0.70	00.74	70.04
12	KNN	03.00	0.00	0.00	00.00	71.00
	CAL	10.00	.70	0.00	07.00	72.00
13	KNN	00.00	0.01	0.70	0.00	00.01
	CAL	00.00	1.00	7.00	10.00	01.01
14	KNN	00.70	0.00	0.00	1.00	00.20
	CAL	00.00	1.70	7.00	0.00	00.10
15	KNN	00.20	0.00	0.00	1.00	00.07
	CAL	00.07	1.70	0.00	0.00	00.10
16	KNN	00.00	0.07	3.00	7.20	73.07
	CAL	00.70	2.00	0.00	17.00	00.00
17	KNN	00.20	0.10	0.00	0.10	07.10
	CAL	00.00	.70	7.00	0.07	00.10
18	KNN	00.20	10.00	1.70	1.00	70.00
	CAL	00.70	7.00	0.00	3.07	00.00
19	KNN	07.70	00.00	0.00	0.00	77.00
	CAL	00.01	0.00	0.00	0.00	01.00
20	KNN	00.00	00.00	3.00	0.20	01.20
	CAL	00.00	10.00	7.00	0.00	07.00
21	KNN	00.70	00.00	1.00	0.20	00.00
	CAL	00.00	10.01	3.20	0.00	01.00
22	KNN	01.00	00.00	1.00	.00	03.00
	CAL	00.70	10.11	0.70	0.10	00.07
23	KNN	0.00	00.00	.00	10.00	70.10
	CAL	3.00	00.01	.00	00.10	00.77
24	KNN	00.00	0.00	0.10	.70	00.00
	CAL	00.00	0.07	0.10	1.00	00.00

SAMPLE		AL	SI	TI	FE	TOTAL
25	KNN	00.00	00.70	1.10	00.00	00.00
	CAL	10.00	10.03	1.00	00.03	10.70
26	KNN	00.00	0.70	1.00	00.00	72.70
	CAL	17.00	0.07	0.03	00.70	00.10
27	KNN	00.00	00.70	7.00	00.00	07.30
	CAL	10.00	10.00	0.00	70.00	00.00
28	KNN	10.20	0.00	.00	00.00	00.20
	CAL	0.00	0.00	1.70	00.00	100.01
29	KNN	0.00	0.00	1.70	03.70	72.10
	CAL	0.01	0.01	0.00	00.00	107.70
30	KNN	00.00	1.10	0.70	10.10	70.30
	CAL	10.10	.30	7.00	00.00	70.30
31	KNN	00.00	1.10	0.00	0.00	00.00
	CAL	03.00	.07	7.77	00.00	00.00
32	KNN	01.30	0.00	0.30	07.00	77.00
	CAL	10.70	1.07	0.01	03.13	00.30
33	KNN	00.00	10.70	1.00	00.00	70.10
	CAL	10.10	3.30	0.03	00.00	00.00
34	KNN	03.70	0.00	1.00	00.00	70.00
	CAL	10.00	0.70	0.00	00.03	77.00
35	KNN	00.00	1.70	0.00	00.00	70.00
	CAL	10.77	.00	0.00	70.10	00.00
36	KNN	00.00	0.20	0.00	10.00	72.00
	CAL	10.10	.00	7.30	00.03	72.00
37	KNN	01.00	.00	0.00	01.00	70.00
	CAL	13.00	.00	0.03	70.07	00.10
38	KNN	00.00	.00	0.30	7.00	00.00
	CAL	00.00	.00	0.00	10.00	00.01
39	KNN	03.70	0.00	1.00	03.70	70.00
	CAL	10.00	1.00	0.03	07.00	70.00
40	KNN	00.00	0.00	1.30	00.30	70.00
	CAL	10.03	1.73	3.30	00.00	73.70
41	KNN	07.00	.70	0.00	00.70	72.00
	CAL	17.00	.01	0.00	00.07	70.00
42	KNN	00.00	0.00	0.00	01.70	70.10
	CAL	10.70	.00	0.03	00.01	70.37
43	KNN	00.00	0.00	1.70	10.30	70.00
	CAL	00.00	.70	0.00	00.07	00.00
44	KNN	00.01	1.30	0.07	10.00	00.03
	CAL	01.00	.07	0.01	00.10	00.70
45	KNN	03.10	.01	0.00	10.00	00.03
	CAL	00.00	.01	7.70	00.00	00.00
46	KNN	00.00	0.00	0.01	7.00	00.33
	CAL	00.00	.00	0.01	10.01	00.30
47	KNN	01.03	.00	0.07	3.01	70.11
	CAL	00.00	.10	10730	0.00	00.00
48	KNN	07.00	1.10	3.00	0.00	00.00
	CAL	00.00	.30	0.00	10.00	00.70

SAMPLE		AL	SI	TI	FE	TOTAL
49	KNN	07.00	.00	0.01	0.10	00.03
	CAL	07.30	.17	13.00	11.00	00.00
50	KNN	03.70	.00	3.30	1.00	00.01
	CAL	11.00	.10	0.13	0.10	00.00
51	KNN	00.00	.03	3.70	3.00	07.70
	CAL	00.20	.10	7.70	0.77	00.00
52	KNN	00.00	.07	3.70	3.10	07.00
	CAL	00.70	.10	0.03	0.00	00.70
53	KNN	00.07	00.00	3.31	.70	00.00
	CAL	00.70	0.00	7.13	1.00	07.10
54	KNN	00.77	00.07	3.30	.00	00.00
	CAL	10.70	10.03	0.03	0.10	00.07
55	KNN	00.00	00.11	1.01	0.00	00.13
	CAL	13.03	00.30	0.07	0.00	00.00
56	KNN	00.00	00.20	3.00	3.30	00.00
	CAL	01.07	0.13	0.00	10.00	00.30
57	KNN	00.00	00.00	0.10	0.00	70.00
	CAL	10.10	11.00	0.00	03.02	00.00
58	KNN	00.00	00.00	0.00	10.10	77.30
	CAL	10.03	7.07	0.07	00.07	00.00
59	KNN	00.30	00.00	1.70	17.30	00.70
	CAL	10.00	0.00	0.00	00.00	00.11
60	KNN	00.10	17.00	0.01	0.10	00.11
	CAL	01.00	0.00	0.01	03.70	00.00
61	KNN	01.00	05.70	1.70	10.00	03.00
	CAL	10.00	10.70	0.07	00.03	00.30
62	KNN	07.00	03.30	1.00	0.00	03.30
	CAL	10.01	01.10	0.00	0.03	00.70
63	KNN	00.00	00.00	1.07	3.00	00.07
	CAL	10.00	11.70	0.70	0.17	07.00
64	KNN	00.00	03.00	1.00	0.00	00.01
	CAL	11.00	01.03	0.07	10.00	00.00
65	KNN	03.00	00.10	1.17	0.00	07.27
	CAL	13.00	00.30	0.01	10.10	01.10
66	KNN	01.00	00.00	0.01	0.00	70.01
	CAL	00.10	7.00	0.30	00.00	00.00
67	KNN	01.70	0.00	0.30	0.70	71.00
	CAL	03.00	0.00	0.01	03.00	00.01
68	KNN	03.00	10.00	1.03	10.00	70.70
	CAL	10.70	0.00	0.00	00.70	00.00
69	KNN	00.00	01.00	0.10	11.00	77.00
	CAL	10.00	7.00	0.01	00.01	00.71
70	KNN	00.00	03.70	1.00	10.00	03.30
	CAL	10.00	11.00	0.30	00.00	00.00
ABSOLUTE ACCURACY		00.00	0.11	0.03	10.01	AVE= 10.00
RELATIVE ACCURACY		00.00	00.00	100.00	100.00	AVE= 000.10

TABLE B-8

CONCENTRATIONS OF 70 BAUXITE SAMPLES (BINARY MIXTURE α COEFF.)

SAMPLE		AL	SI	TI	FE	TOTAL
1	XRF	48.68	.33	3.68	20.06	71.73
	CAL	76.03	.38	5.66	10.07	90.48
2	XRF	47.06	1.00	2.70	18.10	68.64
	CAL	74.08	.83	4.88	15.07	93.31
3	XRF	44.88	3.78	2.48	17.90	70.36
	CAL	70.08	3.19	3.86	14.14	91.26
4	XRF	48.60	2.87	2.81	18.46	71.80
	CAL	75.76	2.86	3.14	17.10	98.86
5	XRF	48.98	2.67	2.43	18.10	72.70
	CAL	73.09	3.06	3.13	16.96	95.18
6	XRF	48.80	.84	2.88	18.86	67.48
	CAL	76.17	.89	1.96	19.88	91.71
7	XRF	47.88	.34	3.21	18.78	70.36
	CAL	74.10	.32	3.79	18.01	96.60
8	XRF	48.98	.84	3.00	17.98	70.78
	CAL	76.88	.89	3.88	16.48	98.07
9	XRF	48.98	6.48	2.83	18.88	78.38
	CAL	68.78	3.82	1.84	18.81	93.78
10	XRF	48.88	8.88	3.83	18.18	78.81
	CAL	76.87	4.78	1.98	18.48	98.18
11	XRF	47.18	3.13	3.71	18.88	72.34
	CAL	73.86	1.88	3.88	18.84	96.81
12	XRF	48.88	8.84	2.88	18.88	71.88
	CAL	78.48	1.23	3.87	18.14	94.23
13	XRF	48.88	8.81	3.78	3.88	68.48
	CAL	88.88	4.88	3.88	3.87	99.88
14	XRF	88.78	3.88	3.88	1.84	68.28
	CAL	88.18	2.88	2.88	1.87	101.81
15	XRF	48.78	4.88	3.88	1.84	88.67
	CAL	88.88	8.88	3.88	1.87	101.88
16	XRF	48.88	8.88	3.88	1.88	72.88
	CAL	88.88	8.88	3.88	1.88	101.88
17	XRF	48.38	3.18	3.88	18.18	87.18
	CAL	88.18	3.88	3.88	1.88	101.38
18	XRF	48.18	88.88	1.78	1.48	78.88
	CAL	88.88	18.38	1.31	1.13	88.36
19	XRF	48.78	38.88	3.88	3.88	77.88
	CAL	77.38	18.38	3.84	1.88	98.18
20	XRF	48.88	38.88	3.88	3.88	81.38
	CAL	88.88	18.48	3.88	3.84	98.88
21	XRF	48.78	28.88	1.78	3.38	88.48
	CAL	78.88	11.38	1.17	1.88	93.18
22	XRF	81.88	88.88	3.88	1.88	88.88
	CAL	81.78	88.88	3.88	1.88	98.88
23	XRF	3.38	88.88	.88	14.38	98.18
	CAL	3.88	88.88	.78	18.88	88.88
24	XRF	88.88	3.88	3.18	.78	88.88
	CAL	88.88	3.88	3.88	.88	188.88

SAMPLE		AL	SI	TI	FE	TOTAL
25	XRF	38.88	38.78	1.18	28.48	88.88
	CAL	58.19	34.58	.78	28.19	97.88
26	XRF	38.48	8.38	1.88	28.88	78.78
	CAL	71.88	8.88	.78	28.14	183.83
27	XRF	83.88	84.78	1.48	28.88	87.38
	CAL	48.84	19.18	.87	23.81	188.47
28	XRF	18.38	8.48	.78	48.88	74.88
	CAL	84.88	8.78	.83	48.31	181.84
29	XRF	8.88	8.88	1.78	83.78	73.18
	CAL	88.98	9.88	1.34	83.87	78.18
30	XRF	38.48	1.18	81.78	18.18	98.38
	CAL	78.78	.88	8.88	17.15	94.87
31	XRF	38.88	1.18	8.88	8.88	88.88
	CAL	88.84	.48	3.88	8.89	97.14
32	XRF	41.38	8.88	3.38	83.88	77.88
	CAL	88.48	3.88	3.18	88.84	87.89
33	XRF	38.48	18.78	7.48	38.48	78.18
	CAL	83.88	8.81	1.48	88.88	84.89
34	XRF	43.78	8.88	1.88	88.88	74.48
	CAL	81.88	8.88	1.78	81.87	89.88
35	XRF	38.88	1.78	8.88	38.88	78.88
	CAL	87.14	.88	1.88	88.88	94.87
36	XRF	38.88	8.38	8.48	18.58	73.88
	CAL	78.89	1.18	8.38	17.87	93.93
37	XRF	81.88	.88	8.88	31.88	78.48
	CAL	88.88	.48	1.88	88.88	98.89
38	XRF	88.88	.88	8.38	7.88	88.38
	CAL	88.84	.48	8.18	8.88	88.48
39	XRF	48.78	4.88	1.88	83.78	78.88
	CAL	88.78	8.38	1.81	88.84	88.87
40	XRF	48.88	8.88	1.38	88.38	78.48
	CAL	87.88	3.83	1.87	18.88	88.89
41	XRF	47.88	.78	8.88	88.78	78.88
	CAL	78.13	.89	8.88	81.41	88.18
42	XRF	48.88	8.88	1.58	81.78	74.18
	CAL	88.51	1.88	1.48	88.44	98.81
43	XRF	88.38	8.88	1.78	18.38	78.88
	CAL	77.19	1.37	1.38	148.88	84.78
44	XRF	88.81	1.88	8.87	78.88	88.83
	CAL	88.38	1.88	8.71	18.48	188.88
45	XRF	83.18	.87	8.48	18.88	88.83
	CAL	84.58	.98	8.48	13.88	181.38
46	XRF	84.84	1.88	4.81	2.48	88.33
	CAL	88.38	.88	3.83	8.88	188.38
47	XRF	81.82	.88	4.87	3.41	78.11
	CAL	87.87	.88	4.81	3.18	188.81
48	XRF	87.84	1.18	3.84	8.48	88.88
	CAL	82.78	.38	2.83	3.78	181.88

SAMPLE		AL	SI	TI	FE	TOTAL
49	XRF	87.88	.83	3.81	4.38	88.83
	CAL	84.88	.38	4.88	4.88	183.38
50	XRF	83.78	.88	3.38	1.48	88.81
	CAL	181.84	.81	3.73	1.38	188.84
51	XRF	88.88	.83	3.18	3.88	87.18
	CAL	84.89	.33	3.86	3.18	181.96
52	XRF	88.88	.87	3.78	3.18	87.88
	CAL	84.87	.38	3.81	3.83	181.84
53	XRF	88.87	88.88	3.87	.78	84.88
	CAL	88.71	18.31	3.87	.81	111.18
54	XRF	38.77	48.87	8.38	.88	88.88
	CAL	88.83	87.84	1.88	.71	87.88
55	XRF	88.34	88.17	1.83	3.88	88.13
	CAL	88.78	43.38	1.81	1.88	98.38
56	XRF	38.88	88.88	3.34	3.38	88.84
	CAL	77.88	12.83	3.88	8.78	94.88
57	XRF	34.98	38.48	8.18	3.88	88.88
	CAL	87.88	18.48	1.87	8.38	87.48
58	XRF	88.88	88.88	3.88	18.18	87.38
	CAL	88.88	13.78	1.88	11.72	98.88
59	XRF	38.38	88.88	1.78	17.88	88.78
	CAL	83.88	18.88	1.81	14.88	88.87
60	XRF	88.18	17.88	3.81	3.18	78.11
	CAL	78.81	3.78	1.88	8.18	87.88
61	XRF	31.88	88.78	1.78	14.88	88.88
	CAL	88.88	88.88	1.18	18.88	84.88
62	XRF	87.88	88.38	1.88	3.88	88.38
	CAL	84.78	38.88	1.84	3.38	84.88
63	XRF	38.88	88.88	1.87	3.88	84.87
	CAL	81.88	38.38	1.88	3.83	84.88
64	XRF	88.88	88.88	1.88	4.88	84.88
	CAL	88.84	37.83	.88	4.77	88.88
65	XRF	83.88	38.18	1.17	4.88	87.27
	CAL	88.888	41.34	.88	2.88	84.83
66	XRF	81.88	38.88	3.81	3.88	78.81
	CAL	72.78	14.81	1.77	4.98	84.88
67	XRF	31.88	8.88	3.38	3.78	71.88
	CAL	84.88	4.88	1.88	3.13	88.87
68	XRF	42.38	16.88	1.88	18.48	78.78
	CAL	78.37	8.48	1.13	13.78	98.18
69	XRF	48.38	21.88	3.18	11.88	77.88
	CAL	78.31	18.88	1.81	18.38	97.38
70	XRF	38.48	23.78	1.88	13.88	88.38
	CAL	88.82	21.38	1.18	12.87	94.88

		AL	SI	TI	FE	TOTAL
ABSOLUTE ACCURACY		87.89	8.87	.48	1.38	AVE= 8.88
RELATIVE ACCURACY		71.88	38.88	18.88	12.81	AVE= 38.74

TABLE B-9

CONCENTRATIONS OF 70 BAUXITE SAMPLES (THEORETICAL α COEFF.)

SAMPLE		AL	SI	TI	FE	TOTAL
1	XRF	48.60	.53	3.58	18.00	71.72
	CAL	67.87	.65	3.37	48.07	119.96
2	XRF	47.30	1.00	3.70	18.10	69.44
	CAL	63.27	1.02	3.97	30.04	100.00
3	XRF	44.60	5.72	2.40	13.90	70.36
	CAL	59.15	6.99	2.56	48.81	111.81
4	XRF	45.30	3.57	2.41	18.40	71.28
	CAL	60.67	4.37	2.58	44.04	117.46
5	XRF	43.80	5.07	2.43	18.10	70.70
	CAL	60.00	6.82	2.76	44.66	117.19
6	XRF	46.80	.64	2.23	18.80	67.49
	CAL	61.98	.84	2.58	43.68	109.88
7	XRF	47.80	.50	2.31	19.70	70.55
	CAL	63.79	.58	2.61	47.68	115.56
8	XRF	46.90	.66	2.65	17.90	70.72
	CAL	60.13	.80	2.98	46.10	113.36
9	XRF	43.90	5.03	2.23	19.60	70.30
	CAL	59.66	7.09	2.46	46.91	126.09
10	XRF	45.60	3.04	2.37	18.10	70.81
	CAL	60.60	10.66	2.64	43.76	117.67
11	XRF	47.10	3.33	2.71	18.00	71.76
	CAL	60.66	4.58	2.84	46.66	114.84
12	XRF	45.60	5.04	2.66	18.06	71.94
	CAL	60.99	3.09	2.96	46.86	113.81
13	XRF	46.00	4.01	2.76	3.80	69.61
	CAL	60.81	5.18	2.99	13.94	91.91
14	XRF	48.30	5.22	2.56	1.04	68.25
	CAL	60.94	6.58	2.58	4.09	83.96
15	XRF	50.20	4.99	2.56	1.04	68.67
	CAL	78.09	6.26	2.61	4.04	88.97
16	XRF	46.80	8.67	1.82	7.80	72.49
	CAL	60.99	13.61	1.13	15.08	90.71
17	XRF	48.30	3.18	2.60	8.10	67.16
	CAL	78.19	5.04	2.89	4.08	81.84
18	XRF	50.10	19.60	1.70	1.40	78.80
	CAL	59.61	24.58	1.81	3.09	88.81
19	XRF	47.70	23.00	2.40	8.00	77.98
	CAL	53.04	29.16	2.87	3.08	88.86
20	XRF	44.40	28.60	2.60	6.30	81.30
	CAL	58.12	36.79	3.08	8.32	98.37
21	XRF	48.70	28.60	1.90	3.30	88.60
	CAL	58.38	38.77	1.81	4.46	96.88
22	XRF	41.60	46.80	1.36	.20	83.96
	CAL	48.83	61.05	1.89	.06	99.83
23	XRF	3.30	60.30	.00	16.60	79.18
	CAL	11.09	79.28	.06	34.57	125.19
24	XRF	50.00	6.60	2.15	.70	69.60
	CAL	69.51	7.97	2.19	1.19	80.46

SAMPLE		AL	SI	TI	FE	TOTAL
25	XRF	25.60	36.70	1.10	23.40	86.86
	CAL	45.12	51.10	1.87	48.75	146.89
26	XRF	34.40	8.70	3.00	28.60	78.70
	CAL	47.33	10.04	3.09	69.86	153.08
27	XRF	33.80	54.70	1.40	36.00	87.30
	CAL	46.65	63.80	1.47	101.21	197.22
28	XRF	16.20	6.60	.90	46.40	74.20
	CAL	47.60	14.78	.99	122.95	186.20
29	XRF	8.90	8.80	1.70	53.30	73.10
	CAL	19.78	18.17	2.04	103.48	143.48
30	XRF	66.40	1.10	2.70	18.10	78.30
	CAL	85.53	1.87	3.38	44.11	114.84
31	XRF	64.60	1.10	2.50	9.00	68.40
	CAL	88.94	1.89	3.09	81.71	94.39
32	XRF	41.30	4.90	2.30	27.40	77.60
	CAL	54.99	7.90	2.97	66.84	127.81
33	XRF	46.60	18.70	1.60	25.40	78.10
	CAL	47.87	13.66	2.05	68.49	132.36
34	XRF	43.70	8.30	1.90	22.80	76.50
	CAL	54.18	11.45	2.48	55.79	123.99
35	XRF	30.60	1.70	2.00	34.90	70.50
	CAL	38.67	2.20	2.58	84.68	148.19
36	XRF	58.00	2.30	2.40	10.50	73.20
	CAL	68.78	2.78	3.00	46.57	116.14
37	XRF	61.60	.90	2.00	31.90	76.40
	CAL	84.83	1.16	2.58	76.84	134.58
38	XRF	59.00	.90	2.30	7.90	69.80
	CAL	78.51	.95	3.07	16.86	98.80
39	XRF	45.70	6.60	1.90	23.70	78.80
	CAL	56.09	8.31	2.66	56.86	131.10
40	XRF	46.50	6.50	1.30	28.30	76.40
	CAL	58.84	7.80	1.63	49.48	116.95
41	XRF	47.20	.70	2.00	22.70	72.00
	CAL	60.59	.90	2.91	54.64	181.09
42	XRF	44.60	8.90	1.60	21.70	76.10
	CAL	60.56	6.84	1.87	52.69	110.38
43	XRF	52.50	2.50	1.70	15.30	72.00
	CAL	66.25	3.18	2.13	37.41	109.91
44	XRF	58.01	1.00	2.07	14.05	69.93
	CAL	78.40	1.09	2.68	37.60	118.30
45	XRF	52.10	.81	2.46	12.00	68.53
	CAL	71.68	1.08	3.03	34.35	111.34
46	XRF	44.84	.80	2.01	19.60	68.23
	CAL	72.19	1.13	3.78	26.99	98.81
47	XRF	61.83	.60	2.07	3.01	70.11
	CAL	76.68	.84	2.90	7.08	87.50
48	XRF	57.54	1.15	2.56	2.60	66.60
	CAL	78.93	1.36	3.88	4.79	98.86

SAMPLE		AL	SI	TI	FE	TOTAL
49	XRF	57.80	.53	3.61	4.30	66.53
	CAL	72.49	.68	4.04	10.68	88.78
50	XRF	63.70	.45	3.30	1.40	69.81
	CAL	76.76	.67	3.92	2.04	83.57
51	XRF	59.50	.53	3.34	3.99	67.76
	CAL	73.46	.75	3.77	5.50	83.69
52	XRF	60.80	.57	3.75	3.10	67.48
	CAL	75.99	.78	3.17	6.44	83.54
53	XRF	60.27	20.09	3.27	.79	84.68
	CAL	65.60	32.07	3.99	1.42	108.17
54	XRF	38.77	28.87	2.38	.98	68.80
	CAL	46.31	47.35	2.86	2.82	95.94
55	XRF	25.54	30.11	1.63	2.05	59.13
	CAL	31.41	41.46	1.84	4.14	98.87
56	XRF	29.80	22.80	2.34	2.20	69.84
	CAL	37.24	34.66	2.43	13.14	87.71
57	XRF	24.90	38.40	2.16	2.60	70.26
	CAL	31.46	36.19	2.80	24.85	115.86
58	XRF	60.40	22.80	2.00	12.10	77.30
	CAL	55.64	28.64	2.89	33.11	119.29
59	XRF	36.30	25.50	1.76	17.20	80.76
	CAL	52.76	32.90	2.04	48.81	136.88
60	XRF	46.10	17.50	2.41	9.10	76.11
	CAL	60.70	20.66	2.33	22.15	106.08
61	XRF	31.60	35.70	1.70	10.90	82.90
	CAL	44.99	44.43	1.68	24.30	120.36
62	XRF	37.40	33.20	1.80	2.50	84.30
	CAL	37.38	37.03	1.83	6.31	103.88
63	XRF	38.60	48.80	1.87	2.80	84.87
	CAL	41.99	51.64	1.90	8.89	120.68
64	XRF	36.80	33.60	1.85	6.80	84.90
	CAL	36.80	41.86	2.15	13.80	118.23
65	XRF	23.60	58.10	1.17	6.50	87.37
	CAL	33.98	66.15	1.88	18.50	116.98
66	XRF	61.60	24.60	2.21	8.80	76.61
	CAL	85.71	30.15	2.84	19.44	100.30
67	XRF	51.70	9.00	2.38	8.70	71.98
	CAL	67.06	10.33	2.24	31.59	101.80
68	XRF	43.50	10.30	1.96	14.60	70.76
	CAL	61.20	20.24	2.88	28.30	119.68
69	XRF	48.60	21.60	2.10	11.60	77.80
	CAL	57.46	27.15	1.98	29.19	115.67
70	XRF	38.40	33.70	1.60	15.60	83.30
	CAL	48.15	42.70	1.64	39.43	131.94
ABSOLUTE ACCURACY		10.76	3.24	.31	19.87	AVE= 9.17
RELATIVE ACCURACY		37.91	23.86	13.70	134.81	AVE= 55.81

TABLE B-10

CONCENTRATIONS OF 70 BAUXITE SAMPLES (FINAL(BAUXITE) α COEFF.)

SAMPLE		AL	SI	TI	FE	TOTAL
1	XRF	46.60	.32	[illegible]	[illegible]	71.73
	CAL	49.91	.35	5.01	19.44	78.81
2	XRF	47.80	1.44	5.70	18.18	69.44
	CAL	48.94	1.33	5.50	16.46	67.33
3	XRF	44.80	5.78	5.46	17.90	78.36
	CAL	43.65	5.11	5.37	17.41	68.36
4	XRF	48.90	3.87	5.41	18.46	71.85
	CAL	48.90	3.81	5.38	15.00	71.63
5	XRF	46.50	5.67	5.43	18.10	75.70
	CAL	46.14	4.79	5.39	16.09	71.40
6	XRF	48.90	.64	5.83	18.86	67.46
	CAL	48.39	.68	5.80	16.87	66.44
7	XRF	47.80	.34	5.21	19.70	78.35
	CAL	[illegible]	.34	5.06	19.63	76.09
8	XRF	49.50	.64	5.68	17.90	78.70
	CAL	47.09	.70	5.52	16.33	69.84
9	XRF	45.90	6.68	5.83	19.66	78.38
	CAL	45.20	6.55	5.10	18.07	76.06
10	XRF	48.60	5.54	5.57	18.18	79.81 C
	CAL	44.89	7.68	5.36	17.78	71.99
11	XRF	47.10	3.13	5.71	18.90	71.74
	CAL	45.09	2.98	5.48	16.94	68.77
12	XRF	48.80	5.64	5.86	20.20	77.44
	CAL	46.11	6.28	5.54	19.04	76.01
13	XRF	48.80	5.81	5.78	5.00	80.41
	CAL	46.81	6.79	5.01	5.56	68.17
14	XRF	50.10	5.85	5.93	1.04	69.35
	CAL	47.06	6.31	5.70	1.62	64.64
15	XRF	50.20	6.02	5.84	1.04	65.47
	CAL	45.73	6.14	5.60	1.61	64.56
16	XRF	50.84	6.87	1.81	1.68	73.00
	CAL	46.89	10.01	1.13	1.96	68.43
17	XRF	48.20	5.18	5.66	5.16	67.16
	CAL	46.52	5.17	5.60	1.67	64.89
18	XRF	50.30	10.00	1.70	1.48	73.80
	CAL	47.83	12.11	1.47	1.88	71.83
19	XRF	45.70	25.80	5.40	5.80	73.96
	CAL	43.15	24.11	5.15	1.89	70.68
20	XRF	44.40	28.80	5.80	6.26	81.36
	CAL	41.73	26.68	5.13	5.34	78.88
21	XRF	48.30	23.56	1.68	5.26	80.48
	CAL	38.34	23.36	1.58	1.79	78.07
22	XRF	41.80	28.80	1.20	.88	83.36
	CAL	39.64	26.65	1.07	.39	78.83
23	XRF	2.38	68.30	.80	16.30	78.18
	CAL	7.68	70.39	.89	16.78	100.00
24	XRF	54.06	6.60	5.18	.78	68.80
	CAL	54.83	6.86	5.38	.83	68.95

SAMPLE		AL	SI	TI	FE	TOTAL
25	XRF	25.60	35.70	1.18	25.40	88.98
	CAL	31.23	35.78	.87	23.23	91.81
26	XRF	26.40	8.78	1.06	25.60	70.78
	CAL	26.55	9.63	.89	26.68	83.46
27	XRF	23.80	24.78	1.46	28.90	87.36
	CAL	31.99	24.13	.97	29.96	97.86
28	XRF	18.30	6.90	.97	48.60	74.88
	CAL	21.74	8.79	.96	48.17	93.31
29	XRF	8.98	8.88	1.78	53.78	73.18
	CAL	13.98	10.61	1.65	55.68	81.84
30	XRF	38.40	1.18	8.78	18.18	72.36
	CAL	48.88	.68	8.67	17.98	78.85
31	XRF	38.80	1.18	8.96	9.88	69.46
	CAL	53.87	.68	8.87	8.77	86.74
32	XRF	41.38	8.98	8.28	27.48	77.98
	CAL	38.15	9.43	8.45	28.87	78.88
33	XRF	48.46	18.78	1.68	25.68	78.18
	CAL	33.26	9.88	1.72	24.89	78.98
34	XRF	43.78	8.88	8.98	22.88	78.68
	CAL	38.38	8.86	8.88	23.81	78.14
35	XRF	38.88	1.78	8.88	28.88	78.58
	CAL	38.38	1.38	1.88	36.68	78.68
36	XRF	48.88	8.38	8.48	18.58	73.58
	CAL	48.18	1.89	8.87	18.78	69.68
37	XRF	41.68	.98	8.88	21.98	74.68
	CAL	38.43	.78	1.96	30.28	78.48
38	XRF	88.88	.98	8.38	7.88	88.38
	CAL	88.17	.73	8.46	6.78	88.11
39	XRF	48.78	8.68	1.88	22.78	73.88
	CAL	48.48	3.68	8.88	24.88	78.74
40	XRF	44.38	8.68	1.38	88.38	74.68
	CAL	48.84	8.13	1.83	88.48	88.88
41	XRF	47.88	.78	8.88	88.78	72.88
	CAL	48.81	.82	8.41	88.88	78.91
42	XRF	48.88	8.88	1.38	21.78	74.18
	CAL	43.82	8.93	1.87	21.88	88.71
43	XRF	53.38	8.38	1.78	18.28	78.88
	CAL	48.81	8.85	1.81	18.18	67.84
44	XRF	88.88	8.88	8.87	14.88	88.93
	CAL	[illegible]	1.88	8.98	14.88	88.87
45	XRF	38.18	.81	8.44	18.88	88.33
	CAL	34.28	1.38	8.86	13.68	78.83
46	XRF	54.84	.88	8.81	7.48	88.35
	CAL	58.38	.83	3.88	6.77	88.81
47	XRF	61.83	.38	8.87	3.81	78.11
	CAL	58.33	.48	8.78	3.19	78.78
48	XRF	57.58	1.18	3.36	6.68	88.88
	CAL	58.89	1.81	3.19	5.89	88.37

SAMPLE		AL	SI	TI	FE	TOTAL
49	XRF	57.88	.53	5.61	6.89	88.83
	CAL	60.41	.51	5.86	6.38	78.89
50	XRF	58.78	.45	3.26	7.46	88.81
	CAL	63.83	.37	3.86	7.36	88.38
51	XRF	59.58	.53	3.76	8.99	87.76
	CAL	58.87	.39	8.91	8.28	88.88
52	XRF	88.88	.87	3.78	3.19	87.88
	CAL	58.77	.37	3.38	8.66	88.32
53	XRF	88.87	88.89	3.27	.79	94.82
	CAL	88.88	88.74	3.14	.88	84.88
54	XRF	38.77	48.87	8.38	.98	88.88
	CAL	38.19	44.88	8.84	.83	83.88
55	XRF	88.84	88.11	1.42	8.88	88.13
	CAL	83.38	83.74	1.33	1.79	88.48
56	XRF	28.88	88.88	8.84	8.38	88.84
	CAL	48.83	88.88	8.83	8.88	73.88
57	XRF	34.88	38.48	8.16	9.88	79.86
	CAL	38.88	38.81	8.16	9.58	81.88
58	XRF	48.88	88.88	8.88	18.18	77.38
	CAL	41.38	81.88	1.88	13.81	77.84
59	XRF	38.78	88.58	1.76	17.88	88.78
	CAL	38.81	84.88	1.68	16.78	88.68
60	XRF	48.18	17.58	8.41	9.18	78.11
	CAL	84.58	16.18	8.87	8.88	72.77
61	XRF	31.68	28.78	1.78	18.98	82.96
	CAL	33.87	28.83	1.84	18.33	84.37
62	XRF	87.48	53.38	1.88	8.88	88.38
	CAL	88.58	84.16	1.79	8.43	88.18
63	XRF	38.68	48.88	1.47	3.88	84.87
	CAL	38.87	48.81	1.88	3.36	88.44
64	XRF	84.88	88.88	1.88	6.88	88.88
	CAL	84.78	87.38	1.89	8.72	91.88
65	XRF	88.68	88.16	1.17	4.38	87.27
	CAL	88.18	88.95	1.84	4.58	93.78
66	XRF	41.88	84.88	8.81	8.88	78.41
	CAL	48.83	88.88	8.88	7.72	78.78
67	XRF	51.98	7.88	8.38	8.78	71.98
	CAL	51.83	7.83	8.18	8.81	78.14
68	XRF	43.88	18.88	1.84	18.48	88.75
	CAL	48.38	18.88	1.81	13.81	78.18
69	XRF	48.58	21.88	8.18	11.48	73.88
	CAL	43.83	88.88	1.86	11.48	77.13
70	XRF	38.48	33.78	1.88	18.48	83.28
	CAL	34.78	38.88	1.48	15.48	84.81
ABSOLUTE ACCURACY		8.88	1.89	-.81	-.38	AVG= 1.83
RELATIVE ACCURACY		9.78	14.18	9.89	8.81	AVG= 18.87

APPENDIX C

COMPUTER PROGRAMS

PROGRAMS AXMSD and AABSD

PURPOSE : To determine matrix effect correction coefficients and interelement effect correction coefficients from elemental concentration and x-ray intensity data for binary mixture samples.

METHOD : Using EQUATIONS 5-2 and 5-3 respectively, an alpha coefficient is determined for each pair of samples. The calculation is carried out for all possible combinations and an average alpha value is determined. A standard deviation of this value is determined.

The alpha coefficient is applied to the measured x-ray intensity data to determine a 100% intensity value. A standard deviation of this value is obtained. The alpha coefficient value is revised by 0.1% increments and the 100% intensity calculation is repeated. This process continues until a minimum standard deviation of the 100% intensity value is obtained.

```
      PROGRAM AXMSD
      COMMON C(10),X(10),CM(10),CIP(10)
      CALL RESET
      WRITE(2,7)
    7 FORMAT("ALFA-XM  [ EFFECT OF (M) ON (X) ]")
    1 AA=0
      DD=0.0
      NX=0
      NCT=0
      N=0
      J=1
      WRITE(2,5)
    5 FORMAT("CONC-X,XRF-X ?")
   10 READ(1,*) C(J),X(J),N
      CM(J)=1.0-C(J)
      J=J+1
      IF(N-1)10,20
   20 J=J-1
      N=1
      WRITE(2,2)
  135 J1=N+1
      DO 100 NN=J1,J
      A=(C(NN)*X(N)-C(N)*X(NN))/
     #(C(N)*X(NN)*CM(NN)-C(NN)*X(N)*CM(N))
      AA=AA+A
      NCT=NCT+1
  100 CONTINUE
      N=N+1
      IF(N-J)135,140,140
  140 AVE=AA/FLOAT(NCT)
      AA=0
      NCT=0
      N=1
   25 J1=N+1
      DO 30 NN=J1,J
      A=(C(NN)*X(N)-C(N)*X(NN))/
     #(C(N)*X(NN)*CM(NN)-C(NN)*X(N)*CM(N))
      D=A-AVE
      DD=DD+D*D
      NCT=NCT+1
   30 WRITE(2,2) N,NN,A
    2 FORMAT(2I3,2X,F12.6)
      N=N+1
      IF(N-J)35,40,40
   35 GO TO 25
   40 WRITE(2,2)
      SD=SQRT(DD/FLOAT(NCT-1))
      WRITE(2,3) AVE,SD
    3 FORMAT("AVERAGE= "F12.6"   STD. DEV. = "F7.4)
  250 WRITE(2,2)
```

```
      AC=0.0
      SP=0.0
      DD=0.0
      NF=0
      FAC=0.001*AVE
      N1=0
      WRITE(2,8)
    8 FORMAT("ABSORPTION CORRECTION"/
     #8X,"DATA",4X,"MATRIX",6X,"100%")
      DO 50 K=1,J
      CI=X(K)*(1.0+AVE*CM(K))
      CIP(K)=CI/C(K)
      AC=AC+CIP(K)
   50 WRITE(2,4) K,X(K),CI,CIP(K)
    4 FORMAT(I3,4F10.6)
      IF(ISSW(15))260,51
  260 CALL RESET
      READ(1,*) AVE
      DD=0.0
      GO TO 40
   51 AAC=AC/FLOAT(J)
      DO 200 K=1,J
      D=CIP(K)-AAC
  200 DD=DD+D*D
      SAC=SQRT(DD/FLOAT(J-1))
      ST=SAC*100.0/AAC
      DN=ST-SP
      IF(NX)201,201,202
  201 IF(DN-0.00001)55,55,45
   45 WRITE(2,203) AVE,AAC,SAC,ST
      FAC=-FAC
      NF=NF+1
      IF(N1)53,53,54
   53 N1=1
      AL=AVE
      GO TO 56
   54 N1=0
      AH=AVE
   56 IF(NF-4)55,150,150
   55 AVE=AVE-FAC
      AC=0.0
      DD=0.0
      SP=ST
      DO 220 K=1,J
      CI=X(K)*(1.0+AVE*CM(K))
      CIP(K)=CI/C(K)
  220 AC=AC+CIP(K)
      GO TO 51
  150 AVE=(AH+AL)/2.0
      NX=1
      GO TO 250
```

```
202 WRITE(2,203) AVE,AAC,SAC,ST
203 FORMAT(F10.6,2F10.0,F10.6)
    WRITE(2,2)
    IF(ISSW(0))99,1
 99 STOP
    END
    ENDS
```

```
      PROGRAM AABSD
      COMMON C(10),X(10),CM(10),CIP(10)
      COMMON CX(10)
      CALL RESET
      WRITE(2,7)
    7 FORMAT("ALFA-XA  [ EFFECT OF (A) ON (X) ]"/
     #"    VARIABLE CONC.-X"/)
    1 AA=0
      DD=0.0
      NX=0
      NCT=0
      N=0
      J=1
      WRITE(2,6)
    6 FORMAT("ALFA-XM")
      READ(1,*) AXX
      WRITE(2,5)
    5 FORMAT("CONC-A,CONC-X,XRF-X ?")
   10 READ(1,*) C(J),CX(J),X(J),N
      CM(J)=1.0-CX(J)-C(J)
      J=J+1
      IF(N-1)10,20
   20 J=J-1
      N=1
      WRITE(2,2)
  135 J1=N+1
      DO 100 NN=J1,J
      X1=CX(NN)*X(N)
      Y1=CX(N)*X(NN)
      A=(Y1-X1+AXX*(Y1*CM(NN)-X1*CM(N)))/
     #(X1*C(N)-Y1*C(NN))
      AA=AA+A
      NCT=NCT+1
  100 CONTINUE
      N=N+1
      IF(N-J)135,140,140
  140 AVE=AA/FLOAT(NCT)
      AA=0
      NCT=0
      N=1
   25 J1=N+1
      DO 30 NN=J1,J
      X1=CX(NN)*X(N)
      Y1=CX(N)*X(NN)
      A=(Y1-X1+AXX*(Y1*CM(NN)-X1*CM(N)))/
     #(X1*C(N)-Y1*C(NN))
      D=A-AVE
      DD=DD+D*D
      NCT=NCT+1
   30 WRITE(2,2) N,NN,A
```

```
    2 FORMAT(2I3,2X,F12.6)
      N=N+1
      IF(N-J)35,40,40
   35 GO TO 25
   40 WRITE(2,2)
      SD=SQRT(DD/FLOAT(NCT-1))
      WRITE(2,3) AVE,SD
    3 FORMAT("AVERAGE= "F12.6"    STD. DEV. = "F7.4)
  250 WRITE(2,2)
      AC=0.0
      NTR=0
      SP=0.0
      DD=0.0
      NF=0
      FAC=0.001*AVE
      N1=0
      WRITE(2,6)
    6 FORMAT("ABSORPTION CORRECTION"/8X,"DATA",
     #4X,"MATRIX",7X,"CORT",3X,"CORT-2ND",6X,"100I")
      DO 50 K=1,J
      C1=X(K)*(1.0+AXX*CM(K))
      C2=X(K)*(1.0+AXX*CM(K)+AVE*C(K))
      CI=C1*(1.0+AVE*C(K))
      CIP(K)=C2/CX(K)
      AC=AC+CIP(K)
   50 WRITE(2,4) K,X(K),C1,C2,CI,CIP(K)
    4 FORMAT(I3,6F10.0)
      IF(ISSW(15))260,51
  260 CALL RESET
      READ(1,*) AVE
      DD=0.0
      GO TO 40
   51 AAC=AC/FLOAT(J)
      DO 280 K=1,J
      D=CIP(K)-AAC
  280 DD=DD+D*D
      SAC=SQRT(DD/FLOAT(J-1))
      ST=SAC*100.0/AAC
      DN=ST-SP
      NTR=NTR+1
      IF(NTR-5000)300,300,301
  300 CONTINUE
      IF(NK)281,281,282
  281 IF(DN-0.000001)55,55,45
   45 WRITE(2,283) AVE,AAC,SAC,ST
      FAC=-FAC
      NF=NF+1
      IF(N1)53,53,54
   54 N1=1
      AL=AVE
```

```
      GO TO 56
   54 N1=0
      AH=AVE
   56 IF(NF-4)55,188,188
   55 AVE=AVE-FAC
      AC=0.0
      DD=0.0
      SP=ST
      DO 220 K=1,J
      C1=X(K)*(1.0+AXX*CM(K))
      C2=X(K)*(1.0+AXX*CM(K)+AVE*C(K))
      CI=CI*(1.0+AVE*C(K))
      CIP(K)=C2/CX(K)
  220 AC=AC+CIP(K)
      GO TO 51
  188 AVE=(AH+AL)/2.0
      NX=1
      GO TO 250
  301 WRITE(2,302)
  302 FORMAT("***** ERROR LIMIT *****")
  252 WRITE(2,203) AVE,AAC,SAC,ST
  203 FORMAT(F18.6,2F10.0,F18.6)
      WRITE(2,2)
      IF(ISSW(0))99,1
   99 STOP
      END
```

PROGRAM AMNLY

PURPOSE : To determine interelement effect correction coefficients from the concentration and x-ray intensity data of the complete set of actual bauxite samples.

METHOD : For each element in the sample there is an equation similar to EQUATION 5-3.

The set of equations is solved by the process of iteration. The initial concentrations are set equal to the intensity ratio and after iteration the calculated concentrations are obtained. This method is the same as that outlined by Lachance and Traill (see ref. 22).

The calculated concentrations are compared to the known concentrations and an absolute-error is determined. The alpha coefficients are revised sequentially by 0.001 or 0.01% (whichever is the largest) and a recalculation of the concentrations is performed. The new absolute error is compared to the old value. The alpha coefficients are so adjusted to produce the minimum absolute error.

```
      PROGRAM ANNLY
      COMMON A(16),X1(4),XOBS(288),CKWN(288),CCAL(288)
      COMMON D(4),SD(4),AD(4),ASC(4),S(78)
      ASC(1)=40514B
      ASC(2)=51511B
      ASC(3)=52111B
      ASC(4)=43105B
  999 CALL RESET
    8 FORMAT(""/F7.4)
      WRITE(2,1)
    1 FORMAT("16 ALFA COEFF. (4 PER LINE)")
      DO 6 I=1,16,4
      I1=I+3
    6 READ(1,*) (A(J),J=I,I1)
      WRITE(2,2)
    2 FORMAT("100% INTENSITIES")
      READ(1,*) (X1(J),J=1,4)
      WRITE(2,7)
    7 FORMAT("SAMPLE NUMBERS ? -")
      READ(1,*) NL,NU
   18 WRITE(2,3)
    3 FORMAT("HS READER"/"KNOWN CONC. , OBS. INTENSITY")
      NLN=4*(NL-1)
      IF(NL-1)144,144,142
  142 DO 143 K=1,NLN
  143 READ(5,*)
  144 ND=NU-NL+1
      NLN=4*ND
      DO 43 K=1,NLN
   43 READ(5,*) CKWN(K),XOBS(K)
  100 CALL PREP3(NLN)
  101 DO 16 K=1,ND
      S(K)=0.0
      K=0
      DO 42 K1=1,NLN,4
      K=K+1
      DO 45 J=1,4
      K2=K1+J-1
   45 S(K)=S(K)+CCAL(K2)
   42 CONTINUE
  102 WRITE(2,5)
      WRITE(2,4) (ASC(J),J=1,4)
    4 FORMAT(8X,4(5X,A2),7X,"TOTAL"/"SAMPLE"/"")
      K=0
      K1=NL-1
      DO 46 J=1,NLN,4
      K=K+1
      K1=K1+1
      CT=0
      DO 41 J1=1,4
```

```
      J2=J+J1-1
   41 CT=CT+CKWN(J2)
      WRITE(2,44) K,CKWN(J),CKWN(J+1),CKWN(J+2),CKWN(J+3),CT
     #,CCAL(J),CCAL(J+1),CCAL(J+2),CCAL(J+3),S(K)
   44 FORMAT(I4," KWN "4F7.2,F10.2/5X,"CAL ",4F7.2,F10.2/" ")
      IF(ISSW(3))468,46
   46 CONTINUE
  468 WRITE(2,8)
      SUM=0.0
      ASU=0.0
      DO 21 K=1,4
      SUM=SUM+AD(K)
   21 ASU=ASU+SD(K)
      AVO=SUM/4.0
      AVA=ASU/4.0
      WRITE(2,18)
   18 FORMAT("ABSOLUTE ACCURACY")
      WRITE(2,19) (AD(J),J=1,4),AVO,(SD(J),J=1,4),AVA
   19 FORMAT(9X,4F7.3,"   AVE="F7.3)
      WRITE(2,8)
      WRITE(2,9) (A(J),J=1,16)
    9 FORMAT(4F10.4)
      WRITE(2,8)
      DO 38 JJ=1,16
      FAC=0.01
      NF=0
      WRITE(2,88) A(JJ)
   88 FORMAT(F7.4"  - ~")
   22 IF(ABS(A(JJ))-0.1)23,24
   23 A(JJ)=A(JJ)+FAC*0.1
      GO TO 5
   24 A(JJ)=A(JJ)+FAC*A(JJ)
    5 CALL PREP3(NLN)
      IF(ISSW(12))999,98
   98 IF(ISSW(13))1000,99
   99 CONTINUE
      SUM=0.0
      DO 25 K=1,4
   25 SUM=SUM+AD(K)
      AVN=SUM/4.0
      IF(ISSW(1))280,282
  280 WRITE(2,281) A(JJ),AVN
  281 FORMAT(/3X,F7.4,F7.2"~")
  282 IF(ISSW(2))283,284
  283 WRITE(2,8)
      GO TO 38
  284 CONTINUE
      IF(AVO-AVN)26,29,29
   26 FAC=-FAC
      NF=NF+1
```

```
      IF(NF-2)29,27,28
   27 AL=A(JJ)
      GO TO 29
   28 AH=A(JJ)
      A(JJ)=(AL+AH)/2.0
      CALL PREP3(NLN)
      SUM=0.0
      DO 20 K=1,4
   20 SUM=SUM+AD(K)
      AVN=SUM/4.0
   50 WRITE(2,13) A(JJ)
   13 FORMAT(F7.4)
   51 DO 17 K=1,ND
   17 S(K)=0.0
      K=0
      DO 48 K1=1,NLN,4
      K=K+1
      DO 47 J=1,4
      K2=K1+J-1
   47 S(K)=S(K)+CCAL(K2)
   48 CONTINUE
      GO TO 30
   29 AVO=AVN
      GO TO 22
   30 CONTINUE
      GO TO 102
 1000 STOP
      END



      SUBROUTINE PREP3(NLN)
      COMMON AAH,AAS,AAT,AAF,ASH,ASA,AST,ASF,ATH,ATA,ATS
      COMMON AFH,AFA,AFS,AFT,XA1,XS1,XT1,XF1
      COMMON XOBS(200),CKWN(200),CCAL(200),D(4),SD(4),
      COMMON AD(4)
      DO 10 J=1,4
      AD(J)=0.0
   10 SD(J)=0.0
      K=0
      DO 20 J=1,NLN,4
      K=K+1
      XA=XOBS(J)
      XS=XOBS(J+1)
      XT=XOBS(J+2)
      XF=XOBS(J+3)
      RA=XA/XA1
      RS=XS/XS1
      RT=XT/XT1
```

```
      RF=XF/XF1
      CM=1.0-RA-RS-RT-RF
      CA=RA*(1.0+AAM*CM+AAS*RS+AAT*RT+AAF*RF)
      CS=RS*(1.0+ASM*CM+ASA*RA+AST*RT+ASF*RF)
      CT=RT*(1.0+ATM*CM+ATA*RA+ATS*RS+ATF*RF)
      CF=RF*(1.0+AFM*CM+AFA*RA+AFS*RS+AFT*RT)
      CM=1.0-CA-CS-CT-CF
  100 OCA=CA
      OCS=CS
      OCT=CT
      OCF=CF
      OCM=CM
      CA=RA*(1.0+AAM*CM+AAS*CS+AAT*CT+AAF*CF)
      CS=RS*(1.0+ASM*CM+ASA*OCA+AST*CT+ASF*CF)
      CT=RT*(1.0+ATM*CM+ATA*OCA+ATS*OCS+ATF*CF)
      CF=RF*(1.0+AFM*CM+AFA*OCA+AFS*OCS+AFT*OCT)
      CM=1.0-CA-CS-CT-CF
      DA=CA-OCA
      DS=CS-OCS
      DT=CT-OCT
      DF=CF-OCF
      DM=CM-OCM
      IF(ABS(DA)-0.00001)120,100,100
  120 IF(ABS(DS)-0.00001)121,100,100
  121 IF(ABS(DT)-0.00001)122,100,100
  122 IF(ABS(DF)-0.00001)123,100,100
  123 IF(ABS(DM)-0.00001)124,100,100
  124 PA=100.0*CA/0.529258
      PS=100.0*CS/0.467439
      PT=100.0*CT/0.599588
      PF=100.0*CF/0.699433
      IF(ISSW(8))118,119
  118 WRITE(2,4) CA,CS,CT,CF,CM
    4 FORMAT(5F9.5)
  119 CONTINUE
      CCAL(J)=PA
      CCAL(J+1)=PS
      CCAL(J+2)=PT
      CCAL(J+3)=PF
      DO 15 J2=1,4
      J3=J+J2-1
      D(J2)=(CCAL(J3)-CKUN(J3))*100.0/CKUN(J3)
      AD(J2)=AD(J2)+ABS(CCAL(J3)-CKUN(J3))
   15 SD(J2)=SD(J2)+ABS(D(J2))
   20 CONTINUE
      DO 25 J2=1,4
      AD(J2)=AD(J2)/FLOAT(K)
   25 SD(J2)=SD(J2)/FLOAT(K)
      RETURN
      END
```

PROGRAM LSERR

PURPOSE : The determination of the least squares equations for the x-ray intensity data of the bauxite samples.

METHOD : The concentrations and the x-ray intensities both measured and corrected are used in the program.
The program takes the measured intensity data and divides by the 100% intensity to give the elemental percentage by the ratio method. The error between the known and the calculated concentrations is determined.
The least squares equations are derived for the measured intensity data and subsequently elemental concentrations are determined from these equations. The error between the known and the calculated concentrations is determined.
The ratio method is performed on the corrected data. and the error is determined.
The least squares method is performed on the corrected data and the error is determined.

The printout compares the measured data to the corrected data for both the ratio method and the least squares method. The average absolute errors are calculated to show the most accurate data set.

```
      PROGRAM LSERR
      COMMON C(70),XI(2,70)
      NC=0
   15 READ(5,7) LA
    7 FORMAT(2X,A1)
      IF(LA-43B)15,20,15
   20 WRITE(2,8)
    8 FORMAT("100% INTENSITY= -")
      READ(1,*) XZ
      F=70.0
      SX=0.0
      SY1=0.0
      SY2=0.0
      SP1=0.0
      SP2=0.0
      SXX=0.0
      DO 50 K=1,70
      READ(5,1) I,C(K),XI(1,K),XI(2,K)
    1 FORMAT(6X,A2,11X,F6.5,F10.0,10X,F10.0)
      C(K)=C(K)*100.0
      SX=SX+C(K)
      SY1=SY1+XI(1,K)
      SY2=SY2+XI(2,K)
      SP1=SP1+C(K)*XI(1,K)
      SP2=SP2+C(K)*XI(2,K)
   50 SXX=SXX+C(K)*C(K)
      SX=SX/F
      SY1=SY1/F
      SY2=SY2/F
      SP1=SP1/F
      SP2=SP2/F
      D=SXX/F-SX*SX
      A1=(SP1-SX*SY1)/D
      A2=(SP2-SX*SY2)/D
      B1=SY1-A1*SX
      B2=SY2-A2*SX
      WRITE(2,2) I,A1,I,B1,A2,I,B2
    2 FORMAT(/"RATIO METHOD"/"  I(MEAS) = "
     #"A2" * I(100%)"//"LEAST SQUARES EQUATIONS"/"  I(MEAS) = "
     #E12.6" ( I "A2" ) + "E12.6,/"  I(CORR) = "E12.6
     #" ( I "A2" ) + "E12.6,3/)
      WRITE(2,3) I,I,I,I
    3 FORMAT(28X"RATIO METHOD  LEAST SQUARES"9X
     #"LEAST SQUARES"/"SAMPLE I"A2"  I(MEAS)  I"A2
     #"  ERROR  I"A2"  ERROR I(CORR)  I"A2"  ERROR"/)
      AERR=0.0
      AEM=0.0
      AEC=0.0
      DO 55 K=1,70
      RM=100.0*XI(1,K)/XZ
```

```
      ERM=RM-C(K)
      AERM=AERM+ABS(ERM)
      PM=(XI(1,K)-B1)/A1
      EM=PM-C(K)
      AEM=AEM+ABS(EM)
      PC=(XI(2,K)-B2)/A2
      EC=PC-C(K)
      AEC=AEC+ABS(EC)
   55 WRITE(2,4) K,C(K),XI(1,K),RM,ERM,PM,EM,XI(2,K),PC,EC
    4 FORMAT("  #"I2,F6.2,F8.0,F6.2,3F7.2,F9.0,F6.2,F7.2)
      AERM=AERM/F
      AEM=AEM/F
      AEC=AEC/F
      WRITE(2,5) AERM,AEM,AEC
    5 FORMAT(/"  AVE. ABS. ERROR = "7X,F5.2,9X,F5.2
     #,17X,F5.2,10/)
      NC=NC+1
      IF(NC-4)15,15,60
   60 STOP
      END
```